NIST TECHNICAL NOTE 1257

U.S. DEPARTMENT OF COMMERCE/National Institute of Standards and Technology

NBS Reactor: Summary of Activities July 1987 Through June 1988

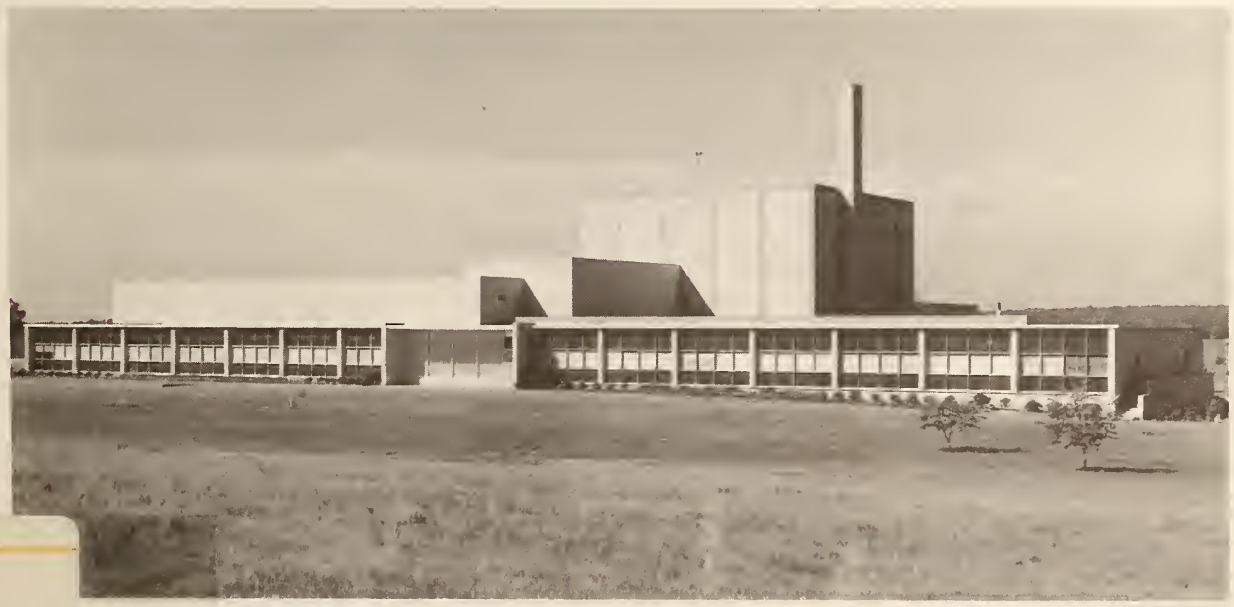

NIST Technical Note 1257

NBS Reactor: Summary of Activities July 1987 Through June 1988

Carol O'Connor, Editor

Reactor Radiation Division
Institute for Materials Science and Engineering
National Institute of Standards and Technology
(formerly National Bureau of Standards)
Gaithersburg, MD 20899

January 1989

NOTE: As of 23 August 1988, the National Bureau of Standards (NBS) became the National Institute of Standards and Technology (NIST) when President Reagan signed into law the Omnibus Trade and Competitiveness Act.

U.S. Department of Commerce
C. William Verity, Secretary

Ernest Ambler, Acting Undersecretary for Technology

National Institute of Standards and Technology
(formerly National Bureau of Standards)
Raymond G. Kammer, Acting Director

National Institute of Standards and Technology Technical Note 1257
Natl. Inst. Stand. Technol. Tech. Note 1257, 227 pages (Jan. 1989)
CODEN: NTNOEF

U.S. GOVERNMENT PRINTING OFFICE
WASHINGTON: 1989

FOREWORD

The National Bureau of Standards (NBS)* Reactor serves the needs of NBS, other government agencies, and outside organizations as a national center for the application of neutron methods to problems of national interest. The Reactor Radiation Division operates the reactor and fosters its scientific and technological use. Toward this end, the Division's small nucleus of scientists is experienced in the use of reactors for a wide range of scientific and technical problems. In addition to pursuing their own research and developing sophisticated experimental facilities, they seek out and encourage collaboration with other scientists engaged in challenging programs whose work can benefit from use of the reactor, but who do not have the reactor experience necessary to take full advantage of the facilities available. The Division also provides irradiation services to a wide variety of users as well as engineering and other technical services.

The reactor operates at 20 MW and supports 25 experimental facilities ranging from intense neutron beams to extensive irradiation facilities. A major expansion of the experimental facilities is currently under way. A cold neutron source was installed and construction of a large neutron guide hall is nearing completion. The guide hall will accommodate 15 new instruments served by seven neutron guides from the cold source. This will be a national facility providing state-of-the-art instruments that are currently unavailable in the United States.

This report summarizes the work done which is dependent on the reactor including a large number of programs outside the Division. The first section summarizes the programs carried out by scientists in the Reactor Radiation Division and their collaborators. The second section summarizes NBS work originating outside NBS for which the Division provides reactor facilities and irradiation services. The remaining sections are self-explanatory.

Appreciation is extended to C. O'Connor for her contributions to the editing, organization, and preparation of this report; F. Shorten for generously sharing his expertise in preparing this report; S. Shatzer for typing manuscripts; and J. Spillman for typing manuscripts and assisting in the preparation of the final copy.

R. S. Carter

R. S. Carter, Chief
Reactor Radiation Division
National Institute of Standards
and Technology

*In August 1988, the name of the National Bureau of Standards (NBS) was changed to the National Institute of Standards and Technology (NIST). Since the work described in this report was done prior to the name change, all references to the Institute read NBS in the body of the text.

ABSTRACT

This report summarizes all those programs which use the NBS Reactor. It covers the period for July 1987 through June 1988. The programs range from the use of neutron beams to study the structure and dynamics of materials through nuclear physics and neutron standards to sample irradiations for activation analysis, isotope production, neutron radiography, and nondestructive evaluation.

KEY WORDS: activation analysis; cold neutrons; crystal structure; diffraction; isotopes; molecular dynamics; neutron; neutron radiography; nondestructive evaluation; nuclear reactor; radiation.

DISCLAIMER

Certain trade names and company products are identified in order to adequately specify the experimental procedure. In no case does such identification imply recommendation or endorsement by the National Institute of Standards and Technology, nor does it imply that the products are necessarily the best available for the purpose.

CONTENTS

CONTENTS

CONTENTS

A. REACTOR RADIATION DIVISION AND COLLABORATIVE PROGRAMS

IN SEARCH OF LOCAL MODE SPLITTING FOR HYDROGEN IN SCANDIUM

T. J. Udovic and J. J. Rush

and

I. S. Anderson
(Paul Scherrer Institute, Villigen, Switzerland)

Recently, incoherent inelastic neutron scattering (IINS) measurements of the hydrogen local mode frequencies in single-crystal samples of α-$YH(D)_{0.18}$ demonstrated a highly unusual potential which was much softer and anharmonic along the c-axis than in the basal plane [1]. Despite nearly cubic local symmetry for the T sites (i.e., a c/a ratio that is only 3% less than the ideal value), the vibrational mode along the c-axis exhibited a frequency that was 25% lower than the frequency of the doubly degenerate vibrations in the basal plane. In addition, the c-axis mode possessed a novel splitting which was attributed to concentration- and temperature-dependent H pairing along the c-axis on either side of an yttrium atom [2].

In order to compare the yttrium results to those for scandium, an analogous rare-earth metal which also retains H in solid solution (α-phase), we have measured preliminary IINS spectra for single-crystal α-$ScH_{0.157}$ using the BT-4 triple-axis spectrometer. Figure 1 illustrates the IINS spectrum for α-$ScH_{0.157}$ using the Be filter ($\Delta E \approx$ 5-9 meV FWHM in the range 80-160 meV) with the Q-vector directed ca. 45° from the c-axis. In this scattering geometry, all H local mode vibrations are present; i.e., the vibrational mode along the c-axis at ca. 103 meV and the vibrational modes in the basal plane at ca. 149 meV. Again, similar to α-YH_x, the vibrational mode along the c-axis is both substantially lower (>30%) in frequency and intrinsically broader than the basal-plane modes. A higher-resolution IINS spectrum of the c-axis mode using the Be/graphite composite filter ($\Delta E \approx$ 2.5 meV FWHM at 100 meV) is illustrated in figure 2. Despite the broadness of the feature, no splitting is observed within the resolution of the measurement. Hence, if splitting is present, it is less than 2.5 meV in contrast to the 3.5-4 meV splitting observed for α-$YH_{0.18}$.

The nature of the potential along the c-axis will be further explored in the near future. In particular, experiments are in progress for determining

the frequency of the corresponding second-excited state as well as the effects of deuterium isotope dilution, hydrogen concentration, and temperature on the α-phase H spectrum.

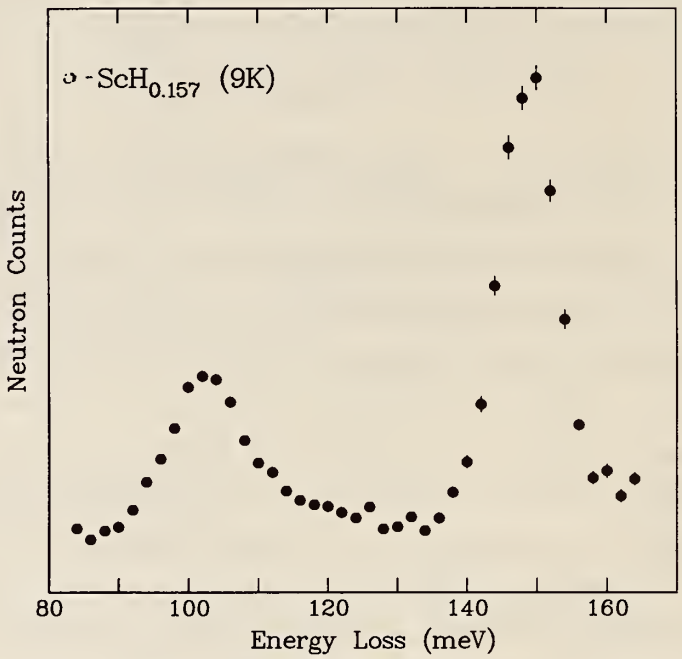

Figure 1. IINS spectrum for single-crystal α-$ScH_{0.157}$ at 9 K using the BT-4 Be-graphite-Be analyzer with the Q-vector directed 45° from the c-axis.

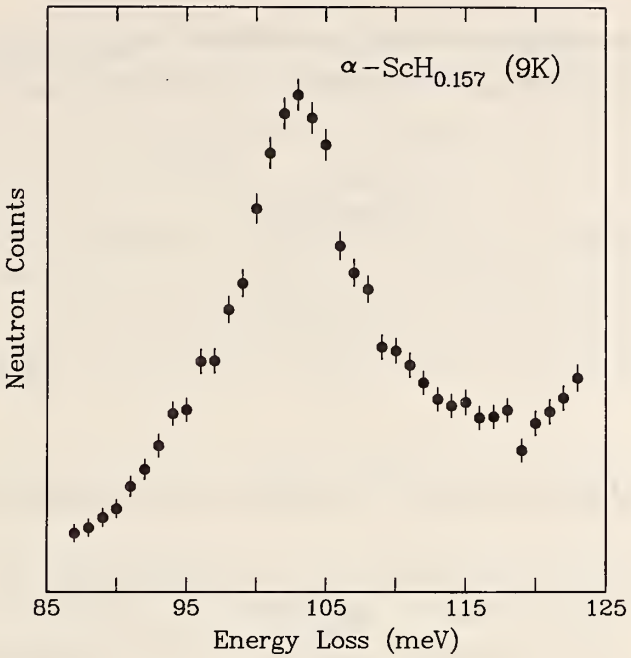

Figure 2. IINS spectrum for the α-$ScH_{0.157}$ c-axis mode at 9 K using the BT-4 Be-graphite-Be analyzer.

References

[1] I. S. Anderson, J. J. Rush, T. J. Udovic, and J. M. Rowe, Phys. Rev. Lett. 57, 2822 (1986).

[2] I. S. Anderson, N. F. Berk, J. J. Rush, and T. J. Udovic, Phys. Rev. B 37, 4358 (1988).

STUDY OF HYDROGEN SITES IN AMORPHOUS $Pd_{85}Si_{15}H_x$ By NEUTRON VIBRATIONAL SPECTROSCOPY

J. J. Rush and T. J. Udovic

R. Hempelmann
(Los Alamos National Laboratory, Los Alamos, NM)

D. Richter
(Institut Laue-Langevin, Grenoble, France)

and

G. Driesen
(Institut für Festkörperforschung, Jülich, West Germany)

$Pd_{1-y}Si_y/H$ is the most intensively investigated amorphous metal/hydrogen system and in some sense can now be considered as a prototype, as Pd/H is for binary crystalline metal/hydrogen systems. The thermodynamics of hydrogen absorption in $Pd_{1-y}Si_yH_x$ were studied by electrochemical methods by Kirchheim et al. The temperature and H concentration dependence of the resulting chemical potential was interpreted in terms of a Gaussian distribution of site energies. The temperature and H concentration dependence of the electrochemically determined H diffusion coefficient was also explained with the same set of microscopic parameters. Further support for the Gaussian model was obtained from high-pressure gas volumetric measurements. The applicability of a Gaussian model is somewhat surprising because such a model neglects H-H interactions which without doubt considerably contribute to the chemical potential at high hydrogen concentration. Recent quasielastic neutron scattering results (Richter et al.) were not consistent with a Gaussian model, but were interpreted in terms of a bimodal distribution of hydrogen sites. These results, however, could not provide information on what kind of sites are involved.

In view of this we have performed a series of neutron vibrational spectra measurements on the high sensitivity Be-filter spectrometer arrangement on the BT-4 instrument to provide an independent probe of the H-bonding states in amorphous $Pd_{85}Si_{15}H_x$, over two orders of magnitude in H concentration (X = .0013 to .08). The results show the existence of two bands H vibrations, roughly around 60 meV and in the 90-130 meV range. From experience with many other metal/hydrogen systems, the former is attributed to octahedral-type sites (Pd_6) and the latter to tetrahedral-types sites (perhaps Pd_3Si). There

is also a tendency of the higher energy scattering intensity to increase with increasing H concentration. Thus at least two different types of H-bonding sites appear to be occupied, with some evidence that the octahedral sites are preferentially filled at lower H concentrations. While the data show that there is a broad and overlapping distribution of site energies, the results are not consistent with the assumption of a Gaussian distribution of hydrogen site energies which has been the basis of interpretation for most of the earlier electrochemical and thermodynamic data on these and similar glasses.

NEUTRON SPECTROSCOPY AS A PROBE OF ZEOLITE FRAMEWORK VIBRATIONS

T. J. Udovic, R. R. Cavanagh, and J. J. Rush

and

J. M. Nicol
(University of Maryland and the National Bureau of Standards)

Incoherent inelastic neutron scattering (IINS) is a particularly useful spectroscopic probe of molecular vibrations involving hydrogen motions in the regime below 250 meV. Indeed, zeolite framework vibrational modes are in an energy regime easily accessible to neutron spectroscopy, yet the low scattering cross sections for framework atoms (e.g., Al, Si, and O) result in low-intensity framework features. The scattering intensity associated with these framework modes can be enhanced dramatically by the presence of framework-coupled hydrogenous counter-cations such as protons or ammonium ions. Such modes can then be more sensitively probed by following the hydrogen motions of these species rigidly attached to the framework lattice. Currently we are interested in using this enhancement technique for investigating the framework vibrations of various zeolites.

As demonstrated by the infrared spectroscopic work of Flanigen et al. [1], zeolites possess two classes of vibrations: (i) structure-insensitive internal vibrations of the framework TO_4 tetrahedra, the primary building units in all zeolite frameworks, and (ii) structure-sensitive vibrations arising from the external linkages between tetrahedra, which are related to secondary building units and building block polyhedra such as double rings and large pore openings. This is exemplified in figure 1 by the IINS spectra of

the protonated forms of Y and rho zeolites. In particular, both zeolite spectra are similar above 70 meV but differ considerably below 70 meV. Force-field analyses of several models of the proton-containing group in H-rho have led to the assignment of the structure-insensitive features at 143 and 131 meV to in-plane and out-of-plane T-O-H bending modes, respectively, and that at 93 meV to a symmetric T-OH stretching mode [2]. Below 70 meV, H-rho exhibits a large-intensity feature at 45 meV in contrast to the narrower and somewhat smaller-intensity feature at 52 meV for H-Y. These structure-sensitive features are attributed to proton-coupled pore-opening modes of the two zeolite frameworks, which contain different external linkages. Recently, it was shown that NH_4-rho possessed, similar to the proton-coupled feature for H-rho, an ammonium-coupled pore-opening feature which was approximately four times as intense due to the presence of four hydrogens instead of one hydrogen per site [3]. In contrast to these hydrogen-containing zeolites, the relatively featureless scattering spectrum of Na-Y, also depicted in figure 1, illustrates the lack of scattering sensitivity in the absence of hydrogenous counter-cations.

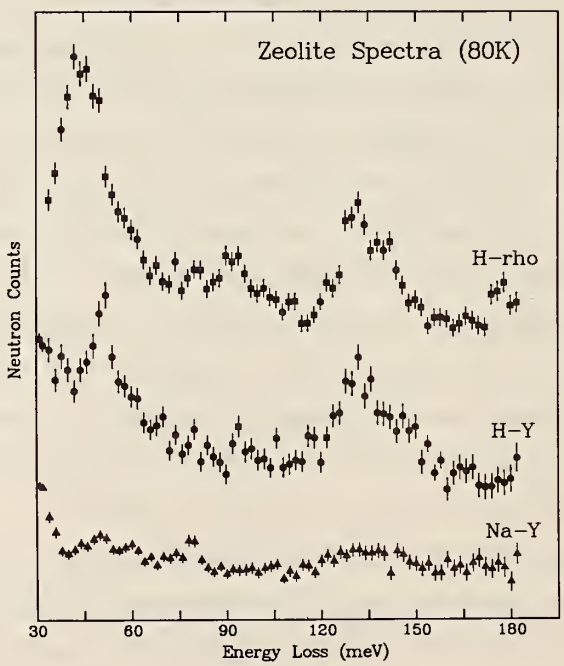

Figure 1. IINS spectra for Na-Y, H-Y, and H-rho zeolites at 80 K.

Work is in progress to investigate other zeolites and counter-cations in order to correlate specific structure-sensitive features to framework geometry.

References

[1] E. M. Flanigen, H. Khatami, and H. A. Szymanski, ACS Adv. Chem. Ser. 101, 201 (1971).

[2] M. J. Wax, R. R. Cavanagh, J. J. Rush, G. D. Stucky, L. Abrams, and D. R. Corbin, J. Phys. Chem. 90, 532 (1986).

[3] T. J. Udovic, R. R. Cavanagh, J. J. Rush, M. J. Wax, G. D. Stucky, G. A. Jones, and D. R. Corbin, J. Phys. Chem. 91, 5968 (1987).

THE MOLECULAR DYNAMICS AND VIBRATIONAL SPECTROSCOPY OF TITANYL PHOSPHATES

J. M. Nicol
(University of Maryland and National Bureau of Standards)

J. J. Rush

and

G. D. Stucky and T. G. Gier
(University of California, Santa Barbara, CA)

Potassium titanyl phosphate ($kTiPO_5$, KTP) is a relatively new nonlinear optical material which because of its high nonlinear optical coefficient, high optical damage threshold, low phase matching temperature sensitivity, and chemical and mechanical stability, is finding increasing application. The structure of KTP is composed of chains of TiO_6 octahedra linked at the corners by long and short bonds. It is these short TiO bonds that appear to be partially responsible for the nonlinear optical properties of KTP. The chains are in turn linked via phosphate bridges to form an open framework structure, in which the charge balancing cations are incorporated within the channels. The K^+ cations may be substituted during synthesis for other cations, which leads to the possibility of modification of the nonlinear optical properties by modification of the internal structure characteristics.

Neutron scattering techniques are being applied to the study of the ammonium analogues of KTP, NH_4TiPO_5 (NTP) and $K_x(NH_4)_{1-x}TiPO_5$ (NKTP), as well as $NH_4H(TiPO_5)_2$ formed by the selective deammoniation of NTP. The molecular

dynamics of the ammonium ions are being probed by quasielastic scattering using TOF methods, while the vibrational spectroscopy is being investigated by inelastic neutron scattering using the Be-graphite-Be analyzer on BT-4. In addition it is hoped that information will be obtained on hydronium ions (H_3O^+) that are formed during synthesis of titanyl phosphates by hydrothermal techniques, by comparing the results with materials synthesized by flux methods.

THE DYNAMICS OF MOLECULAR HYDROGEN ADSORBED IN CoNa-A ZEOLITE

J. M. Nicol
(University of Maryland and National Bureau of Standards)

J. Eckert
(Los Alamos National Laboratory, Los Alamos, NM)

and

J. Howard
(Imperial Chemical Industries, Wilton, England)

Detailed knowledge of the dynamics and interaction of adsorbate molecules in the cavities of zeolites is crucial for a better understanding of the catalytic properties of these materials. Although a considerable amount of information has been obtained on the interaction of small molecules, such as ethyne, ethene, carbon monoxide etc., with the exchangeable cations in zeolites, only limited information is available on the interaction of molecular hydrogen with the cations. Detailed knowledge of the adsorption properties of H_2 would be of enormous interest because of the simplicity and prototypical nature of this system, as far as the catalytic activity of zeolites is concerned. We are undertaking a program to study molecular hydrogen adsorption in a series of transition metal exchanged zeolites by inelastic neutron scattering (IINS). The sensitivity of IINS to the rotational and vibrational transitions involving H_2, as well as the ability of neutrons to induce transitions within the librational ground state by nuclear spin flips, that are generally not allowed in optical spectroscopies, makes IINS a particularly useful probe of bound hydrogen.

Neutron scattering spectra of H_2 adsorbed in $Co_{4.1}Na_{3.8}$-A (CoNa-A) have been obtained in the energy range 1-40 meV using the time-of-flight (TOF, incident energy 14.8 meV: 1-13 meV) and BT-4 (Be/graphite filter configuration: 12-40 meV) spectrometers. Hydrogen was adsorbed to a coverage of 0.5 molecules per supercage in the fully dehydrated zeolite at 50 K. The sample was cooled to 12 K for data collection.

The IINS spectra of molecular H_2 adsorbed in CoNa-A zeolite are depicted in figures 1a and 1b. In both cases the "background" measurement of the dehydrated zeolite before H_2 adsorption was subtracted using a scale factor determined by the relative monitor counts of the respective data sets. While in the energy range of the TOF data the dehydrated zeolite background was featureless, an intense band at 21 meV was observed in the BT-4 data (fig. 1c). The difference spectrum (fig. 1b) therefore contains a few data points in the region of 21 meV which are believed to be the result of the incomplete subtraction of this "background" feature. The origin of this peak in the dehydrated zeolite spectrum may be accounted for by the presence of $Al(OH)_4$ complexes in the β-cages. These species have been identified in diffraction studies of CoNa-A [1]. The high intensity and low energy of the mode suggests that it is due to a torsional mode of the complex.

In figures 1a and 1b the low energy excitation at 3.8 meV, which occurs with nearly equal intensity in both neutron energy gain and loss, a rather sharp peak at 15.3 meV and the broad, structured band at 27.5 meV are due to molecular H_2 adsorbed within the CoNa-A framework. Annealing the sample at room temperature and subsequent recooling to 12 K did not reveal any noticeable change in the IINS spectrum, indicating that even at room temperature little if any dissociation of H_2 occurs. By considering the predictions of a variety of models for adsorbed diatomic molecules, the observed peaks can be assigned to the rotational and vibrational excitations of H_2 molecules that are weakly bound, presumably to the Co transition metal cations [2]. A two-fold cosine potential with 2° of rotational freedom in which the H_2 is bound end-on to the Co cations best accounted for the observed features [3-5]. Within this model the assignment of the peak at 3.8 meV (0.5 B, where B is the rotational constant) to rotational transition (or librational ground state splitting) of the H_2 molecule, implies a barrier height of about 1.4 Kcal/mol (7.4-9.2 B). Two transitions to the excited rotational states are then predicted at 4.2 B and 3.7 B (31.9 and 28.1 meV),

in good agreement with the broad band observed at about 27.5 meV in figure 1b. The potential energy level diagram for this model, with the rotational transitions to the excited states indicated is shown in figure 2. The remaining peak at 15.3 meV would then be assigned to a vibrational excitation within this model.

Following the success of the assignment of the spectrum of molecular H_2 in CoNa-A, we are now investigating the interaction of H_2 with other transition metal ion-exchanged zeolites by IINS.

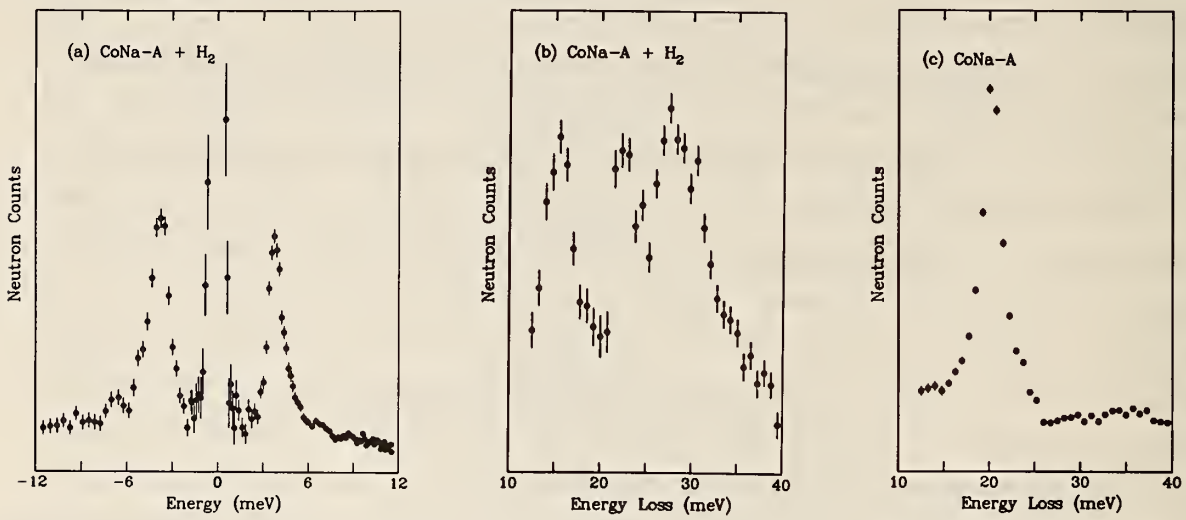

Figure 1. The IINS spectra of 0.5 molecules of H_2 per supercage adsorbed in CoNa-A zeolite at 12 K. (a) TOF spectrum of adsorbed H_2; (b) BT-4 spectrum of adsorbed H_2; (c) BT-4 spectrum of the dehydrated zeolite background.

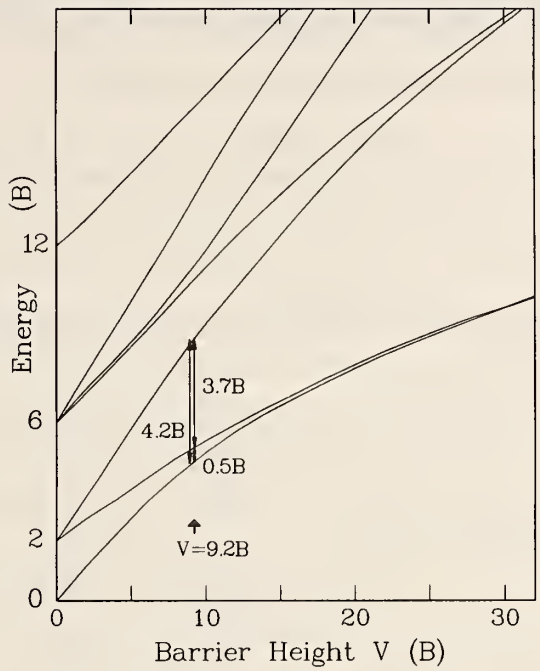

Figure 2. The energy levels of a two-dimensional hindered rotor in a double minimum potential [3]. The observed transitions for H_2 adsorbed in CoNa-A are indicated by arrows. The energy levels and rotational barriers are given in terms of the rotational constant B.

References

[1] J. M. Adams and D. A. Haselden, J. Solid State Chem. 55, 209 (1984).

[2] J. M. Nicol, J. Eckert, and J. Howard, J. Phys. Chem. (in press).

[3] R. F. Curl, H. P. Hopkins, Jr., and K. S. Pitzer, J. Chem. Phys. 48, 4064, (1968).

[4] D. White and E. N. Lassettre, J. Chem. Phys. 32, 72 (1960).

[5] A. A. Evett, J. Chem. Phys. 33, 789 (1960).

INELASTIC NEUTRON SCATTERING STUDY OF TETRAMETHYLAMMONIUM PILLARED MONTMORILLONITE

D. A. Neumann and J. J. Rush

J. M. Nicol
(University of Maryland and the National Bureau of Standards)

and

N. Wada
(Schlumberger-Doll Research, Ridgefield, CT)

Montmorillonite is a member of a naturally occurring class of expandable layered silicates known as smectite clays in which the two-dimensional oxyanions are separated by layers of intercalated cations. Permanent porosity, such as is present in zeolites, can be induced in these minerals by exchanging large cations; e.g., tetramethylammonium, for the naturally occurring ones. The resulting material is known as a "pillared clay" and the large cations which prop the host layers apart are referred to as "pillars". Despite the obvious utility of such structures as catalysts or catalyst supports, relatively little information is available concerning the details of the pillar-host interaction. We have therefore undertaken an inelastic neutron scattering study of the low energy internal modes of tetramethylammonium pillars in montmorillonite. This energy range includes the torsional excitations of the methyl groups which have recently been shown to be quite sensitive to the nature of their environment [1] and which are Raman and infrared inactive.

The experiment was performed at the BT 4 spectrometer using the Be-graphite-Be analyzer, currently the most sensitive instrument of its kind in the world. Two different configurations were used for the primary spectrometer. The first employed a Cu(220) monochromator with collimations of 60′-40′ before and after the monochromator which yielded an energy resolution of roughly 2-5 meV over the energy range of 35-90 meV. For the lower energy portion of the spectra, a graphite (002) monochromator was used with a collimation of 40′-20′, which gave a resolution of about 1.8-2.8 meV over the energy range of 20-40 meV. Data collection time was about 6 hours.

Four internal modes of the $(CH_3)_4N^+$ ion are observed in the data (fig. 1). These are the singly-degenerate, symmetric, torsional mode which belongs to the A_2 symmetry group; the triply-degenerate, antisymmetric torsional

excitation possessing F_1 symmetry; and two C-N bending excitations of symmetry E (doubly-degenerate) and F_2 (triply-degenerate) which are observed because the H atoms ride along on these modes. In addition, a broad feature is observed at about 60 meV. While several modes of the montmorillonite host probably contribute to this scattering, the most important is almost certainly the libration of the hydroxyl groups. The energies of the torsional modes, 27.4 and 38.0 meV, are intermediate to the values obtained for tetramethylammonium ions occluded in the sodalite cage of the zeolite ZK-4 (30.4 and 40.3 meV) [1] and in the gmelinite cage of zeolite omega (25.9 and 36.3 meV) [1].

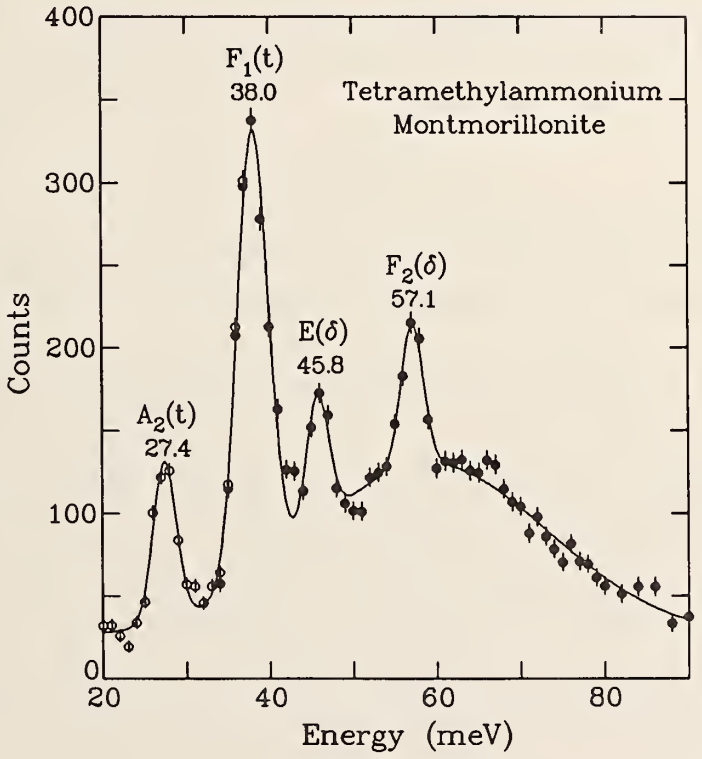

Figure 1. Inelastic neutron scattering spectra of montmorillonite pillared with tetramethylammonium ions taken at 80 K. The solid line represents a fit which includes five Gaussians and a constant background. None of the peaks are resolution limited.

This result indicates that the $(CH_3)_4N^+$ ion interacts more strongly with its environment in montmorillonite than in gmelinite cages but more weakly than in the slightly smaller sodalite cages. In addition, the widths of all of the observed excitations (after correcting for instrumental resolution) for tetramethylammonium ions in montmorillonite are quite similar to those measured by Brun et al. [1] for these ions occluded in gmelinite cages. A

more quantitative analysis of the data awaits further theoretical work on the relationship between these modes and the local environment of the $(CH_3)_4N^+$ ion.

References

[1] T. O. Brun, L. A. Curtiss, L. E. Iton, R. Kleb, J. M. Newsam, R. A. Beyerlein, and D. E. W. Vaughn, J. Am. Chem. Soc. 109, 4118 (1987).

SANS STUDIES OF CHROMIA-PILLARED CLAYS

A. Moini, T. D. Brewer, and T. J. Pinnavaia
(Michigan State University, East Lansing, MI)

and

D. A. Neumann

Pillared clays are a recently discovered class of microporous materials with interesting catalytic and adsorption properties. They are typically prepared by the insertion of thermally stable cations into the galleries of smectite clays. The intercalated ions function as molecular pillars between the host layers. Upon removal of the co-intercalated solvent, a two-dimensional permanently porous network is formed. The most interesting pillaring agents studied so far are the polyoxocations which are prepared via hydrolysis reactions. Upon dehydration, the intercalated polyoxocations are converted to small clusters of metal oxide units which act as pillars [1,2].

The goal of this present small angle neutron scattering (SANS) study was to learn more about the structural characteristics of chromia-pillared clays [3]. The synthesis of these materials involved the addition of anhydrous sodium carbonate to a solution of chromium nitrate followed by aging for 36 hours at 95 °C. A suspension of clay (montmorillonite or fluorhectorite) was then added dropwise, and the mixture was aged for 1.5 hours. The resulting products were washed free of excess salt, air-dried, and then calcined at 350 °C.

The SANS curve for a calcined chromia-pillared clay is shown in figure 1. The log-log plot of these data appears in figure 2. There is clearly a power-law behavior in the Q-range 0.013-0.031 $Å^{-1}$ with a slope of -3.46. This relatively high slope is consistent with the formation of a network of face to face layers crosslinked by the pillaring chromia aggregates. Particles with

more two-dimensional or exfoliated structures should exhibit much lower power-law slopes.

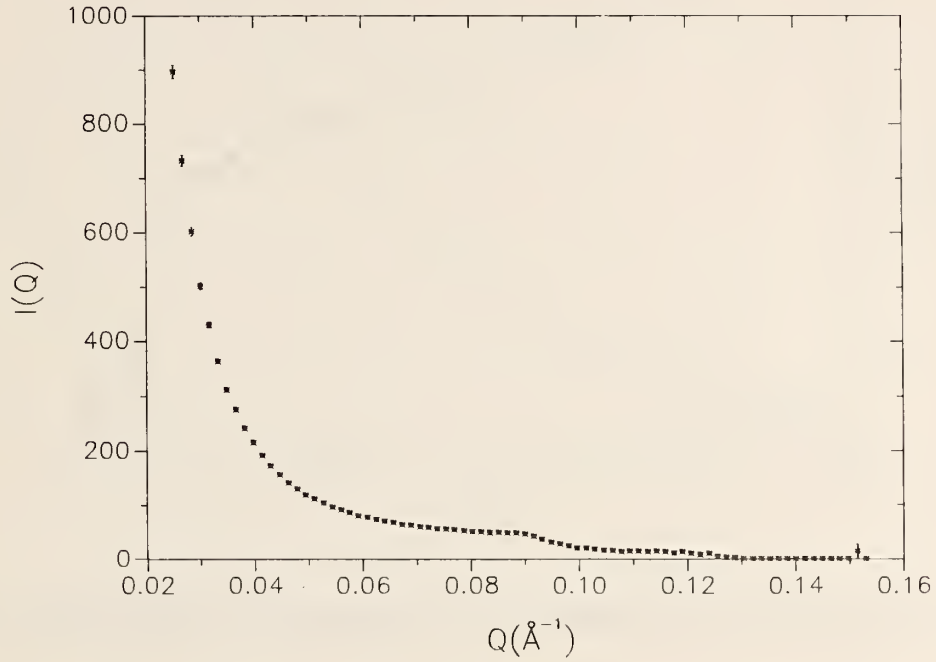

Figure 1. SANS data for chromia-pillared montmorillonite.

The peaks in the high-Q region ($Q > 0.08$ Å^{-1}) are probably due to scattering from the pillars. The two peaks corresponding to 70 and 51 Å are most likely indicative of the lateral interpillar distances taken from the center of the particles. Adsorption studies on this complex have revealed the presence of pores between 10 and 15 Å in diameter. If this free space is taken into account, the width of the pillars would be between 45 and 55 Å. Considering the vertical dimension of the particle, as determined from the interlayer distance (~ 12 Å), these pillars may be described as highly anisotropic clusters.

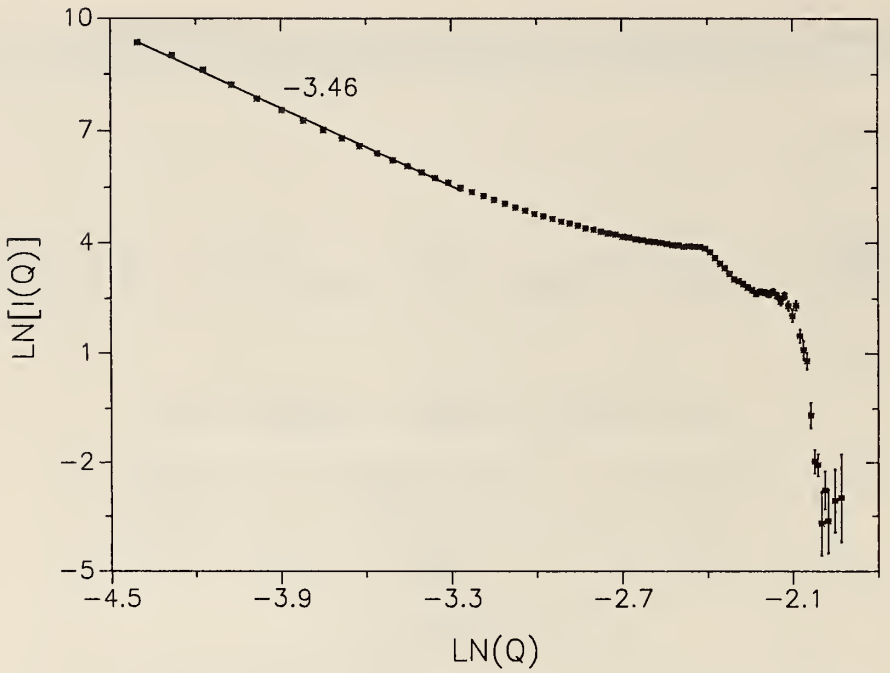

Figure 2. Log-log plot of the SANS data for chromia-pillared montmorillonite.

The scattering curve for chromia-pillared fluorhectorite is shown in figure 3. The power-law behavior for this clay is observed in the Q-range 0.015 - 0.036 $Å^{-1}$ with a slope of -3.73. The scattering in the high Q region differs from the behavior observed for chromia-montmorillonite. This is an indication that the structure of the pillars could vary to a great extent depending on the charge density of the clay. In the case of fluorhectorite, it is possible that much larger particles are formed and that the structure is not as uniform as chromia-montmorillonite. Further studies are needed to elucidate the relationships between pillar distribution and the charge density of the host clay.

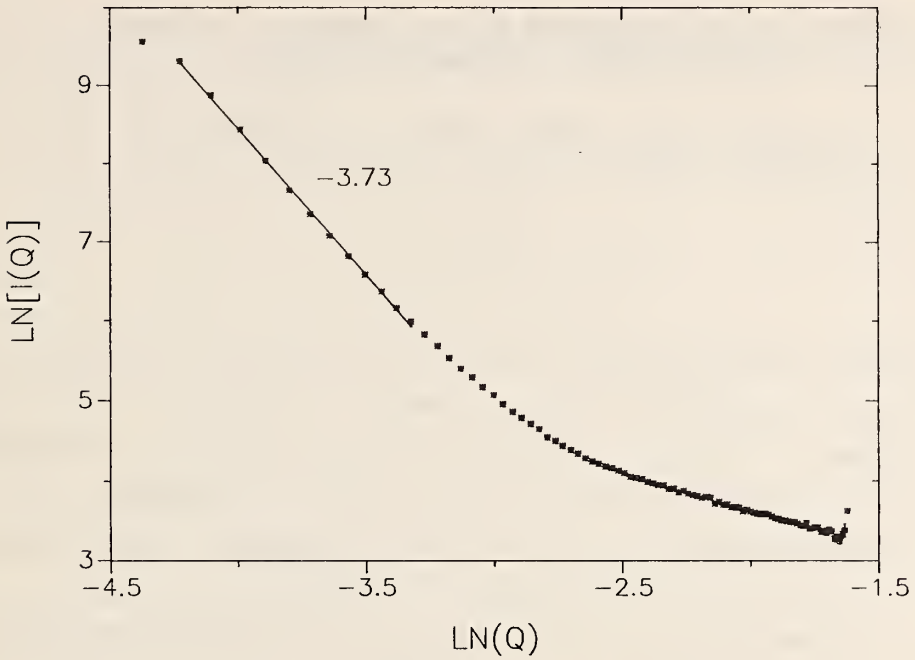

Figure 3. Log-log plot of the SANS data for chromia-pillared fluorhectorite.

References

[1] T. J. Pinnavaia, Science 220, 365 (1983).

[2] R. M. Barrer, Zeolites and Clay Minerals as Sorbents and Molecular Sieves, Academic Press, New York (1973).

[3] T. J. Pinnavaia, M.-S. Tzou, S. D. Landau, J. Am. Chem. Soc. 107, 4783 (1985).

STUDIES ON THE DISPERSION OF CLAY PARTICLES IN EPOXY BY SMALL-ANGLE NEUTRON SCATTERING

A. Moini, M. S. Wang, and T. J. Pinnavaia
(Michigan State University, East Lansing, MI)

and

D. A. Neumann

The rational design of advanced organic composite materials with improved performance characteristics has been of growing interest in recent years. Typical approaches to preparing such materials have included the embedding of chemically modified inorganic particles with plate-like geometry. We have been studying the interaction of clay minerals with epoxy to form new types of composite materials with improved mechanical properties.

A series of commercially available natural clays and modified organoclays were mixed with epoxy resin (DER 331 or EPON 828) at 50 °C. This step was followed by the addition of melted metaphenylenediamine (MPDA) which served as the curing agent. The final mixture was cured in a vacuum oven at 75 °C.

One of the features of interest in the formation of these clay-epoxy composites is the degree of clay dispersion in the polymeric medium. Previous investigations [1,2] have suggested that the clay layer stacking/aggregation in aqueous suspensions can be studied by small-angle neutron scattering. The slopes obtained from the log-log plots of SANS data appear to be closely related to the dimensionality of the particles. For stacked clay layers, these slopes usually approach the limiting value of -4.0, indicating the presence of smooth three-dimensional particles. On the other hand, when the layers are separated from one another upon dispersion in a swelling liquid, the increased anisotropy lowers the absolute values of the observed slopes. In the present project, we have investigated the SANS properties of clay dispersions in epoxy matrices.

The six types of commercial clays studied were HPM-20, Microfine, Bentonite, Mica 4, Claytone 40 (CT 40), and Claytone PS (CT PS). The first three have similar general compositions ($Na^{+}_{0.33}(Al_{1.67}Mg_{0.33})Si_4O_{10}(OH)_2$), Mica 4 is a muscovite with the general formula $H_2K(AlSiO_4)_3$, and the Claytones are organoclays prepared from montmorillonite. SANS data were collected on a series of clay-epoxy composites prepared from these clays. The results,

obtained on composites were compared with the data on the pure clays and their aqueous/organic suspensions .

The data for HPM-20 and HPM-20/epoxy composites can be used as a representative example. The log-log plot of the SANS data for the pure clay (fig. 1) showed a power-law behavior with a slope of -3.70 between Q = 0.015 and 0.0509 $Å^{-1}$. This value agrees with the expected results for particles which are close to three-dimensional as a result of stacked clay layers.

A log-log plot of the SANS data for a 16% HPM-20/epoxy composite is shown in figure 2. A slope of -3.29 was obtained in the region from Q = 0.014 to Q = 0.030 $Å^{-1}$. A similar decrease in the slope also was observed for clay-epoxy phases containing lower concentrations of HPM-20, as shown in table 1. This change in power-law dependence suggests the presence of more anisotropic particles at lower concentrations. As a reference, a 5% suspension of HPM-20, in D_2O was studied which gave a slope of -2.12 in the region from Q = 0.015 to 0.030 $Å^{-1}$. This value may be compared with that obtained for a 7% composite (-2.69 for Q = 0.015 to 0.028 $Å^{-1}$).

The same type behavior, decreasing power-law slope with decreasing concentration of clay, was observed for all of the other systems, as shown in table 1. It is obvious that, at low concentrations, all clay types show some degree of dispersion in the epoxy. Indeed, all of the data collected on composites with very low clay contents (< 5%) gave very similar low slopes. This feature, in addition to the low scattering power at these low clay contents, prompted us to concentrate more closely on the products with higher clay contents.

The most promising clays showed reasonable dispersion even at very high concentrations. An example of such behavior was a 30% Microfine/epoxy composite which had a slope of -2.83 in the Q-range from 0.015 to 0.041 $Å^{-1}$.

The slopes obtained for the pure organoclays were lower than those obtained for the nonfunctionalized clays. This feature is probably due to a more limited face-to-face stacking of the clay layers in the presence of the organic phase. The epoxy composites prepared using these organoclays showed lower power-law slopes compared to the other clays. Comparison of the results for the 7% composites prepared from HPM-20, Mica 4, and Claytone PS clearly demonstrates this point. The degree of dispersion of organoclays in epoxy was comparable to or better than that observed for suspensions of these clays in ethanol/water mixtures.

The above results suggest that SANS studies on clay-epoxy composites reveal the degree of platelet interaction and anisotropy within the individual clay particles. This must be distinguished from dispersion which takes place on a more macroscopic level. It may be possible to couple this technique with other measurements; e.g., SEM and mechanical strength, to reach a better understanding of the formation of clay-epoxy composites.

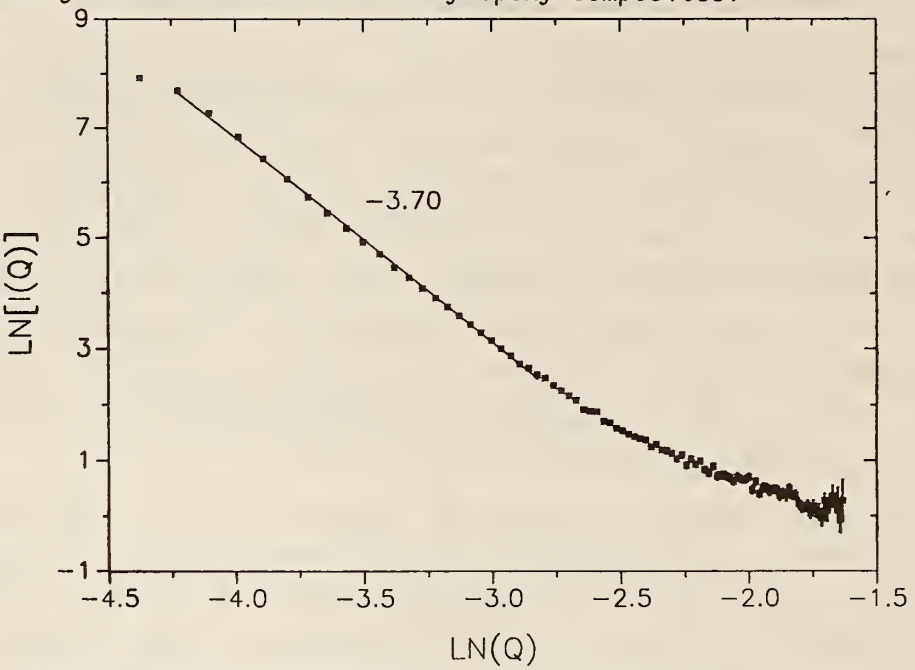

Figure 1. Log-log plot of SANS data for HPM-20 clay powder.

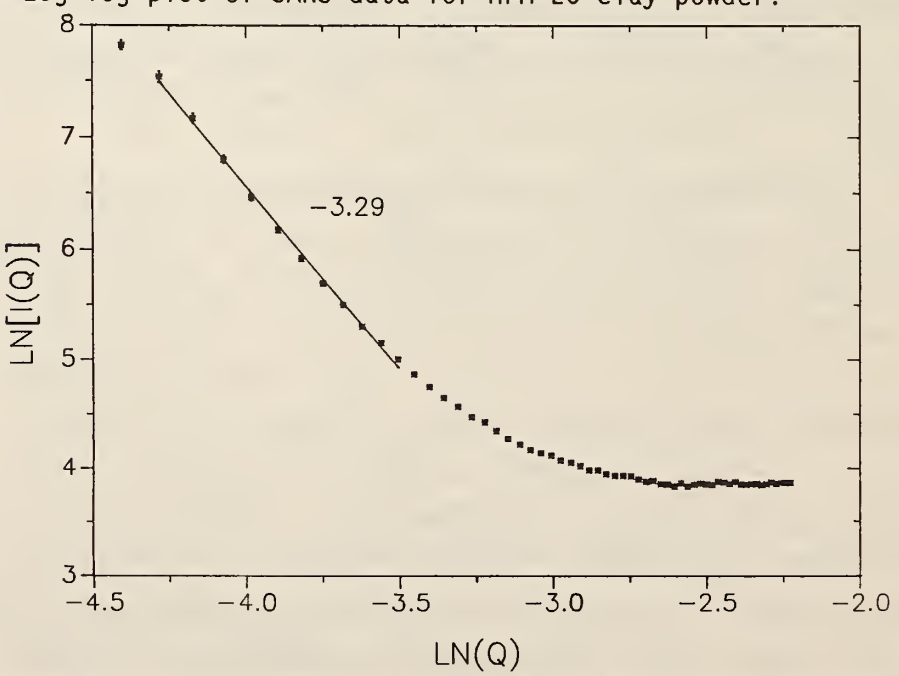

Figure 2. Log-log plot of SANS data for 16% HPM-20/epoxy composite.

Table 1. Slopes (and the Q-ranges, $Å^{-1}$) obtained from the log-log plots of SANS data for clay-epoxy composites

clay conc.(wt. %)	HPM-20	MICA 4	MICROFINE	BENTONITE	CT 40	CT PS
100 %	-3.70 (0.015-0.059)	-4.20 (0.015-0.044)			-3.41 (0.012-0.033)	
30 %			-2.83 (0.015-0.041)			
25 %		-3.26 (0.015-0.026)				
16 %	-3.29 (0.015-0.030)				-2.58 (0.012-0.022)	
7 %	-2.69 (0.015-0.028)	-2.39 (0.015-0.022)				-1.58 (0.015-0.025)
5 %	-2.12[a] (0.015-0.033)				-2.84[b] (0.015-0.028)	

[a] clay suspension in 50 % D_2O/H_2O

[b] clay suspension in 50 % D_2O/EtOH

References

[1] D. J. Cebula, R. K. Thomas, and J. W. White, J.C.S.Faraday I **76**, 314 (1980).

[2] T. J. Pinnavaia, V. Rainey, M.-S. Tzou, and J. W. White, J. Mol. Catal. 27, 213 (1984).

MAGNETO-ELASTICITY AND STRUCTURE OF Er|Y SUPERLATTICES

R. W. Erwin and J. J. Rhyne

and

J. Borchers, M. B. Salamon, R. Du, and C. P. Flynn
(University of Illinois, Urbana, IL)

In the rare-earth superlattices which have been extensively studied, $[Dy_x|Y_y]$ [1] and $[Gd_x|Y_y]$ [2], the magnetic order can be described in terms of the conventional indirect exchange coupling as applied to the heavy rare-earth elements [3], and the range and strength of the interactions through the Y layers find a reasonable interpretation in the context of a conduction-band spin-density-wave. By studying $[Er_x|Y_y]$ superlattices, we move to a system where the exchange is considerably weaker compared to magneto-elastic

energies, which have already been shown to be significantly perturbed in the $[Dy_x|Y_y]$ superlattices [1]. This enhances the possibility of controlling the magnetic structure, and further understanding the details of the magneto-elasticity of Er.

The samples for this study were grown at the University of Illinois [1], by depositing 120 - 200 alternating layers of Er and then Y onto 1.6 cm^2 $(11\bar{2}0)$ sapphire following buffer layers of approximately 1000 Å of Nb and 300 Å Y, so that the hcp c-axis of the superlattice is perpendicular to the growth plane. They have been shown to be good single crystals (mosaic $\approx$ 30′) with sharp interfaces (only several atomic planes wide) between the layers.

The neutron diffraction measurements employed 13.5 meV neutrons with resolution of 0.021 $Å^{-1}$ along Q and 0.008 $Å^{-1}$ transverse to Q when Q is near 2.0 $Å^{-1}$.

Neutron diffraction scans along c* are shown in figure 1 for $[Er_{32}|Y_{21}]$. Since the neutron cross-section selects only magnetic scattering from moments perpendicular to Q, the scans through (002) measure only the basal-plane components, while the scans marked (101) select predominantly the c-axis components.

The fact that no additional magnetic intensity appears on the (101) down to 5 K, indicates that the ferromagnetic phase transition found in bulk Er at 18 K is suppressed. This same effect was found in the Dy-Y superlattices, and here is the first hint that the magneto-elastic energy is significantly different than in bulk Er.

The appearance of magnetic sidebands of the (101) indicates linear-spin-density-wave ordering (LSDW) of the c-axis components at $T_N \approx 78 \pm 1$ K. This 7% reduction from the 84 K value of bulk Er is typical of superlattices [1,2], and may be due to interfacial alloying and/or other finite size effects. That the difference is not great indicates that the exchange interactions are very near bulk values. This is also confirmed by our determination of the turn angle between successive Er basal planes.

Also below 35 K, magnetic intensity appears about the 002 Bragg peaks, as the basal-plane components of the moments order. These ordering temperatures are almost a factor of two lower than in bulk Er, and so must be strongly influenced by magneto-elastic energetics. In fact, the basal-plane ordering in bulk Er is near the 54 K lock-in transition to the $\omega = 2\pi/7$ state, where the temperature derivative of ω first changes sign. The low temperature

saturation moment in all three superlattices is about 8.5 μ_B, suggesting some residual disorder of the spins. This is consistent with a shorter coherence length for the basal-plane components than the c-axis components.

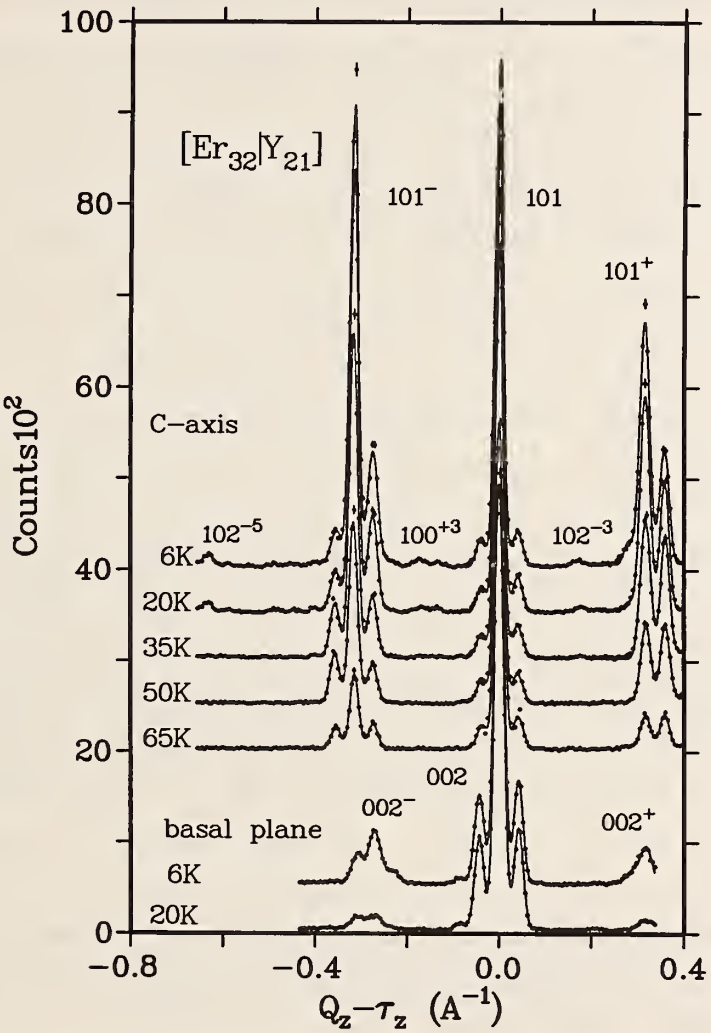

Figure 1. Neutron diffraction scans along the c* direction, through (101) and (002) for $[Er_{32}|Y_{21}]$ show the development of a linear-spin-density-wave state with moments along the c-axis, which then "squares-up" upon lowering the temperature (indicated by the appearance of higher order harmonics). The coherence length for the c-axis components is estimated as 3 bilayers. Below about 30 K the basal-plane components order, as indicated by the satellites of (002). This ordering has a shorter coherence range (about 1.5 bilayers) and a different turn angle than the c-axis components.

We have fit our diffraction data to obtain ω in the separate Er and Y layers. These values are plotted in figure 2 along with ω for bulk Er [4]. The magneto-elastic terms in the Hamiltonian favor smaller ω, and are responsible in bulk Er for the turn down below 54 K, as well as the ferromagnetic phase transition below 18 K. None of these features are present in the superlattices, which all show ω clamped at its high temperature value, with only a slight decrease (about 1°) from 50 K to 5 K. Rough calculation of the driving energy for ferromagnetism shows that it is reduced from 2.2 K/atom for bulk Er to about 1.4 K/atom in the superlattices. One difficulty with these calculations, not heretofore addressed, is the contribution of the c-axis modulated magneto-elastic waves observed by Gibbs et al. [4]. It would be interesting to see if such waves exist in the superlattices.

The ω in the Y layers as given in figure 2 are seen to be the approximate 50° found in the other superlattices and dilute Y alloys [1,2]. In fact, the data suggest that the $2\pi/7$ lock-in state is stable over an extended temperature range. In addition, our fits give total phase shifts across the Y layers which cannot be explained as simple multiples of π. As in the Dy-Y superlattices, the coupling across the Y is not scalar.

Finally it is obvious from examining the raw data that the basal-plane and c-axis ω are not equivalent at low temperatures in the superlattices, since the centroids of the magnetic scattering are at different Q values. This is born out by our data analysis. We again invoke the strength of the magneto-elastic energies compared to the exchange as an explanation for this effect. It can be argued that exchange alone would tend to produce the same ω for basal-plane and c-axis components. In the superlattice the c-axis ω may be more strongly clamped than the basal-plane ω.

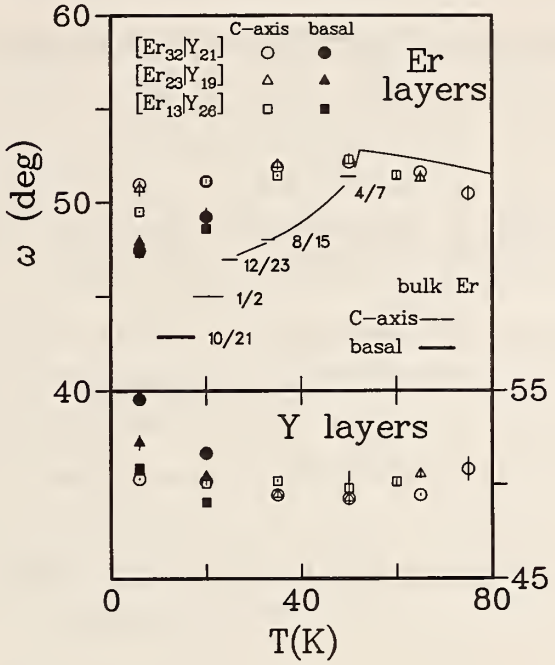

Figure 2. The turn angles in the Er and Y layers are shown and compared to bulk Er. In the Er layers ω is "clamped" near the high-temperature lock-in value of bulk Er ($2\pi/7$), although it is difficult to ascertain if a lock-in occurs in the superlattices. The low temperature basal-plane ω appears to be less "clamped" than the c-axis ω. The ω in the Y layers is near the 50° found in other superlattices and dilute Y alloys. The total phase shift across the Y layers is not a simple multiple of π.

References

[1] J. J. Rhyne, R. W. Erwin, J. Borchers, Shantnau Sinha, M. B. Salamon, R. Du, and C. P. Flynn, J. Appl. Phys. 61, 4043 (1987); R. W. Erwin, J. J. Rhyne, M. B. Salamon, J. Borchers, Shantnau Sinha, R. Du, J. E. Cunningham, and C. P. Flynn, Phys. Rev. B35, 6808 (1987).

[2] J. Kwo, E. M. Gyorgy, D. B. McWhan, M. Hong, F. J. DiSalvo, C. Vettier, and J. E. Bower, Phys. Rev. Lett. 55, 1402 (1985); C. F. Majkrzak, J. W. Cable, J. Kwo, M. Hong, D. B. McWhan, Y. Yafet, J. V. Waszczak, and C. Vettier, Phys. Rev. Lett. 56, 2700 (1986).

[3] A. J. Freeman, in Magnetic Properties of Rare-Earth Metals, edited by R. J. Elliot, Plenum, New York, (1972), p. 314, and ref. therein.

[4] D. Gibbs, J. Bohr, J. D. Axe, D. E. Moncton, and K. L. D'Amico, Phys. Rev. B34, 8182 (1986).

FIELD DEPENDENCE OF THE STRUCTURE OF Er|Y SUPERLATTICES

R. W. Erwin and J. J. Rhyne

and

J. Borchers, M. B. Salamon, R. Du, and C. P. Flynn
(University of Illinois, Urbana, IL)

We have previously obtained the structure in zero field of Er|Y single crystal superlattices grown by molecular-beam-epitaxy techniques [1]. Sapphire substrates were used with buffer layers of approximately 1000 Å of Nb and 300 Å of Y, so that the hcp c-axis of the superlattice is perpendicular to the growth planes. We found long-range order of the c-axis Ising-like Er moments extending through the "magnetically dead" Y layers as was found for the X-Y superlattices Dy|Y [2]. The Er layer turn angles for the linear-spin-density-wave are nearly temperature independent at $\omega \approx 2\pi/7$, the high temperature commensurate lock-in value in bulk Er [3], although we could not claim with certainty that the lock-in state is stabilized. The ferromagnetic transition is completely suppressed, because the magneto-elastic energy density is considerably reduced in the superlattice compared to the bulk.

We have now studied the magnetic structure of these materials in an applied field along the c-axis by neutron diffraction and SQUID magnetometry. The bulk magnetization is plotted vs. internal field for two of the superlattices in figure 1. The low-field ($\leq$ 15 kOe) low-temperature ($\leq$ 35 K) states have a magnetization of $\approx$ 1/7 of the saturation value. The $[Er_{13}|Y_{26}]$ superlattice shows evidence of an intermediate fan state.

In figure 2 we show neutron diffraction data for $[Er_{13}|Y_{26}]$. The overlap of superlattice peaks results from the poor resolution for scans directed out of the scattering plane. At T = 10 K (fig. 2a) the application of a 10 kOe field (7 kOe internal) slightly shifts the centroid of the scattering for the magnetic superlattice peaks on each side of τ = (110). This indicates that the Er layer turn angle increases. Our data analysis shows that the field-induced state has the commensurate value $\omega = 2\pi/7$ (51.4°), which is shifted from the zero-field value (50.3° in agreement with our previous analysis). The original analysis [1] of the zero-field low-temperature data suggested that $\omega = 2\pi/7$ is the stable value of the turn angle. The absence of any shift in q at 10 kOe (a slight broadening is evident) confirms this as the stable state.

At 40 K (fig. 2b), the zero-field ω has the stable value $2\pi/7$ and is not shifted by a 10 kOe field. Higher fields strongly shift the magnetic scattering to smaller q, indicating the development of the linear fan state. The average turn angle for the Er layers in this state is $\approx 35°$, which is much lower than found in any bulk Er state. Of the superlattices we have studied this is the one with the smallest ratio of Er to Y, and thus has the least magneto-elastic energy density. This is consistent with the theories of fan states where large anisotropy or magneto-elastic energies favor a direct transition from the modulated to ferromagnetic states [4]. These theories do not yet take into account the perturbation of the turn angle by magneto-elastic effects in the fan state.

Finally, the zero-field remanence state returns to the zero-field-cooled value of ω, but with a reduced coherence length.

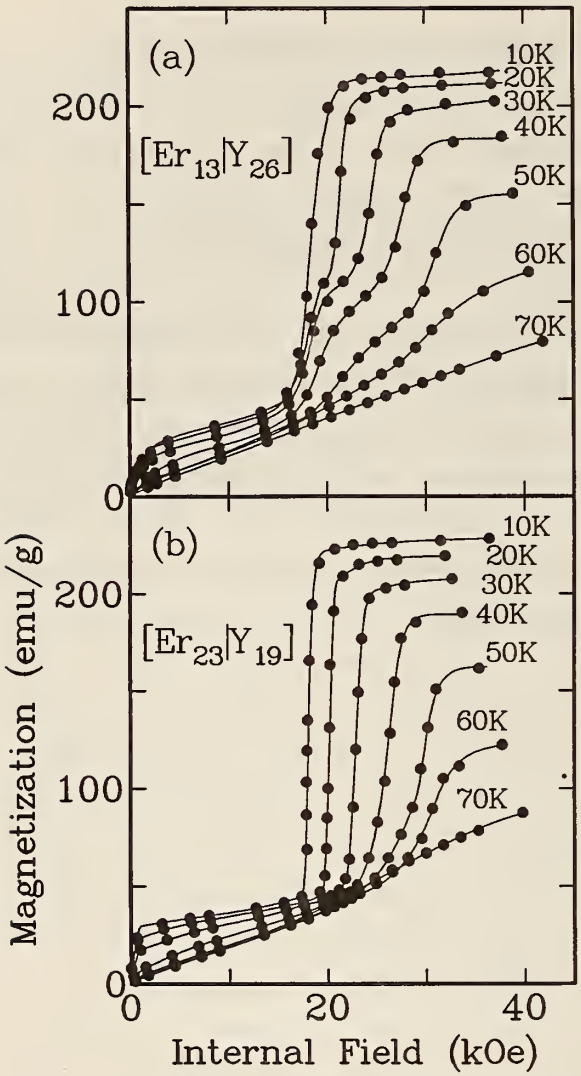

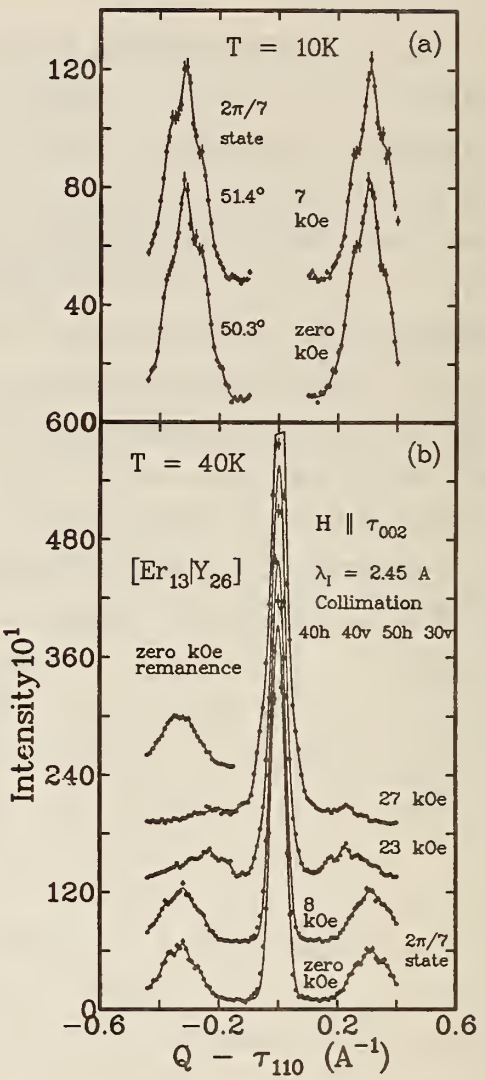

Figure 1. (left) Magnetization vs. internal field along the c-axis for the (a) $[Er_{13}|Y_{26}]$ and (b) $[Er_{23}|Y_{19}]$ superlattices. The low-field low-temperature states have a magnetization of approximately 1/7 of the saturation value corresponding to the net c-axis moment of the $2\pi/7$ lock-in state. The $[Er_{13}|Y_{26}]$ superlattice shows evidence of an intermediate fan state.

Figure 2. (right) (a) Neutron diffraction scans along (11ξ) for $[Er_{13}|Y_{26}]$ at T = 10 K with the applied field along the c-axis. The calculated Er turn angle shifts from 50.3° to the commensurate value, $2\pi/7 = 51.4°$, with little or no loss of coherence when the field is raised from zero to 10 kOe (7 kOe internal). (b) At T = 40 K there is no shift in the Er layer turn angle as the field is raised, indicating that $\omega = 2\pi/7$ is the zero-field state. The sharply reduced q of the peaks ($\omega \approx 35°$) at 23 and 27 kOe internal field indicates the development of fan states corresponding to the magnetization plateaus in figure 1a.

References

[1] R. W. Erwin, J. J. Rhyne, J. Borchers, M. B. Salamon, R. Du, and C. P. Flynn, J. Appl. Phys. 63 3461 (1988); J. Borchers, M. B. Salamon, R. Du, C. P. Flynn, J. J. Rhyne, and R. W. Erwin, ibid. page 3458.

[2] R. W. Erwin, J. J. Rhyne, M. B. Salamon, J. Borchers, Shantanu Sinha, R. Du, J. E. Cunningham and C. P. Flynn, Phys. Rev. B35 6808 (1987).

[3] D. Gibbs, J. Bohr, J. D. Axe, D. E. Moncton, and K. L. D'Amico, Phys. Rev. B34 8182 (1986).

[4] Y. Kitano and T. Nagamiya, Progress Theoret. Phys. 31, 1 (1964).

MAGNETIC STRUCTURE OF CUBIC $Tb_{0.3}Y_{0.7}Ag$

J. A. Gotaas

M. R. Said and J. S. Kouvel
(University of Illinois, Chicago, IL)

and

T. O. Brun
(Argonne National Laboratory, Argonnne, IL)

The CsCl-type compounds RAg (R = rare earth) exhibit a fine balance between ferromagnetism and antiferromagnetism of various forms. The dilution of the rare earth by the chemically similar nonmagnetic yttrium should certainly lead to reductions in ordering temperatures, perhaps to modifications in the magnetic structures, and ultimately to spin-glass behavior. Magnetization studies of the series $Tb_xY_{1-x}Ag$ and $Gd_xY_{1-x}Ag$ [1] have shown that for $x < .5$, thermoremanences appear along with associated time dependences which are indicative of spin-glass behavior. We have carried out neutron diffraction measurements to clarify the nature of the magnetic state in these systems, starting with a polycrystalline sample of $Tb_{0.3}Y_{0.7}Ag$, which exhibited the largest remanence effects.

The neutron diffraction was performed on BT-6 and BT-9, using a pyrolytic graphite (PG) monochromator at 2.46 Å and a PG analyzer and filter to improve the signal to noise ratio of the data. A diffraction pattern taken at 4 K showed a set of additional peaks appearing at distinct positions from the nuclear peaks observed at 60 K. These could be associated with the set of indices $(h + 1/2, k + 1/2, \ell)$. This type of antiferromagnetic structure has

been observed in other RAg compounds, including TbAg. The ($\pi\pi$0) structure consists of moments ferromagnetically aligned in [110] planes, with neighboring planes antiferromagnetically coupled; the resulting magnetic lattice has tetragonal symmetry with a doubling of the cell axes in two directions. The structure observed here is a more complex variant of the ($\pi\pi$0) structure. Figure 1 shows the first peak in the diffraction pattern, in which two reasonably sharp peaks are superimposed on a broad peak, approximately centered on the (1/2, 1/2, 0) position. The broad central peak corresponds to the ($\pi\pi$0) spin structure and the pair of satellites represent an incommensurate modulation of the basic antiferromagnetic structure. Such a modulated structure has been observed in HoAg, TmAg, ErAg and DyAg.

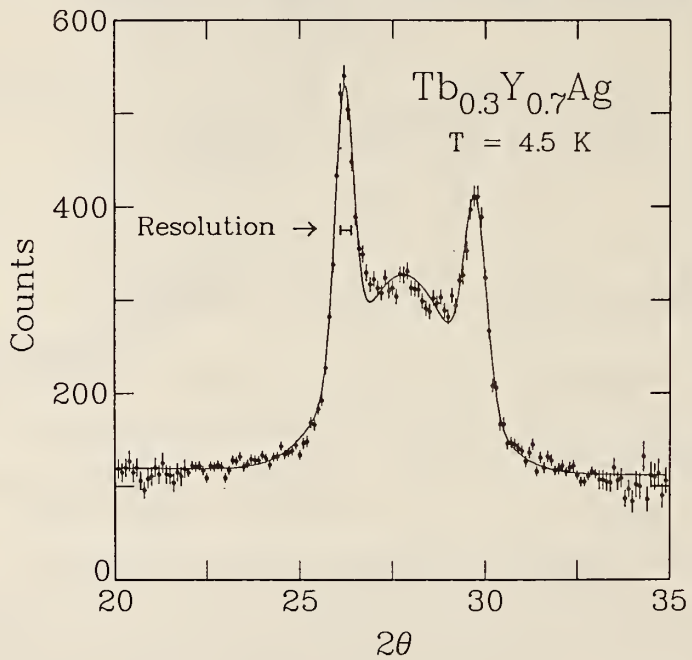

Figure 1. Multiple peak structure observed at (1/2, 1/2, 0) position at T = 4.5 K. Instrumental resolution is indicated.

The magnetic peaks are not resolution limited, indicating that the correlation lengths are finite even at 4 K. The central ($\pi\pi$0) peak is very broad, indicating a correlation range of only ~ 42 Å, which is approximately 12 chemical unit cells. The satellite peaks, while considerably sharper, still possess an intrinsic width corresponding to a correlation length of ~ 290 Å. Assuming that the structures are similar to those found in the related RAg compounds, the diffraction pattern is consistent with the

coexistence of a short-range ordered ($\pi\pi$0)-type structure and an incommensurate modulated structure of the type found in HoAg. In this structure, the individual moments are parallel to the unique c-axis; the propagation vector for the modulated state is directed along the cube edges, allowing for a set of domains (h $\pm$ δ, k, ℓ), (h, k $\pm$ δ, ℓ), etc. The separation of the satellites from the (1/2, 1/2, 0) position indicates that modulation wave vector has a magnitude of 0.059(2π/a), corresponding to about 17 chemical unit cells.

Figure 2 shows the temperature dependence of the integrated intensity of the central peak as well as the sum of the integrated intensities of the satellites. As indicated in the figure, there is still measurable intensity at 37.5 K, persisting above the nominal transition derived from magnetization measurements. As the peaks have broadened still further, it is difficult to distinguish the satellite positions and the integrated intensities; some scattering remains up to 45 K. Clearly most of the magnetic order develops below approximately ~ 36 K, in agreement with the bulk measurements. Although the breadth of the peaks makes the precise determination of the peak positions difficult, the data are consistent with a temperature dependent modulation wavelength, as is found in HoAg and TmAg.

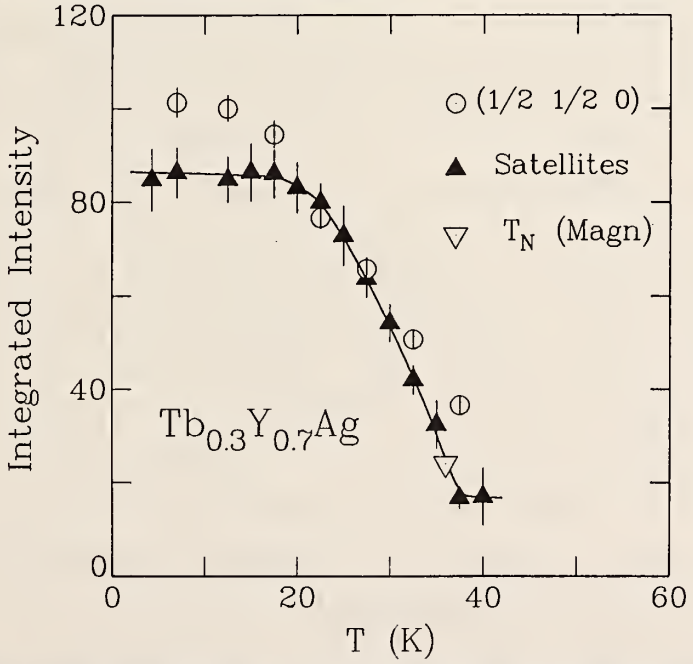

Figure 2. Temperature dependence of the integrated intensities of the central (1/2, 1/2, 0) peak and the sum of the satellite peaks.

References

[1] M. R. Said, J. S. Kouvel, and T. O. Brun, J. Appl. Phys. 63, 4340 (1988).

MAGNETIC STRUCTURE OF $Y_{0.97}Er_{0.03}$

J. A. Gotaas and J. J. Rhyne

L. E. Wenger
(Wayne State University, Detroit, MI)

and

J. A. Mydosh
(Rijks-Universiteit Leiden, 2300 RA Leiden, The Netherlands)

The nature of the magnetic state in dilute alloys remains a problem of considerable interest, with the rare-earth elements substituted into yttrium forming an interesting series of systems with varying exchange interactions and single-ion anisotropies. It has been shown that long range order persists down to rare-earth concentrations less than 2-5%, depending on the particular element. We have continued a systematic study of these systems by investigating $Y_{0.97}Er_{0.03}$. Measurements were performed on a single-crystal sample oriented with the a- and c-axes in the scattering plane, using BT-6 and BT-9. The sample was mounted in a pumped ^{3}He cryostat which could be cooled to a minimum temperature of 0.3 K.

The crystal field anisotropies in both bulk erbium and the dilute yttrium alloys are such that the erbium moments lie predominantly along the c-axis. The spin orientation factor in the neutron scattering cross-section then implies that the satellites resulting from an incommensurate modulated structure will occur only around the allowed nuclear peaks in the basal plane [e.g. (110)], displaced along the c* reciprocal axis by $(2\pi/c)\delta$, where δ is the modulation wave vector of the ordered phase. Such magnetic peaks were observed displaced from the (110) nuclear peaks, with δ = 0.275. The scattering at the satellite position displayed two components: a sharp component that appeared at 3.25 K and was resolution-limited in width, implying true long range order, and a secondary weaker component (approximately 5% of the main peak at 0.3 K) which persisted to temperatures up to ~10 K, with a diffraction width corresponding to a finite correlation length of only about 80 Å. The presence of precursor critical scattering is typical, but the persistence of the scattering down to 0.3 K is rather unusual. The net magnetic intensity, which is proportional to the square of the magnetic order parameter, is displayed in figure 1, where it is denoted by (1, 1, 0.275). No differences were observed in the magnetic intensities on cooling

and warming. The intensity shown contains the contribution of both components of the scattering, since it is experimentally difficult to uniquely separate them.

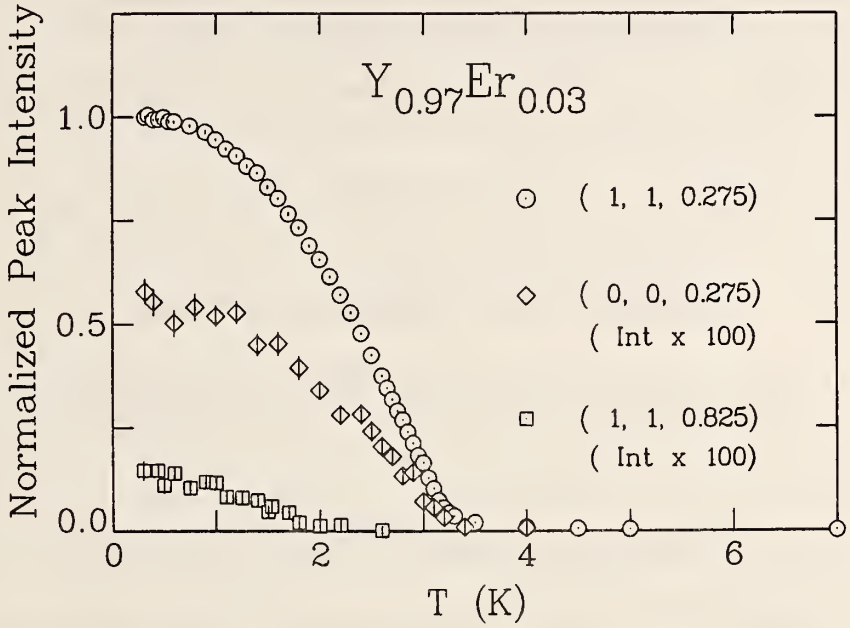

Figure 1. Normalized magnetic peak intensity versus temperature for (110^{+}) [⊙], (000^{+}) [ ] and (110^{3+}) [□] satellites. Note that the latter two intensities are scaled up by a factor of 100.

A careful search for c-axis satellites revealed the presence of an (000^{+}) peak with an intensity only 0.6% of the main (110^{+}) satellite, indicating the existence of a small basal-plane component in the ordered state. This component shows the same temperature dependence (displayed as (0, 0, 0.275) in fig. 1) as the main c-axis structure and represents only about 0.1 μ_B. The absence of significant basal-plane anisotropy suggests that this basal plane moment forms a helical component, which would make the structure similar to that observed in pure erbium between 20 and 52 K.

A careful search for higher harmonics of the c-axis structure was carried out, since general thermodynamic arguments predict that the disorder in the moment at every site must vanish as $T \rightarrow 0$. A peak corresponding to a third-harmonic component was found to develop at temperatures below approximately 2 K, with an intensity at 0.3 K of only 0.15% of the primary satellite, indicating that the sinusoidal structure begins to square up. The intensity of this peak is shown in figure 1 as (1, 1, 0.825).

MAGNETIC RARE-EARTH SUPERLATTICES

C. F. Majkrzak

D. Gibbs, P. Böni, and A. I. Goldman
(Brookhaven National Laboratory, Upton, NY)

J. Kwo, M. Hong, T. C. Hsieh, R. M. Fleming, D. B. McWhan, and Y. Yafet
(AT&T Bell Laboratories, Murray Hill, NJ)

J. W. Cable
(Oak Ridge National Laboratory, Oak Ridge, TN)

J. Bohr
(Risφ National Laboratory, Denmark)

H. Grimm
(IFF, Kernforschungsanlage, Jülich, West Germany)

and

C. L. Chien
(Johns Hopkins University, Baltimore, MD)

Recent advances in molecular-beam epitaxy (MBE) techniques have made it possible to grow single-crystal, rare-earth (RE) superlattices with a high degree of perfection and limited interdiffusion [1-3]. Magnetic layers consisting of a discrete number of atomic planes can be deposited alternately with nonmagnetic or other magnetic layers of a given thickness. The effects of reduced dimensionality on the magnetic ground state and corresponding critical behavior can be investigated. Because the magnetic RE moments interact through long-range, indirect exchange, a modulation of the magnetic properties in certain synthetically layered RE structures might also be expected. Furthermore, since the detailed, microscopic magnetic structures of the RE metals result from the competition between the isotopic indirect-exchange and the anisotropic crystal-field and magnetoelastic interactions, the study of synthetic RE superlattices with a tailored composition and/or strain profile can, in principle, give valuable information about such phenomena as the lock-in transitions from incommensurate to commensurate phases recently described by a spin-slip model [4-6].

The periodicity of the multilayer structure makes it possible to study its magnetic state by diffraction and polarized neutrons are especially useful in determining the more-complicated, noncollinear magnetic structures which can occur in some of the RE superlattices. The magnetic structures of several

single-crystal, magnetic RE superlattice systems grown by MBE are currently being studied by neutron diffraction. In particular, investigations of long-range magnetic order and interlayer interactions in Gd-Y, Dy-Y, and Ho-Y periodic superlattices have already shown that the magnetic structure is propagated coherently across the intervening non-magnetic Y layers [7]. In the Gd-Y system, an antiphase domain structure develops for certain Y layer spacings, whereas modified helical moment configurations are found to occur in the other systems. In Gd-Dy superlattices, a number of different magnetic structures are observed, some of which are commensurate and others which are incommensurate with the chemical superlattice wavelength. Theoretical interaction mechanisms have recently been proposed to account for the magnetic states of these novel materials [8].

Interlayer interaction studies of the Gd-Y superlattice system involving more-exotic layered structures, specifically arrangements where two different Y layer thicknesses corresponding to ferromagnetic and antiferromagnetic interactions between Gd layers are propagated in a Fibonacci sequence, are also in progress. The expectation is that something can be learned about the long-range order, or the lack thereof, in such a quasiperiodic heterostructure with competing interactions.

An attempt to measure the magnetization profile as a function of temperature in a ferromagnetic $[Gd_{10}\text{-}Y_{20}]_{100}$ sample by neutron diffraction has also been made in order to study the effect of reduced dimensionality and interface anisotropy on the magnetic critical behavior. However, it turns out that it is necessary to determine the chemical compositional and strain modulation profiles very accurately. In this particular case the problem is complicated by a strongly temperature-dependent strain profile and more-comprehensive measurements must be performed before any conclusions can be made regarding critical point exponents.

These RE superlattice studies have only just begun and much work remains to be done. Nevertheless, new and interesting results have already been obtained [9].

References

[1] J. Kwo, D. B. McWhan, M. Hong, E. M. Gyorgy, L. C. Feldman, and J. E. Cunningham, in Layered Structures, Epitaxy and Interfaces, Matls. Res. Soc. Symp. Proc. No. 37, p. 509, edited by J. H. Gibson and L. R. Dawson, Materials Research Society, Pittsburgh, PA (1985).

[2] S. Sinha, J. E. Cunningham, R. Du, M. B. Salamon, and C. P. Flynn, in Proceedings of the International Conference on Magnetism, edited by J. J. Rhyne, B. R. Cooper, D. L. Huber, N. C. Koon, and R. C. O'Handley, North-Holland, Amsterdam (1985).

[3] J. Kwo, E. M. Gyorgy, D. B. McWhan, M. Hong, F. J. DiSalvo, C. Vettier, and J. E. Bower, Phys. Rev. Lett. 55, 1402 (1985).

[4] D. Gibbs, D. E. Moncton, K. L. D'Amico, J. Bohr, and B. H. Grier, Phys. Rev. Lett. 55, 234 (1985).

[5] J. Bohr, D. Gibbs, D. E. Moncton, and K. L. D'Amico, Physica 140A, 349 (1986).

[6] D. Gibbs, J. Bohr, J. D. Axe, D. E. Moncton, and K. L. D'Amico, Phys. Rev. B34, 8182 (1986).

[7] See, for example, the review article by C. F. Majkrzak, D. Gibbs, P. Böni, A. I. Goldman, J. Kwo, M. Hong, T. C.Hsieh, R. M. Fleming, D. B. McWhan, Y. Yafet, J. W. Cable, J. Bohr, H. Grimm, and C. L. Chien, J. Appl. Phys. 63, 3447 (1988) and relevant references therein.

[8] See, for example, the review article by Y. Yafet, J. Kwo, M. Hong, C. F. Majkrzak, and T. O'Brien, J. Appl. Phys. 63, 3453 (1988).

[9] C. F. Majkrzak, J. W. Cable, J. Kwo, M. Hong, D. B. McWhan, Y. Yafet, J. V. Waszczak, H. Grimm, and C. Vettier, J. Appl. Phys. 61, 4055 (1987).

ANTIFERROMAGNETIC STRUCTURE AND CRYSTAL FIELD SPLITTINGS IN THE CUBIC HEUSLER ALLOYS $HoPd_2Sn$ AND $ErPd_2Sn$

W.-H. Li, J. W. Lynn, and H. B. Stanley
(University of Maryland and the National Bureau of Standards)

T. J. Udovic

and

R. N. Shelton and P. Klavins
(University of California, Davis, CA)

The Heusler alloy series of general composition RPd_2Sn, with R = Sc, Y, and the heavier rare earths from Tb to Lu, crystallize into the cubic Cu_2MnAl-type structure (Fm3m), with the rare-earth ions occupying sites of cubic point symmetry. In particular, the coexistence of antiferromagnetic order and superconductivity has been reported for both $YbPd_2Sn$ [1] and $ErPd_2Sn$ [2]. This new class of systems possesses two features which make them particularly interesting candidates for study. First, they contain a substantially higher

percentage of magnetic ions in comparison to the RRh_4B_4 [3] and RMo_6S_8 [4] materials. Second, there is no clear isolation of the magnetic and superconducting sublattices. The nearest-neighbor distance between magnetic ions, for example, is substantially smaller than for the RRh_4B_4 and RMo_6S_8 systems, which leads to a larger exchange interaction between rare-earth ions themselves, and the rare-earth ions and conduction (4d) electron spins. In the present paper we report diffraction and inelastic neutron scattering measurements which have been used to determine the magnetic structure and the crystal-field splittings.

Measurements were carried out on the BT-9 triple-axis spectrometer as well as time-of-flight (TOF) spectrometer. Powder diffraction patterns were taken with a neutron incident energy fixed at 14.8 meV (λ = 2.351 Å) using pyrolytic graphite (002) as monochromator, and no analyzer. A pyrolytic graphite filter was used to reduce higher order wavelength contaminations. Horizontal collimations of 40′, 25′, and 25′ (FWHM) before and after the monochromator, and after the sample, were employed. In the study of the crystal field excitations, on the other hand, the TOF technique is ideally suited since the excitations are dispersionless. The data collected for many detectors may be summed to improve the statistical accuracy, while the momentum dependence of the intensities may also be readily extracted from the experimental data. The 64 detectors of the TOF machine were placed to cover scattering angles over a range from 6.3 - 114.5°. Neutrons with an incident energy of E_i = 13.8 meV (λ = 2.435 Å) were used for these measurements.

To study the nature of the long-range magnetic order which developed at low temperatures, sets of complete diffraction pattern were taken at various temperatures. To extract the magnetic component, we employed the subtraction technique [5], where data at high temperatures are subtracted point by point from the data in the ordered phase. The magnetic diffraction pattern thus obtained is shown in figure 1 for $HoPd_2Sn$. Four magnetic Bragg peaks are evident, and may be indexed as {1/2,1/2,1/2}, {1/2,1/2,3/2}, {1/2,3/2,3/2}, and {1/2,1/2,5/2} + {3/2,3/2,3/2} reflections of an fcc type-II antiferromagnet. This sequence of half-integral reflections shows that the magnetic unit cell doubles along all three directions with respect to the chemical unit cell. The basic is the same as that for $ErPd_2Sn$ [6].

The temperature dependence of the {1/2,1/2,1/2} peak intensity is shown in figure 2, where a Neel temperature of $T_N \approx 5$ K is indicated for this

system. Comparing the integrated intensity of the {1/2,1/2,1/2} reflection with the {004} nuclear peak yields an ordered magnetic moment of 5.81(8) μ_B at T = 0.34 K. However, note that there is substantial smearing of the transition. In addition, the widths of the Bragg peaks are significantly larger than instrumental resolution at all temperatures, which we interpret as indicating substantial intrinsic disorder. The nuclear peaks, in contrast, are resolution limited in width.

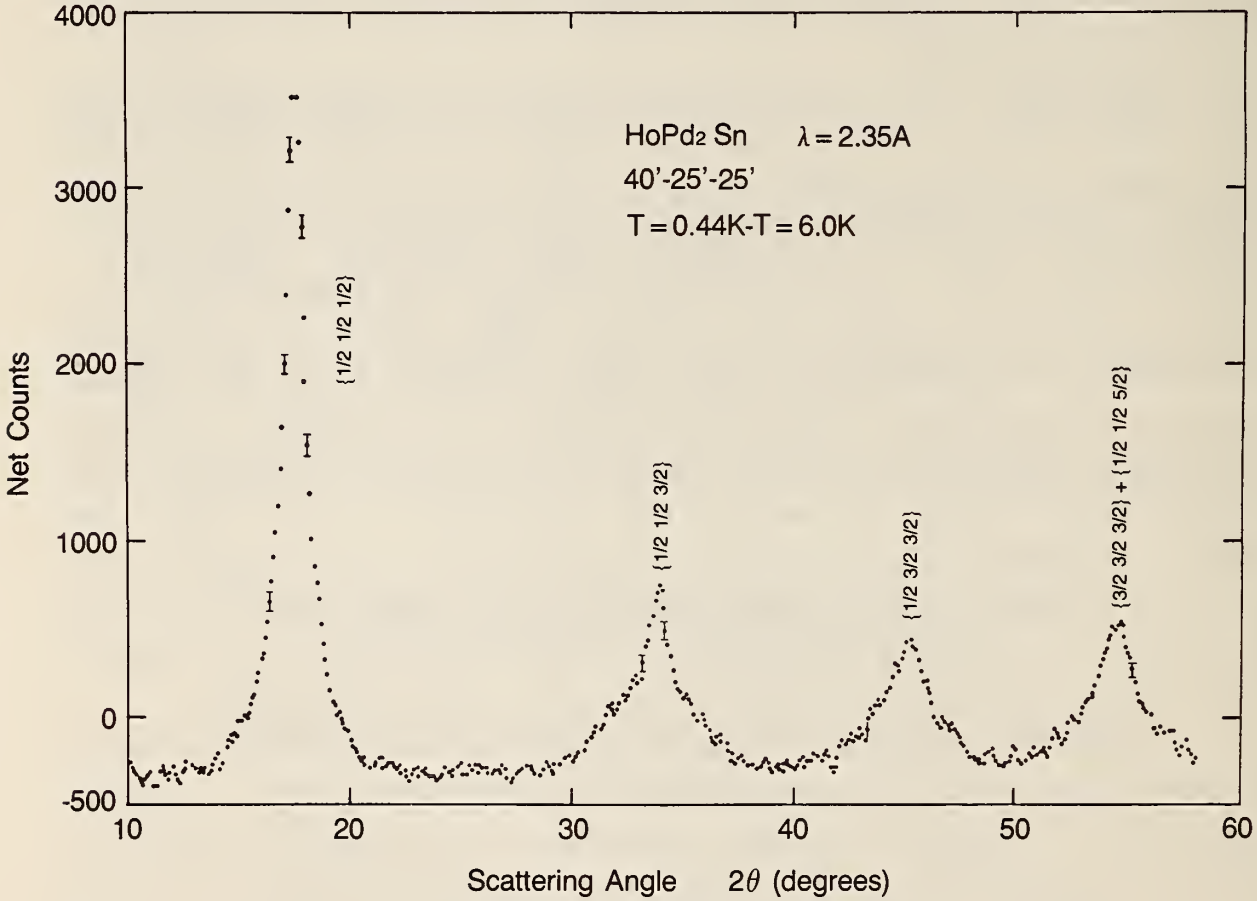

Figure 1. Magnetic powder diffraction pattern for $HoPd_2Sn$, obtained by subtracting the data measured at T = 6 K from the data at T = 0.44 K.

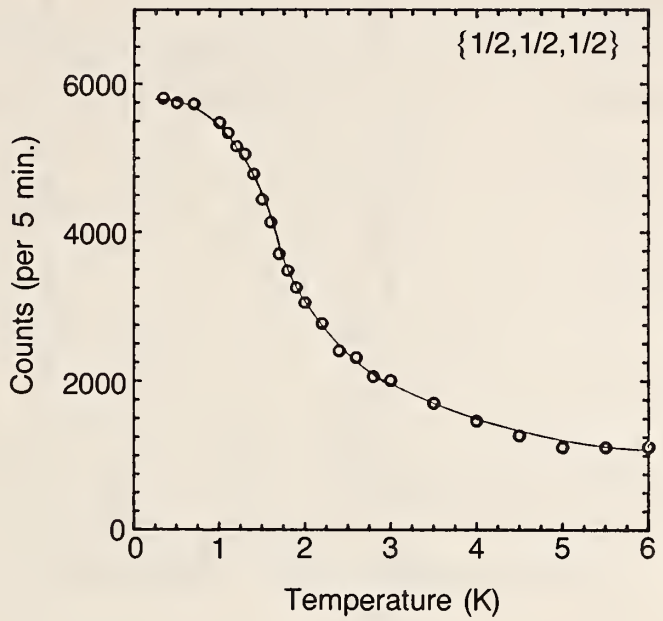

Figure 2. Temperature dependence of the {1/2,1/2,1/2} antiferromagnetic peak intensity. The rounding of the transition at T_N = 5 K is due to either critical fluctuations or a distribution of T_N's. The solid curve is a guide to the eye.

Measurements of the crystal field excitations on the $HoPd_2Sn$ powder sample were taken at six different temperatures in the range from 0.44 to 40 K using the TOF spectrometer. The scattering spectra that were obtained by summing over data acquired by 60 detectors at T = 0.44, 10.0, 23.0, and 40.0 K are shown in figure 3. At low temperatures, where the thermal energy is small in comparison with the excitation energies (e.g., T = 0.44 and 10.0 K), two dispersionless excitations are clearly observed, with energies of 3.52(1) and 6.65(1) meV at T = 10 K, and correspond to transitions out of the ground state. At elevated temperatures, when the higher energy crystal field levels become thermally populated (e.g., T = 23.0 and 40.0 K), one additional transition on the neutron energy gain side (E < 0) is also evident. This energy was determined to be -3.5(2) meV at T = 40.0 K. We noted that the intensities of the transitions at both 3.52 and 6.65 meV decreased with increasing temperature, as expected due to the depopulation of the crystal field ground state.

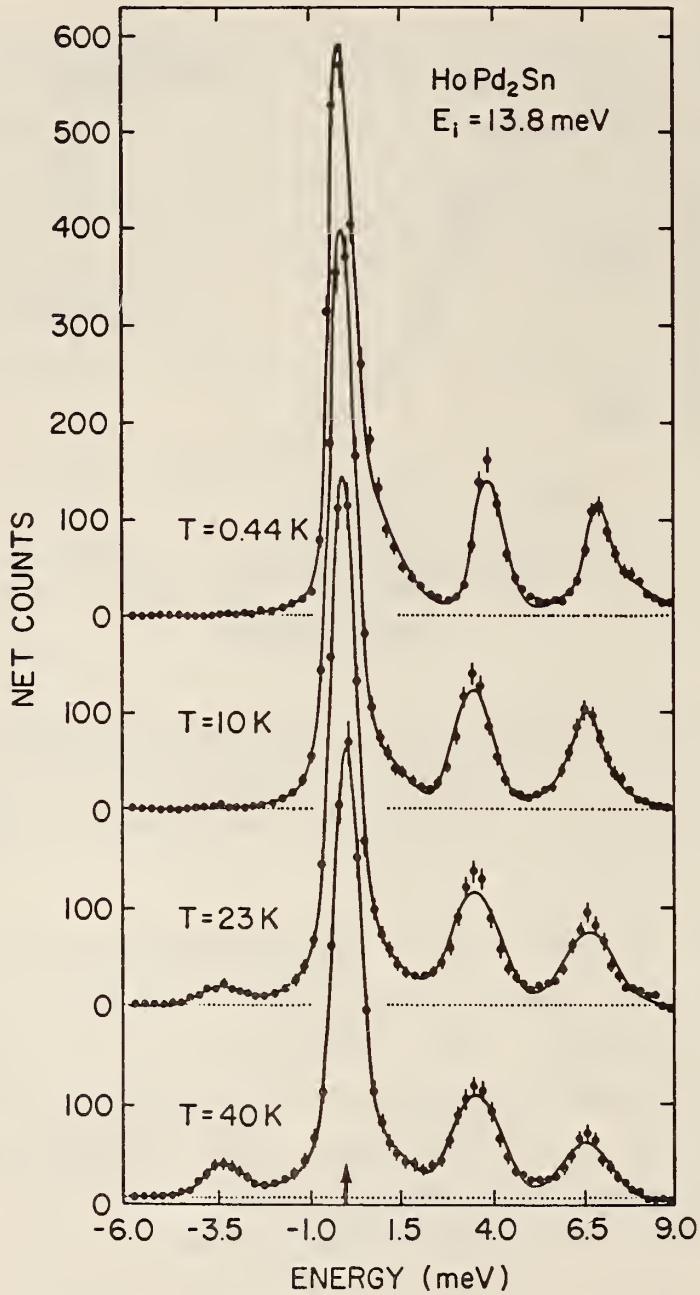

Figure 3. Elastic and inelastic scattering observed on powder $HoPd_2Sn$ with the time-of-flight technique. To improve the statistics, spectra shown were obtained by summing over data acquired on 60 detectors spanning a Q range from 0.48 to 3.85 Å . At T = 23.0 and 40.0 K, transitions from higher energy levels to low energy levels are also evident in neutron energy gain side (E < 0).

To determine the Lea, Leask, and Wolf [7] (LLW) crystal field parameters W and x, we start with the data obtained at T = 10 K. Utilizing the energies of the transitions from the ground state, there are nine sets of

data which are consistent with the experimental data. However, only one set yields the correct observed transition probabilities, and gave W = 0.0287(2) meV and x = 0.3248(8). These LLW parameters give a crystalline electric field (CEF) energy level sequence $\Gamma_5^{(1)}$ - $\Gamma_3^{(1)}$ - $\Gamma_4^{(1)}$ - $\Gamma_5^{(2)}$ - Γ_1 - $\Gamma_4^{(2)}$ - $\Gamma_3^{(2)}$, with an overall energy splitting of 17.56 meV at T = 10 K, and the magnetic triplet $\Gamma_5^{(1)}$ (Bethe's notation [8]) as the ground state. The temperature dependent data are completely consistent with this set of parameters. Similar measurements were also taken on the $ErPd_2Sn$ powder sample. Following the same analysis procedure as for the Ho systems, the crystal field parameters for this system were determined to be W = -0.0450(4) meV and x = 0.3022(6). These LLW parameters give a CEF energy level sequence $\Gamma_8^{(3)}$ - Γ_6 - $\Gamma_8^{(2)}$ - $\Gamma_8^{(1)}$ - Γ_7 with an overall energy splitting of 20.32 meV at T = 10 K, and the magnetic $\Gamma_8^{(3)}$ as the ground state.

Reference

[1] H. A. Kierstead, B. D. Dunlap, S. K. Malik, A. M. Umarji, and G. K. Shenoy, Phys. Rev. B32, 135 (1985).

[2] R. N. Shelton, L. S. Hausermann-Berg, M. J. Johnson, P. Klavins, and H. D. Yang, Phys. Rev. B34, 199 (1986).

[3] W. A. Fertig, D. C. Johnson, L. E. DeLong, R. W. McCallum, M. B. Maple, and B. T. Matthias, Phys. Rev. Lett. 38, 987 (1977).

[4] M. Ishikawa and O. Fischer, Solid State Commun. 23, 37 (1977).

[5] J. W. Lynn, J. A. Gotaas, R. N. Shelton, H. E. Horng, and C. J. Glinka, Phys. Rev. B31, 5756 (1985).

[6] H. R. Stanley, J. W. Lynn, R. N. Shelton, and P. Klavins, J. Appl. Phys. 61, 3371 (1987).

[7] K. R. Lea, M. J. M. Leask, and W. P. Wolf, J. Phys. Chem. Solids 23, 1381 (1962).

[8] H. Bethe, Ann. Phys. Opz. 3, 133 (1929).

ANTIFERROMAGNETIC ORDER OF THE Cu IN $RBa_2Cu_3O_{6+x}$

J. W. Lynn and W.-H. Li
(University of Maryland and National Bureau of Standards)

H. A. Mook and B. C. Sales
(Oak Ridge National Laboratory)

and

Z. Fisk
(Los Alamos National Laboratory)

The magnetic properties of the oxide superconductors have been of particular interest due to the intrinsic interest in magnetism as well as because of the possibility that the magnetic fluctuations are responsible for the superconducting pairing [1]. The $RBa_2CU_3O_{6+x}$ (R = rare earth) system orders antiferromagnetically [2-4] for small x ($x \leq 0.4$), where the system is tetragonal and nonsuperconducting. The magnetic structure consists [3,4] of a simple antiparallel arrangement of Cu spins both within the Cu-O planes as well as along the tetragonal c-axis, while the oxygen deficient Cu planes possess no ordered moment. The three-dimensional ordering can be quite high ($T_{N1}(x \approx 0) \sim 450$ K), indicating that the magnetic interaction energies are large. The 3-d transition temperature is also very sensitive [2] to the oxygen concentration x, decreasing rapidly with increasing x and approaching zero for $x \sim 0.4$.

A second magnetic phase transition has recently been observed [5,6], in which the oxygen-deficient Cu "chain" layers also order magnetically. We have been investigating the nature of this ordering and the effect of oxygen concentration on T_{N2} and have now obtained results on a number of single crystal specimens of $NdBa_2Cu_3O_{6+x}$. We find that at small x and low T the basic magnetic structure consists of a simple antiferromagnetic arrangement of spins both within the planes as well as along the c-axis. In particular, we find an unexpectedly large magnetic moment on the Cu chain sites. At intermediate temperatures the spin arrangement is a superposition of the high T and low T configurations, and is noncollinear in nature. We also find that both transition temperatures decrease with increasing x, with the lower transition T_{N2} being much more sensitive to x than the higher transition T_{N1}.

The neutron measurements were carried out at the National Bureau of Standards Research Reactor using standard triple-axis instruments.

Unpolarized diffraction data were collected with an incident energy of either 14.8 or 13.7 meV using a pyrolytic graphite PG(002) monochromator. Polarized neutron measurements were then taken to establish that the new peaks are magnetic in origin, and this procedure has been described previously [4]. The Bragg peak corresponding to the (1/2,1/2,3/2) reflection is shown in figure 1. Even though the Cu moments are quite small, the crystal is sufficiently large (~ 50 mg) to obtain an excellent signal-to-noise ratio. Polarized neutron measurements were employed to establish that the observed half-integral peaks are wholly magnetic in origin. The half-integral value for the third index demonstrates that the magnetic structure is doubled along all three crystallographic directions in comparison to the chemical unit cell. This contrasts with the spin configuration observed [3,4] in the higher temperature magnetic phase, where the ℓ index is integral and the magnetic and chemical unit cells are the same size along the tetragonal c-axis.

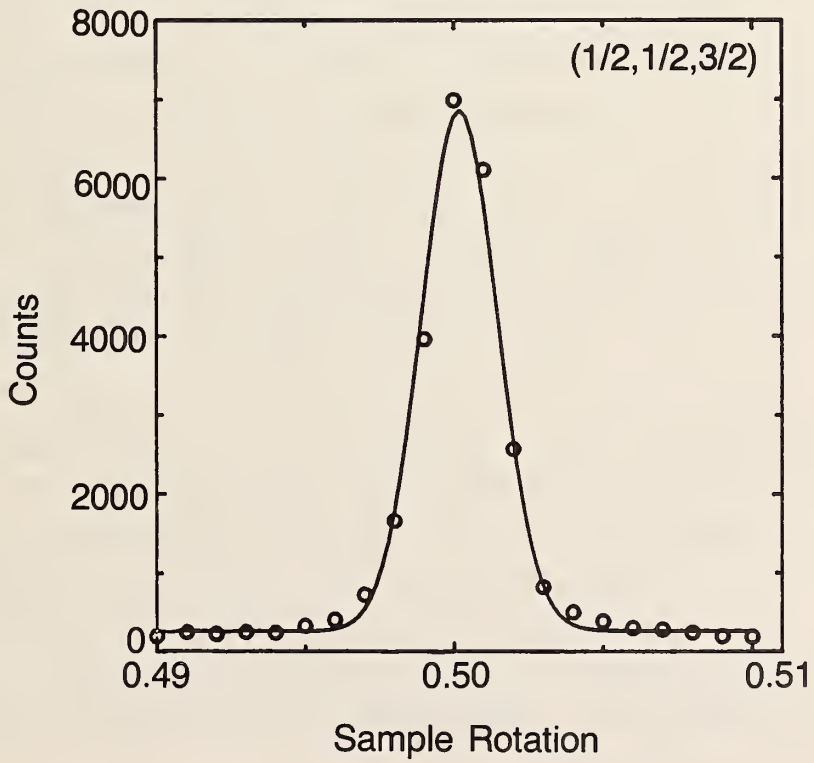

Figure 1. Observed magnetic Bragg peak for the (1/2,1/2,3/2) peak at low temperatures.

The temperature dependence of the (1/2,1/2,3/2) peak is shown in the bottom portion of figure 2. For this value of oxygen concentration ($x \approx 0.1$)

the lower phase transition occurs at $T_{N2} \approx 80$ K. The top portion of the figure compares the intensity of the whole-integral peaks such as (1/2,1/2,2), which are associated with the higher temperature phase transition; for the present sample $T_{N1} = 430$ K. There is a dramatic downturn in the intensity of the whole-integral reflections at low temperatures which is associated with the development of the intensities of the half-integral peaks. It is clear that the half-integral peaks dominant at low T, and hence they correspond to the ground state spin configuration of the system. The T = 0 structure consists of a simple collinear arrangement of spins, with the spin direction in the tetragonal plane. The nearest-neighbor spins within the Cu-O planes (designated M_P, for planes) are aligned antiparallel as they are in the high T phase. However, along the c-axis the oxygen-deficient Cu moment (designated M_C, for chains) is nonzero, and aligned antiparallel to the spins in the Cu-O layers. The doubling of the unit cell along the c-axis direction results because the sense of the spins is reversed in going from one chemical unit cell to another.

The values of the ordered moments we obtain at low temperatures are $M_P = 0.97 \pm 0.09\mu_B$ for the Cu-O planes (assumed equal), and $M_C = 0.46 \pm 0.06\mu_B$. This compares with $M_P \sim 0.6\mu_B$ for the maximum moment found [4] above T_{N2}. The essential difference between the two structures is of course the moment M_C. We remark that the conventional viewpoint for the $RBa_2Cu_3O_{6+x}$ class of materials is that the Cu valence in the Cu-O_2 planes is 2+, with an associated magnetic moment, while the Cu "chain" layers contain Cu^{1+} which is non-magnetic. The unexpectedly large ordered moment which we have observed on the Cu "chain" layers demonstrates that the Cu state is not an appropriate description of the electronic configuration of the "chain" layers in these materials. It is reasonable to assume that the chain-layer moment is a result of strong hybridization of the (band) electronic wave functions within this (as well as the Cu-O) Cu plane, rather than as a result of a perturbation caused by the remnant oxygen in the layer as has been suggested [6]. Further work on the magnetic properties of these systems as a function of concentration, magnetic field, and pressure is underway.

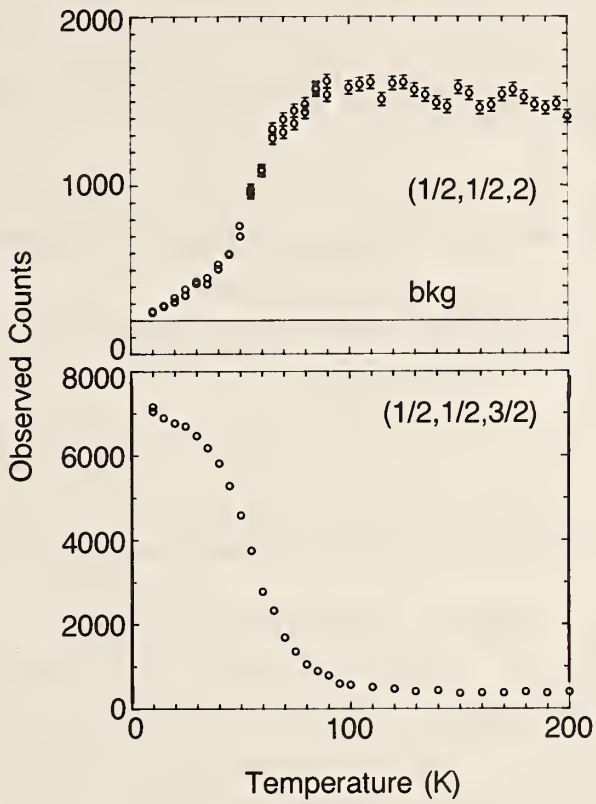

Figure 2. Magnetic intensities for the $NdBa_2Cu_3O_{6.1}$ crystal. The downturn of the intensity of the (1/2,1/2,2) peak coincides with the development of half-integral peaks such as the (1/2,1/2,3/2) peak shown the in bottom portion of the figure.

References

[1] See, for example, P. W. Anderson, Science 235, 1196 (1987). P. W. Anderson, G. Baskaran, Z. Zou, and T. Hsu, Phys. Rev. Lett. 58, 2790 (1987). V. J. Emery, Phys. Rev. Lett. 58, 2794 (1987). R. H. Parmenter, Phys. Rev. Lett. 59, 923 (1987). J. E. Hirsch, Phys. Rev. B35, 8726 (1987); Phys. Rev. Lett. 59, 228 (1987). J. R. Schrieffer, X.-G. Wen, and S.-C. Zhang, Phys. Rev. Lett. 60, 944 (1988).

[2] D. C. Johnston, S. K. Sinha, A. J. Jacobson and J. M. Newsam, Physica B (to be published, Interlaken Conference), and references therein. See also J. H. Brewer et al. Phys. Rev. Lett. 60, 1073 (1988).

[3] J. M. Tranquada, D. E. Cox, W. Kunnmann, H. Moudden, G. Shirane, M. Suenaga, P. Zolliker, D. Vaknin, S. K. Sinha, M. S. Alverez, A. J. Jacobson, and D. C. Johnston, Phys. Rev. Lett. 60, 156 (1988).

[4] W.-H. Li, J. W. Lynn, H. A. Mook and B. C. Sales, Bull. Am. Phys. Soc. 33, (1988). W.-H. Li, J. W. Lynn, H. A. Mook, B. C. Sales and Z. Fisk, Phys. Rev. B37, 9844 (1988).

[5] J. W. Lynn, W.-H. Li, H. A. Mook, B. C. Sales, and Z. Fisk (to be published).

[6] H. Kadowaki, M. Nishi, Y. Yamada, H. Takeya, H. Takei, S. Shapiro, and G. Shirane, Phys. Rev. B37, 7932 (1988).

NEUTRON DIFFRACTION IN $Co_pMg_{1-p}O$ SOLID SOLUTIONS

T. M. Giebultowicz
(University of Notre Dame, Notre Dame, IN)

J. J. Rhyne

and

M. S. Seehra and R. Kannan
(West Virginia University, Morgantown, WV)

$Co_pMg_{1-p}O$ offers an excellent prototypical example for the study of percolation effects in diluted antiferromagnets. The system retains the original structure of CoO (NaCl-type) in the entire $0 < p < 1$ composition range [1]. The magnetic Co^{++} ions form a randomly diluted fcc lattice with predominantly next-nearest neighbor (NNN) AF coupling due to the mediating role of the oxygen anions.

Recent studies [1] of DC magnetic susceptibility $\chi(T)$ carried out for $Co_pMg_{1-p}O$ with $0.10 < p < 1$ in a broad T range indicate that the percolation threshold for this system is $p_c \approx 0.13$, in agreement with the theoretical value of $p_c = 0.136$ for a fcc lattice with NN and NNN interaction. The variation of the reduced Néel temperature $\tau = T_N(p)/T_N(p = 1)$ with p also reveals a crossover effect at $p = 0.45$. It is of interest that the system shows a remarkable similarity [2] to $Eu_pSr_{1-p}Te$ [3], which suggests that such a crossover behavior is universal for diluted Type II antiferromagnets. However, the mechanism of this phenomenon, as well as the nature of the magnetic state in CoO below p_c (superparamagnetic particles, or a spin glass?) is not yet fully understood, and neutron scattering measurements are necessary to obtain more insight into these issues.

We have carried out neutron diffraction measurements on several $Co_pMg_{1-p}O$ powder specimens with various Co concentrations ($p = 0.25$, 0.37, 0.42, 0.47, 0.54, 0.60, and 0.90). At low temperatures, the systems exhibited the expected pattern of superstructure peaks corresponding to the Type II AF structure. Examples of the composition dependence of the $(111)_M$ magnetic

peaks are displayed in figure 1 for the range $0.37 \leq p \leq 0.54$. For $p = 0.90 - 0.54$ the reflections showed no detectable broadening beyond the instrumental resolution, confirming the existence of a LRO AF phase in this concentration region. In contrast, the peaks observed for $p \leq 0.47$ are broadened and are of Lorentzian shape, indicating a transition to a SRO state. The inverse correlation length (κ) data plotted in figure 2 clearly suggest that the LRO→SRO transition in the system has a sharp composition dependence, and that the critical concentration for this process is slightly higher than $p = 0.47$. The sharp nature of this transition is also indicated by the behavior of the integrated intensity of the $(111)_M$ reflection vs. p, which is plotted in figure 2 normalized by the intensity of the nuclear reflection $(200)_N$. The results clearly show a sharp discontinuity in the magnetic scattering intensity at p_c.

The results of our neutron diffraction studies of $Co_pMg_{1-p}O$ demonstrate that the previously reported crossover behavior in the magnetic susceptibility at $p \approx 0.45$ really reflects the breakdown of the LRO magnetic phase in the system. Since it is believed that a similar type of transition (LRO → spin glass) occurs in $Eu_pSr_{1-p}Te$ for $p \leq 0.50$ [3], these results also indicate why the magnetic characteristics of the two systems are similar at higher p values.

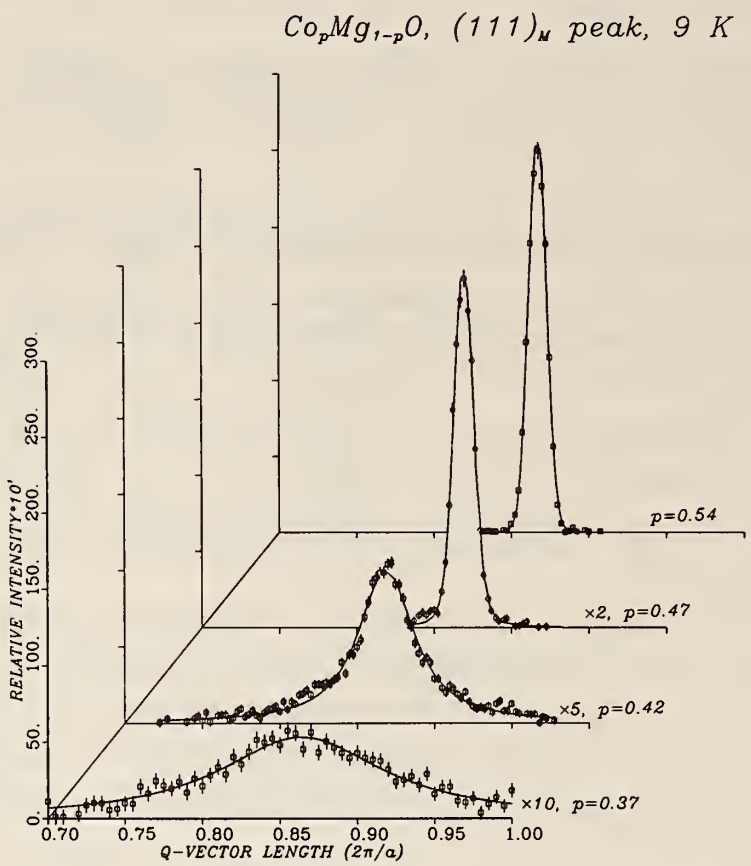

Figure 1. The $(111)_M$ magnetic peaks in $Co_pMg_{1-p}O$ for several different Co concentrations. Solid lines are the results of fitting Lorentzian lineshapes folded with the Gaussian instrumental resolution function to the experimental points (for p = 0.54 only a Gaussian line has been fitted).

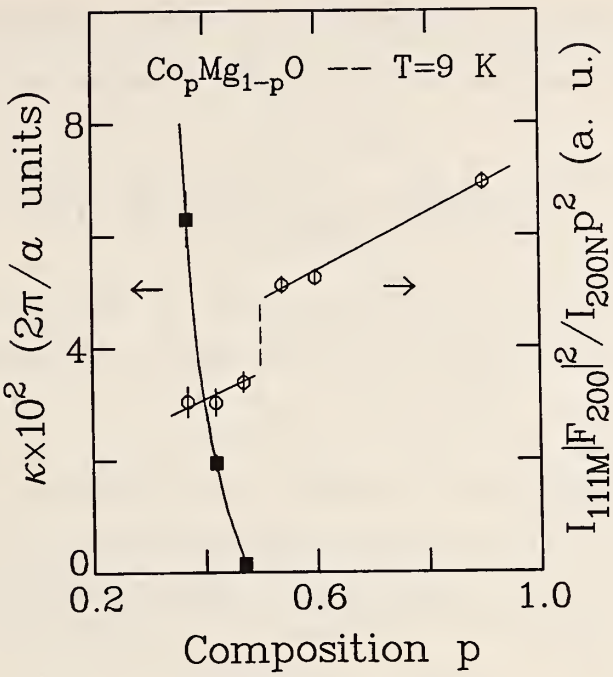

Figure 2. Left plot: the dependence of the inverse correlation length κ on concentration p in the SRO phase in $Co_pMg_{1-p}O$. Right plot: relative intensity of the $(111)_M$ reflection as a function of p (see text). The lines plotted in both graphs are guides for the eye.

References

[1] R. Kannan and M. S. Seehra, Phys. Rev. B35, 6847 (1987).

[2] M. S. Seehra, J. C. Dean, and R. Kannan, ibid. B37, 5864 (1988).

[3] F. J. Borgermann, H. Maletta, and W. Zinn, ibid. B35, 8454 (1987).

SUPERCONDUCTIVITY IN LANTHANUM BARIUM CUPRATE PEROVSKITES

S. Miraglia, A. Santoro, and F. Beech

and

S. A. Sunshine, L. F. Schneemeyer, J. V. Waszczak, and D. W. Murphy
(AT&T Bell Laboratories)

Samples in the system $Ba_{2-x}La_{1+x}Cu_3O_{7-\delta}$ ($0.0 \leq x \leq 0.5$; $0 < \delta < 0.25$) have been prepared and characterized by x-ray powder diffraction, magnetic susceptibility, electrical resistivity, and for $x = 0.5$, powder neutron diffraction. This neutron diffraction study on $Ba_{1.5}La_{1.5}Cu_3O_{7.25}$ indicates that the structure is similar to the 92 K superconductor $Ba_2YCu_3O_7$ with two exceptions. First, the "Ba site" contains 75% Ba and 25% La and second, the symmetry is tetragonal. At $x = 0.5$ the material is a semiconductor, but as x decreases, metallic behavior and superconductivity are observed. Compositions with $x < 0.2$ contain traces of $BaCuO_2$, but exhibit $T_c^{onset} \approx 90$ K and $R = 0$ near 80 K. For $x = 0.2 - 0.3$, $T_c^{onset} \approx 60$ K and $R = 0$ near 50 K are observed. For $x \leq 0.1$ orthorhombic symmetry is observed. These results provide further evidence that oxygen stoichiometry and details of the oxygen ordering are important to superconductivity.

CRYSTAL CHEMISTRY OF SUPERCONDUCTORS: A GUIDE TO THE TAILORING OF NEW COMPOUNDS

A. Santoro and F. Beech

and

M. Marezio and R. J. Cava
(AT&T Bell Laboratories, Murray Hill, NJ)

The crystal structures of the known superconducting copper oxides can be described in terms of two basic structural types. The series $LaCa_{n-1}Cu_nO_{2n+2}$, $(Tl, Bi)_2(Ba, Sr)_2Ca_{n-1}Cu_nO_{2n+4}$ and $TlBa_2Ca_{n-1}Cu_nO_{2n+3}$ can be viewed as made of alternating slices having the rock salt and perovskite structure. The compounds $Ba_2YCu_4O_8$ and $Ba_4Y_2Cu_7O_{14+x}$, on the other hand, comprise perovskite blocks alternating with blocks in which a crystallographic shear is present. The effect of this shear is that of forming double chains of edge sharing squares with oxygen atoms at the corners and copper atoms at the center. The

superconductor $Ba_2YCu_3O_7$ can be described in terms of both structural types and may be considered as an intermediate type between the other two. The basic building blocks of these superconducting materials can be further broken down into constituent nets (or meshes). This description allows one to envisage new structures built from these meshes containing the key structural elements present in the currently known superconductors. As such, the structural schemes used in this description may be used as a guide in the preparation of new materials with interesting electronic properties.

NEUTRON AND ELECTRON DIFFRACTION STUDY OF $YBa_2Cu2_2Cu1_{.77}Fe_{.23}O_{7.13}$

P. Bordet, J. L. Hodeau, P. Strobel, and M. Marezio[1]
(Laboratoire de Cristallographie, C.N.R.S.)
([1]also at AT&T Bell Laboratories, Murray Hill, NJ)

and

A. Santoro

The compound of formula $YBa_2Cu_{2.7}Fe_{0.3}O_{7.13}$ has been analyzed by neutron and electron diffraction techniques. The material is tetragonal with lattice parameters a = b = 3.8674(1), c = 11.6687(2) A and space group P4/mmm. The Fe cations substitute only the Cu cations located on the basal plane of the structure and can adopt three different types of coordination (tetrahedral, pyramidal and octahedral) depending upon the content and distribution of the extra oxygen atoms on the plane. Calculations of the effective valence of iron cations seem to indicate the Fe^{3+} is present in tetrahedral coordination and Fe^{4+} in pyramidal and octahedral coordination, while values of $Cu^{2.2+}$ and $Cu^{2.47+}$ were found for the copper cations located at (00z) and (000), respectively. The electron diffraction experiments show diffuse scattering planes parallel to (110) and (1$\bar{1}$0). Crosses of strong intensity are visible at reciprocal nodes located between the lattice layers. This diffuse scattering is interpreted in terms of linear clusters of iron cations extending along the [110] and [1$\bar{1}$0] directions having a width of a few cations. The clusters are separated by domains of orthorhombic $YBa_2Cu_3O_{6+x}$ having the same orientation or rotated of 90° one with respect to the other.

STRUCTURE AND CRYSTAL CHEMISTRY OF $La_2CaCu_2O_6$ AND $La_2SrCu_2O_6$ BY POWDER NEUTRON DIFFRACTION

R. J. Cava
(AT&T Bell Laboratories, Murray Hill, NJ)

and

A. Santoro and F. Beech

The structures of $La_2CaCu_2O_6$ and $La_2SrCu_2O_6$ were refined with the Rietveld method using neutron powder diffraction data collected with the high-resolution five-counter diffractometer at the NBS Reactor. The initial model of the structure was build in both cases by substituting the layers of $-(CuO_2)_{o,c}-$[1] in the structure of La_2CuO_4 with blocks of three layers having composition and sequence $-(CuO_2)_{o,c}-(M/La)_{c,o}-(CuO_2)_{o,c}$, where M is either a Ca or a Sr atom and M/La indicates that the site may be occupied by M and/or La atoms.

The refinements show that although the general structural configuration of $La_2CaCu_2O_6$ and $La_2SrCu_2O_6$ is the same, the distribution of the atoms in the crystallographic sites is quite different in two cases. We may point out these differences by representing the two structures as sequences of layers with the following scheme:

$$[-(CuO_2)_o-(Ca)_c-(CuO_2)_o-(LaO)_c-(LaO)_o-$$
$$(CuO_2)_c-(Ca)_o-(CuO_2)_c-(LaO)_o-(LaO)_c-](CuO_2)_o-..$$

and

$$[-(CuO_2)_o-(La)_c-(CuO_2)_o-(MO)_c-(MO)_o-$$
$$(CuO_2)_c-(La)_o-(CuO_2)_c-(MO)_o-(MO)_c-](CuO_2)_o-...$$

where M ≃ 70% La + 30% Sr and where the content of a unit cell of the structure is included in the square brackets. From these schemes we see that the (CuO_2) layers are separated by (Ca) layers in $La_2SrCu_2O_6$ and by (La) layers in $La_2SrCu_2O_6$. This different distribution of atoms may be understood by considering that the ionic radius of Sr^{2+}(IX) is larger than that of La^{3+}(IX) (1.31 Å versus 1.22 Å) and for this reason the strontium atoms will prefer sites with nine-fold coordination and will displace La^{3+} into the eight-fold coordinated sites located between the (CuO_2) layers of $La_2SrCu_2O_6$.

Both the calcium and strontium compounds analyzed in this study are terms of the homologous series $La_2M_{n-1}Cu_nO_{2n+2}$ with n = 2. This series may be considered as a particular case of a more general class of compounds having formula

$$(AO)_x\ (A'O)_y\ (M)_{n-1}\ (CuO_2)_n$$

and belonging to a structural type in which blocks $(AO)_x\ (A'O)_y$ with rock-salt structure alternate with blocks $(M)_{n-1}(CuO_2)_n$ having a defective perovskite distribution. The condition of equality between cation and anion valences requires that

$$2(2n + x + y) = px + qy + s(n-1) + mn, \qquad (1)$$

where p, q, s, and m are the valences of A, A', M, and Cu, respectively. If m = s = 2 (case of Ca^{2+} and Cu^{2+}) we have from (1):

$$x(p-2) + y(q-2) = 2 \qquad (2)$$

and, for y = 0 and p = 3 (case of La^{3+}) we obtain

$$(AO)_2\ (M)_{n-1}\ (CuO_2)_n$$

i.e.,

$$A_2^{3+}\ M_{n-1}^{2+}Cu_n^{2+}O_{2n+2}$$

which is the homologous series of the title compounds[2].

---

[1] In this work, the composition of a layer is specified by the chemical symbol, and the location of the atoms in the unit mesh of the layer is indicated by the subscripts o (cation at the origin of the mesh) and c (cation at the center of the mesh). Thus, the symbol $(CuO_2)_o$, for example, indicates that the copper atom is at the origin of the mesh and the oxygen atoms at the mid-points of each side, and $(LaO)_c$ indicates that the lanthamum atom is at the center and the oxygen atom at the origin of the mesh.

[2] Note that for q = 2, y may assume any value. For y = 2 we obtain

$$(AO)_2)\ (A'O)_2\ (M)_{n-1}\ (CuO_2)n$$

i.e.,

$$A_2\ A'\ M_{n-1}\ Cu_n\ O_{2n+4}$$

which is the homologous series of the well-known compounds

$$Bi_2Sr_2Ca_{n-1}Cu_nO_{2n+4} \text{ and } Tl_2Ba_2Ca_{n-1}Cu_nO_{2n+4}$$

Attempts to prepare other terms of this series, as well as some of the many other possible compounds derivable with the above formulas, are underway at the present time.

PHASE EQUILIBRIA IN THE SYSTEM Ba-Y-Cu-O-CO_2 IN AIR

F. Beech

and

R. S. Roth, C. J. Rawn, J. D. Whittler, and J. O. Anderson
(Ceramics Division)

Work has continued on this important phase diagram and its current status is shown in figure 1.

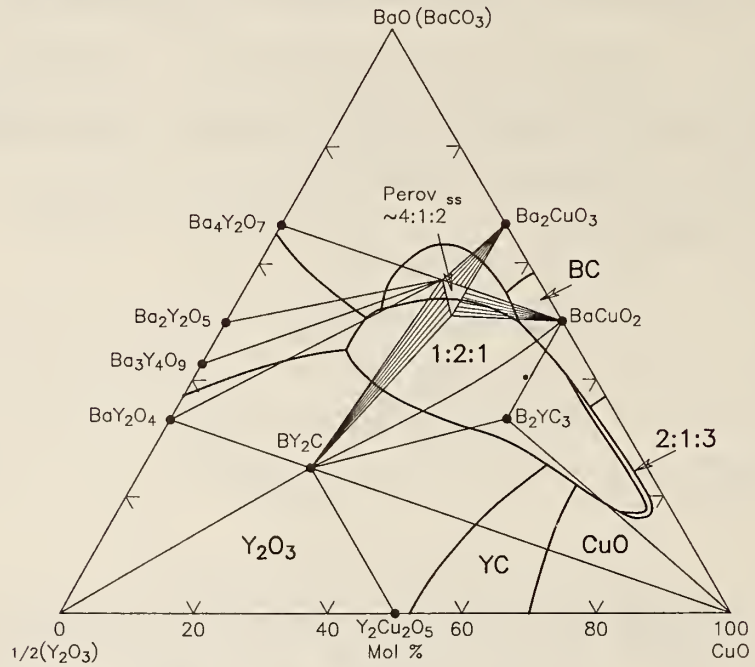

Figure 1. Phase Diagram for Ba-Y-Cu-O-CO_2 at 950 °C.

Features worthy of note are that the phase previously described as 3:1:2 with the "ordered" perovskite-like lattice $\underline{a} = \sqrt{2}\ \underline{a}'$, $\underline{c} = 2\underline{a}'$ has been shown to be a solid solution series containing CO_2 as an integral part of the structure. This solid solution region which encompasses the formula $Ba_{3.2}Y_{0.8}Cu_{2-x}O_{6.4+x} \cdot (yCO_2)$ strongly influences the melting relations of the compositions around the $Ba_2YCu_3O_{6+x}$ superconducting phase. The superconductor phase melts through a four-phase region, tetragonal $Ba_2YCu_3O_{6+x}$, BaY_2CuO_5, $BaCuO_2$ and liquid from about 950°C to 1002 $\pm$ 2 °C in air. This four-phase region is apparently due to the presence of a fourth component, CO_2, acting as an integral part of one or more of these phases, probably mainly in the liquid. The presence of CO_2 in one or more of the crystalline

phases, including the superconductor, is inferred. The tetragonal → orthorhombic transition occurring upon oxidation of $Ba_2YCu_3O_{6+x}$ is concluded to be metastable. No large primary phase field consisting of only $Ba_2YCu_3O_{6+x}$ plus liquid has been identified in the melting relations of the Ba-Y-Cu-O system in air.

SIGNIFICANCE OF PLANE VERSUS CHAIN SITES IN 1-2-3 SUPERCONDUCTORS

J. J. Rhyne, J. K. Stalick, and J. A. Gotaas

and

C. L. Chien, G. Xiao, M. Z. Cieplak, D. Musser, A. Gavrin, and F. H. Streitz
(The John Hopkins University, Baltimore, MD)

Atomic site substitution is one of the effective experimental means of studying the mechanism behind the high T_c superconductivity in the new perovskite superconductors. For example, it has been shown for $YBa_2Cu_3O_7$ that substitution of the Y atom by one of the heavy rare earths (e.g., Gd) which possesses a large magnetic moment does not degrade the superconducting transition temperature. This suggests that the Y site is well shielded from the superconducting electrons, and the imposition of a large local moment at this site does not produce pair breaking. These materials do show magnetic order for $T < 4K$ due to dipole-dipole coupling.

One of the outstanding questions in high T_c $YBa_2Cu_3O_7$ superconductors is the relative importance of the Cu-O_2 planes (Cu(2)-site) and the Cu-O chains (Cu(1)-site). We have used Zn, Ga, Fe, Co, Ni, and Al to selectively substitute the Cu(2) and Cu(1) sites while maintaining the oxygen content near 7 as determined using neutron diffraction. Bulk results show that Zn strongly suppresses the T_c of the material even for concentrations as low as 6%, $T_c \approx$ 40 K. The other elements also depress T_c to some degree but in general remain in the range 80 K and above for substitutions in the 6% range, except for Co in which the local magnetic moment of Co is presumed to have an adverse effect on the electron pairing mechanism.

The neutron diffraction studies have shown that the substituted ions do not stoichiometrically populate the Cu(1) and Cu(2) sites. Rather the 3+ ions (Ga and Al) and the ions for which the 3+ oxidation state is possible (Fe and Co) substitute for Cu primarily on the Cu(1) site, and in consequence destroy

the integrity of the chain site Cu-O ordering. In addition the orthorhombic symmetry distortion is gradually eliminated with increasing concentration of the substituted ion and the material becomes tetragonal. However, the materials remain high T_c superconductors in the tetragonal state.

In contrast to the 3+ ions substitutions, Zn(2+), for which the 3+ oxidation state is unknown, is found to largely substitute for the Cu(2) ion in the plane site and the orthorhombic symmetry is preserved. The resulting disorder in the Cu-O planes, however, severely degrades the superconductivity.

The results for Ni ion substitution are intermediate between those for the 2+ and 3+ ions. At the 3% substitution level the material remains orthorhombic, with Ni probably occupying both the Cu(1) and Cu(2) sites. Attempts to prepare materials with a higher concentration of Ni have not resulted in single-phase samples. However, Ni appears to have a larger negative effect on T_c than do the 3+ ions.

The neutron diffraction results have also shown that all the materials exhibit total oxygen concentrations near seven, which means that incomplete oxidation is not the origin of the depressed T_c in Zn. The Co and Fe materials actually show oxygen levels above 7 resulting from the increase in average valence on the Cu(1) site due to the partial substitution of the 3+ ion for the lower valency Cu.

In summary, the neutron results for the site occupancies of the atoms substituted for Cu, combined with bulk data, have demonstrated that the integrity of the planes is much more important than that of the chains in sustaining high T_c superconductivity. The results also show that the orthorhombic cell distortion is not critical for high transition temperatures.

INELASTIC NEUTRON SCATTERING STUDY OF H ABSORBED IN $YBa_2Cu_3O_{7-\delta}$

D. A. Neumann

and

P. F. Miceli, J. M. Tarascon, P. Barboux, and L. H. Greene
(Bell Communications Research, Red Bank, NJ)

An inelastic neutron scattering study of hydrogen absorbed in the high temperature superconductor, $YBa_2Cu_3O_{7-\delta}$, has been initiated using the Be filter analyzer at BT4. Preliminary results obtained for two concentrations, 0.4 and 4.0 H atoms per Y, are shown in figure 1, along with the generalized density of states of the pure material [1]. For x = 4.0, scattering due to H modes is observed over nearly the entire energy range of 40-220 meV which indicates that many different H sites are populated in this material or that there is a great deal of interaction between the H atoms or both. There are, however, two principal peaks which occur at about 78 meV and 100 meV and two

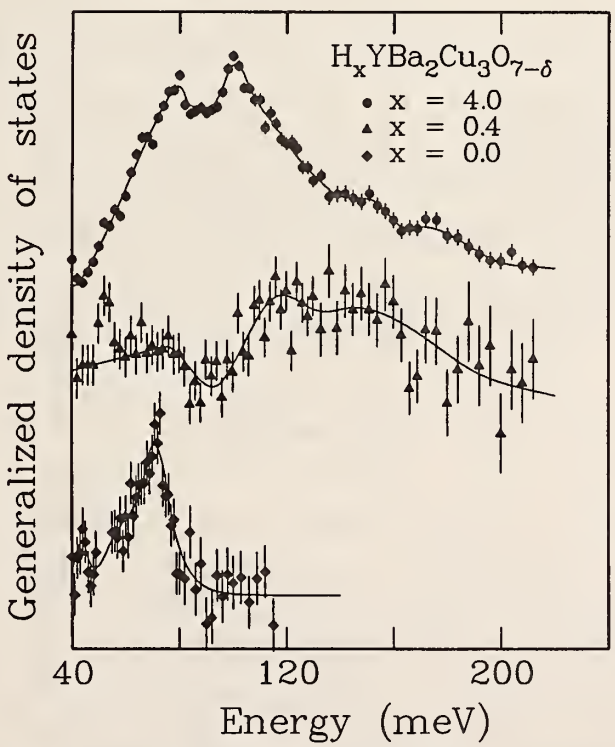

Figure 1. Generalized density of states for H absorbed in $YBa_2Cu_3O_{7-\delta}$. The scattering is dominated by the modes involving the H atoms.

shoulders at energies of roughly 150 and 175 meV. The 78 meV peak is probably due to H atoms riding along on the Cu-O stretching excitations, while the 100 meV peak may be a Cu-H bond-bending mode. The shoulders could then be stretching excitations involving the H atoms since they have smaller displacements and would therefore be less intense than the bending modes. Similar features are observed for the x = 0.4 sample, however better counting statistics are required before a reliable comparison can be made.

References

[1] J. J. Rhyne, D. A. Neumann, J. A. Gotaas, F. Beech, L. Toth, S. Lawrence, S. Wolf, M. Osofsky, and D. U. Gubser, Phys. Rev. B36, 2294 (1987).

THEORETICAL MODELS FOR HIGH-TEMPERATURE SUPERCONDUCTIVITY

R. C. Casella

I have carried out an analysis of the effects of certain electronic energy-band features on gap ratios $2\Delta/kT_c$ for high-T_c superconductors, including the possibility of multigap systems. In addition to phonons, other intermediate bosons (IB) mediating the superconducting interaction have been considered (in a quite general way). Interesting results are obtained when one includes the possibility of an IB with energy ω exceeding the width(s) of one or more narrow peak(s) in the density-of-states associated with distinct sub-bands, each presumably associated (in the tight-binding sense) with distinct substructures, such as the multi-stacked copper-oxide planes. Because of the complex nature of the known high-T_c materials, one feature which might distinguish this class is the possibility of two sets of carriers in distinct substructures (e.g., different Cu-O planes) such that the amplitude for an electronic transition between them is small, but such that the carriers of each substructure can nonetheless interact with those of another via the exchange of the IB between them. I have considered theoretical models which represent extreme examples of this general class; namely models in which superconductivity results solely from the exchange of the IB between the carriers in distinct substructures. That is, taken separately, each substructure is assumed to be nonsuperconducting (or at best the intraband IB exchange would lead to low-T_c superconductivity and is ignored in the analysis). The fermionic operators $c^{\dagger}$ and d^{+} for carriers in

each group create normal-state excitations in sub-bands C and D, respectively, and enter in a BCS-like generalized Hamiltonian H of the type invoked some years ago by Suhl et al. [1] to describe the interplay between s and d electrons. The equations of motion in the Heisenberg picture are ($\hbar = 1$),

$$-i\,\dot{c}_{\vec{k}\uparrow} = -\,\epsilon_C(\vec{k})\,c_{\vec{k}\uparrow} + \Delta_C(\vec{k})\,c^{+}_{-\vec{k}\downarrow}$$
$$-i\,\dot{d}_{\vec{k}\uparrow} = -\,\epsilon_D(\vec{k})\,d_{\vec{k}\uparrow} + \Delta_D(\vec{k})\,d^{+}_{-\vec{k}\downarrow}\,. \tag{1}$$

Where, e.g., $\epsilon_C(\vec{k})$ is normal-state excitation relative to the ground state in sub-band C and where, in general,

$$\Delta_C(\vec{k}) = -\sum_{\vec{k}'} V_{CC}(\vec{k}-\vec{k}')\,\langle c_{-\vec{k}'\downarrow}(0)\,c_{\vec{k}'\uparrow}(0)\rangle$$
$$-\sum_{\vec{k}'} V_{CD}(\vec{k}-\vec{k}')\,\langle d_{-\vec{k}'\downarrow}(0)\,d_{\vec{k}'\uparrow}(0)\rangle\,. \tag{2}$$

Here

$$\langle c_{-\vec{k}\downarrow}(0)\,c_{\vec{k}\uparrow}(0)\rangle = (\Delta_C/2E_C)\tanh(\beta E_C/2), \tag{3}$$

where $E_C = (\epsilon_C^2 + \Delta^2)^{1/2}$ and $\beta = 1/kT$. Let B_I denote the widths of the sub-bands for I = C, D. For the conventional wide-band class ($\omega \ll B_I$), in weak coupling ($g^2 = \lambda_{CD}\,\lambda_{DC} \ll 1$ and $kT_c = 1.13\,\omega\exp(-1/g)$), and assuming $\lambda_{CC} = 0 = \lambda_{DD}$,

$$\Delta_C = 2\omega\,\alpha^{-1/2}\exp(-1/g)\,,\quad \Delta_D = 2\omega\,\alpha^{1/2}\exp(-1/g),$$
$$2\Delta_C/k_BT_c = 3.5\,\alpha^{-1/2},\quad 2\Delta_D/k_BT_c = 3.5\,\alpha^{1/2}. \tag{4}$$

Here, $\alpha^2 = N_C(0)/N_D(0)$.

In contrast, when ω exceeds the width of one or more peak in the sub-band density-of-states (as shown in fig. 1), a Taylor series expansion about the density-of-states at the Fermi surface, $N_C(\epsilon) = N_C(0) + \ldots$, is no longer valid and the excitations within the narrower band C extend throughout the peak. That is, in the presence of IB exchange, the peak consists of a foam of elementary excitations. For the band structure characterized in figure 1 and neglecting interband carrier mixing, I find

$$\Delta_C = B\,\alpha^{-1/2}\exp(-1/g), \quad \Delta_D = B\,\alpha^{1/2}\exp(-1/g),$$

$$2\Delta_C/k_BT_c = 3.5\,\alpha^{-1/2}\exp(\Lambda/g), \tag{5}$$

$$2\Delta_D/k_BT_c = 3.5\,\alpha^{1/2}\exp(\Lambda/g),$$

where

$$\Lambda = \left[1 + \left(\frac{g\ln R}{2}\right)^2\right]^{1/2} - 1,$$

$$\alpha^2 = \langle N_C \rangle / N_D(0), \tag{6}$$

$$B = (2\omega B_C)^{1/2}, \quad R = (2\omega/B_C).$$

$\langle N_C \rangle$ denotes the mean density-of-states, averaged over the narrow band C (c.f., fig. 1). This work was motivated in part by early reports of various values of $2\Delta/kT_c$ differing from the classic BCS value 3.5, as determined via several different types of experiments (tunneling, infrared absorbtion, nuclear-spin relaxation) in the La-Sr-Cu-O and Ba-Y-Cu-O high-T_c systems. A scenario such as that illustrated in figure 1 readily accommodates the precise spin-relaxation data obtained for the $Ba_2\,Y\,Cu_3O_{7-\delta}$ system [2]. I find $g \simeq 0.24$ and an IB energy $\omega \gtrsim 1$ eV, suggesting that the IB is not a phonon. However, the two gap interpretation [2a] of the spin relaxation data is not unique [2b]. A more complete description of my analysis has been submitted for publication [3].

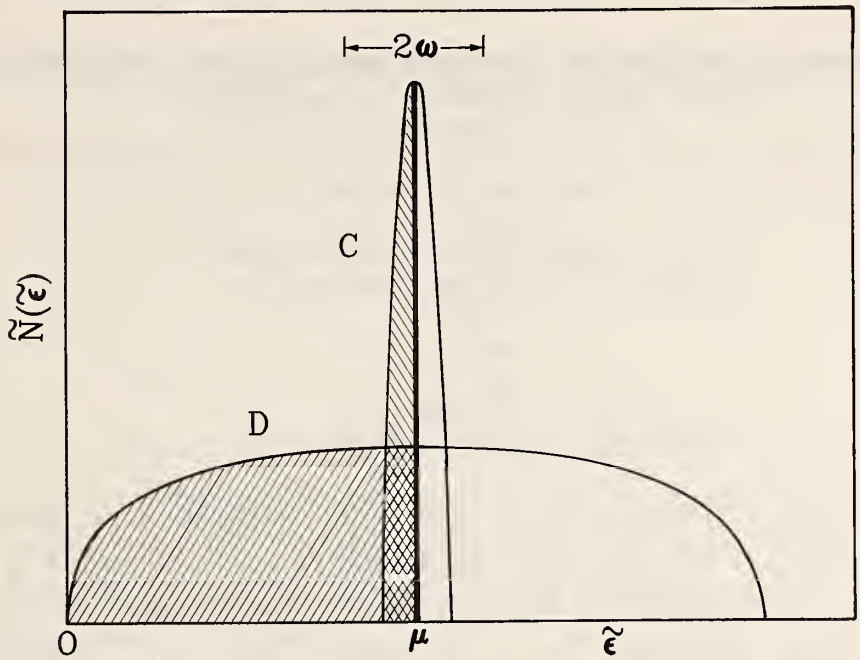

Figure 1. Density-of-states and assumed electronic occupancy in the absence of the intermediate boson (IB) exchange leading to pair condensates. ω is the IB energy, which for the case illustrated, satisfies, $B_C < 2\omega << B_D$. B_I denotes the width of the Ith sub-band (I = C, D).

References

[1] H. Suhl, B. T. Mathias, and R. L. Walker, Phys. Rev. Lett. 3, 552 (1959).

[2] (a) W. W. Warren Jr., R. E. Walstedt, G. F. Brennert, G. P. Espinoza, and J. P. Remeika, Phys. Rev. Lett. 59, 1860 (1987),
(b) R. E. Walstedt, Bul. Am. Phys. Soc. II, 33, 337 (1988).

[3] R. C. Casella, Nuovo Cimento D (in press).

NEUTRON POWDER DIFFRACTION STRUCTURE AND ELECTRICAL PROPERTIES OF THE DEFECT PYROCHLORES $Pb_{1.5}M_2O_{6.5}$ (M = Nb, Ta)

F. Beech and A. Santoro

W. M. Jordan and C. R. A. Catlow
(University College, London, UK)

and

B. C. H. Steele
(Imperial College, London, UK)

Powder neutron diffraction and Rietveld analysis have been used to investigate the crystal structures of the defective pyrochlores $Pb_{1.5}Nb_2O_{6.5}$ and $Pb_{1.5}Ta_2O_{6.5}$. Both materials crystallize with the symmetry of space group Fd3m, with lattice parameters a = 10.5647(2) and a = 10.5558(2) Å, respectively. No evidence has been observed of oxygen or lead vacancy ordering in these compounds. This result is interpreted in terms of a model in which all lead present in the structure has seven-fold pyramidal coordination and forms domains separated by regions of lead vacancies with hexagonal or bipyramidal configurations of the oxygen atoms. This model, built on the assumption that the driving force in the formation of this type of defect pyrochlores is the coordination of lead, leads us to conclude that the system $Pb_{1+x}M_2O_{6+x}$ (M = Nb, Ta) may exist over a range of compositions with $0.33 \leq x \leq 0.6$, and may also explain results obtained in other studies of related materials. The electric measurements show that both compounds are predominantly electronic conductors and that the ionic contribution to the total conductivity is very small even at the highest temperatures used in the study.

A NEUTRON POWDER DIFFRACTION STUDY OF Na,Cs ZEOLITE RHO

W. H. Baur and A. Bieniok
(Johann Wolfgang Goethe University, Frankfurt an Main, West Germany)

R. D. Shannon
(Du Pont Company, Wilmington, DE)

and

E. Prince

Several studies [1,2] have shown a simple relation between the lattice constant of zeolite rho and the degree of elliptical distortion, and therefore the pore size, of the "double eight ring" that is the basic structural element. A previous study [3] of a rho sample containing sodium and cesium, however, was clearly discordant with the general trend. Because of this a neutron powder diffraction study of a rho sample with a similar composition was undertaken to determine whether the discrepancy was due to a real exception to the rule or to an insufficiently precise structure determination.

A set of neutron powder diffraction data was collected at 373 K from a sample of zeolite rho with the approximate composition $Na_{7.6}Cs_{3.2}Si_{36.4}Al_{11.6}O_{96} \cdot 5D_2O$. The structure was refined by the Rietveld method to R_{wp} = 8.01%, giving the parameter values shown in table 1. If the eight ring is undistorted, the $\underline{x}$ parameters of O(2) and O(3) are equal. The ratio of these parameters is a measure of the elliptical distortion. In an extensive set of structures this ratio is related to the lattice constant, to a good approximation, by EL = 13.866 - 0.839$\underline{a}$. In this structure $\underline{a}$ = 14.66Å, giving EL = 1.566, in good agreement with the observed value, 1.569. The structure of Na,Cs rho is not, therefore, an exception to this rule. Figure 1 shows the observed ellipticity parameter, and the pore size derived from it, plotted against the lattice constant for a variety of samples of zeolite rho.

Table 1. Structural parameters for Na,Cs zeolite rho: C is the number of atoms per unit cell. Cell constant, a = 14.6566(4) Å

atom	x	y	z	B	C	Wyckoff position	site symmetry
Si/Al	.2692(7)	.1207(10)	.4200(7)	1.0(2)	48	48(h)	1
O(1)	.0294(5)	.2099(6)	.3864(8)	2.0(2)	48	48(h)	1
O(2)	.2092(6)	.2092(6)	.3949(10)	2.1(3)	24	24(g)	m
O(3)	.1333(6)	.1333(6)	.6232(9)	1.6(2)	24	24(g)	m
Cs	.00	.00	.50	2.9(13)	3.2	6(b)	42m
Na(1)	.305(7)	.305(7)	.305(7)	3.0	2.0(5)	8(c)	3m
Na(2)	.040(8)	.040(8)	.504(9)	3.0	4.2(7)	24(g)	m
OW(1)	.218(8)	.218(8)	.120(15)	3.0	2.1(5)	24(g)	m
OW(2)	.169(10)	.040(8)	.040(8)	3.0	2.2(4)	24(g)	m
OW(3)	.432(11)	.432(11)	.282(15)	3.0	1.9(5)	24(g)	m

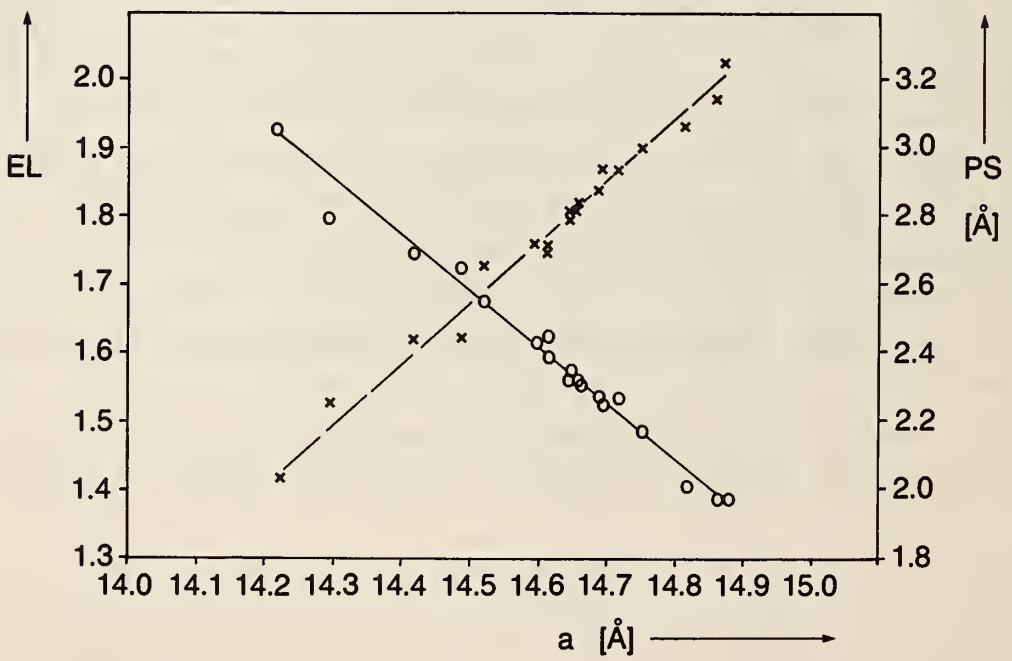

Figure 1. Variation of the ellipticity parameter EL (left axis, circles), and pore size, PS (right axis, crosses), with cell constant, a, in a variety of samples of zeolite rho.

References

[1] J. B. Parise, L. Abrams, T. E. Gier, D. R. Corbin, J. D. Jorgenson, and E. Prince, J. Phys. Chem. 88, 2303 (1984).

[2] W. H. Baur, R. X. Fischer, and R. D. Shannon, Proc. Int. Symp. Innovation in Zeolite Materials Science, Amsterdam, Elsevier 281-292 (1988).

[3] L. B. McCusker and C. Baerlocker, Proceedings of the 6th International Zeolite Conference, 812. Guildford: Butterworth (1984).

THE STRUCTURES OF η-, γ- AND θ-ALUMINA

R. S. Zhou and R. L. Snyder
(Alfred University, Alfred, NY)

and

E. Prince

When aluminum hydroxide, which exists as $Al(OH)_3$ (bayerite) and as AlOOH (boehmite), is heated, water is driven off. The ultimate end product is corundum, α-Al_2O_3, but, before corundum is formed, other phases appear that are very reactive, catalytic materials. Bayerite transforms to a cubic phase designated η-alumina. Boehmite transforms to a slightly different, cubic phase designated γ-alumina. On further heating, both of these phases transform to a monoclinic phase, designated θ-alumina, before recrystalizing as corundum. Because neither the starting materials, bayerite and boehmite, nor the final product, corundum, is catalytically active, there has been considerable interest in the structures of the "transitional" phases in attempts to understand their properties.

Neutron powder diffraction patterns were collected from samples of η-alumina, γ-alumina and θ-alumina on the five detector powder diffractometer. Particle sizes for all three samples were very small, so that the diffraction peaks were much broader than typical ones produced by well crystallized materials on that instrument. It proved to be possible, nevertheless, to perform Rietveld-method structure refinements with the data and to extract useful, structural information from them. All three structures are spinel like, with oxygen atoms arranged in approximate cubic close packing and aluminum atoms occupying tetrahedral and octahedral interstices. η and γ are both cubic, with very similar cell constants, but the intensity distributions

in their diffraction patterns are clearly distinct. The hypothesis that these phases are hydrogen spinels, with the composition DAl_5O_8, is ruled out; there is no ordered hydrogen in the structure. In η and γ some of the octahedral aluminum, roughly the right proportion to be considered to be on the surfaces of very fine particles, is considerably displaced along a threefold axis from the center of the octahedron. In η the displacement is sufficient to make the coordination be effectively three. The proportion of aluminum found in this distorted environment was 13% in η and 25% in γ.

θ-alumina is an apparently well-ordered structure, with 50% of the aluminum in each of tetrahedral and octahedral interstices. It is formed by a displacive transformation from η or γ, but is apparently metastable with respect to corundum, to which it transforms by recrystallization on further heating.

Figure 1 shows the configuration of oxygen atoms in four successive (111) layers in cubic close packing, with the positions of the tetrahedral and octahedral interstices and the additional sites occupied in η and γ.

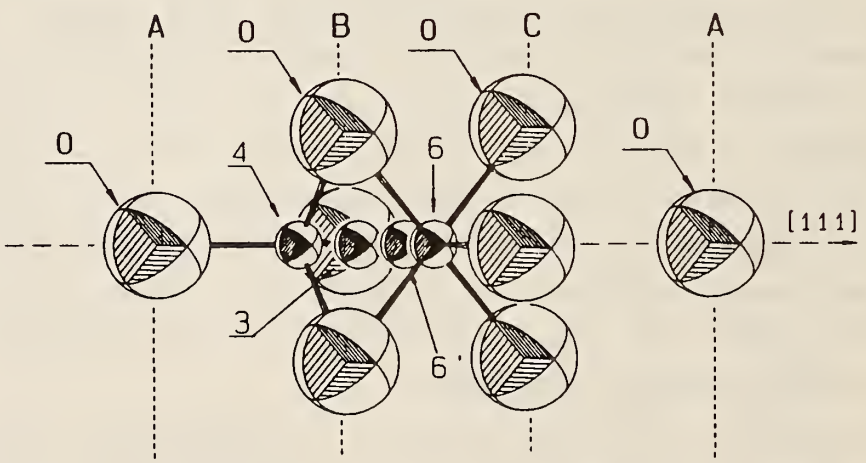

Figure 1. A cluster of oxygen atoms in cubic close packing, showing the tetrahedral and octahedral interstices. The 3-coordinated position is occupied in η-alumina, and the G^1 position is occupied in γ-alumina.

N-DIMENSIONAL CRYSTALLOGRAPHIC DESCRIPTION OF THE ICOSAHEDRAL PHASES; THE EXAMPLE OF THE $Al_{73}Mn_{21}Si_6$ QUASIPERIODIC STRUCTURE

D. Gratias, M. Bessier, Y. Calvayrac, S. Lefebvre, and A. Quivy
(C.E.C.M./C.N.R.S.)

and

J. W. Cahn and B. Mozer

Icosahedral phases in aluminum based alloys have been extensively studied by means of x-ray, neutron and electron diffraction [1]. Many spectra have been collected, but no fully satisfying crystallographic model that matches properly the observed diffracted intensities has been proposed. The structural characterization of quasiperiodic phases is a formidable task owing to the numerous parameters which have to be determined in addition to those of standard 3-D crystallography [2].

The present paper reports experiments carried out on a reproducibly created and well characterized icosahedral $Al_{73}Mn_{21}Si_6$ ternary alloy which has been investigated by x-ray [3] and neutron diffraction [4]. The crystallographic analysis is based on the following heuristic hypotheses:

i. Nonredundant indexing requires only six-indices; the 6-D space description has therefore been used. (This, however, does not necessarily imply that the actual structure in 6-D would fit with atomic 3-D surfaces depending only on the perpendicular space variable, $x_\perp$.);

ii. The powder diffraction patterns have been indexed using the scheme proposed by Cahn, Shechtman, and Gratias [5] assuming a primitive 6-D hypercubic lattice; actually, two other equivalent lattices with same multiplicity could have been considered as well: the D_6+ and D_6- (dual to each other) lattices defined by,

$$D_6(\pm) = F(2A) + (1/2,1/2,1/2,1/2,1/2, \pm 1/2)F(2A),$$

where F(2A) designates the face-centered hypercubic 6-D lattice with parameter 2A, are consistent with both the icosahedral symmetry and the extinction rules observed in single domain electron diffraction. These lattices lead to projected quasilattices τ times smaller (for D_6+) or larger (for D_6-) than the one obtained for the primitive 6-D lattice.

iii. The 6-D point group of the structure has been assumed to be m35. It is obvious, even from powder diffraction patterns, that the 6-D point group is m35 and not a supergroup of m35 (intensities of equivalent reflections in

the B_6 holohedral point group are clearly different). Although the hemihedral noncentrosymmetric 235 group could have been chosen as well, convergent beam electron diffraction [6] and recent neutron contrast experiments [7] have shown that the motif is most likely to be centrosymmetric.

References

[1] International Workshop on Aperiodic Crystals, J. de Physique 7, Colloquium 3 (1986).

[2] P. Bak Phys. Rev. Lett 54 1517 (1985); Phys Rev. B32 5764 (1985); Phys. Rev. Lett 56, 861 (1986); J. de Physique 7, Colloqium 3 136 (1986).

[3] M. Bessiere et al. (in preparation).

[4] R. Bellissent et al. (in preparation).

[5] J. W. Cahn, D. Shechtman, and D. Gratias, J. Mat. Res. 1, 13 (1986).

[6] L. Bendersky and M. J. Kaufman, Phil. Mag. B53, L75 (1986).

A 6-D STRUCTURAL MODEL FOR THE ICOSAHEDRAL (Al,Si)-Mn QUASICRYSTAL

J. W. Cahn
(Institute for Materials Science and Engineering)

D. Gratias
(C.E.C.M./C.N.R.S.)

and

B. Mozer

A 6-dimensional (6-D) periodic model is proposed for the Al-Mn-Si icosahedral quasiperiodic crystal. The model results from an embedding of the periodic cubic α structure in 6-D. In the Janner-Janssen-Bak description, it consists of three concentric spherical shells of respectively Mn, Al and Al aligned in perpendicular space around the lattice nodes and two additional shells of Al around the body centers. This model is shown to match the x-ray powder diffraction data with a satisfactory residual R-factor of 0.128.

NEUTRON DIFFRACTION STUDIES OF THE MARTENSITIC TRANSFORMATION IN SODIUM METAL

R. Berliner
(University of Missouri, Columbia, MO)

H. G. Smith
(Oak Ridge National Laboratory, Oak Ridge, TN)

J. R. D. Copley
(University of Maryland and the Reactor Radiation Division)

and

J. Trivisonno
(John Carroll University, Cleveland, OH)

Neutron powder diffraction experiments on polycrystalline sodium metal have shown that it undergoes a martensitic phase transformation at about 35 K from the bcc structure to a new hexagonal form [1,2]. The structure of the new phase, as given by the powder diffraction patterns, appears to be the same as the structure adopted by lithium metal at low temperature; i.e., the 9R Samarium type structure [3]. Recent reports [4] and theoretical work [5] have claimed that this structural transformation in sodium is partly the result of softening of the Σ_4 phonon branch along the [110] symmetry direction.

We have measured the phonon dispersion curve for the Σ_4 branch as a function of temperature, and the structure of the transformed phase at 30 K, using the triple axis spectrometer BT9. No substantial softening of the phonon branch was observed. The crystallography of the transformed phase is somewhat different to the one observed earlier in lithium metal [6]. About each bcc [110] direction, diffracted intensity corresponding to four trigonal variants of the new phase can be observed. Studies of the (10ℓ) reflections showed that the new phase contains both a 9R (Samarium type) structure and a substantial fraction of an hcp phase. Preliminary investigations of both phases show that they evidence the same kind of shifting and broadening that was observed in lithium. Careful monitoring of the diffraction pattern as the crystal warmed showed that there was a substantial temperature range, starting at 55 K, over which the 9R phase transformed to bcc leaving the hcp phase intact. Upon further warming the hcp phase also reverted to bcc, and the system remained a single crystal in its original orientation up to a

temperature in the range from 250 K and 300 K, where it broke into several pieces, probably due to too fast a warming rate in this latter region.

References

[1] C. S. Barrett and O. R. Trautz, Trans. Am. Inst. Min. Metall. Pet. Engr. 175, 579 (1948).

[2] R. Berliner, O. Fajen, H. G. Smith, and R. J. Hitterman, Bull. Am. Phys. Soc. 33, 615 (1988).

[3] R. Berliner and S. A. Werner, Phys. Rev. B34, 3586 (1986).

[4] O. Blaschko and G. Krexner, Phys. Rev. B30, 1667 (1984).

[5] R. J. Gooding and J. A. Krumhansl, Bull. Am. Phys. Soc. 33, 615 (1988).

[6] H. G. Smith, Phys. Rev. Lett. 58, 1228 (1987).

CRYSTAL STRUCTURE STUDY BY X-RAY DIFFRACTION.

H. L. Ammon
(University of Maryland, College Park, MD)

and

C. S. Choi
(ARDEC, Picatinny Arsenal, NJ and Reactor Radiation Division)

There is considerable interest in the synthesis and chemistry of cubane derivatives within the explosives community which is searching for new types of energetic materials based on high-density and highly-strained molecules. During the reporting period, we have studied the crystal structures of four newly synthesized compounds. Due to the unexpectedly long delay of the restoration of the NBS x-ray single crystal diffractometer, the experiments were conducted at the x-ray Laboratory of the Department of Chemistry, University of Maryland. The data collections were done by using Mo radiation with an incident beam monochromator and an Enraf-Nonius CAD-4 diffractometer throughout.

1. Crystal Structure of 1,4-diiodocubane

The crystal, $C_8H_6I_2$, crystallizes in monoclinic, $P2_1/c$, with the cell dimensions, a = 7.137(1), b = 7.269(2), c = 8.991(2)Å, β = 111.69(2), V = 433.4(3)Å^3,with two molecules per unit cell. The calculated density was D_x =

$2.73 gcm^{-3}$. The structure was solved with Patterson methods. Final R = 0.036 and wR = 0.053 for 714 reflections with $I > 3\sigma(I)$. The molecular structure is shown in figure 1. The molecule possesses a center of symmetry, with the two I atoms positioned on opposite corners of the cube.

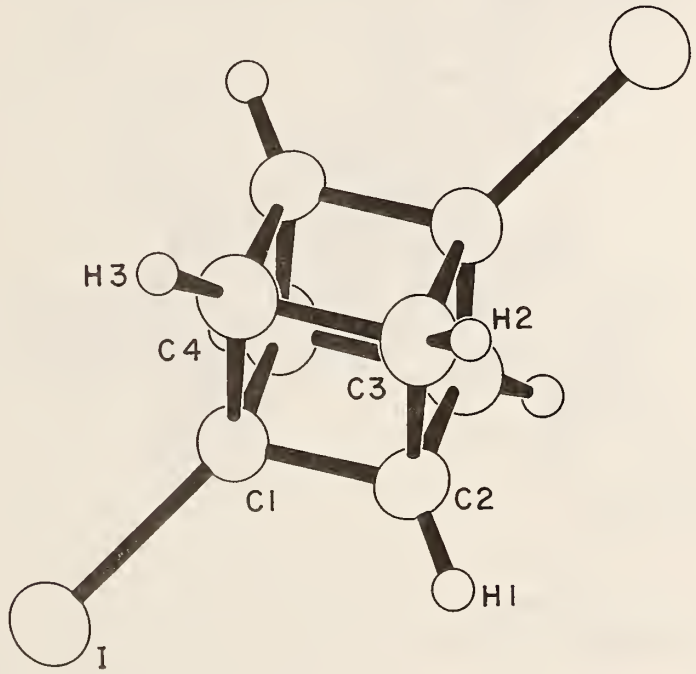

Figure 1. ORTEP drawing of 1,4-diiodocubane molecule.

2. Crystal Structure of 1,4-diammoniumcubane-(Bis-trinitromethide)

The compound, $C_{10}H_{12}N_8O_{12}$, crystallizes in monoclinic, C2/m, with cell dimensions, a = 14.298(2), b = 8.408(1), c = 7.354(2) Å, V = 859.9(5) $Å^3$, with two molecules per unit cell. The calculated density is, $D_x = 1.68 gcm^{-3}$. The structure was solved with MITHRILL direct methods. Final R = 0.039 and wR = 0.054 for 672 reflections with $I > 3\sigma(I)$. ORTEP drawing of the molecole is given in figure 2. The diammoniumcubane cation possesses 2/m symmetry and the trinitromethide anion mirror symmetry. The cation is linked to six trinitromethide anions, three at each end, by three different N-H•••O hydrogen bonds for each anion, as shown in figure 2. The diammoniumcubane moiety undergoes intense libration motions about the long N1•••N1 molecular axis (the axis with the smallest moment of inertia), with r.m.s. amplitude of 17°.

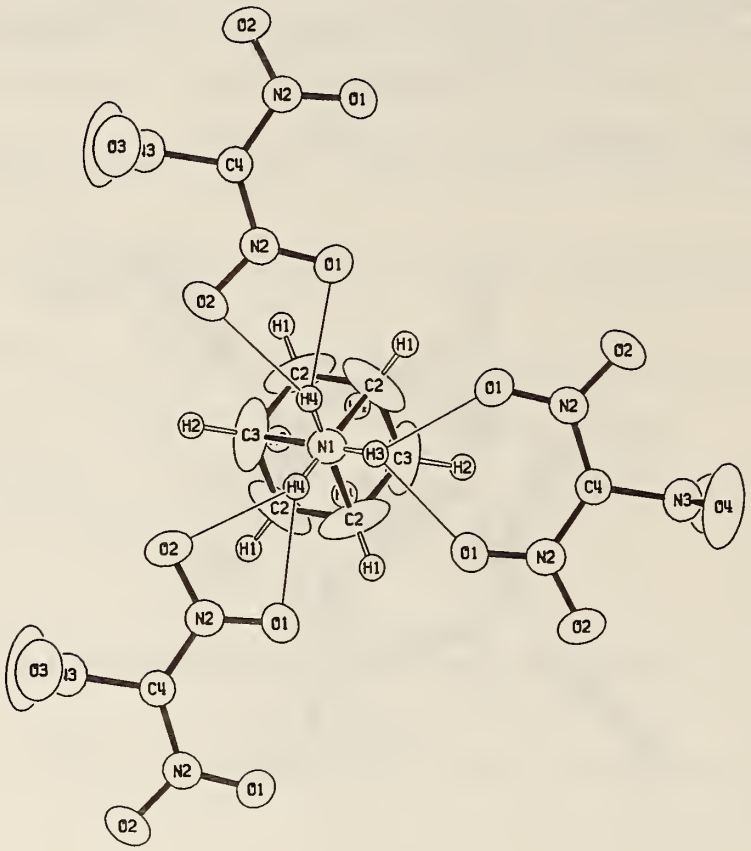

Figure 2. ORTEP drawings of diammoniumcubane cations and trinitromethide anion, viewed along the long axis direction of the cation (N1•••N1). The cation possesses 2/m symmetry (H3,N1,C1,C3 on the mirror plane), and linked to six anions by strong H-bonds. The H-bondings at one end of the cation are shown here. The cation possesses a pseudo-threefold symmetry, and undergoes an intense libration motion (r.m.s. amplitude of 17°) about the axis as demonstrated by the elongated thermal ellepsoids (isotropic H atoms).

3. Structure of 1,4-di(N,N-diisopropylaminomethyl)-2,7-diphenyl-cubane

The compound, $C_{34}H_{46}N_2$, crystallizes in monoclinic, $P2_1/n$, a = 9.641(2), b = 15.900(5), c = 10.864(2) Å, β = 117.92(1), V = 1472(1)Å^3, with two molecules per unit cell. The calculated density is D_x = 1.09gcm^{-3}. The structure was solved with MITHRIL direct methods. Final R = 0.054 and wR = 0.060 for 1348 reflections with I > 3σ(I). ORTEP drawing of the molecule is shown in figure 3. The molecule possesses a center of symmetry, with the two phenyl groups and the two isopropyl groups positioned on opposite corners of the cube, respectively.

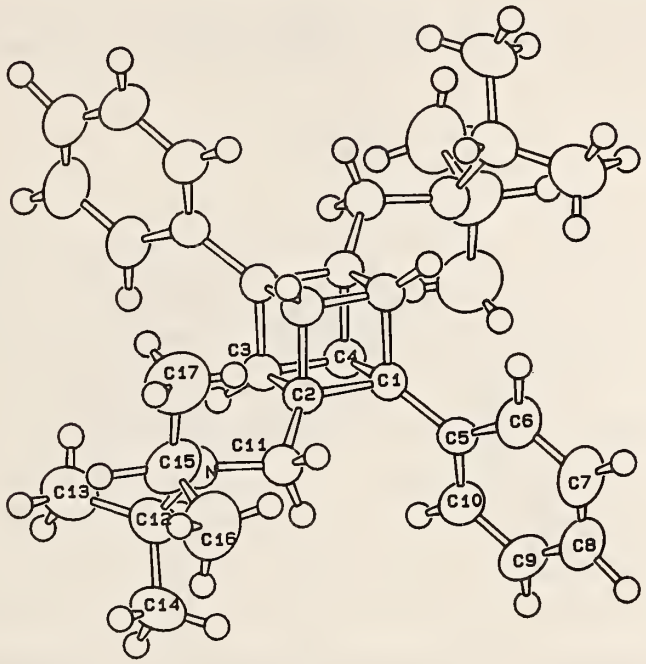

Figure 3. ORTEP drawing of 1,4-di(N,N-diisopropylaminomethyl)-2,7-diphenylcubane.

4. Structure of 1-adamantanylammonium trinitromethide

The compound, $C_{11}H_{18}N_4O_6$, crystallizes in orthorhombic, Pnma, a = 23.802(9), b = 8.431(3), c = 7.166(2)Å, V = 1438.0(8) $Å^3$, with four molecules per unit cell. The measured and calculated densities are, D_m = 1.37(5)gcm^{-3}, D_x = 1.396gcm^{-3}, respectively. The structure was solved with MITHRIL direct methods. Final R = 0.048 and wR = 0.061 for 860 reflections with I > 3σ(I). ORTEP drawing of the molecule is given in figure 4. Both the adamantanylammonium cation and trinitromethide anion possess mirror symmetry. The cation is linked to three trinitromethide anions by six N-H•••O hydrogen bonds through the three ammonium hydrogens.

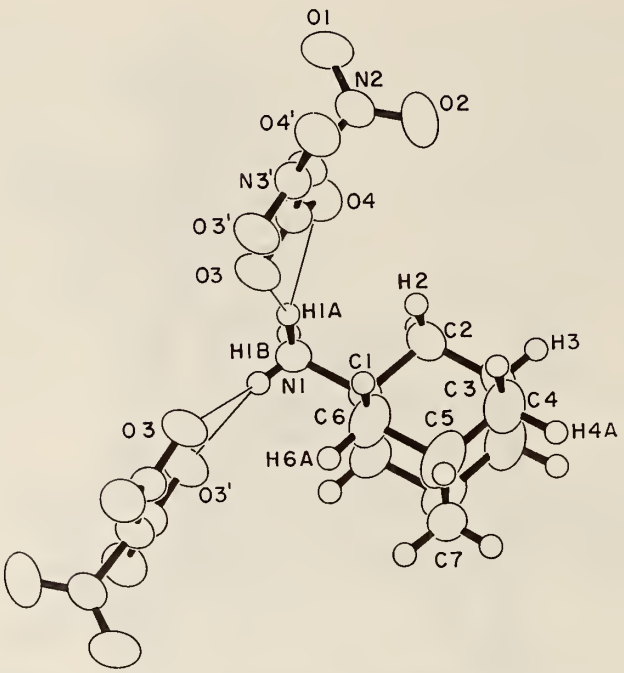

Figure 4. ORTEP drawing of adamantanylammonium cation, and two out of the three nearest trinitromethide anions linked by N-H···O hydrogen bonds. A third anion is related by mirror symmetry to the H1A-linked anion; it is not shown here for clarity.

PHASE DIAGRAM OF ALLOYS IN THE Ti-Al SYSTEM

R. M. Waterstrat
(American Dental Association Health Foundation Research Unit)

and

E. Prince

There has been widespread interest in the effects of impurities, particularly oxygen, on the phase diagram of alloys in the titanium-aluminum system. To study impurity effects, it is obviously necessary to have a good knowledge of the properties of the pure, binary system, but most previous studies have been on quenched samples, which are subject to ambiguous interpretations. Because of the high penetrating power of the neutron, neutron powder diffraction is a useful tool for studying materials at high temperatures, and, because of the negative scattering length of titanium, it is particularly sensitive to the presence of ordered phases in this system.

We have performed two types of high-temperature, neutron diffraction experiments on alloys in the system $Ti_{1-\underline{x}}Al_{\underline{x}}$ with $\underline{x}$ in the range from 0.14 to 0.45. Full diffraction patterns at 900 °C and 1000 °C were taken on samples that had previously been equilibrated at those temperatures for up to 2 weeks, in order to determine the composition range within which the ordered, hexagonal, α_2 phase was present. For some compositions, the strongest peaks characteristic of the α_2 phase, the disordered, hexagonal, α phase, and the disordered, body centered-cubic, β phase were observed as the temperature was raised in order to verify the approximate transition temperatures and the identities of the phases on either side of the boundary. Figure 1 shows the Ti-Al phase diagram given recently by Murray [1], modified to be compatible with our observations and with our data points shown. For the most part previous observations are confirmed, but there are two features of particular interest. First, for $\underline{x}$ = 0.16 at 900 °C and for $\underline{x}$ = 0.16 and $\underline{x}$ = 0.18 at 1000 °C the α_2 phase is not observed, but the background in the diffraction pattern was abnormally high, and the α phase peaks were very weak. This may be attributed to displacement effects due to short range order. Second, when the sample with $\underline{x}$ = 0.40 was heated up, the β phase was not found. A full diffraction pattern at 1200 °C had only one peak. That peak is compatible with a disordered, hexagonal structure, as in the α phase, but not with the β phase. Because the scattering lengths of Al and Ti are nearly equal in

magnitude, but opposite in sign, a disordered alloy with $\underline{x}$ = 0.50 would be a "null matrix", which would give no neutron diffraction pattern at all. $\underline{x}$ = 0.40 is close enough to this so that the weakness of the diffraction pattern is not surprising.

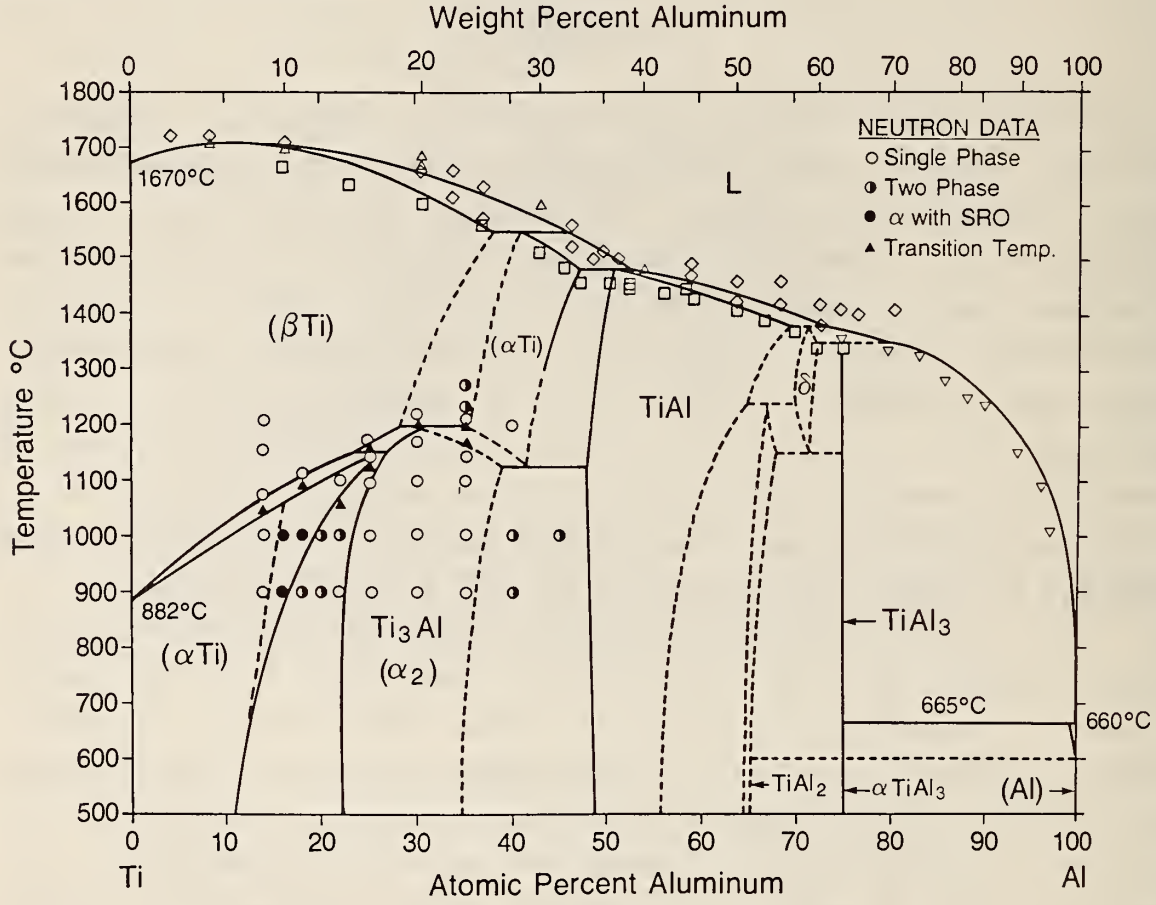

Figure 1. Ti-Al phase diagram with neutron diffraction observations shown. Solid black dots indicate the region of apparent short range order.

References

[1] J. L. Murray, Calculation of the Titanium-Aluminum Phase Diagram, Met. Trans. 19A, 243 (1988).

NEUTRON DIFFRACTION STUDY OF TEXTURES OF MATERIALS

C. S. Choi and H. J. Prask
(U.S. Army, ARDEC, Dover, NJ and Reactor Radiation Division)

We have studied textures of three different type of materials: cold-worked depleted uranium (DU) alloys, a magnetically oriented high T_c superconductor, and the standard sample prepared by the international pole figure standard project committee. The diffraction patterns and pole figure data were measured with 1.275 Å neutrons using the four-circle single crystal neutron diffractometer. The background was determined from the off-Bragg intensities of the powder pattern. The random-distribution intensity, R, was determined from the observed pole figure data, $F(\phi,\chi)$, by:

$$R = \{\sum_{\chi} R(\chi)\cos(\chi)+R(90)/n\}/(\sum_{\chi} n\cdot\cos\chi+1),$$

where $R(\chi) = \sum_{\phi} F(\phi,\chi)$ and $n = 360/\Delta\phi$.

The pole density was expressed in terms of the m.r.d. (multiples of a random distribution) unit (which was calculated by $F(\phi,\chi)/R$), and was presented by the equal-area projection type pole figures.

1. Textures of the cold-worked DU alloys

U-0.75 wt% Ti is an important material in the military armament area because of its high density and mechanical strength. Previously, we studied the textures of small experimental samples as a function of heat-treatment and cold-work. During this reporting period, we studied the textures of full-scale samples: a standard induction sample, two cold-worked samples, and two phase III samples. Among them the measurements of the two cold-worked samples were completed. The pole figures, as given in figure 1, showed clear fiber-texture with the slip system similar to small-scale, 70% swaged samples studied previously. Assuming that the orientation distributions are ideal fiber-textures, the two-dimensional pole-figures were converted to a one-dimensional χ-angular distribution by circular averaging of the intensities at each χ-angle. There are two important parameters in the texture analysis: a slip system (fiber-axes here) and a degree of texture. The degree of texture may be expressed by the weighted sum of the pole-density variation

from the complete random density. For fiber texture, it can be calculated from χ-angular distribution:

$$\text{degree of texture} = [\Delta_{90}+\Sigma(72\cos(\chi_i)\Delta_i))/(1+\Sigma(72\cos(\chi_i)]$$

where, Δ_i refers to the deviation at χ_i, the number 72 corresponds to the number of ϕ-angles in each χ-angle. The degree of texture as defined above depends heavily on the number of peaks and the peak positions in the the chi-angular distribution function. Therefore, its usage should be limited to comparison between the same (hkl) poles. The degree of texture obtained for the full-size samples were compared with those of the small-scale laboratory samples in table 1. The (111) pole distribution is least sensitive to the degree of texture because of the evenly spaced peak positions. The degree of texture of the others in the table shows a close correlation with the degree of cold-work of the sample.

2. Texture of a magnetically oriented $HoBa_2Cu_3O_7$ superconductor

Several rare earth-Ba-CuO high temperature superconductor materials were made by Claudia Orstertag in the Ceramic Division, by applying high magnetic field. The orientation distribution of one of the samples, Ho-Ba-CuO, was determined by interpretation of neutron diffraction patterns and pole figures. Two diffraction patterns, one with the scattering vector parallel and the other perpendicular to the direction of the applied magnetic field, were measured. It was clear from the diffraction profiles that the sample was heavily textured with the crystallographic c-axis parallel to the applied field direction. The details of the orientation distributions were attained by the pole figure measurements as shown in figure 2. Since the diffraction peaks of (003), (100), and (010) are overlapping, the 003 pole figure contains 100 and 010 distributions. The figure shows that 001 poles have a one-dimensional distribution (along the north-south direction in the figure) and 100 and 010 poles have a two-dimensional distribution (in the plane perpendicular to the N-S direction). The pole density distributions along the equator could be described reasonably well with a Lorentzian function (FWHM = 33(1)°), as shown in figure 3.

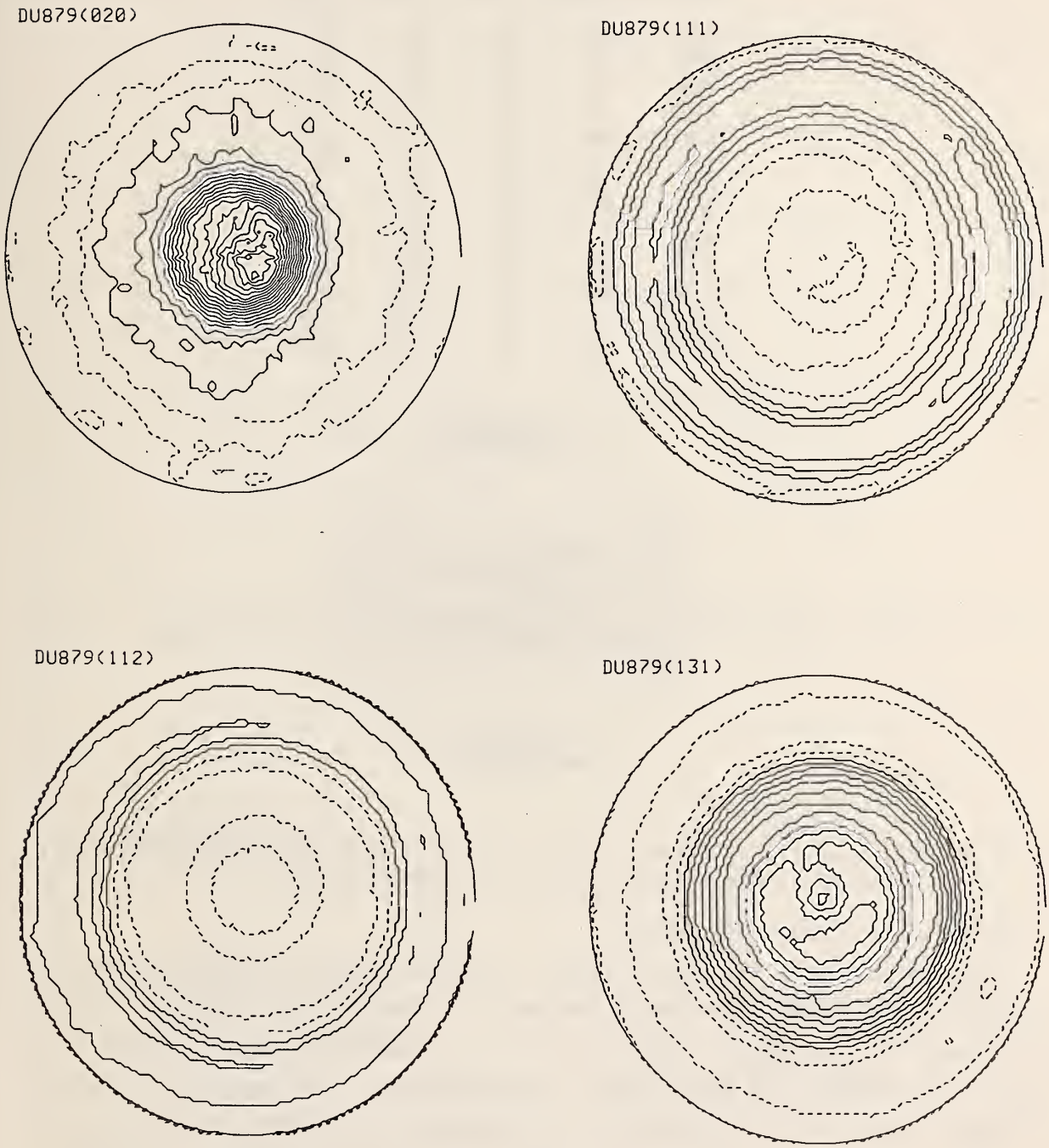

Figure 1. The pole figures of one of the two full scale DU samples. The contour levels equal or higher than 1 m.r.d. (multiples of a random distribution) are given by solid and lower than 1 by dotted lines. The contour intervals are 0.4 m.r.d. for 020 pole figure, and 0.2 m.r.d. for all the others.

Table 1. The Degree of Texture

Sample	(010)	(111)	(112)	(131)
30A	.59	.18	.22	.21
40A	.72	.18	.28	.29
60A	.67	.25	.35	.39
60B	.77	.24	.33	.42
60D	.86	.25	.36	.42
60E	.71	.28	.37	.40
60F	.88	.26	.37	.46
60G	.71	.26	.35	.40
60H	.76	.29	.36	.39
70A	.98	.29	.43	.57
70B	1.03	.27	.39	.60
879D	.93	.32	.39	.56
892A	.96	.37	.38	.58

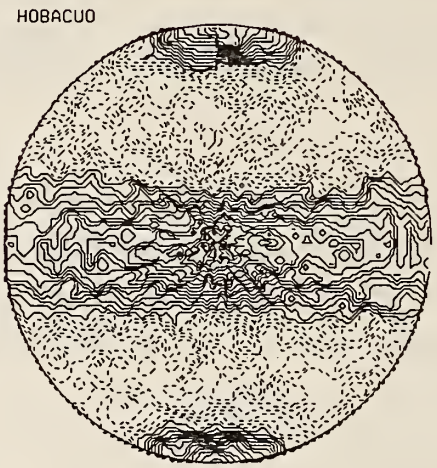

Figure 2. 003 pole figure (containing 100 and 010) of the magnetically oriented sample with 0.1 m.r.d. contour interval.

3. Pole Figure Standard Project

The purpose of the pole figure standard project is to determine the limitations of various experimental methods. A fine-grained limestone, $CaCO_3$, was chosen as a standard sample since its diffraction pattern includes many closely spaced peaks and weak peaks. The sample was experimentally deformed in pure shear at T = 400 °C , P = 100 MPa, $\dot{\epsilon} = 3.6 \times 10^{-7} s^{-1}$, to a strain $\epsilon_1 = 35\%$, $\epsilon_2 = -3\%$, $\epsilon_3 = -36\%$. Crystal data are, trigonal $R\bar{3}2/m$, a = 4.989 Å, c = 17.061 Å. The 012, 104, 006, 110, 113, 202, 108 and 116 pole figures were measured. Among them, 108 and 116 diffraction peaks overlapped because of instrumental resolution and occurred as a distorted peak in the diffraction pattern. A visual inspection of all the pole figures showed excellent

agreement with those of other laboratories: ILL, Jülich and Geesthacht. The two pole-figures, 108 and 116, are shown in figure 4.

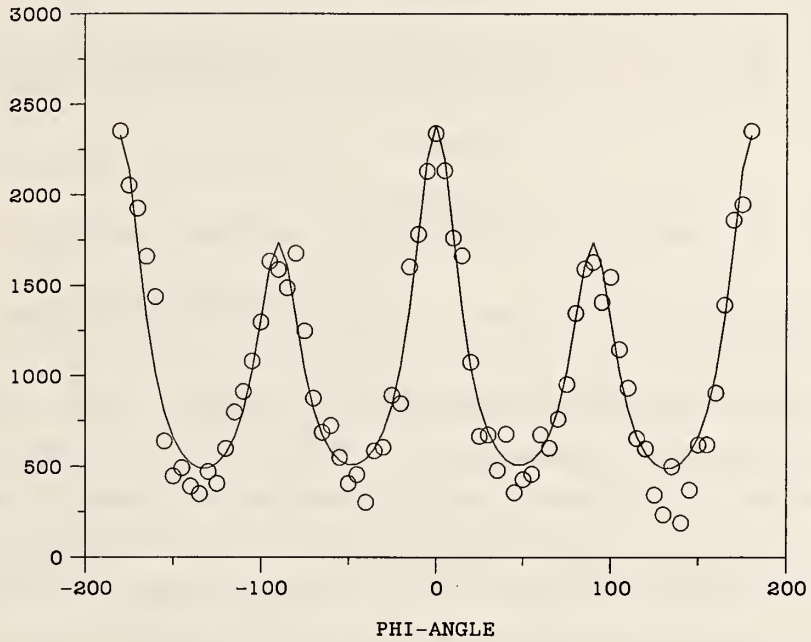

Figure 3. The equatorial distribution of 003 and 100/010 pole density of the magnetically oriented sample with 0.001 m.r.d. unit.

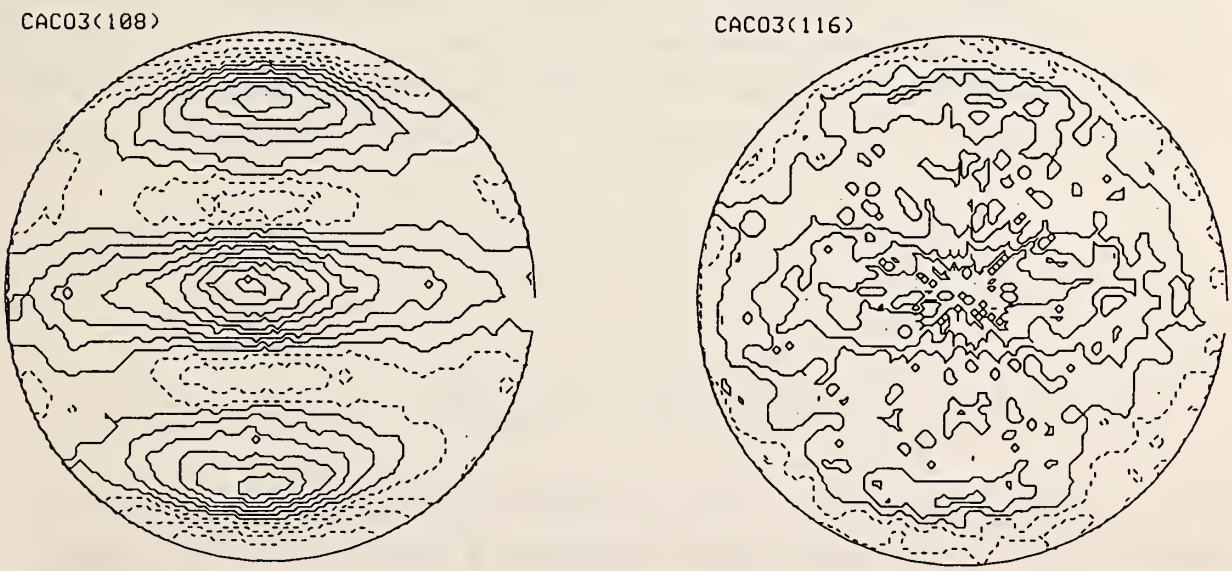

Figure 4. 108 and 116 pole figure of the standard sample ($CaCO_3$), with 0.1 m.r.d. contour interval.

A MAXIMUM-ENTROPY DENSITY DISTRIBUTION THAT FITS AN ARBITRARILY LARGE SET OF FOURIER AMPLITUDES

E. Prince

D. M. Collins
(Laboratory for the Structure of Matter, Naval Research Laboratory)

and

L. Sjölin
(Chalmers University of Technology, Göteborg, Sweden)

In crystallography, as in a number of branches of physics, the observable quantities are related to the Fourier transform of some density distribution, and the problem is to infer what that distribution looks like. Because the Fourier transform can only be measured in a finite region of reciprocal space, the data are inherently incomplete, and the problem is underdetermined. If the density distribution is everywhere nonnegative, the principle of maximum entropy provides a powerful criterion for deciding which of the possibly infinite set of distributions that satisfy the observations is, in some sense, the best one. Although the solution is conceptually simple, application of the principle to practical problems has come slowly because the process of finding the maximum entropy distribution for a large object with a large data set appeared to be formidable. We have developed a procedure for finding the maximum entropy distribution that is applicable to macromolecular structures with modest computing resources and reasonable times.

Consider a unit cell divided into $\underline{n}$ pixels, and let the mean density in the $\underline{k}$th pixel be $\rho_{\underline{k}}$. We wish to maximize

$$S(\rho) = -\sum_{\underline{k}=1}^{\underline{n}} \rho_{\underline{k}} \ln \rho_{\underline{k}}, \tag{1}$$

subject to

$$|F_{\underline{map}}| = (V/\underline{n}) \left| \sum_{\underline{k}=1}^{\underline{n}} \rho_{\underline{k}} \exp(2\pi i \mathbf{h}_{\underline{j}} \cdot \mathbf{r}_{\underline{k}}) \right| = |F_{\underline{obs}}(\mathbf{h}_{\underline{j}})| \tag{2}$$

for a set of $\underline{m}$ reflections. This is a constrained optimization problem in $\underline{n}$ dimensions, and, for a macromolecular structure, $\underline{n}$ can be a very large number. It can be shown, however, that the constrained maximum of $S(\rho)$ is equal to the unconstrained minimum of

$$\Phi(\mathbf{x}) = -\sum_{\underline{k}=1}^{\underline{n}} \rho'_{\underline{k}}(\mathbf{x}) \ln \rho'_{\underline{k}}(\mathbf{x}) + \sum_{\underline{j}=1}^{\underline{m}} [|F_{\underline{map}}(\mathbf{h}_{\underline{j}})| - |F_{\underline{obs}}(\mathbf{h}_{\underline{j}})|], \tag{3}$$

where

$$\rho'_{\underline{k}}(\mathbf{x}) = \exp[\sum_{\underline{j}=1}^{\underline{m}} \underline{x}_{\underline{j}} \cos(2\pi \mathbf{h}_{\underline{j}} \cdot \mathbf{r}_{\underline{k}} - \phi_{\underline{j}})], \tag{4}$$

which is the value of $\rho_{\underline{k}}$ for which

$$-\rho_{\underline{k}} \ln \rho_{\underline{k}} + \sum_{\underline{j}=1}^{\underline{m}} \underline{x}_{\underline{j}} \cos(2\pi \mathbf{h}_{\underline{j}} \cdot \mathbf{r}_{\underline{k}} - \phi_{\underline{j}}) \tag{5}$$

is maximum for a given $\mathbf{x}$. Here $\phi_{\underline{j}}$ is the best previously available estimate of the phase of $F(\mathbf{h}_{\underline{j}})$. Finding the minimum of $\Phi(\mathbf{x})$ is an unconstrained optimization in $\underline{m}$ dimensions, where $\underline{m}$ is, in general, very much less than $\underline{n}$. The phase of $F_{\underline{map}}(\mathbf{h}_{\underline{j}})$ becomes a better estimate of $\phi_{\underline{j}}$.

Because the Fourier transform of $\rho(\mathbf{r})$ is a linear function of $\rho(\mathbf{r})$, $\Phi(\mathbf{x})$ can be shown to be everywhere convex, and it must have a unique minimum. Many of the modern techniques for nonlinear optimization are applicable. Preliminary studies using a quasi-Newton type algorithm on a problem with 560000 pixels and 21 reflections gave an estimate of running time, on a Microvax computer, of 3 minutes per 100000 pixels per reflection. Obvious modifications to the code should reduce that time by at least a factor of ten and possibly as much as a hundred. It remains to be determined how large an initial set of phases, $\phi_{\underline{j}}$, must be for phases to be extended by maximum entropy to an acceptable structure.

D-SPACING/FORMULA INDEX FOR PHASE IDENTIFICATION BY ELECTRON, NEUTRON OR X-RAY DIFFRACTION

V. L. Himes, A. D. Mighell, and J. K. Stalick

The NBS/Sandia/ICDD Electron Diffraction Database is a new computerized Standard Reference Database designed for phase characterization by electron, neutron or x-ray diffraction methods. The Database and associated software [1] permit highly selective identification procedures for microscopic as well as macroscopic crystalline materials. The Database and software are available to the scientific community on magnetic tape. A subset of the data will be made available as a printed D-Spacing/Formula INDEX. Work on the INDEX was carried out in collaboration with the Sandia National Laboratories and the International Centre for Diffraction Data.

The Electron Diffraction Database, containing approximately 71,000 entries, was derived from two well-known Databases -- NBS CRYSTAL DATA [2] and the PDF-2 [3]. The database contains chemical, physical and crystallographic information on a wide variety of materials including minerals, metals, intermetallics and general inorganic compounds. It is comprehensive as numeric and factual data have been taken from over 1200 journals. All of the data have been critically evaluated and transformed to standard forms with NBS*AIDS83 [4] which is a database building and evaluation program. In addition, essential derivative data have been calculated.

The Electron Diffraction Database has been designed to include all the data required to identify materials using computerized d-spacing/formula matching techniques. The data for each entry include: the conventional cell, reduced cell, lattice type, space group, calculated or observed d-spacings, chemical name, chemical and empirical formulas, materials class indicators, references and other parameters. To permit selective d-spacing/formula matching procedures, all the required d-spacings for each material are explicitly stored in the Database. Thus in each entry, there are up to 60 interplanar spacings including all the largest d-spacings (low two theta) that are most diagnostic for identification purposes. The d-spacings are either calculated (approximately 86%) or observed. For those cases in which the cell is known, the d-spacings were systematically calculated starting with the largest d-values and ending at the cutoff value of 0.83 Å. Known space group and centering data were used to eliminate d-spacings corresponding to

geometrically extinct reflections. For those cases in which the cell is unknown, observed d-spacings were used.

The printed INDEX was derived from the comprehensive Database. It contains a critical subset of the data necessary for identification and is designed to be used independently of or in conjunction with the computer database. For each compound, the INDEX contains one line of data which includes: up to four "high Z" elements (Z > 10) in alphabetical order; up to two "low Z" elements (Z < 11) in alphabetical order; the first ten low-angle d-spacings rounded to three significant figures; the chemical formula; the first two symbols of Pearson's code; the first Crystal Data Determinative Ratio; the unique PDF and CD numbers. These unique pointers permit the experimentalist to obtain additional information for a compound in NBS CRYSTAL DATA and in the Powder Diffraction File which are available on magnetic tape and on CD-ROM. A more detailed description of the data is given in "NBS*AIDS83: A Manual Describing the Data Formats used in NBS*AIDS83" [5]. The total number of entries in the INDEX is less than the computer version of the Electron Diffraction Database. The latter permits multiple entries with the same chemical and d-spacing information but different in other respects such as the reference to the original literature. To save space, only the entry with the latest reference is kept in the printed INDEX.

The INDEX is arranged so that the experimentalist can readily identify a material with the chemical and diffraction data routinely collected in the analytical laboratory. The INDEX is organized as follows: 1) the primary sort is an alphabetical sort on the "high Z" elements that are present in the chemical formula; 2) the secondary sort is on ascending magnitude of the d-spacings; and 3) compounds without any "high Z" elements are at the end of the INDEX and are sorted only on ascending magnitude of the d-spacings. The "high Z" elements in the INDEX correspond to those that can routinely be observed in x-ray Energy Dispersive Spectra (EDS) commonly taken in the analytical laboratory. To prepare the primary sort key, the "high Z" elements were extracted from the chemical formula and alphabetized. If there were greater than four different elements of this type in the formula, only the first four in ascending order were included in the sort key.

The D-Spacing/Formula INDEX will prove a practical tool for electron diffractionists because the experimental data obtainable from the analytical electron microscope (AEM) is precisely that required to reliably identify and

characterize unknown phases. Extensive experience with online searching of NBS CRYSTAL DATA [6] and the results of an EMSA-JCPDS Electron Diffraction Practices Questionnaire [7] show that search/match procedures based on chemistry and calculated d-spacings (fig. 1) are extremely reliable. A knowledge of elements present and absent in an unknown is usually sufficient to give a limited set of potential candidates when searching the entire database. (For example, if it is known from qualitative EDS chemistry that an unknown contains the elements Cr, Fe, and Ni only those elements, then a search of the database yields only three potential compounds.) Likewise experience has shown that a knowledge of low-angle d-spacings is highly diagnostic. Matching these d-spacings of an unknown against the Database also yields a limited answer set. Consequently, when these two sets (D-spacings and formulas) are intersected, the experimentalist usually obtains a relatively short, but complete, list of all compounds that could cause the observed experimental data. Due to the quantity and quality of the reference data available in the INDEX, the d-spacings/formula method can routinely be used for compound identification in the analytical laboratory.

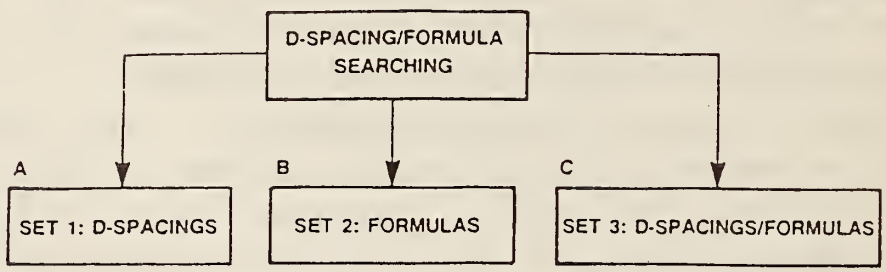

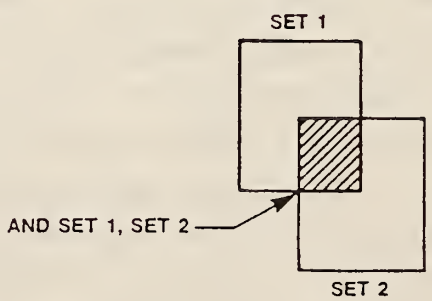

A. SET 1 = The set of compounds resulting from the d-spacing search.
B. SET 2 = The set of compounds resulting from the formula search.
C. SET 3 = AND SET 1, SET 2 = the compounds in the Electron Diffraction Database that have the same or related d-spacings/formulas as the unknown.

Figure 1. Identification by d-spacing/formula matching.

References

[1] M. J. Carr, W. F. Chambers, D. K. Melgaard, V. L. Himes, J. K. Stalick, and A. D. Mighell, NBS/Sandia/ICDD Electron Diffraction Database (1987); Sandia Report, SAND87-1992, UC-13, Sandia National Laboratories, Albuquerque, NM 87185.

[2] NBS CRYSTAL DATA (1987). A magnetic tape of chemical, physical and crystallographic data compiled and evaluated by the NBS Crystal Data Center, National Bureau of Standards, Gaithersburg, MD 20899.

[3] PDF-2. A magnetic tape of chemical, crystallographic and x-ray powder data compiled and evaluated by the JCPDS--International Centre for Diffraction Data, Swarthmore, PA 19081.

[4] NBS*AIDS80: A FORTRAN Program for Crystallographic Data Evaluation. A. D. Mighell, C. R. Hubbard, and J. K. Stalick, Natl. Bur. Stand. (U.S.). Tech. Note 1141 (1981); NBS*AIDS83 is an expanded version of NBS*AIDS80. A copy of the program for research applications may be obtained by writing the NBS Crystal Data Center.

[5] NBS*AIDS83: A manual describing the data formats used in NBS*AIDS83. This manual (1987) contains a detailed description of the data items in the Powder Diffraction File and in NBS Crystal DATA. It may be obtained from the JCPDS--International Centre for Powder Diffraction Data or from the NBS Crystal Data Center.

[6] CRYSTDAT (1987). An online search, retrieval and analysis system for NBS CRYSTAL DATA developed jointly by the National Research Council of Canada and the National Bureau of Standards.

[7] A Max-D Alphabetic Index to the JCPDS Database. R. Anderson and G. G. Johnson, Jr., EMSA Bull. 8, No. 1 (1979); and the Proceedings of the 1979 EMSA Meeting.

GRAZING INCIDENCE NEUTRON DIFFRACTION FROM Si(110)

J. F. Ankner and H. Zabel
(University of Illinois, Urbana, IL)

and

D. A. Neumann and C. F. Majkrzak

During the past decade, there has been a great deal of interest in the properties of surfaces and a corresponding development of surface-sensitive experimental techniques. Of these techniques, surface x-ray diffraction using glancing incidence has proven to be particularly useful because of two important facts. For one, the interaction of x-rays with matter is weak, allowing comparatively simple structure factor calculations. Secondly, grazing incidence x-ray diffraction is the only probe providing surface as well as substrate information within the same experimental setting: the depth of penetration of the x-rays into the surface can be controlled by varying the incident grazing angle ϕ below the critical angle for total external reflection ϕ_c. Neutrons possess both of these virtues and their sensitivity to light adsorbates and magnetic structures qualifies them as an ideal complement to x-rays. Unfortunately, neutron fluxes are considerably smaller than the x-ray fluxes available at synchrotrons, which has prevented a parallel development of neutron and x-ray grazing-incidence diffraction techniques. However neutron fluxes are large enough to observe surface diffracted beams. To demonstrate this fact, we have performed the first surface neutron diffraction experiment using grazing incidence.

The geometry for grazing incidence diffraction is shown in figure 1. A beam of neutrons of wave-vector $\vec{k}$ strikes the (110) surface of a perfect Si crystal at a glancing angle ϕ and undergoes specular reflection ($\vec{k}_s$). The sample is oriented such that $\vec{k}$ satisfies the transmission diffraction condition for the $(1\bar{1}1)$ reflection in the plane of the surface. The diffracted beam then reflects from the crystal surface with wave-vector $\vec{k}_G$ and angle ϕ_G. Under glancing incident angle conditions, the transmitted beam intensities decay exponentially into the bulk, so only the topmost layers of the crystal interact with the neutrons.

The experimental arrangement is shown in figure 2. A 4.43 Å beam of neutrons ($\Delta\lambda/\lambda = 0.008$), collimated to 0.3 mrad by a pair of Cd slits, struck the (110) face of a Si crystal at glancing angle ϕ. This wavelength was

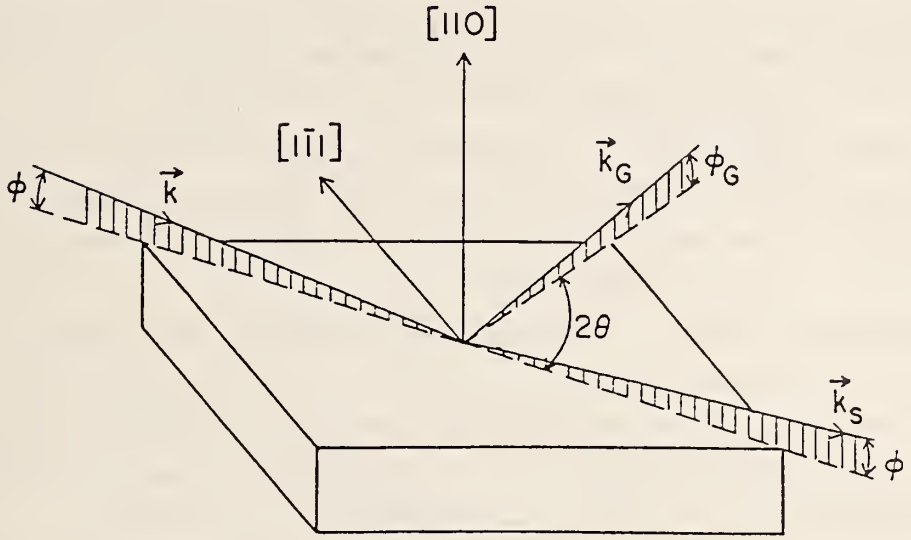

Figure 1. Grazing incidence diffraction geometry. $\vec{k}$, $\vec{k}_S$, and $\vec{k}_G$ are the initial, reflected and reflected-diffracted wave-vectors, respectively.

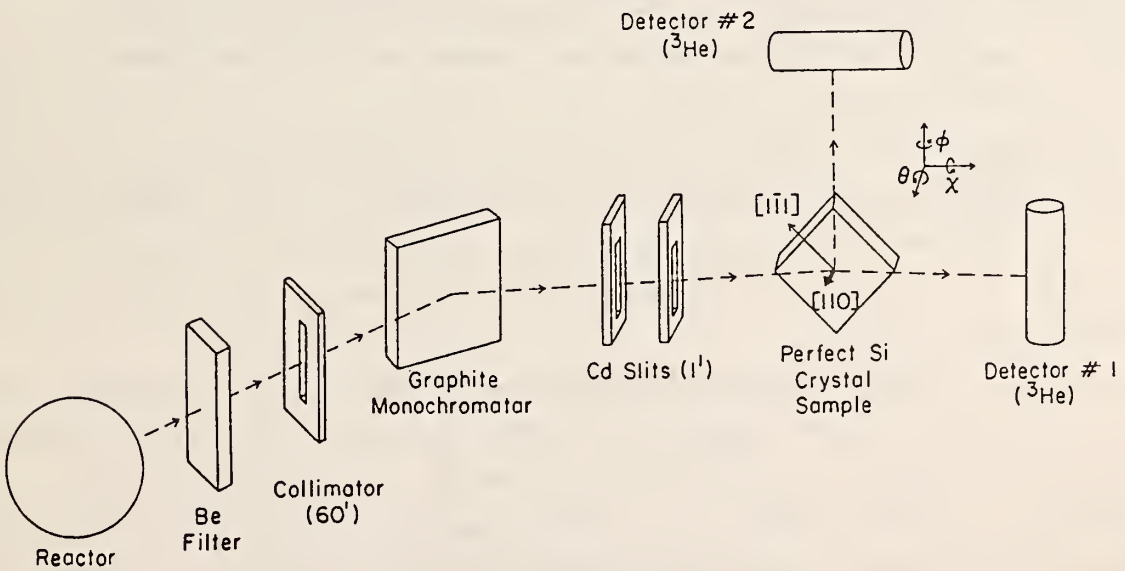

Figure 2. Experimental arrangement. The beam was collimated to 1′ by the Cd slits.

chosen for two reasons. The first was that a long wavelength produces a large critical angle (3.6 mrad for Si at 4.43 Å), which allows one to relax the collimation for the glancing angle ϕ and thereby increase the intensity. Secondly, λ = 4.43 Å is the wavelength for which the Bragg angle of the Si($1\bar{1}1$) diffracted beam is 45°, which is convenient because the diffracted beam detector could then be mounted directly above the sample. The specularly reflected incident beam intensity was recorded by the conventional triple-axis detector (detector #1) simultaneously with that of the reflected-diffracted beam (detector #2). The sample was a perfect Si crystal of dimensions 2.75" × 2.8" × 0.5" with a syton polished (110) face.

The data shown in figure 3 were obtained by scanning the incident angle ϕ through the critical angle ϕ_c with angles θ and χ set to satisfy the diffraction condition. Since the beam was broad by dynamical diffraction standards, only a small fraction of the incident intensity was diffracted and therefore the specularly reflected beam intensity may be treated as a simple specular reflection (the one beam approximation). The specularly reflected beam intensity (plotted as squares in figure 3) has therefore been fit with a modified Fresnel function [1]. The reflected-diffracted beam for the same scan is shown as the open circles in figure 3. Detector #2 was left wide open and so performed an integration of the intensity distribution over the diffracted beam exit angle ϕ_G. The reflected-diffracted intensity rises to a maximum near ϕ_c^d as the evanescent wave penetrates into the sample and then dies out above the critical angle as the intensity is transmitted to the transmitted-diffracted beam. The reflected diffracted beam was fit using the two-beam approximation of dynamical diffraction theory and the result is shown as a solid line. The good correspondence conclusively demonstrates the existence of a Si($1\bar{1}1$) reflected-diffracted beam excited under grazing incidence conditions.

The development of grazing-incidence neutron diffraction techniques opens up a wide variety of experimental studies in surface and interface physics which are difficult or impossible to perform using other methods. In particular, neutron studies of surface magnetic structures, magnetic thin films and interfaces, and low atomic number adsorbates and films promise to be very fruitful lines of future research due to the insensitivity of x-rays to these systems and the difficulty of quantitative analysis and lack of depth-specific information of electron and ion diffraction techniques. The present

work has resulted in the first observation of a reflected-diffracted neutron beam under grazing-incidence conditions and demonstrates the feasibility of this technique to these and other surface and interface problems.

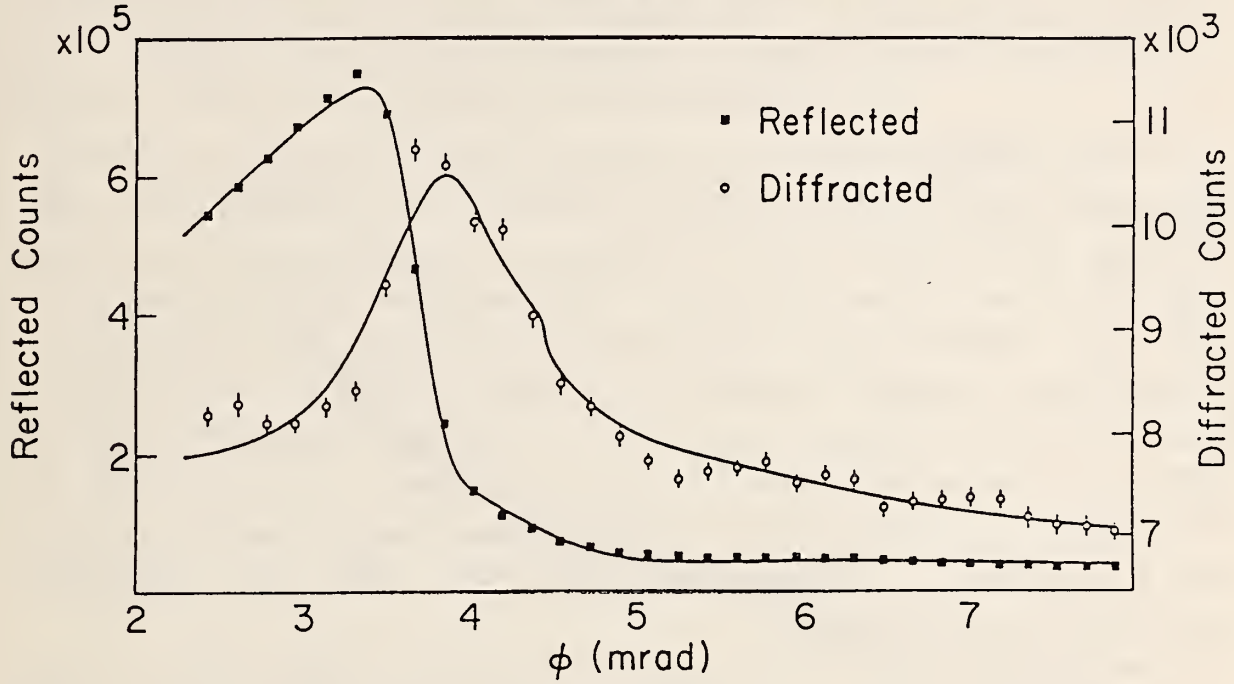

Figure 3. Data fit using the dynamical theory of neutron diffraction. The specularly reflected beam is shown as squares, while the reflected diffracted beam is indicated by circles. This result conclusively demonstrates the existence of a reflected-diffracted beam.

References

[1] M. Born and E. Wolf, Principles of Optics, 6th ed., Pergamon Press, Oxford (1970).

SURFACE ORDERING AND LAMELLAR FORMATION IN DIBLOCK COPOLYMERS

S. H. Anastasiadis and T. P. Russell
(IBM Alamaden Research Center, San Jose, CA)

and

S. K. Satija and C. F. Majkrzak

Block copolymers are one of the most interesting classes of synthetic high-polymer materials which have great potential for speciality and high-technology applications [1]. For example, block copolymers are increasingly being used in applications such as thin films, adhesives and surfactants. A fundamental understanding of their surface phenomena is therefore essential. The technique of neutron reflectometry is ideally suited for the study of polymer surfaces where one can utilize selective deuterium labelling to highlight scattering from specific parts of the polymer. In this report we give results of recent neutron reflectivity measurements from thin films of diblock copolymer of hydrogenated polystyrene (PSH) and deuterated polymethylmethacrylate (DPMMA).

The diblock copolymer with a molecular weight M_W = 30,000 (15 for PSH and 15 K for DPMMA) was dissolved in toluene (~ 3g/100cc). The polymer solution was spin coated onto a highly polished fused silica block (3" x 1" x 1/2"). The specimen was then placed in vacuum to remove any residual solvent in the polymer film.

Figure 1 shows the neutron reflectivity measured from the sample. The filled diamonds is the data from the as cast film. This profile can be well represented by a calculated profile from a smooth homogeneous 1150 Å film of the block copolymer. The open diamonds are the data after the sample was annealed at 178 °C for 16 hours. The dramatic change in the reflectivity profile is due to reorientation of lamellar morphology parallel to the film surface [2,3]. The peak in reflectivity at Q = .04 $Å^{-1}$ can be thought of as a Bragg peak from the highly ordered lamellae with a repeat distance of 175 Å. Preliminary fits to the data show that the reflectivity profile of the annealed sample can be fit to a periodic varying density profile throughout the thickness of the film, starting with PSH at the top of the film. A more stringent fit to the data will help in better determining the interfacial thickness and interfacial profiles between A and B blocks of the copolymer.

The oscillatory composition profiles in diblock copolymers near the free surface have been recently predicted [3]. These interesting profiles occur due to the connectivity of blocks and because the surface modifies the Flory interaction parameter and the chemical potential in the adjacent copolymer layer. More detailed studies of dependence of lamellae formation on molecular weight and temperature are being conducted presently.

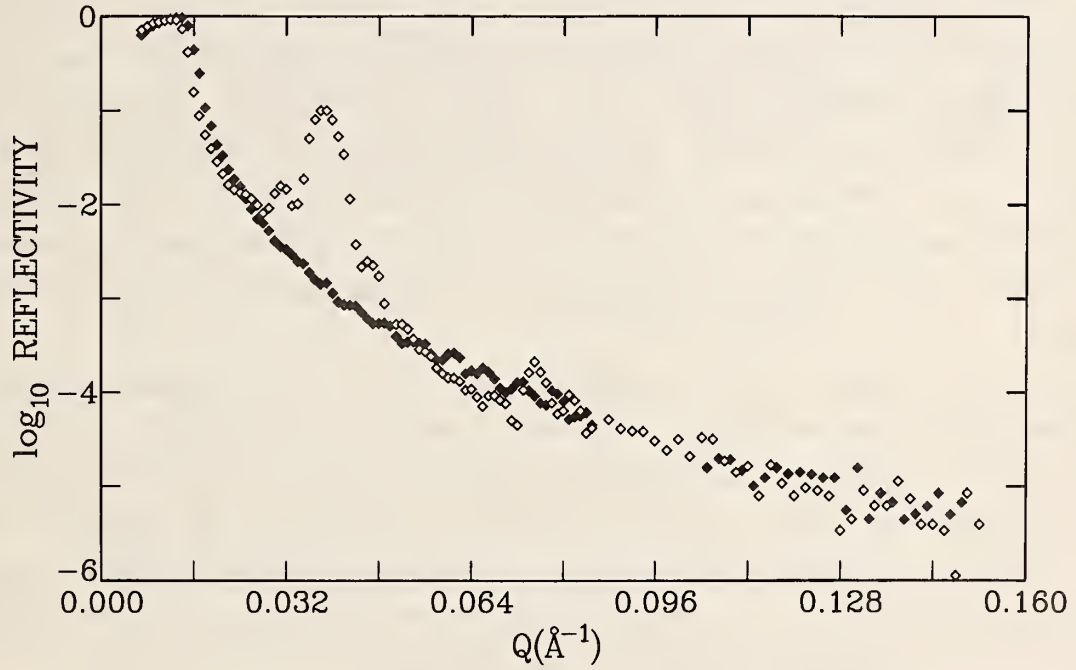

Figure 1. The filled diamonds are the neutron reflectivity from as cast film of PSH-DPMMA. The open diamonds represent the reflectivity from the same sample after annealing at 178 °C for 18 hours.

References

[1] Processing, Structure and Properties of Block Copolymers; M. J. Folkes, Ed.; Elsevier, New York,(1985).

[2] H. Hasegawa and T. Hashimoto, Macromolecules 18, 589 (1985).

[3] G. H. Fredrickson, Macromolecules 20, 2535 (1987).

THE SIGNIFICANCE OF MULTIPLE SCATTERING IN THE INTERPRETATION OF SMALL ANGLE NEUTRON SCATTERING EXPERIMENTS

J. R. D. Copley
(University of Maryland and the National Bureau of Standards)

The multiple scattering of neutrons in small angle neutron scattering experiments has been studied using the technique of Monte Carlo simulation [1]. This technique is in general more versatile than analytic techniques, in that there is (at least in principle) virtually no limit to the complexity of the sample geometry and/or the sample's differential scattering cross section. Complications such as inelastic scattering, the scattering from a container, and effects due to instrumental resolution, may also be included. On the other hand analytic calculations are essentially exact and they proceed much faster, but in general a new computer program must be written for each problem.

As a test (and demonstration) of the Monte Carlo approach we have calculated single and multiple scattering intensities for strongly scattering samples of a system of monodisperse spheres in vacuo: our results are in excellent agreement with the semi-analytic calculations of Schelten and Schmatz [2] over a wide range of values of the dimensionless parameter $\sigma_P \rho_N z$, where σ_P is the total scattering cross section per particle, ρ_N is the number density of particles, and z is the sample thickness.

The scattering by systems of monodisperse spheres embedded in a medium has also been studied: the scattering cross section and number density of the medium were chosen to represent light water. Simulations were run for 1 mm thick samples with volume fractions f in the range from 0.01 to 0.20, and an "empty" run on the pure medium was also performed. The standard procedure for subtraction of the scattering by the medium, which involves normalization of the "empty" run using the factor $(1-f)T_S/T_M$, where T_S and T_M are the transmissions of the sample and the medium respectively, slightly over-subtracts the multiple scattering due to the medium alone, since this scattering scales with a higher power of (1-f) than the single scattering. This is shown in figure 1, which also illustrates the magnitude of the multiple scattering correction remaining after subtraction of the scattering by the medium.

In view of its importance as a normalization standard which is frequently used in small angle scattering experiments, we have attempted to calculate

single and multiple scattering intensities in experiments on 1 mm thick samples of light water. The Egelstaff-Schofield kernel [3] was used to describe the double differential scattering cross section, using appropriately chosen parameters. We have computed the forward direction enhancement factor $g(\lambda)$, introduced by Jacrot [4] (p 937), and it is compared with experimental measurements [5,6] in figure 2. The lack of good agreement at the longer wavelengths is very possibly due to inadequacies in the model scattering function. The problem of determining (and understanding) the behavior of $g(\lambda)$ (as well as the angular dependence of the scattering at small angles) is widely recognized, and it is to be hoped that additional calculations and measurements will be undertaken in the future.

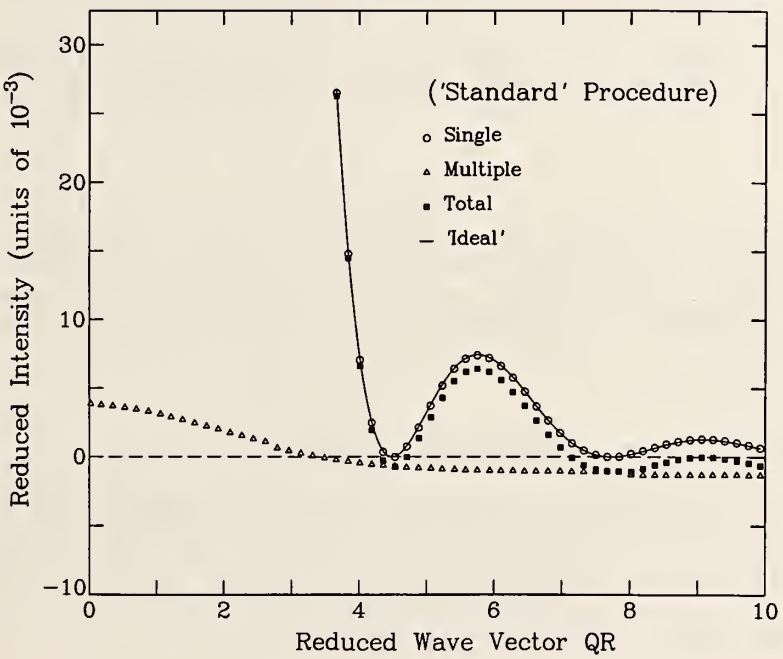

Figure 1. Corrected single, multiple, and total scattered intensities for a system of particles immersed in a medium, with a volume fraction of 10%. The "ideal" intensity (i.e., the normalized intensity of scattering by an infinitely thin sample) is shown as a solid line. The normalization of the intensities is such that the "ideal" intensity is unity at QR = 0.

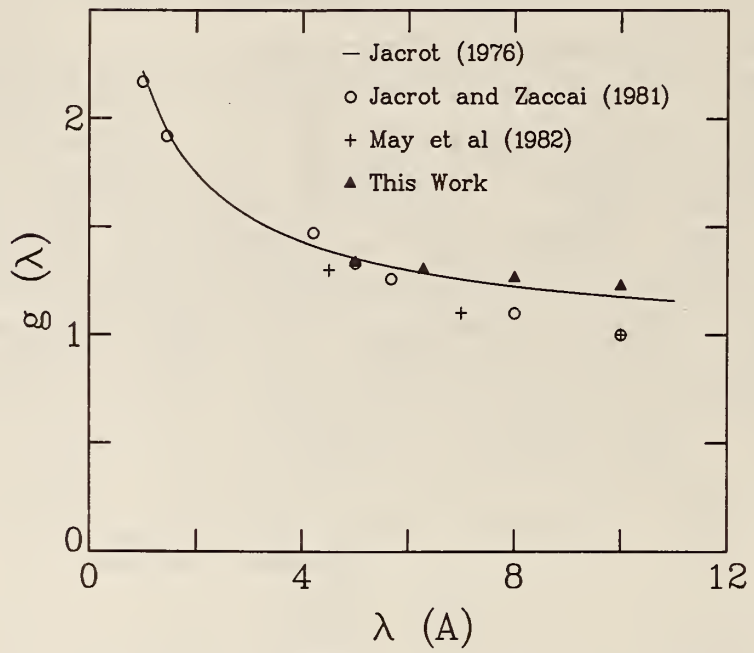

Figure 2. Calculated and measured values of the forward scattering enhancement factor $g(\lambda)$. The solid line is the function $[1 - \exp(-0.6\sqrt{\lambda})]^{-1}$ suggested by Jacrot (1976). The results of May et al. (1982) were normalized to unity at λ = 10 Å.

References

[1] J. R. D. Copley, J. Appl. Cryst. (in press).

[2] J. Schelten and W. Schmatz, J. Appl. Cryst. 13, 385-390 (1980).

[3] P. A. Egelstaff and P. Schofield, Nucl. Sci. Eng. 12, 260-270 (1962).

[4] B. Jacrot, Rep. Prog. Phys. 39, 911-953 (1976).

[5] B. Jacrot and G. Zaccai, Biopolymers 20, 2413-2426 (1981).

[6] R. P. May, K. Ibel, and J. Haas, J. Appl. Cryst. 15, 15-19 (1982).

MODEL BICONTINUOUS STRUCTURE WITH FRACTAL SURFACES

N. F. Berk

We have shown previously [1] that an algorithm originally invented by Cahn [2] to simulate morphology influenced by spinodal decomposition in isotropic two-phase systems can be adapted to the description of the scattering properties of microdispersed and microporous systems distinguished by a morphology with a well defined length scale, including microemulsions, controlled pore glasses, and polymer mixtures. Our generalization of Cahn's scheme associates an interface between two material phases of uniform densities with a level-set (contour) of a random standing wave, $S_N(\vec{r})$, composed of N sinusoids having isotropic random wavevectors, $\vec{k}$, with wavenumbers distributed according to density P(k), and with uniformly distributed phase constants, ϕ_n:

$$S_N(\vec{r}) = \frac{1}{N\langle A^2\rangle} \sum_{n=1}^{N} A_n \cos(k\hat{k}_n \cdot \vec{r} + \phi_n), \qquad (1)$$

where A_n are random amplitudes. The continuously connected space between level sets α and β is then given uniform density $\rho(\vec{r}) = \Theta_{\alpha\beta}[S_N(\vec{r})]$, where $\Theta_{\alpha\beta}(x) = 1$ for $x \epsilon (\alpha,\beta)$, zero otherwise.

If the wavenumber distribution P(k) has finite second moment, then it can be shown rigorously that the interfaces generated by the model are smooth and lead to classical Porod law scattering: $I(q) = 1/q^4$ as scattering wavenumber $q \to \infty$. However, if P(k) behaves asymptotically as

$$\lim_{k\to\infty} P(k) = 1/k^{1+2H}, \quad 0 < H < 1, \qquad (2)$$

(so that P(k) is normalizable but has no second moment) then it can be shown that the scattering intensity behaves asymptotically as

$$\lim_{q\to\infty} I(q) = 1/q^{3+H}, \qquad (3)$$

corresponding to a surface with fractal (self affine) dimension D = 3-H, with $2 < D < 3$. It is interesting that P(k) with property (2) is the power spectrum of a 1-dimensional Brownian process, $B_H(z)$. Numerical simulations

(H = 1/2, D = 5/2) of the interfaces reveal fractal-like visualizations consistent with this mathematical description.

References

[1] N. F. Berk, Phys. Rev. Lett., 58, 2718 (1987); see also R. W. Hopper, J. Non-Crystalline Solids 49, 263 (1982).

[2] J. W. Cahn, J. Chem. Phys. 42, 93 (1965).

PHASE SHIFT DEPENDENCE OF STRONG MULTIPLE SCATTERING

N. F. Berk

We have developed a new formulation [1] of the phase shift dependence of incoherent multiple scattering that extends our earlier work [2]. We find in the limit $\bar{z} >> 1$, where $\bar{z}$ is the sample thickness divided by the scattering mean free path, that the width, Δ, of the multiple scattering intensity satisfies the scaling relation,

$$\Delta_\beta(\bar{z}_\beta) = \beta(\nu)\Delta_1(\bar{z}_\beta), \tag{1}$$

where

$$\bar{z}_\beta = \bar{z}_1/\beta^2(\nu), \tag{2}$$

and

$$\bar{z}_1 = \frac{3}{2} z\phi\rho^2\lambda^2 R. \tag{3}$$

In (3), z is the thickness, ϕ is the scattering volume fraction, ρ is the scattering length density, λ is the incident beam wavelength, and R is the spherical particle radius. The function $\beta(\nu)$ in (2) is $\nu/[2\alpha(\nu)]^{1/2}$, where

$$\alpha(\nu) = 2\text{-}4(\nu\sin(\nu)+\cos(\nu)-1)/\nu^2, \tag{4}$$

and ν is the single particle scattering phase shift. If Δ_1 is proportional to $(\bar{z}_1)^{1/2}$, as in naive treatments of multiple scattering, then (1 and 2) indicate that the width of multiple scattering is independent of the phase shift, i.e., independent of the diffractive ($\nu << 1$) or refractive ($\nu >> 1$) nature of the underlying single particle scattering. In fact, Δ_1 contains

logarithmic corrections to the naive result stemming from the Porod law behavior of the single particle scattering, and it is these, alone, which effectively distinguish between the different phase shift regimes [1]. Thus, incoherent multiple scattering from thick samples tends to be insensitive to the cross-over from diffractive to refractive behavior.

References

[1] N. F. Berk and K. A. Hardman-Rhyne, J. Appl. Cryst. (1988) in press.

[2] N. F. Berk and K. A. Hardman-Rhyne, J. Appl. Cryst. 18, 467 (1985), Physica 136B, 218 (1986).

DYNAMICAL THEORY FOR THE SCATTERING OF POLARIZED NEUTRON BEAMS FROM MAGNETIC SPIRAL AND RELATED STRUCTURES

N. F. Berk and C. F. Majkrzak

We are involved in the study of polarized neutron scattering from magnetic spiral and multilayered structures using dynamical scattering theory. The investigation is motivated by increasing interest in a wide variety of possible applications of polarized beams to the study of magnetic systems and to the use of magnetic components in neutron scattering instrumentation. The neutron magnetic interaction with spiral structures depends on the chirality (handedness) of the spiral. Thus, while a spiral has no net magnetization, it can distinguish between up and down neutron spin states in an incident beam and scatter them differently. Spiral magnetic structures occur frequently in rare earth materials but usually without net chirality. However, MnSi, which has a noncentrosymmetric unit cell, is known to form domains favoring a single chirality. Alternatively, magnetic spirals can be synthesized as multilayers in which the magnetization, uniform over a single layer, rotates between successive layers. Such piecewise spirals also present the possibility of alternating the nonmagnetic nuclear interaction from layer to layer, so that interference between the chiral nuclear interaction and the spatially varying magnetic interaction may bias the conversion of one spin state into another.

Both continuous and multilayer magnetic spirals require solution of the coupled one-dimensional Schroedinger equations of the form,

$$\psi_+''(z) + (\tilde{Q}/2)^2\psi_+(z) - pe^{-i(Gz+\phi)}\psi_-(z) = 0$$

$$\psi_-''(z) + (\tilde{Q}/2)^2\psi_-(z) - pe^{+i(Gz+\phi)}\psi_+(z) = 0, \qquad (1)$$

where $\psi_{\pm}(z)$ represent the components of the neutron spinor wave function. The magnetic interaction with the spiral is given by the exponential terms, where p is the scattering length density of the magnetization, which lies in the x-y plane at angle ϕ from the x-axis, and G is the wavevector of the spiral along the z-axis. Also in (1), $\tilde{Q} = \sqrt{(Q^2 - 16\pi b)}$, where b is the uniform nuclear interaction, and $Q = 2\underline{k}\sin(\theta)$ is the neutron scattering vector for a beam of momentum $\underline{k}$, incident at glancing angle θ. The essential physical assumption in (1) is that G is small compared to crystalline reciprocal lattice vectors, so that b and p represent cell averages; then (1) is valid for values of Q satisfying the same criterion as G. From the formal solutions of (1) it is possible to construct a 4X4 transfer matrix $A(z_1,z_0)$ that connects the spinor and its first derivative at the incident surface, $z = z_0$, to its values at the exit surface, $z = z_1$:

$$\Psi(z_1) = A(z_1,z_0)\,\Psi(z_0), \qquad (2)$$

where Ψ is a four component column matrix. At $z = z_0$, Ψ defines the amplitudes for the incident and reflected spinor beams, while at $z = z_1$, it defines the amplitude of the transmitted spinor. For the multilayer spiral, (1) is solved for G = 0, corresponding to a uniform magnetic slab between z_1 and z_2. In that case $A(z_2,z_1)$ depends only on $z_2 - z_1$, and the solution for the multilayer of thickness T, composed of N slabs of thicknesses T_n, is represented by

$$\Psi(T) = A_N(T_N)\ldots A_1(T_1)\Psi(0). \qquad (3)$$

We have solved (1) analytically for arbitrary G and have obtained the transfer matrix. Analytical results for the reflection and transmission coefficients have been obtained for the continuous spiral, while a computer program to calculate (3) and its consequences has been developed for the multilayer. The dependence of the reflection and transmission properties of such model systems on interaction parameters and on the direction of the laboratory guide field (quantization axis) for various incident polarization states is being determined.

PHASE CONTRAST MATCHING IN LAMELLAR STRUCTURES COMPOSED OF MIXTURES OF LABELED AND UNLABELED BLOCK COPOLYMER FOR SMALL-ANGLE NEUTRON SCATTERING

Y. Matsushita, Y. Nakao, R. Saguchi, K. Mori,
H. Choshi, Y. Muroga, I. Noda, and M. Nagasawa
(Nagoya University, Nagoya, Japan)

and

T. Chang, C. J. Glinka, and C. C. Han

The conformation of a single polymer chain in bulk can be determined by measuring small-angle neutron scattering (SANS) from a random mixture of deuterium-labeled and unlabeled polymers with the same chain length at any mixing ratio. The same method is applicable for determining the conformation of a block chain of diblock copolymer even in a micro-domain structure if strong diffraction intensities from the micro-domain structure can be eliminated. Three methods were employed to eliminate the diffraction. In the first method a single-chain scattering function is obtained as the difference between the coherent scattering from a blend of labeled and unlabeled block copolymers and its corresponding unlabeled block copolymer. This method is straightforward, but it is difficult to obtain reliable data for a single-chain conformation [1] because the diffraction intensity due to the domain structure is much more intense than the single-chain scattering and also because identical domain structures are required for both specimens in order to compensate for the scattering due to the domain structure.

The second method utilizes the anisotropy of oriented micro-domain structures. Single-chain scattering from labeled and unlabeled blocks can be observed with minimum interference when the incident neutron beam is perpendicular to the lamellar surface because the diffraction from the lamellae is suppressed in this orientation. Hadziioannou et al. [2] and Hasegawa et al. [3] used this approach to investigate conformations of polystyrene block in a lamellar structure of styrene-isoprene copolymers. Since the orientation of lamellae was never perfect in any experiment, results of accurate block chain dimensions are also difficult to obtain.

In the third method, the diffraction is eliminated by matching the average scattering lengths between the two phases ("phase contrast matching") using random mixtures of labeled and unlabeled block chains. This method was first proposed for polymer blends by Jahshan and Summerfield [4] and subsequently extended to block copolymers by Koberstein [5]. In principle,

this is the best method, one should observe the single-chain scattering in a microdomain structure only if one can match the scattering length of A and B phases. However, this requires that $\beta_{AH} < \beta_B < \beta_{AD}$ (where β_{AH}, β_B and β_{AD} are scattering length of hydrogenated A chain, B chain and deuterated A chain respectively) and also a uniform distribution of deuterated block chain in the A phase.

Diblock copolymers of styrene and 2-vinylpyridine with narrow molecular weight distributions were used in this study to investigate the applicability of this method. Three labeled diblock copolymers with different molecular weights, two triblock copolymers with partially labeled styrene blocks, and their corresponding unlabeled copolymers used as partners in blends were employed as shown in table 1. Phase contrast ratio for 3 diblock copolymer samples are shown in figure 1 and for 2 triblock copolymer samples are shown in figure 2 together with theoretical predictions.

It is clear from figures 1 and 2 that phase contrast matching is successful for the samples with the low molecular weights (3.4×10^4 for the labeled portions) but not for the samples with the higher molecular weights (9.2 and 16.2×10^4) and the samples with partially deuterated blocks. We conclude that the mismatching is caused not only by non-uniform distribution of deuterated species along the direction perpendicular to the lamellae due to difference in positions and lengths of the labeled and unlabeled blocks but also by concentration fluctuations in mixtures of hydrogenated and deuterated polystyrenes in domains.

Table 1. Molecular characteristics of samples

	Sample Code	Mn_{-5} ($\chi 10^{-5}$)	Mw/Mn (GPC)	Cs[a]) (wt%)	Cd[b]) (%)
I	DP-33	0.34 0.66	1.07 1.04	49	100
	SP-33	0.37 0.63	1.10 1.03	50	0
II	DP-77	0.92 1.67	1.02 1.09	48	100
	SP-77	0.77 1.49	1.02 1.02	51	0
III	DP-15	1.62 2.80	1.05 1.10	47	100
	SP-15	1.19 2.43	1.01 1.06	48	0
IV	SPD-4	1.52 1.97 4.01	1.03 1.06 1.08	50	19.1
	SP-12	2.11 3.88	1.04 1.03	50	0
V	DSP-1	0.31 1.37 2.34	1.01 1.05 1.04	48	22.7
	SP-15	1.19 2.43	1.01 1.06	48	0

a) Cs are the total polystyrene content in the sample. Values for DP-33 and SP-33 are determined by pyrolysis gas chromatography, others are determined by elemental analysis.

b) Cd are the styrene-d8 content in the total polystyrene part.

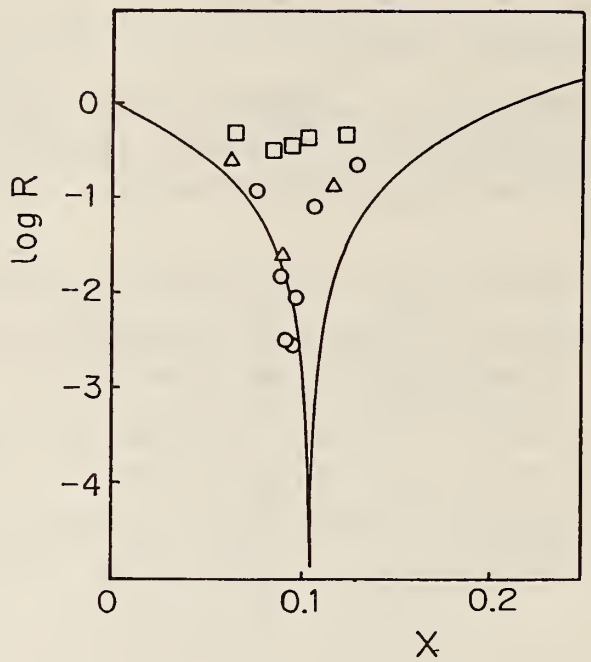

Figure 1. Variation of contrast factor R as a function of X, the volume fraction of deuterated polystyrene, on semilogarithmic scale. Solid line is the theoretical prediction. Open Circles - DP-33/SP-33, Open triangles - DP-77/SP-77, Open squares - DP-15/SP-15.

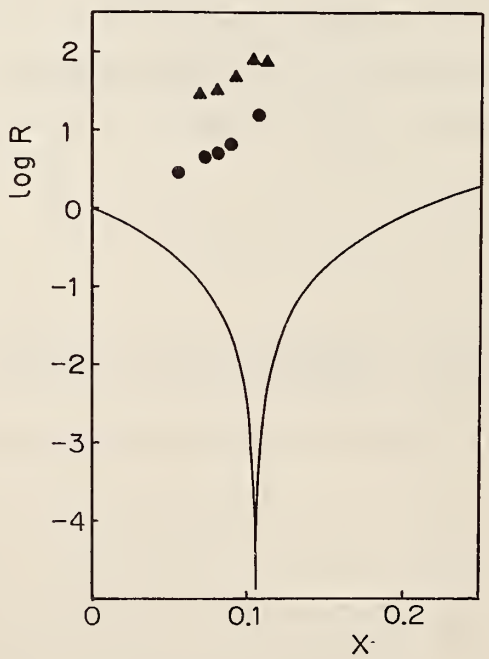

Figure 2. Variation of contrast factor R as a function of X on semilogarithmic scale. Solid Circles - SDP-4/SP-12, Solid squares - DSP-1/SP-15 and the solid line is the theoretical prediction.

References

[1] R. W. Richards and J. L. Thomason, Polym. 22, 581 (1981).

[2] G. Hadziiannou and A. Skoulios, Macromol. 15, 267 (1982).

[3] H. Hasegawa, T. Hashimoto, H. Kawai, T. P. Lodge, E. J. Amis, C. J. Glinka, and C. C. Han, Macromol. 18, 67 (1985).

[4] S. N. Jahshan and G. C. J. Summerfield, Polym. Sci., Polym. Phys. Ed. 18, 1859 (1980).

[5] J. T. J. Koberstein, Polym. Sci. I., Polym. Phys. Ed. 20, 593 (1982).

TEMPERATURE, COMPOSITION AND MOLECULAR WEIGHT DEPENDENCE OF BINARY INTERACTION PARAMETER OF POLYSTYRENE/POLY(VINYLMETHYLETHER) BLENDS

C. C. Han, B. J. Bauer, and J. C. Clark
(Polymers Division)

Y. Muroga and Y. Matsushita
(Nagoya University, Nagoya, Japan)

M. Okala
(Tokyo Institute of Technology, Tokyo, Japan)

Q. Tran-Cong
(Kyoto Institute of Technology, Kyoto, Japan)

and

T. Chang
(Korean Research Institute for Chemical Technology, Chungnam, Korea)

The technical importance of polymer blends has been well recognized in recent years [1]. Making polymers miscible through chemical structure modification is a very important topic, but miscibility may not be the ultimate characteristic one is looking for. This is because synergistic effects which enhance the property of a phase separated material mainly come from molecular alignment, reinforcement, phase domain size and morphology.

In order to understand and possibly control the domain sizes and morphology due to phase decomposition, one has to understand thermodynamics (statics) as well as phase separation kinetics (dynamics). We understand that statics and dynamics are inseparable subjects if we wish to talk about phase behavior of even a simple binary system. The most important quantity needed in both static and dynamic characterization is the free energy (of mixing) of

the system as a function of temperature and composition. For the case of polymer systems, we also need to know the molecular weight dependence of the free energy function.

Small angle neutron scattering (SANS) has been used [2-4] to measure the effective or scattering binary interaction parameter, X_{eff}, (for convenience, we will drop the subscript "effective" or "scattering" throughout this paper and define $X_{eff} = X_{scatt} = X$) for a deuterated polystyrene/poly(vinyl- methylether) (PSD/PVME) system. This technique offers a rather simple, fast and accurate method of obtaining the X parameter. Therefore, a systematic study of this X parameter as a function of composition (ϕ), temperature (T) and molecular weight (MW) is possible.

The extraction of the X parameter from SANS measurements depends on the mean¬field nature of the polymer system and the random phase approximation (RPA) calculation [5,6]. Nevertheless, within our measurement error, we have found this procedure quite satisfactory. Furthermore, we should point out that the parameter extracted from this procedure is different from the X_F-parameter in the Flory-Huggins free energy function as long as the X_F-parameter is allowed to be compositionally dependent. The exact origin of this compositional dependence of X_F is not certain, it could be caused by residual entropic effects of monomer size difference between the two components; by the local packing orientations; by the chain end effect; etc. [7-10]. We have allowed the X_F to be compositionally dependent which is different from the original definition of the Flory¬Huggins X-parameter. But, as long as the interaction between the two types of monomer can be described by a single q-independent potential function $U(\phi, T)$ at a given ϕ and T, the RPA calculation will provide a general scattering structure factor S(q), which allows the extraction of the effective interaction parameter, X, from the scattering experiment.

In this paper, we present a systematic study of the effective X parameter as a function of ϕ, T and MW for high molecular weight and narrow molecular weight distribution deuterated polystyrene/poly(vinylmethylether) systems by the SANS technique.

In figure 1, X/V_0 values are plotted against 1/T for a typical high molecular weight series sample at various compositions as indicated in the figure. At any given composition, the X/V_0 values follow the 1/T dependence as is clearly indicated by the straight lines in this figure. This is a

necessary condition if a polymer system does follow the mean-field behavior. Then, through the compositional dependence of X, the free energy function can be constructed following the calculation by Sanchez [11].

The calculated free energy curves at several temperatures for the H series are shown in figure 2 together with the corresponding spinodal curve and measured spinodal temperatures.

It is clear that the binary interaction parameter, X_F, can be obtained according to Sanchez theory and free energy function can be generated with an empirical functional form of the measured X/V_0. Spinodal temperatures and cloud point curves have been generated and compared with experimental values successfully.

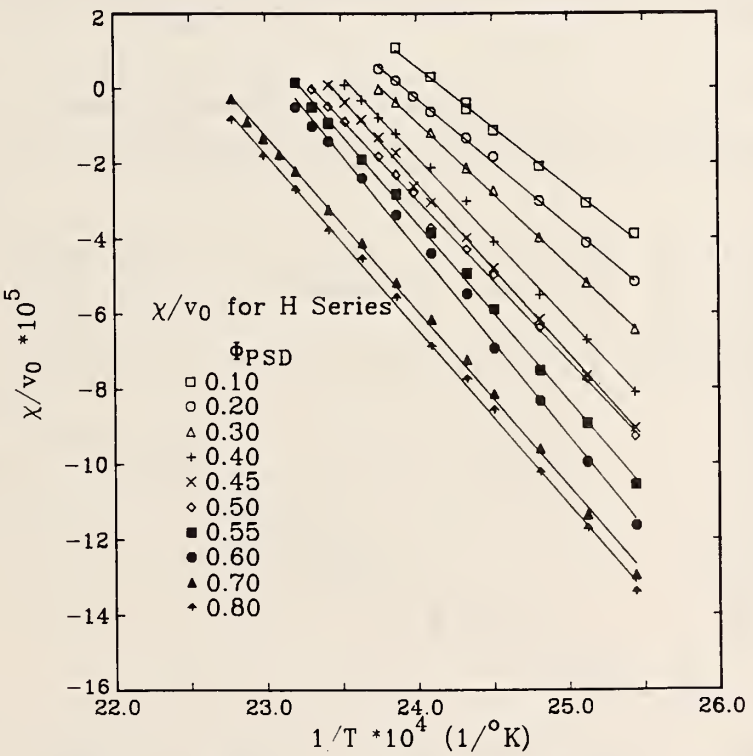

Figure 1. Reciprocal temperature dependence of X/V_0 for various composition of the H-series sample (MW of PSD = 593×10^3 and PVME = 1.1×10^6) is displayed.

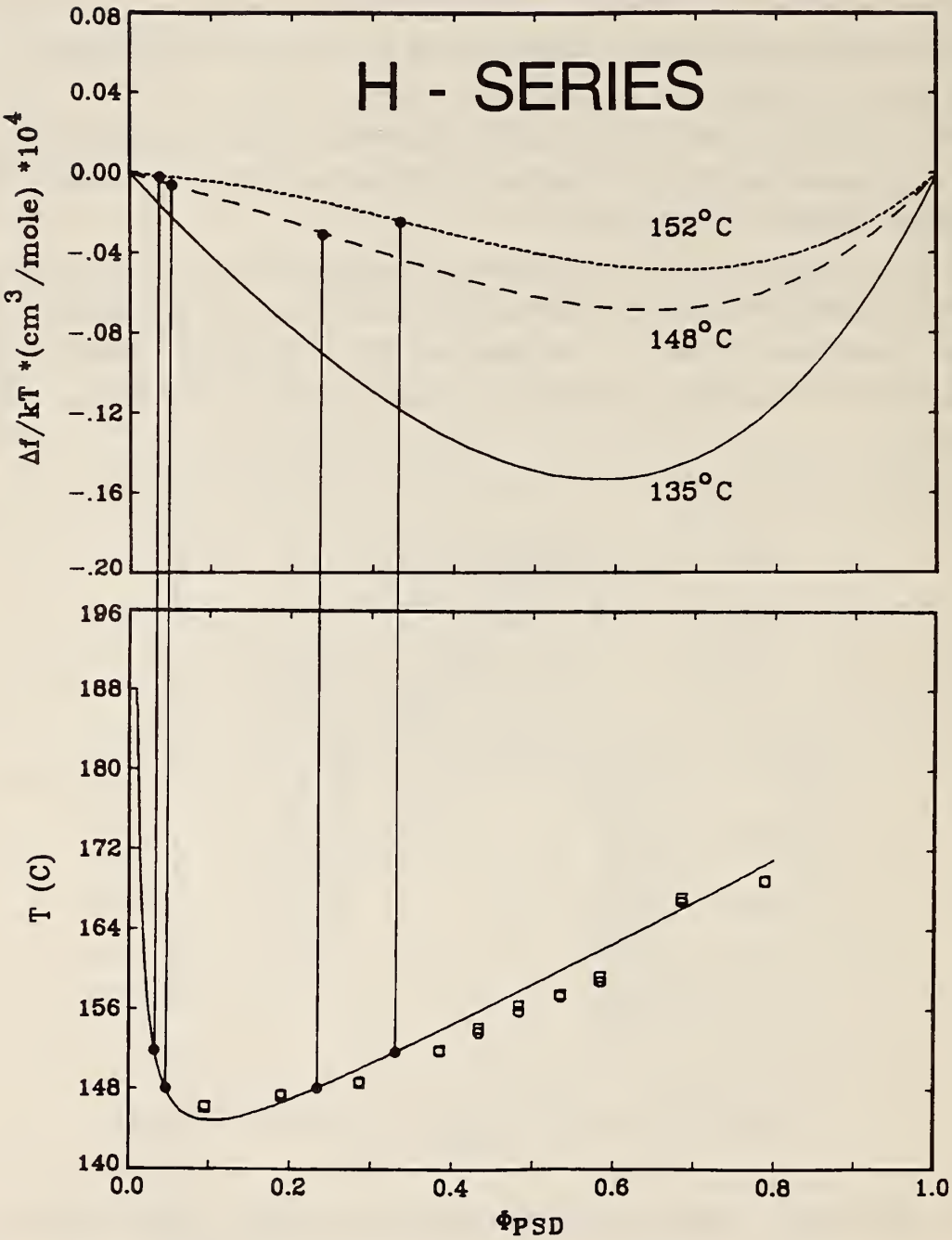

Figure 2. Free energy of mixing obtained for the H-series at 152 °C, 148 °C and 135 °C below (critical temperature) are plotted against ϕ_{psd} in the upper part of the figure. Spinodal temperature line together with experimental data points (in open circle and square) are displayed in the lower part. The calculated spinodal points at 152 °C and 148 °C are also shown in filled circles.

References

[1] (a) D. R. Paul and S. Newman, eds., Polymer Blends, Volume I and II, Academic Press, New York (1978). (b) O. Olabishi, L. M. Robeson, and M. T. Shaw, "Polymer-Polymer Miscibility," Academic Press, New York (1979).

[2] C. Herkt-Maetzky and J. Schelton, Phys. Rev. Lett. 51, 896 (1983).

[3] H. Yang, M. Shibayama, R. S. Stein, and C. C. Han, Polym. Bull. 12, 7 (1984).

[4] M. Shibayama, H. Yang, R. S. Stein, and C. C. Han, Macromol. 18, 2179 (1985).

[5] (a) P. G. de Gennes, J. de Physique 31, 235 (1970). (b) P. G. de Gennes, Scaling Concepts in Polymer Physics, Cornell University Press, New York (1979).

[6] K. Binder, J. Chem. Phys. 79, 6387 (1983).

[7] D. Patterson, S. N. Bhattacharyya, and P. Picker, Trans. Faraday Soc. 64, 648 (1968).

[8] (a) I. G. Sanchez and R. H. LaCombe, J. Phys. Chem. 80, 2352 (1976). (b) R. H. LaCombe and I. C. Sanchez, J. Phys. Chem. 80, 2568j (1976).

[9] (a) R. Koningsveld, L. A. Kleintjens and H. M. Schoffleers, Pure Appl. Chem. 39, 1 (1974). (b) K. Koningsveld, Advan. Colloid., Interface Sci. 2, 151 (1968).

[10] M. Muthukumar, J. Chem. Phys. 85, 4722 (1986).

[11] I. Sanchez, private communication.

CHARACTERIZATION OF POLYQUINOLINE BLOCK COPOLYMER USING SMALL ANGLE SCATTERING TECHNIQUES

W.-L. Wu
(Polymers Division)

and

J. K. Stille, J. W. Tsang, and A. J. Parker
(Colorado State University)

Polyquinoline is a major candidate for molecular composites. In a molecular composite, rigid rod molecules are dispersed in a matrix of flexible polymer. The molecular rods act as the reinforcing fiber. Molecular composites offer processing advantages while retaining excellent performance properties at high temperature. In the ultimate molecular composite each molecular rod should be completely surrounded by flexible polymer molecules to separate on a larger scale, which must be overcome by modification of chemical compositions.

This work is aimed at demonstrating that small angle scattering (SAS) is a viable technique for the structure determination of rigid rod polymers in solid state. The presence of microvoids in this type of material has hampered the use of SAS in rigid rod polymers and their blends as a quantitative measurement technique. To circumvent this difficulty, both small angle neutron and x-ray measurements were carried out on the same specimen. Due to the difference in the scattering contrast factors of the voids between x-ray and neutron scattering the void contribution to the scattering intensity can then be removed. A block copolymer of alternating rigid rod and flexible polyquinoline was studied using the above scheme to determine the compatibility between the rigid and the soft components. The average molecular weight for each block was about 17,000. The SANS and SAXS results, both in an absolute intensity scale, are given in figures 1 and 2, respectively. The calculated molecular structure factor and the void scattering are given in figure 3. Based on the peak height of the molecular structure factor, it is concluded that the block copolymer was not phase segregated; however, a strong intermolecular correlation was observed within the same component.

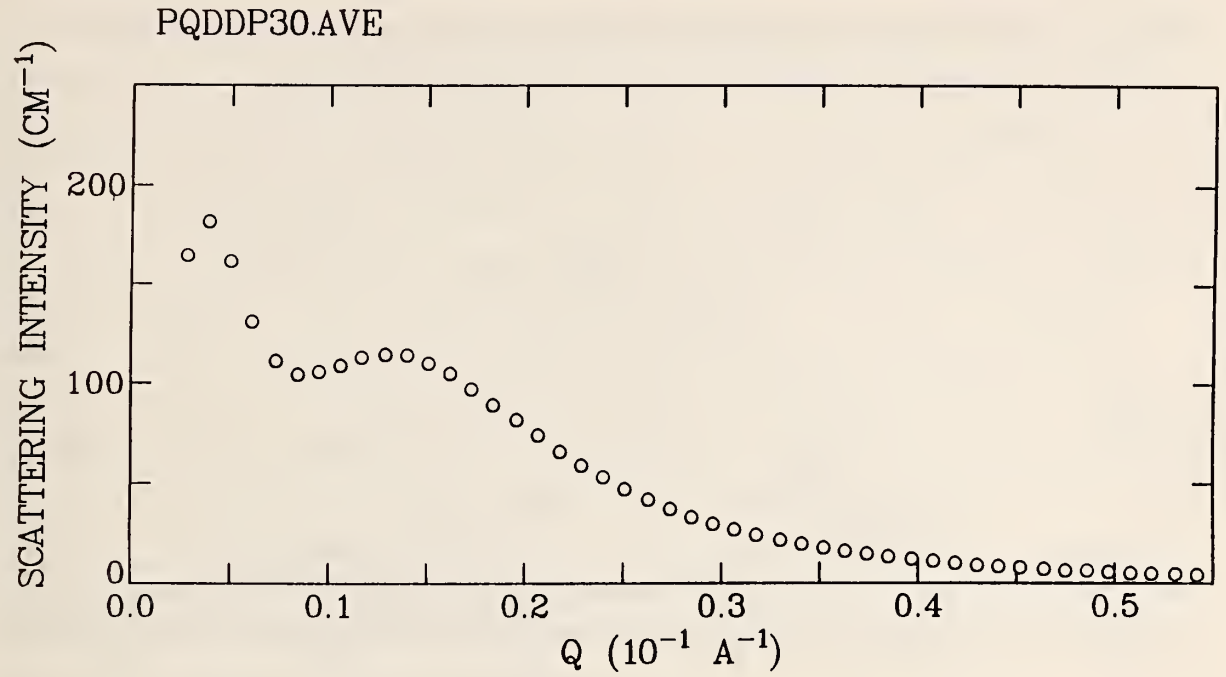

Figure 1. SANS result of polyquinoline multi-block copolymer. The soft block is partially deuterated. The intensity is in absolute scale.

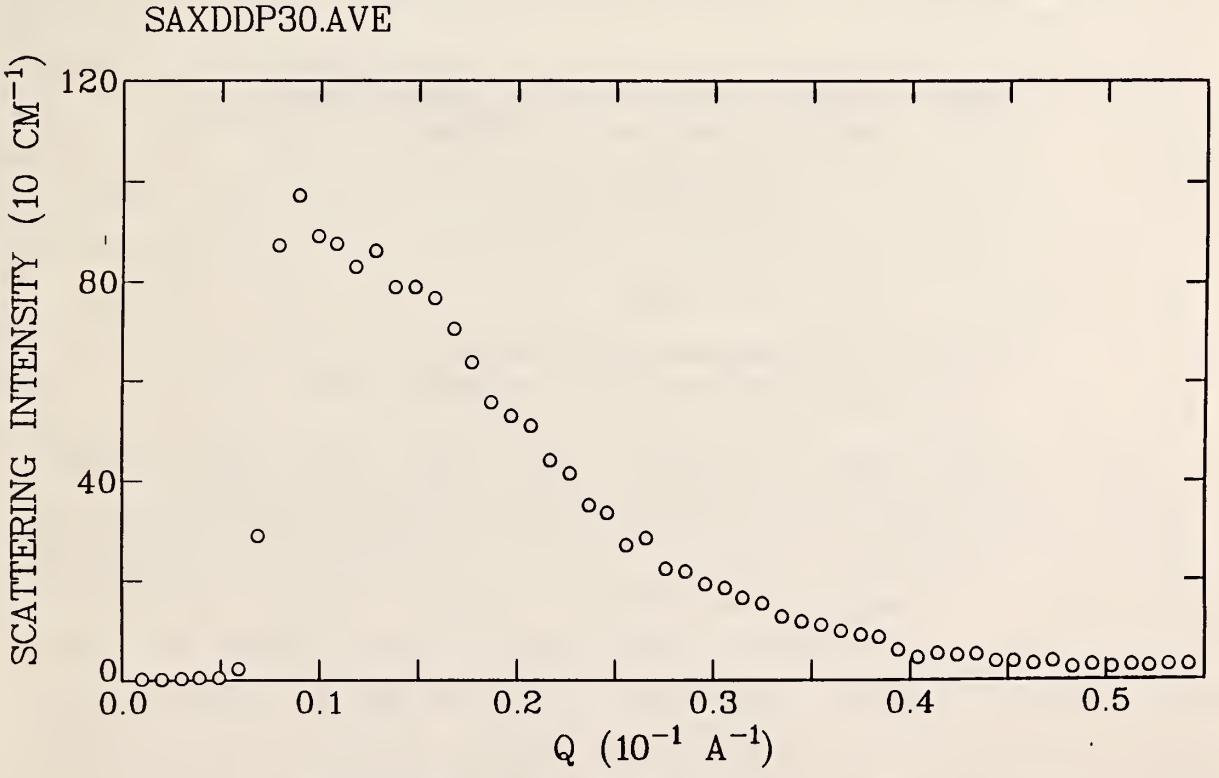

Figure 2. SAXS result of the sample of figure 2. The intensity is in absolute scale.

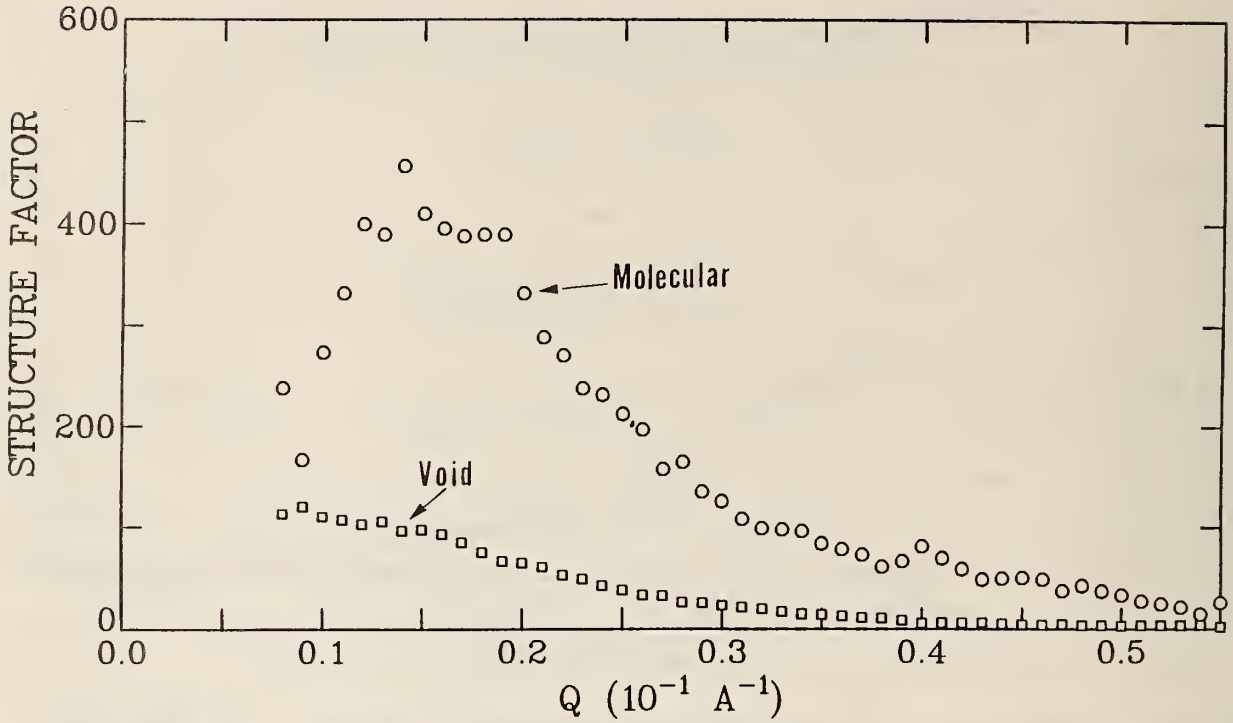

Figure 3. The calculated structure factors of the voids and the multi-block copolymer.

NEUTRON SCATTERING STUDIES OF LIPID TUBULES FORMED FROM A POLYMERIZABLE SURFACTANT

C. Han and S. Krueger
(Polymers Division)

and

P. E. Schoen and R. Treanor
(Naval Research Laboratory, Washington, DC)

Small angle neutron scattering (SANS) and wide angle neutron diffraction studies have been initiated to determine the structure of tubules formed by the polymerizable lipid, 1,2-bis(10,12-tricosadiynoyl)-sn-glycero-3-phosphocholine. A conversion from spherical liposomes to hollow, thin-walled, cylinders (tubules) occurs as the lipid is slowly cooled through its chain melting phase transition temperature [1]. The tubules typically have diameters between 0.3 and 1 μm and lengths ranging from a few to several hundred micrometers and can be irreversibly polymerized by irradiation with 254 nm light. Lipids cooled too rapidly tend to form small planar shards, rather than tubules.

Preliminary SANS and wide angle measurements have been made on suspensions of tubules and shards in D_2O. The SANS measurements are useful for determining the bilayer spacing. As shown in figure 1, a pronounced peak can be observed at $q_m \simeq 0.095$ Å^{-1} for tubules in D_2O with concentration C = 30 mg/ml. This corresponds to a bilayer spacing $d = 2\pi/q_m \simeq 66$ Å. In figure 2, a similar experiment has been carried out, but on a suspension with less tubule conversion. It is clear that the peak at $q_m = 0.095$ Å^{-1} is much weaker. Yet, the position is unchanged. This confirms the idea that the bilayer thickness is being measured, while the intensity of the peak is related to the concentration of the tubules. No obvious diffraction signal has been detected from the wide angle measurements conducted on the same material. This supports the notion that, due to the tight crystal-like packing of the lipid chains, water is completely excluded from the hydrophilic region. Therefore, there is no scattering contrast between the lipid chains to give any neutron diffraction signal.

SANS measurements have also been initiated on partially deuterated lipid chains in tubule form. Figure 3 displays the SANS data obtained from a suspension of tubules in which the lower half of both lipid chains are deuterated. Again, the tubules are in D_2O and the concentration is 30 mg/ml. A more pronounced peak is observed at $q_m \simeq 0.1$ Å^{-1} and a secondary structure may also exist. SANS measurements in an extended q range are planned in order to further study this sample. In addition, use of the contrast variation [2,3] technique should allow the mapping of a more detailed bilayer structure.

Eventually, the data will be compared with model calculations of the scattering function S(q) determined for various packing arrangements of the hydrocarbon chains. The locations of the atoms determined from the data taken on the planar shards will be used as initial positions in a computer modeling of the equilibrium placement of the molecules in the cylindrical tubules. This should provide some insight into the cause of the bending of the sheets into tubules.

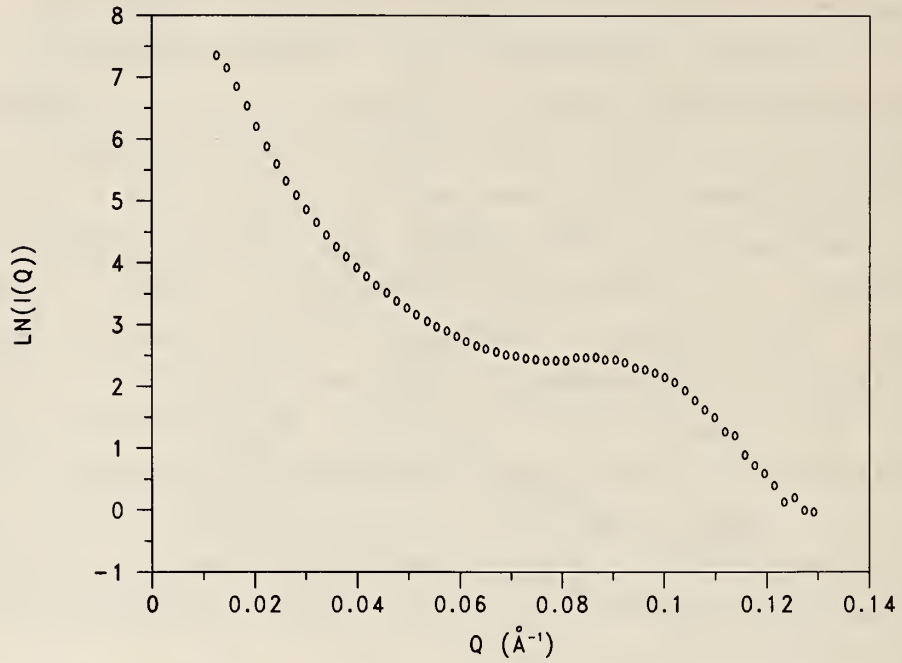

Figure 1. SANS data from lipid tubules in D_2O with C = 30 mg/ml.

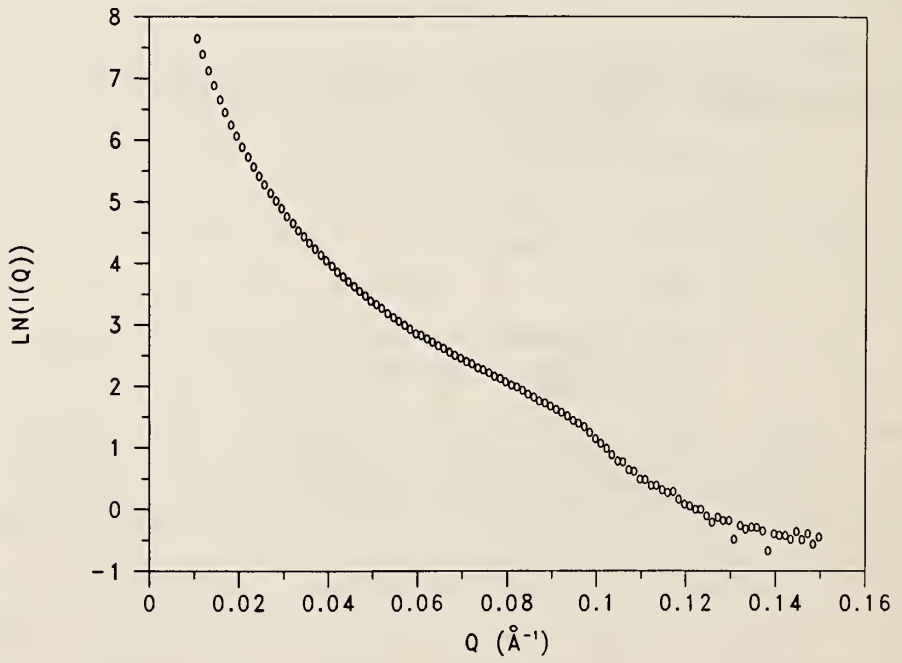

Figure 2. SANS data from lipid tubules in D_2O with C = 30 mg/ml, but with incomplete conversion from liposomes to tubules.

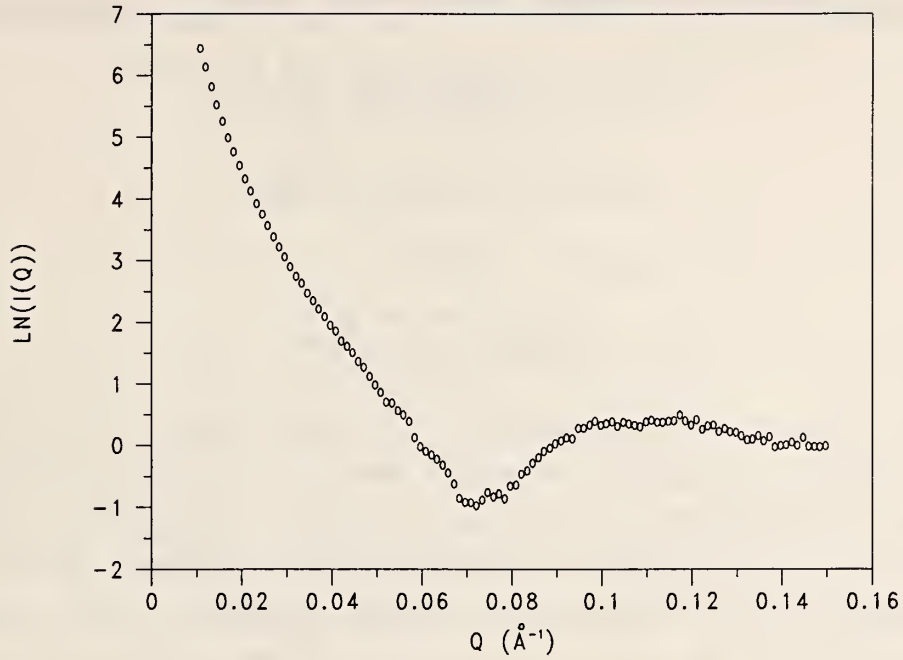

Figure 3. SANS data from partially deuterated lipid tubules in D_2O with C = 30 mg/ml.

References

[1] P. Yager, P. E. Schoen, C. Davies, R. Price, and A. Singh, Biophys. J. 48, 899 (1985).

[2] B. Jacrot, Rep. Prog. Phys. 39, 911 (1976).

[3] H. B. Stuhrmann and A. Miller, J. Appl. Cryst. 11, 325 (1978).

SMALL ANGLE NEUTRON SCATTERING OF POLY(VINYLALCOHOL) - AQUEOUS SOLUTION

M. Shibayama, H. Kurokawa, and S. Nomura
(Kyoto Institute of Technology)

S. Roy and R. S. Stein
(University of Massachusetts)

and

L. D. Coyne and W. Wu
(Polymers Division)

Two kinds of poly(vinylalcohol) PVA aqueous gels; i.e., hydrogels (PVA aqueous solution) and alkaline gels (PVA aqueous solution containing borate ions), were investigated using small angle neutron scattering as a function of temperature and concentration. For both gels the scattered intensity, I(q), rises anomalously as q approaches 0 when the system was in gel state, where q is the magnitude of the scattering vector. When the system is in sol state, the correlation length can be obtained, which is a few times greater than the radius of gyration of the PVA molecules, indicating the existence of PVA clusters even in sol state. The scattering exponent, μ in $I(q) \sim q^{-\mu}$, was evaluated to be around 1.6 to 2.0 for the gels. Its value decreases abruptly around the gel-to-sol transition temperature. This scattering exponent observed is in accordance with the value of theoretically predicted values based on fractals [1,2].

References

[1] D. Stauffer, Phys. Rep. 54, 1 (1979).

[2] L. Leibler and F. Schoesseler, Phys Rev. Lett. 55, 1110 (1985).

SMALL ANGLE NEUTRON SCATTERING STUDIES OF ISOLATED NEUROSECRETORY VESICLES

S. Krueger
(Polymers Division)

and

R. Nossal
(National Institutes of Health, Bethesda, MD)

Small angle neutron scattering (SANS) was used to study the state of the dense cores within intact neurosecretory vesicles (NSV). These vesicles transport the neurophysin proteins (NP), along with their associated hormones, oxytocin (OT) or vasopressin (VP), from the posterior pituitary gland to the bloodstream, where the entire vesicle contents are released. Knowledge of the vesicle core structure is important in developing an understanding of this release mechanism. Since the core constituents exist in a dense state at concentrations which cannot be reproduced (in solution) in the laboratory, a method was developed to determine the core structure from SANS experiments performed on intact neurosecretory vesicles.

The H_2O/D_2O ratio in the solvent can be adjusted, using the method of contrast variation [1,2] such that the scattering due to the vesicle membranes is minimized, thus emphasizing the scattering originating from the cores. The applicability of this method for examining the interior of biological vesicles was tested by performing an initial study [3] on human red blood cells (RBCs), which are similar in structure to other biological vesicles. Changes in intermolecular hemoglobin interactions, occurring when the ionic strength of the solvent was varied or when the cells were deoxygenated, were examined. The results agreed with those expected for dense protein solutions, [4] indicating that the method developed was suitable for the study of hemoglobin within the cells. Similar SANS studies were then performed on intact NSV.

A contrast variation series was performed on NSV membrane suspensions in H_2O as well as in 10, 20, 40 and 70% D_2O buffers. The results, shown in figure 1, suggest that the scattering from the NSV membranes is minimized when the solvent contains between 10 and 20% D_2O. The data, fit using the flat sheet approximation [5], yielded a membrane match point of $18 \pm 2\%$ D_2O.

Initial data (see fig. 2) taken on intact NSV in 21% D_2O, covering a range of Q values such that $0.015 \leq Q \leq 0.28$ $Å^{-1}$, showed no evidence of

scattering beyond the small angle peak. In order to determine the extent of the core contribution to the scattering at small angles, the scattering from the NSV membranes alone was subtracted from that due to the intact NSV. Suspensions of intact NSV as well as NSV membranes were measured in 20% and 40% D_2O buffers. Then, a subtracted scattering curve, $I_{sub}(Q) = I_v(Q) - C \cdot I_m(Q)$, where $I_v(Q)$ is due to the intact NSV and $I_m(Q)$ is due to the NSV membranes, was obtained for the samples in each solvent. The constant, C, is the factor which normalizes $I_m(Q)$ to $I_v(Q)$. As the vesicle core contains mostly protein, its match point is assumed to be approximately that of a typical protein, i.e., around 40% D_2O. Since the only contribution to $I_v(Q)$ is due to the vesicle membrane, the scattering curves in 40% D_2O were used to find the normalization factor, C. As a check on this procedure, C was also verified independently through biochemical means [6].

In 20% D_2O, the contribution to the scattering intensity due to the vesicle membranes is small. Therefore, after subtracting the normalized membrane scattering, $I_{sub}(Q)$ is approximately equal to $I_c(Q)$, the scattering due to the protein core. Figure 3 illustrates $I_{sub}(Q)$ as obtained from the measured scattering intensities of both intact NSV and NSV membranes in 20% D_2O.

A Guinier fit [1] (see fig. 4) in the Q range $0.010 \leq Q \leq 0.020$ Å^{-1} yielded a radius of gyration, $R_g \simeq 183 \pm 7$ Å. Since the core is dense, it is probable that this represents the size of the spaces between the proteins rather than the particles themselves. The curvature in the $\ell n[I_{sub}(Q)]$ vs Q^2 plot suggests that a distribution of sizes of particles (or spaces) is present in the NSV cores.

The "openness" of the NSV core structure was tested by fitting a straight line to the linear region occurring at small Q values in a log-log plot of $I_{sub}(Q)$ versus Q in order to find its fractal dimension [7]. As illustrated in figure 5, an average fractal dimension of $D = 2.8 \pm 0.2$, based on several fits made in the range $0.010 \leq Q \leq 0.06$ Å^{-1}, was obtained, thus confirming the dense nature of the NSV core.

The SANS data, along with accompanying biochemical analysis, suggest that the NSV core constituents form long, flexible aggregates which fold to form a compact, but not solid, structure. Additional data obtained at smaller angles, made possible by the recent installation of a cold source at the NBS Reactor, should provide a more complete picture of the NSV core structure.

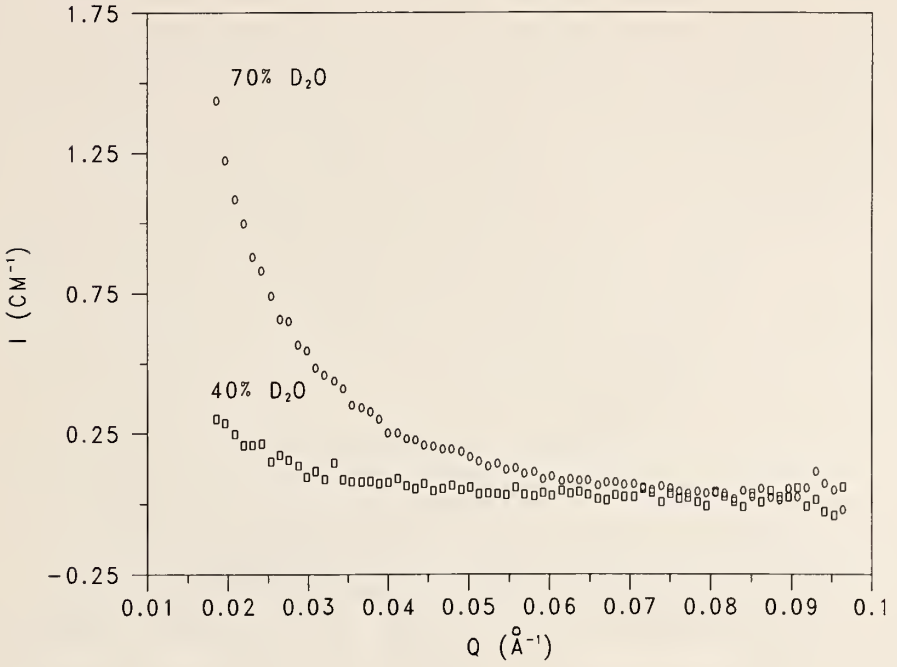

Figure 1a. Contrast variation series for NSV membranes. Plot of I(Q) vs Q for NSV membranes in 70% and 40% D_2O.

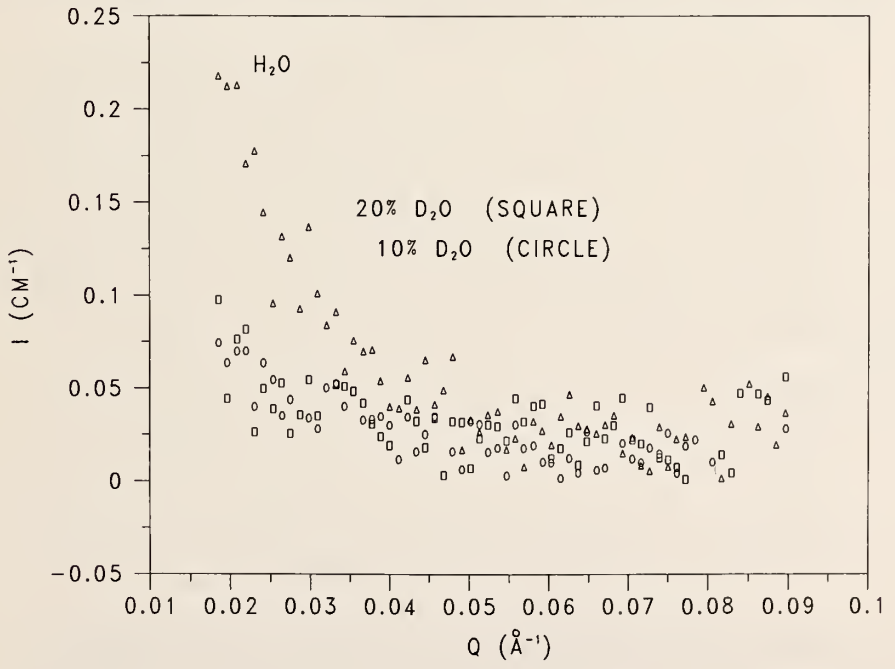

Figure 1b. Contrast variation series for NSV membranes. Plot of I(Q) vs Q for NSV membranes in 20% and 10% D_2O as well as in H_2O.

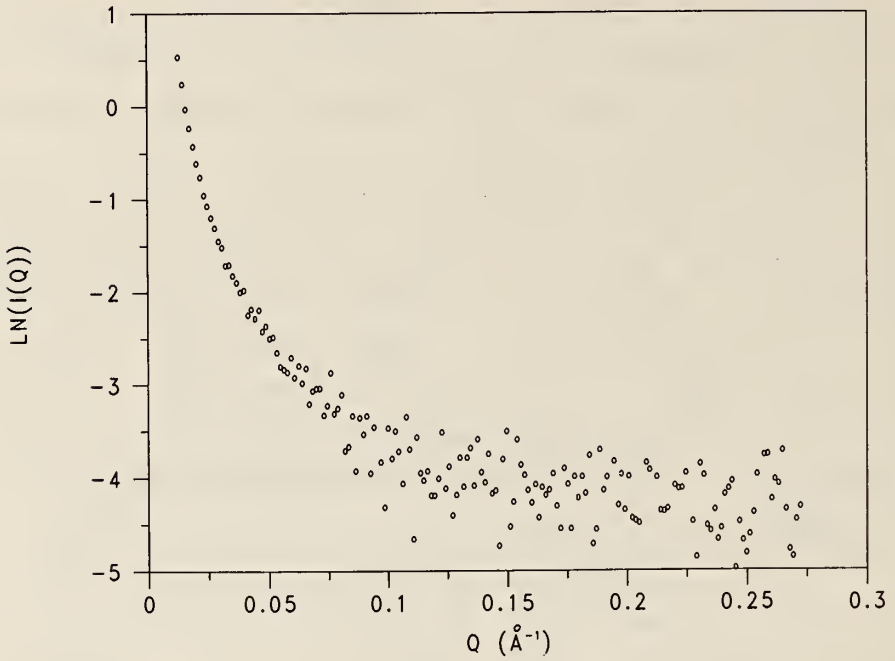

Figure 2. $\ell n(I(Q))$ vs Q plot of intact NSV in 21% D_2O covering the range of Q values from $0.015 \leq Q \leq 0.28$ $Å^{-1}$.

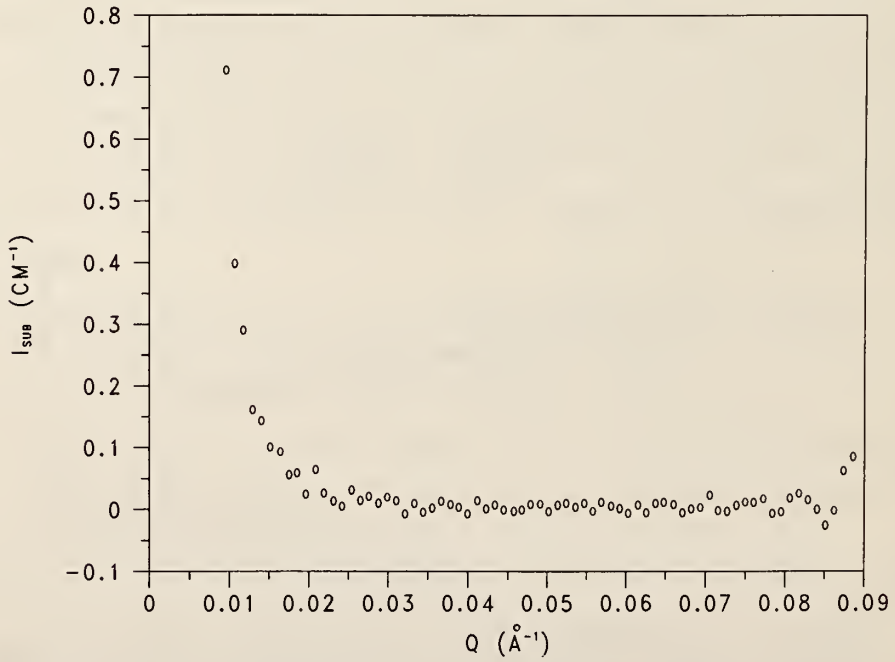

Figure 3. Scattering due to the NSV core protein, $I_{sub}(Q)$, in 20% D_2O, obtained by subtracting the (normalized) NSV membrane scattering from the intact NSV scattering.

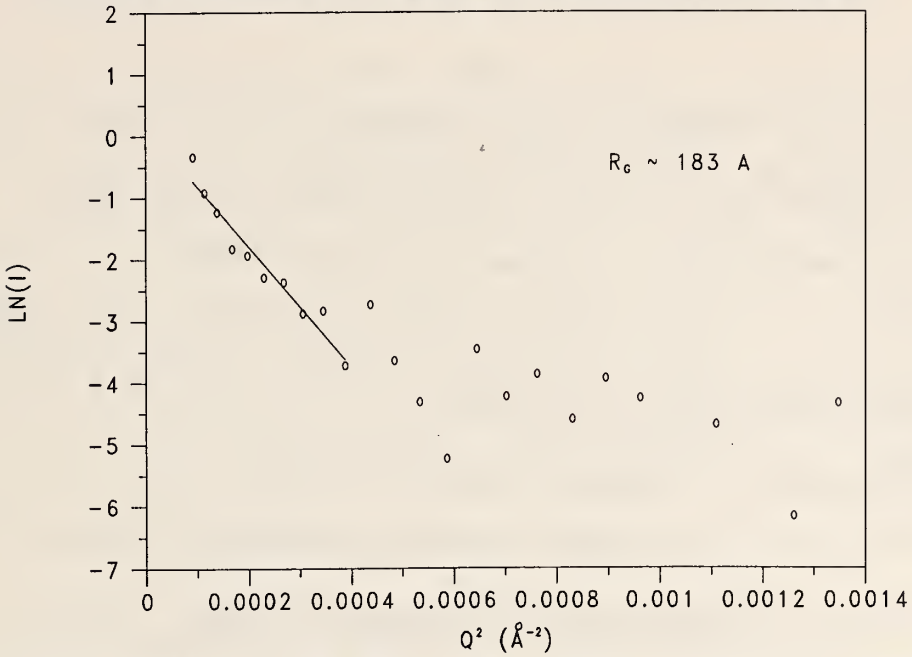

Figure 4. Guinier fit to the NSV core protein scattering in 20% D_2O. A radius of gyration, $R_g \simeq 183 \pm 7$ Å, was obtained in the region fit. The smooth curvature of the $\ell n(I_{sub}(Q))$ vs Q^2 plot suggests a distribution of sizes can be found over the Q range plotted.

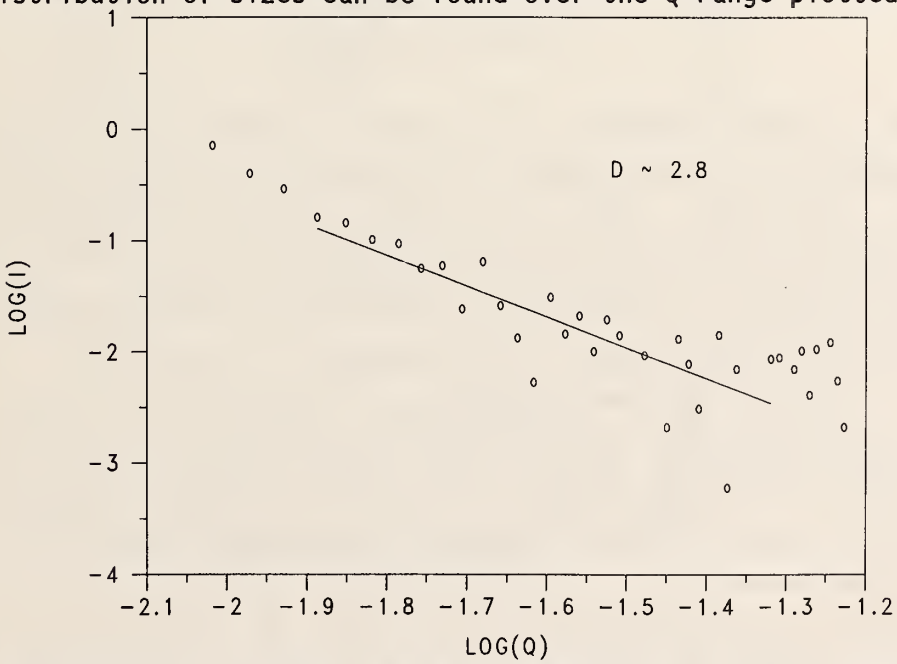

Figure 5. Log-log plot of $I_{sub}(Q)$ vs Q for the NSV core protein scattering in 20% D_2O. The line is a representative fit, made in the range $0.013 \leq Q \leq 0.05$ Å^{-1}. The calculated fractal dimension, $D = 2.8 \pm 0.2$, is an average of several fitted values obtained using slightly different Q ranges.

References

[1] B. Jacrot, Rep. Prog. Phys. 39, 911 (1976).

[2] H. B. Stuhrmann and A. Miller, J. Appl. Cryst. 11, 325 (1978).

[3] S. Krueger and R. Nossal, Biophys. J. 53, 97, (1988)

[4] R. Nossal, C. J. Glinka, and S.-H. Chen, Biopolm. 25, 1157 (1986).

[5] G. Porod in Small Angle X-Ray Scattering, O. Glatter and O. Kratky, eds., Academic Press, New York, 17 (1982).

[6] S. Krueger and J. T. Russell, unpublished results.

[7] T. A. Witten and L. M. Sander, Phys. Rev. B27(9), 5686 (1983).

DENSIFICATION OF MICROPOROUS SILICA

G. G. Long
(Ceramics Division)

and

S. T. Krueger
(Polymers Division)

The sol-gel technique can be used to prepare novel glasses, fibers, thin and thick films with chemical homogeneity and unique structural and electrical properties. High purity, crack-free silica bodies with "made-to-order" narrow pore-size distributions have been formed as model systems for the investigation of the relationships between the physical properties of this class of material and the amount and character of porosity. The present research focuses on the characterization of such porous bodies by small angle neutron scattering (SANS) and multiple small angle neutron scattering (MSANS) since it has been demonstrated that thermal processing and the resultant microstructure bear a strong influence on the dielectric and other properties of the product material.

Samples were prepared [1] by the Shoup [2] technique from 85 wt.% potassium silicate and 15 wt.% colloidal silica. The porosity of the precursor body was between 81 and 86%. The average pore radius in the precursor body was 0.10 μm as measured by Hg porosimetry. Since the calculated density was within 2% of that derived from simple geometric measurements, the pores must be mostly open. Each of the samples measured in

this study was subjected to a firing temperature above the onset of sintering which occurs at 1150-1200 °C depending on the average pore size of the dried precursors. The porosities of the SANS samples were 40, 35, 30, 5, and 2%, and for several of these both thin samples for diffraction measurements and thick samples for multiple scattering measurements were available.

MSANS [3,4] was used to measure the average pore sizes present during the intermediate stages of thermal processing, where the radii could be expected to be in the 0.08-10 μm range. Total surfaces areas were estimated from the single scattering Porod curves. Pore populations were studied in the late stages of processing by means of diffraction measurements with 14 Å incident neutrons. The results are shown in table 1.

Table 1. Pore radii and surface scattering areas for the microporous silica samples

Sample No.	Density	Pore Radius (μm)	Total surface area (cm^2)
1	0.60	0.185	5.89×10^4
2	0.65	0.243	8923
4	0.70	0.224	
6	0.95	<0.08	1198
9	0.98	<0.08	127

These results indicate that densification during the intermediate stages is accompanied by pore coarsening. Although pore coarsening had previously been observed in the earlier stages of thermal processing, this result was unexpected since the pores are generally expected to undergo shrinkage in order for the body to densify. The observed pore coarsening eventually levels off and by the time the material is 95% dense, one cannot detect any pores with radii greater than 0.08 μm. SANS measurements on the 95% dense sample using 14 Å incident neutrons reveal the presence of populations of pores with radii 330 Å and less.

References

[1] We are grateful to R. A. Gerhardt, Center for Ceramics Research, Rutgers University for providing the samples used in this study.

[2] R. D. Shoup, Colloid and Interface Sci. 3, 63 (1976).

[3] N. F. Berk and K. A. Hardman-Rhyne, J. Appl. Crystallogr. 18, 467 (1985).

[4] K. A. Hardman-Rhyne and N. F. Berk, J. Appl. Crystallogr. 18, 473 (1985).

COLD NEUTRON PROJECT

J. R. D. Copley, C. J. Glinka, J. A. Gotaas, G. Greene, W. Knill, J. LaRock, C. J. Majkzrak, C. O'Connor, D. Pierce, J. M. Rowe, S. Satija, I. G. Schroder, T. J. Udovic, and R. Williams

The neutron guide hall and office/laboratory building construction contract was awarded in fall of 1987. The bids received indicated that the design package was good, and the successful bidder has proved to be responsible and reliable. Construction began in November, 1987 and at present is 2/3 complete. The contract requires completion of the building before January, 1989, and actual completion and beneficial occupancy should occur substantially before this date. No major problems have arisen in this phase of the project.

The neutron guide tubes have been ordered from Cilas-Alcatel in France. Actual fabrication of components has begun, and the first delivery of neutron guides will occur in the spring of 1989, with installation beginning immediately. Concurrently, the detailed design of the in-reactor components of the guide support systems and reactor penetrations is essentially complete, with fabrication to begin in September. In the first stage of the neutron guide installation, the three guides that run along the east side of the guide hall will be installed and developed. The remaining four guides will be installed later, possibly at the same time as a new cold source which is presently being designed is ready. This schedule has been chosen to minimize reactor down time, while allowing for an orderly development of the full complement of instruments. The layout of the initial three guides and instruments is shown in figure 1.

The design of the first complement of instruments as shown in figure 1 is underway, with different instruments at quite different stages. Two of the instruments shown, the short small angle neutron scattering facility (SANS) and the time-of-flight (TOF) spectrometer already exist inside the reactor building, and will be moved, with some improvements and modifications, to the guide hall immediately. As the new instruments come on line, these two will be replaced, but in the development stage, they will be available to carry on currently ongoing research. When the first guides are installed, the port currently allocated to the TOF machine will be modified to become the neutron depth profiling station. The Exxon/NBS high resolution SANS will be ready for installation when the guides are installed, as will the first experiment to be

performed at the fundamental neutron physics station. The other instruments shown will be ready for installation in stages during the following year. A brief description of some of the instruments is given below.

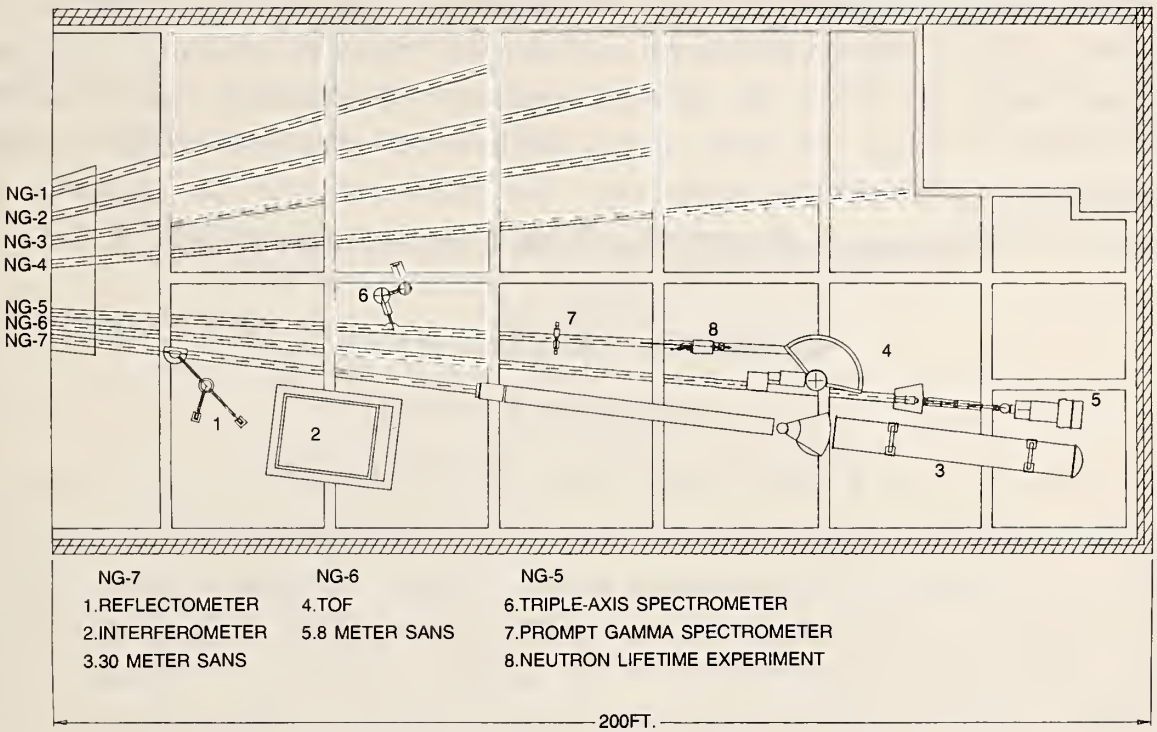

Figure 1. Cold Neutron Research Facility layout showing initial instrumentation complex.

NEUTRON REFLECTOMETER

S. Satija

In the past 10 years there has been growing interest in a variety of surface sensitive techniques including, most recently, neutron reflection from surfaces. Current measurements show this to be a powerful probe of surface properties; e.g., the study of density profiles as functions of depth and surface roughness. One unique advantage of neutrons is the ability to use deuterium labelling to highlight scattering from selected components in a film. We have initiated a program in neutron reflectivity measurements on a variety of surfaces and interfaces using a modified triple axis spectrometer in order to develop methods and techniques to be used in a new reflectometer now being designed for installation in the guide hall. The design goal for this new instrument is the ability to do measurements of reflectivities of

order 10^{-7}. The spectrometer will use a pyrolytic graphite crystal to both monochromate and vertically deflect the neutron beam onto a horizontal sample. This configuration will allow the measurement of reflectivities of liquid surfaces. The instrument will have two detectors--one at small angles to measure specular reflectivities, and another capable of scanning a large angular range in order to perform surface diffraction measurements. Independent movement of both sample and detector will be provided to allow measurement of off-specular scattering. The resolution will be variable by means of automated slits adjustments within a range of $\Delta Q/Q$ of 0.05-0.15.

NEUTRON DEPTH PROFILING FACILITY

R. G. Downing and B. Grazman

Construction of a neutron depth profiling facility for installation at the cold source has begun. In order to provide the maximum flexibility in the final configuration of the presample section of the instrument, the in-pile plug has been designed to allow easy replacement of the initial collimator with a converging neutron guide or other optical devices. After extensive research into the properties of various single crystal filters for removal of fast neutrons from the beam, a filter of 13 inches of sapphire has been chosen as the optimum configuration for this application. The detailed design of the in-reactor components, collimators and shielding is now underway, with fabrication scheduled for the fall of 1988. At the same time, several new techniques for the actual profiling are under study, including a cooperative NBS/Texas A&M collaboration on time-of-flight techniques. The final facility will be ready for installation when the neutron guides are installed in 1989.

PROMPT γ ACTIVATION ANALYSIS FACILITY

R. M. Lindstrom and C. A. Stone

Preliminary design of this facility has focussed on two topics. The first has been the high count rates expected from typical samples (in excess of 50 K counts per second). At this count rate, we have already achieved a resolution of better than 1.9 keV at 1332 keV. These count rates also allow us to consider more advanced counting techniques, which are currently under study. The second has been the possibility of using γ-γ and γ-conversion

electron coincidence counting in analytical measurements. Experiments performed this past year at the Brookhaven HFBR using a four-detector coincidence system showed that the intensity of several weak γ-ray peaks could be determined to within 3%. Standard counting techniques give uncertainties of 200% for the same counting time. The design of this facility will be complete within 3 months, and construction will be completed in time for installation in the guide hall in 1989.

HIGH RESOLUTION SMALL ANGLE SCATTERING SPECTROMETER

C. J. Glinka

and

S. K. Sinha
(Exxon Engineering and Research Company)

Much of the detailed mechanical design of the vacuum flight path for the 30 m long, high resolution SANS spectrometer, being built jointly by NBS and the Exxon Research and Engineering Co., has been completed and fabrication is well underway. Within this flight path, the effective source-to-sample distance can be varied in steps from 5-15 m, through the insertion of neutron guide tube sections, and the sample-to-detector distance varied continuously from 2-15 m. A motorized carriage for positioning a large two-dimensional position-sensitive detector inside the post-sample flight path has been built and is currently being instrumented. The remaining mechanical design work should be completed by the end of 1988 with fabrication of components continuing until mid-1989. Delivery of many of the major commercial components of the instrument, including two advanced type velocity selectors and the guide tube sections for the incident flight path, is also expected during this period.

A novel feature of this instrument will be the use of a doubly curved, grazing incidence mirror, 2.4 m long, to focus the incident beam onto the detector. If successful, such a mirror would provide up to a fourfold increase in flux on the sample, for a given minimum Q-value, over what can be obtained with either single or multi-beam converging pinhole collimation. As currently planned this mirror will consist of eight, 30 cm long x 5 cm high, concave cylindrical segments that will be aligned tangent to an arc 1700 m in radius. Each segment will be slightly bent to conform approximately to this

1700 m arc to achieve focusing in the horizontal plane. Calculations indicate that this arrangement of bent cylindrical mirrors will give about 95% of the flux gain that an ideally figured toroidal mirror would provide for a small fraction of the cost of a single mirror of the required length, shape and surface finish.

The SANS flight path has been designed to accommodate either conventional pinhole collimation or a focusing mirror. Actual performance tests will dictate the final choice of beam collimation.

DESIGN OF A HIGH RESOLUTION TIME-OF-FLIGHT SPECTROMETER

J. R. D. Copley

The high resolution time-of-flight spectrometer, primarily designed to provide an energy resolution of 10-15 μeV using an incident wavelength of 6 Å, is intended to be highly versatile so that rapid measurements with relatively poor resolution can be performed prior to the more definitive high resolution studies. The instrument will use at least six high speed disk choppers, each fitted with several widely separated neutron windows, in order to achieve this purpose. We also hope to include an option to use a multiple-slot system (see "On the Use of Multiple-Slot Multiple Disk Chopper Assemblies to Pulse Thermal Neutron Beams," by J.R.D. Copley, elsewhere in this report) to achieve high resolution with additional intensity. The choppers will run on magnetic bearings, and recent tests of the extent of jitter in such systems suggest that the multiple-slot concept will work. If the full width of the neutron guide (6 cm) is to be used, a converging guide will be required, since the sample size can only be of order 1-2 cm in order to achieve the desired resolution. Studies of converging guides have been performed, but no definite decision has as yet been made.

WORKSHOP ON MICROSTRUCTURE AND MACROMOLECULAR RESEARCH WITH COLD NEUTRONS

C. J. Glinka, J. A. Gotaas, and C. O'Connor

On April 21-22, 1988, over 160 scientists, including 25 from industry, 70 from universities and 30 from Government laboratories and agencies (not including NBS), gathered at NBS, Gaithersburg, for a Workshop on Microstructure and Macromolecular Research With Cold Neutrons. This workshop was one of a series, each devoted to a major area of research with cold neutrons, that are being held in conjunction with the development of the Cold Neutron Research Facility (CNRF) at the NBS 20 MW research reactor as a National, user-oriented research facility. The dual aims of this workshop were to highlight research opportunities in the application of cold neutron techniques to the study of submicron structure in materials and macromolecular systems, and to inform and involve the scientific community in the planning for instrumentation for the CNRF.

The workshop's goal of highlighting research opportunities with cold neutrons was addressed in two sessions in which invited speakers reviewed current work in a variety of disciplines and discussed future extensions utilizing cold neutrons. Talks by T. Russell (IBM Almaden Research Center), J. Hayter (Oak Ridge National Laboratory), G. Zaccai (Institut Laue-Langevin), and R. Page (Southwest Research Institute) covered applications in Polymer Science, Chemistry, Biology and Ceramics, respectively. Metallurgical applications, with an emphasis on time-resolved studies, were described by B. Gaulin (Oak Ridge National Laboratory) while S. Sinha (Exxon Research and Engineering Co.) presented a general formalism for using scattering measurements to characterize fractal behavior in materials. In addition, the use of cold neutrons to study the structure of surfaces and interfaces was the subject of talks be R. Thomas (Oxford University) and H. Zabel (University of Illinois) who discussed the relatively new techniques of neutron reflectometry and grazing incidence diffraction.

One session of the workshop was devoted entirely to reviewing the current status and future plans for the NBS CNRF. NBS Deputy Director Ray Kammer opened the session by outlining the overall scope of the CNRF as a National user facility open to all qualified researchers on the basis of scientific merit. Kammer's policy overview was followed by a technical overview by J. M. Rowe who described the architectural design of the experimental hall and

office wing (scheduled for completion in early 1989) associated with the CNRF, and the network of totally reflecting guide tubes that will transport neutrons from the reactor cold source to the CNRF. He also presented data on the performance of the D_2O-ice cold source now in operation in the reactor and gave a timetable for projected instrument development. The remaining four talks in this session each focused on a specific cold neutron technique and presented design concepts for its implementation in the CNRF. Described were a novel SANS instrument that would utilize a doubly curved mirror to focus a beam onto a detector, the current state of development of neutron supermirrors and their use both to enhance flux and to produce polarized neutron beams, a neutron reflectometer suitable for measurements on both solid and liquid surfaces, and an improved facility for Neutron Depth Profiling which would utilize a converging neutron guide to increase the sensitivity of this technique by more than one order of magnitude over what is now possible using thermal neutrons.

The last session of the workshop consisted of three discussion sessions which provided participants with the opportunity to comment upon or inquiry further about any aspect of the CNRF. The discussions were wide-ranging and touched upon the need for advanced cold neutron instrumentation for inelastic scattering, recent progress in neutron optical devices and the practical needs of potential users of the CNRF.

One clear impression that emerged from the workshop is that there is a strong and growing interest in the scientific potential of the relatively new techniques of neutron reflectometry and grazing incidence diffraction for the study of near surface and interface structure. As a result of this expressed interest, the development of a state-of-the-art neutron reflectometer for the CNRF will be given increased priority. This instrument, along with a 30 m SANS machine, are expected to be the first instruments to go into operation when the CNRF guide hall is completed.

Copies of the workshop program containing the abstracts of the invited talks, and a 12-page booklet describing the CNRF may be obtained by contacting Carol O'Connor, National Bureau of Standards, Bldg. 235 Rm. A-106, Gaithersburg, MD 20899 (phone: 301-975-6240).

NBSR COLD NEUTRON SOURCE

R. S. Carter, P. Kopetka, J. M. Rowe, J. J. Rush, D. Fravel, and J. A. Gotaas

The NBSR cold source was installed in August 1987 and became operational in October 1987. The source is a 16 L block of D_2O ice maintained at 35 K with a large (8" diam.) reentrant hole. In anticipation that its performance could be improved by the addition of some H_2O, a series of tests were performed over a period of several months with different H_2O concentrations. The optimum H_2O concentration was found to be 7 1/2%. (See "Cold Source Spectrum and Flux Measurements" elsewhere in this report.)

The gain in cold neutron intensity ($\lambda > 4$ Å) achieved by the cold source was determined in several ways. These included the gain relative to the best intensity that could be obtained from the best beam hole available without a cold source; the gain versus the cold source empty; and the gain versus the cold source full, but warm. The gains were 3, 5, and 10 respectively. (For more detail see "Cold Source Spectrum and Flux Measurements" elsewhere in this report.)

Radiation damage studies were performed by measuring the release of H_2, O_2, and the production of H_2O_2 as a function of radiation exposure. After a specified number of megawatt-hours of operation, the reactor was shutdown and the system allowed to warm up gradually. As the system warmed, the release of D_2 and O_2 was measured. The rate of gas release as a function of ice temperature typically showed two peaks, one at ~ 200 K and the other near the melting point. In general most of the release was deuterium with very little oxygen. Analysis of the water after melting showed that most of the oxygen could be accounted for by the formation of D_2O_2 found in the water. As expected, based on earlier results in the literature, the D_2 released tended towards a saturation value as shown in figure 1. The D_2 releases are well within those anticipated and do not present any safety threat to the integrity of the cold source. From the figure, it is concluded that extended periods of operation pose no safety concerns. In fact, the exposure limit of the ice is set by the tritium level generated in the D_2O ice by neutron capture rather than the buildup of radiolytic products. After about 12 weeks of irradiation at 20 MW reactor power (three reactor operating cycles), the tritium level in the cold source ice begins to exceed that in the reactor (D_2O moderated and

reflected) primary cooling system. Therefore, it is deemed prudent to melt the ice after three reactor cycles and replace it with fresh material.

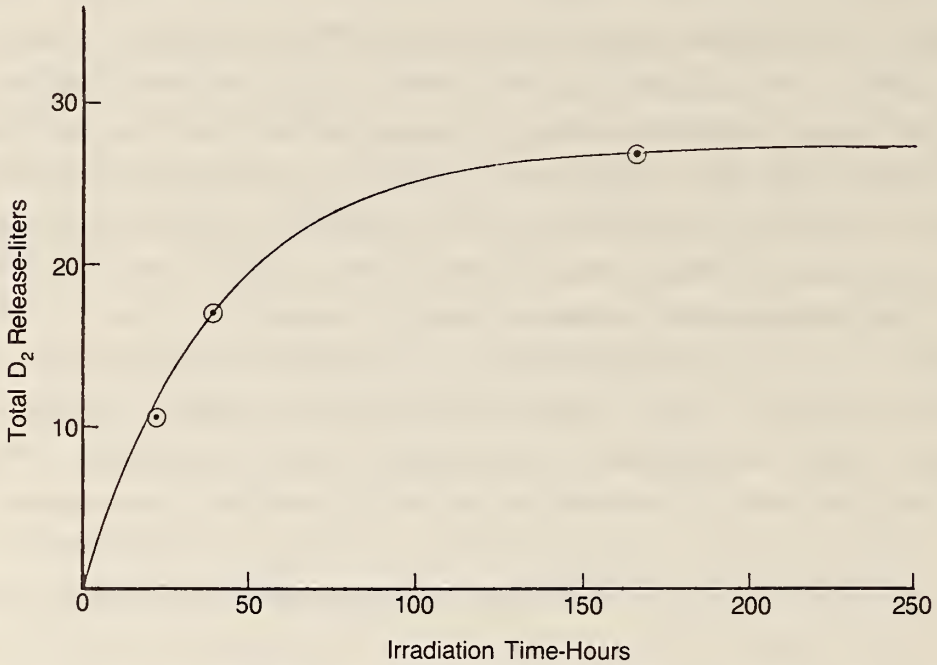

Figure 1. Total D_2 release vs. irradiation time at 20 MW.

A phenomena that was not anticipated and that further limits the long term buildup of radiolytic products was the occurrence of spontaneous recombination of these products even when the ice is cold. This may be due to local hot spots that allow some recombination and energy release. This process or "burp" causes a significant fraction of the accumulated radiolytic products to recombine releasing enough energy to cause the ice temperature to rise to 80 to 90 K. Although this energy is easily absorbed in the ice, the rapid temperature rise perturbs the refrigerator which cools the ice, and may cause it to shutdown if unattended. This "burp" phenomena appears to occur about every 3 days or so at full reactor power. Therefore, every 2 days the ice temperature is intentionally raised by decreasing the refrigerator cooling to initiate a "burp" in a controlled fashion.

This procedure, which warms up the ice for about 1 hour every 48 hours, permits long term continuous operation without uncontrolled perturbation of the refrigerator cooling system.

Thus, the length of time that ice may be maintained in the cold source is not limited by the buildup of radiolytic products, but by the operational

desire to limit the buildup of tritium to a readily manageable level. This requires the melting and replacement of the ice only four times a year. To assure that the ice can be maintained frozen for such long periods of time, a simple, backup refrigerator capable of maintaining the ice below freezing temperature is available on standby if the main refrigerator should fail.

SMALL ANGLE NEUTRON SCATTERING FACILITY

J. A. Gotaas and C. J. Glinka

The installation in the fall of 1987 of a 20-liter , D_2O-ice cold source in the reactor has resulted in a flux increase at the 8 meter SANS spectrometer that ranges from 2.75 at 5 A to nearly 4 at about 15 A. The beam current at the sample is now 1 x 10^6n/sec, for a minimum accessible Q-value of 0.015 A^{-1}, and is 2 x 10^4n/sec, for a minimum Q of 0.004 A^{-1}, for example. For strong scatterers, the low Q limit of the instrument is less than 0.003 A^{-1}. This is illustrated in figure 1 which shows a SANS pattern for a highly porous glass where the first data point outside the beamstop is at Q = 0.0024 A^{-1}

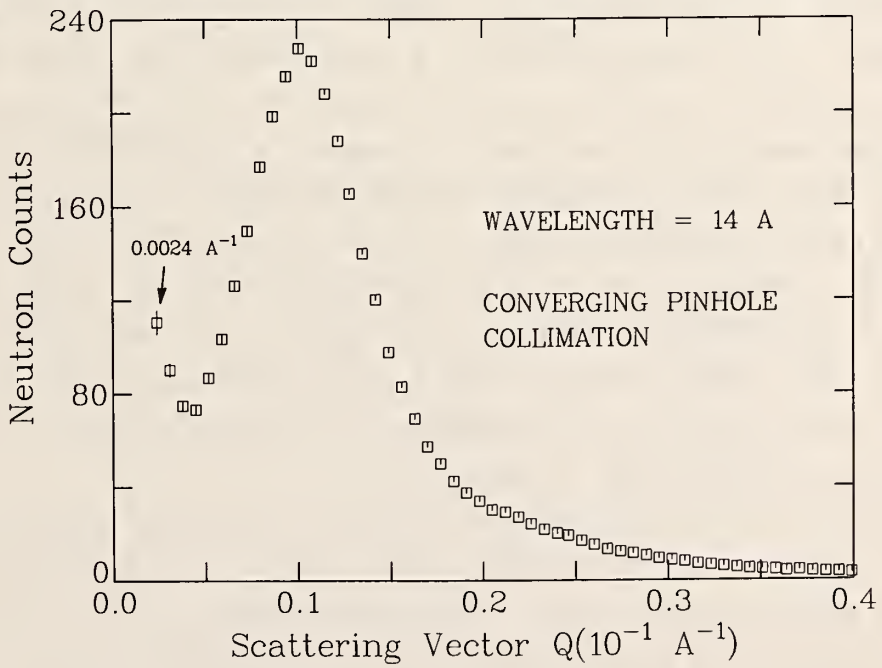

Figure 1. Small angle scattering from a porous silica glass measured using converging pinhole collimation and 14 A neutrons from the cold source. The first data point lying wholly outside the instrument's beamstop is a Q = 0.0024 A^{-1}.

COLD SOURCE SPECTRUM AND FLUX MEASUREMENTS

C. J. Glinka, T. J. Udovic, J. M. Rowe, and J. J. Rush

and

D. M. Gilliam and G. P. Lamaze
(Center for Radiation Research)

Summarized below are the results of a series of measurements made between October 1987 and April 1988 to characterize both the spectral shape and the absolute flux of neutrons from the 16 liter D_2O-ice cold source installed in the fall of 1987. The measurements were of three types: 1) time-of-flight measurements of the spectral shape, 2) absolute measurements with a double fission chamber of the total cold neutron flux (wavelengths above 4A), and 3) beam monitor count rates to estimate the gain as a function of wavelength.

1) Spectrum Shape

Time-of-flight measurements of the wavelength distribution of neutrons from the cold source were made at the SANS beam port (CTE) soon after the installation of the source and prior to reinstalling the SANS and TOF instruments. For these measurements a Fermi chopper was set up at the SANS velocity selector position and was followed by a 3.5 m evacuated flight path with fission monitors at both ends. Attempts to measure the total, unfiltered spectrum from the cold source failed because the chopper in its closed position was not sufficiently opaque to the epithermal and fast neutrons in the beam. Consequently, most of the measurements ere made with 9 inches of liquid-nitrogen-cooled, single-crystal quartz in the beam immediately preceding the chopper. The data were subsequently corrected for background , chopper transmission, the 1/v dependence of the beam monitor efficiency, and the tabulated transmission of quartz at 77 K.

A typical corrected wavelength spectrum with the cold source at 30 K is shown in figure 1. Although the complete spectrum is not Maxwellian in shape, a single Maxwellian curve with a temperature of 65 K gives a reasonably good fit to the data from 3 to 9 A (solid curve in fig. 1).

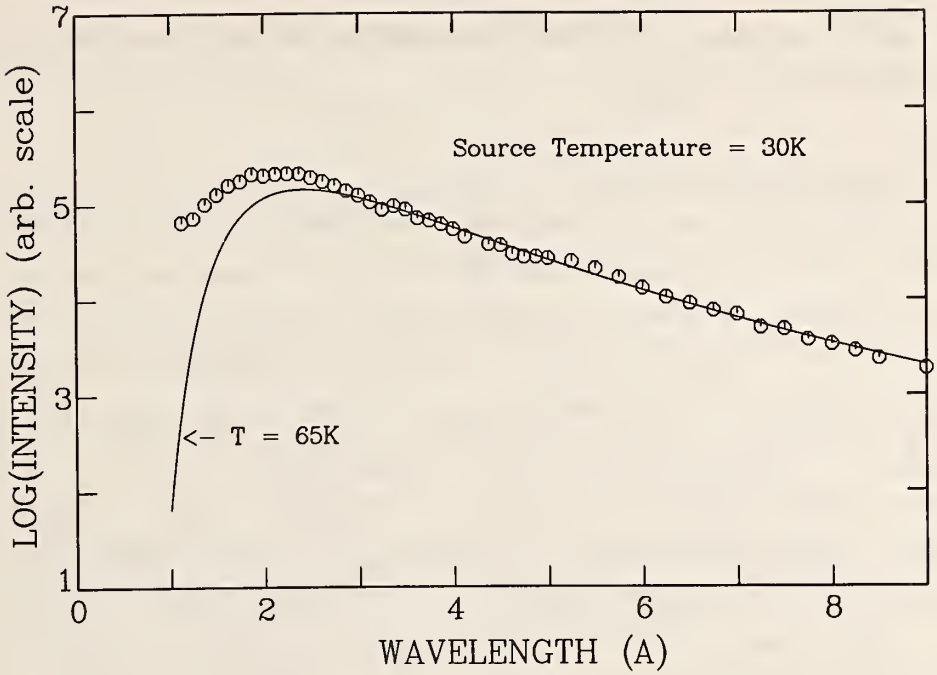

Figure 1. A typical corrected wavelength distribution, measured by time-of-flight, with the cold source operating at 30 K with 7.5% H_2O homogeneously mixed in the D_2O. The solid curve is a Maxwellian spectrum at a temperature of 65 K that gave the best fit to the data from 3 to 9 A.

2) Absolute Flux Measurements

An absolute value for the neutron flux from the cold source was derived from fission rates measured with a double fission chamber placed at the entrance to the SANS instrument's pre-sample flight path for direct comparison with similar measurements made in 1981 when the SANS instrument was first installed. For this measurement the liquid-nitrogen-cooled SANS filter, consisting of 8 inches of single-crystal bismuth and 8 inches of polycrystalline beryllium, was in place, but the velocity selector was removed. Thus the measured fission rates represent an integration over all wavelengths greater than 3.95 A, the Bragg cutoff for beryllium, weighted by the 1/v cross section of the fission foils.

The flux inferred from measurements with three fission foils of known mass, including one foil that was used for the 1981 flux measurement, was 4.94×10^7 n/cm^2-sec (assuming a Maxwellian spectrum for wavelengths greater than 4 A with a characteristic temperature of 65 K) with an uncertainty of about 7%. This is an increase in cold neutron flux ($\lambda > 3.95$A) of $2.5 \pm .2$

over the value measured in 1981 (scaled to 20 MW) which was based on a Maxwellian temperature of 350 K.

3) Flux Gains Versus Wavelength

After reinstalling and calibrating the SANS velocity selector, beam monitor count rates were measured versus wavelength under various cold source operating conditions. The ratios of count rates measured with the cold source temperature at 30 K (with 7.5% H_2O in the D_2O ice) and with the source empty are plotted in figure 2. The measured gains under this condition increase from about 4.5 to 5.5 over the wavelength range from 5 to 12 Å

SANS beam monitor count rates were also used to assess the effect of substituting a small percentage of H_2O for D_2O in the cold source in an effort to optimize the moderating and transmission characteristics of the source. The best results were obtained with a homogeneous mixture containing about 7.5% H_2O which gave about a 20% increase in flux compared to having pure D_2O in the source.

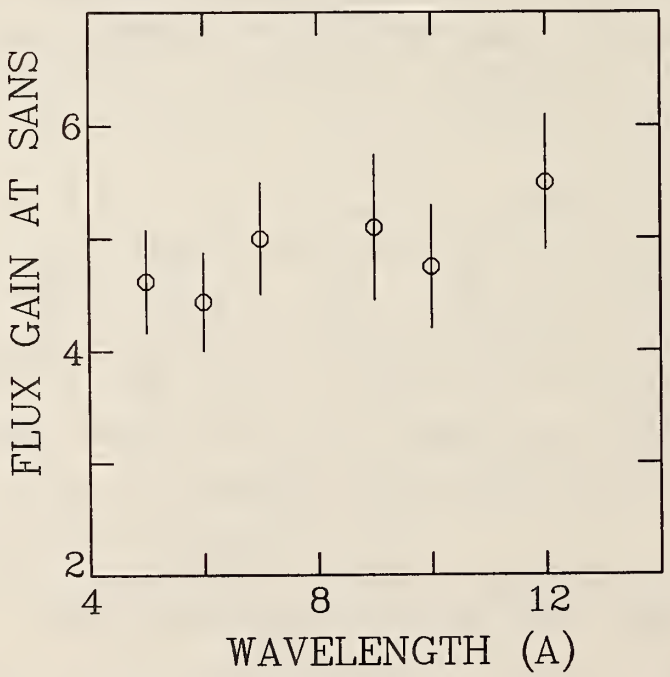

Figure 2. Data points are ratios of beam monitor count rates measured at the SANS instrument with the cold source at a temperature of 30 K (with 7.5% H_2O in the D_2O ice) to those measured with the source empty.

SUPERMIRROR DEVELOPMENT

C. F. Majkrzak and D. A. Neumann

J. R. D. Copley
(University of Maryland and National Bureau of Standards)

and

R. P. DiNardo
(Brookhaven National Laboratory, Upton, NY)

Polarized neutrons play an important role in scattering studies of condensed matter [1]. Consequently, an efficient means of polarizing a neutron beam is very valuable. In addition to conventional, bulk single-crystal polarizers such as the Heusler alloy Cu_2MnAl, polarizing mirrors are often used for this purpose. This is possible because for most materials the refractive index for neutrons is less than unity so that external reflection occurs from flat surfaces in air or vacuum at glancing angles up to a critical angle of the order of 0.1 deg/Å neutron wavelength. Furthermore, because the neutron possesses a magnetic dipole moment, its propagation through ferromagnetic materials is determined by a birefringent refractive index. Thus for a ferromagnetic material which is magnetized parallel to its reflecting surface, the critical angle depends on the neutron spin state so that only one spin state is effectively reflected between two distinct critical angles. For many applications it is advantageous to reflect one spin over as wide a range of angles as possible with a high efficiency. To this end polarizing supermirrors, first suggested by Mezei [2] and Turchin [3] have been developed in recent years [4,5] which in effect extend the critical angle of reflection for one spin state by constructive interference of the neutron wave in a thin-film, multi-layered structure consisting of a ferromagnetic and nonmagnetic material. Reviews of these devices and their applications are given in references [6-8]. Nevertheless, it has not yet been possible to produce polarizing supermirrors with high reflectivity beyond about twice the critical angle of ordinary Ni (0.1 deg/Å). Current efforts are focussed primarily on: 1) extending the critical angle of both polarizing and non-polarizing supermirrors out to a critical angle equal to three times that of ordinary Ni; and 2) obtaining, simultaneously, a uniform reflectivity approaching unity. Recently, direct evidence has been obtained by electron microscopy performed at ORNL [9] which suggests that the primary reason for

reduced reflectivity in supermirrors is a progressive roughening of the layers, presumably due to lattice mismatch, thermally induced strain, or microcrystallite size and orientation. Deposition conditions favoring amorphous growth and reduced stress are therefore being sought.

Work on Fe-Si [10] and Fe-W [11] polarizing multilayers and supermirrors deposited by sputtering techniques at Brookhaven National Laboratory is in progress. Non-polarizing supermirrors, which have a potentially important application as guide tube coatings to improve beam transport properties, are being developed in collaboration with two commercial film coaters, the Ovonics Co., Troy, MI, and the Opto-Line Co., Andover, MA. In particular, Ni-Ti, C-Al, and C-V systems are being investigated.

In addition, measurements of the flux enhancement gained with converging guide segments constructed of both ordinary mirrors and supermirrors have been performed. The measured gains are in good agreement with the predicted values as shown in figure 1 [12].

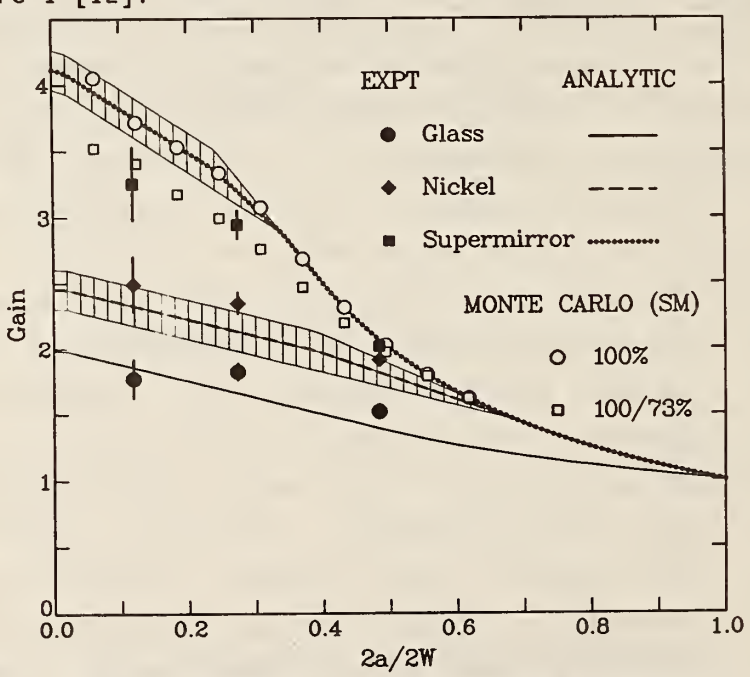

Figure 1. Measured and calculated gains, plotted as a function of the exit window width 2a to the entrance window width 2 W, for converging guide systems. The experimental measurements and the analytic calculations are shown as closed symbols and lines respectively. The hatched areas represent the uncertainties in the calculated gains due to the uncertainties in the critical angle ratios m. The error bars on the experimental results are due to uncertainties in the widths 2a. The open symbols represent Monte Carlo calculations, assuming 100% reflectivity to Q_c = 0.043 $Å^{-1}$ (circles), and 100% reflectivity to 0.020 $Å^{-1}$, 73% reflectivity from 0.020 to 0.043 $Å^{-1}$ (squares).

References

[1] R. M. Moon, T. Riste, and W. C. Koehler, Phys. Rev. 181, 920 (1969).

[2] F. Mezei, Comm. Phys. 1, 81 (1976).

[3] V. F. Turchin, Deposited Paper, At. Energy 22, No. 2 (1967).

[4] O. Scharpf, AIP Conf. Proc. 89, 182 (1981).

[5] T. Ebisawa, N. Achiwa, S. Yamada, T. Akiyoshi, and S. Okamoto, J. Nucl. Sci. Tech. 16, 647 (1979).

[6] R. Pynn, Rev. Sci. Instrm. 55, 837 (1984).

[7] C. F. Majkrzak, Applied Optics 23, 3524 (1984).

[8] C. F. Majkrzak et al. Physica B, to be published.

[9] H. Mook and J. Bradshaw, private communication.

[10] R. P. DiNardo, C. F. Majkrzak, and D. A. Neumann, Fabrication of Neutron Polarizing Multilayers by Sputtering, Proc. of the 32nd Annual Int'l. Tech. Symposium on Optical and Optoelectronic Applied Science and Engineering, SPIE, August, 1988, San Diego, CA to be published.

[11] C. F. Majkrzak, D. A. Neumann, J. R. D. Copley, and R. P. DiNardo, Fe-W Supermirrors for Polarizing Neutrons, Proc. of the 1987 Fall Meeting of the Materials Research Society, in press.

[12] J. R. D. Copley and C. F. Majkrzak, Converging Neutron Guides, Proc. of the 32nd Annual Int'l. Tech. Symposium on Optical and Optoelectronic Applied Science and Engineering, SPIE, August, 1988, San Diego, CA, to be published.

NEUTRON REFLECTION STUDIES OF SURFACES AND INTERFACES

S. K. Satija and C. F. Majkrzak

In the past ten years there has been growing interest in a variety of surface sensitive techniques including more recently, neutron reflection from surfaces. Current developments show this to be a powerful probe of surface properties; e.g., density profile with depth and surface roughness etc. One unique advantage of neutrons is that selective deuterium labelling can be used to highlight scattering from selected components in a film. At the NBS research reactor we have initiated a comprehensive program in neutron reflectivity measurements from a variety of surfaces and interfaces in anticipation for an expanded capability in the cold neutron guide hall.

In order to differentiate between various models of surfaces, it is crucial to measure reflectivities to very low levels. Recently we have demonstrated the ability to measure reflectivities down to ~ $1x10^{-6}$. An example of such a measurement is shown in figure 1. The points in figure 1 show the measured neutron reflectivity from a highly polished single x-tal of quartz. The line shows calculated reflectivity from quartz surface assuming a root mean square surface roughness of 5 Å. With the completion of a new dedicated instrument in the cold neutron guide hall we will be able to measure neutron reflectivities in $1x10^{-7}$ range. This would be better than any instrument currently available in the world.

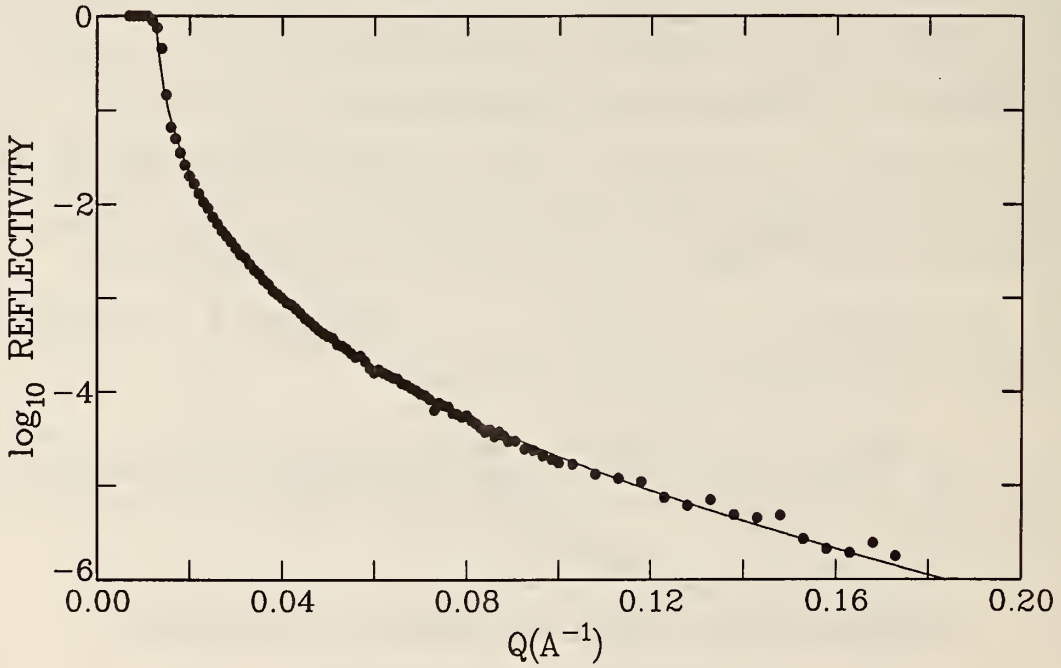

Figure 1. Neutron reflectivity from a highly polished quartz single x-tal. The data has been corrected for background and contribution due to off specular scattering. The solid line is the calculated reflectivity for quartz surface with an RMS surface roughness of 5 Å.

SIMULATION OF THE PHASE SPACE TRANSFORMATION OF NEUTRONS BY BRAGG REFLECTION FROM MOVING MOSAIC CRYSTALS

D. A. Neumann

Backscattering has proven to be an extremely valuable tool for the study of single particle motions in condensed matter, primarily due to the excellent energy resolution ($\lesssim$ 1 μeV) of these instruments. The principal limitation of this technique has been the rather small flux on the sample ($\approx$ 10^4 neutrons/cm^2/sec at both the Institut Laue-Langevin and Jülich) partially linked to the extremely good energy resolution. There is also, however, a substantial mismatch of the angular resolution of the primary and secondary sides of all cold neutron backscattering instruments currently in operation because the divergence of the incident beam is limited by the neutron guide on which the instrument is installed, while the angular resolution of the secondary spectrometer is quite low due to the large area analyzing crystals and the detector geometry. Therefore it is possible to increase the flux at the sample position without degrading the energy resolution by increasing the angular divergence of the incident beam. This has in fact been done to some extent at Jülich through the use of a converging supermirror guide placed immediately before the sample. However it seems impossible to match the $\vec{Q}$ resolution of the primary spectrometer to that of the secondary spectrometer with current supermirror technology. To overcome this difficulty Schelten and Alefeld have proposed a novel neutron phase space transformation which uses moving mosaic crystals to change a well-collimated, white neutron beam into a divergent, nearly monochromatic one [1]. Physically, this occurs because the slower moving neutrons are diffracted at higher angles and therefore get a "push" from the moving crystal, while the Bragg condition is satisfied at smaller angles for the faster neutrons causing diffraction to occur from crystallites moving away from the incident neutrons thereby reducing their speed. In order to assess the possible gains for a backscattering spectrometer built at the Cold Neutron Research Facility, a simulation of this type of transform has been performed incorporating parameters relevant to the NBSR.

A backscattering spectrometer built at the NBS would be located on a ^{58}Ni guide of dimension 6 $\times$ 15 cm^2. Therefore the beam must be compressed in order to achieve a reasonable sample size of 3 $\times$ 3 cm^2. It is envisaged that this would be accomplished with a converging supermirror nose with a critical angle of about twice that of Ni. Simulations of this element indicate that the beam

divergence η after such a compression would be approximately twice the critical angle of Ni in the horizontal plane ($\eta_h = 2\theta_c$) and about three times θ_c in the vertical direction ($\eta_v = 3\theta_c$).[2] For the purposes of this simulation, the phase space crystal was chosen to be pyrolytic graphite (d = 3.354 Å and θ_o = 69.181°) with a thickness of 5 mm. The incident distribution of neutrons was taken to be a 65 K Maxwell-Boltzmann distribution (in accord with measurements of the flux from the NBS cold source) truncated at 4 Å to simulate a Be filter in the incident beam and at 10 Å because wavelengths longer than this have essentially no probability of being diffracted by the moving crystal. This distribution was then multiplied by the square of the incident wavelength in order to account for the fact that θ_c is proportional to the wavelength. The horizontal and vertical mosaics and the velocity of the graphite crystal were included as input parameters. The reflectivity of graphite was accounted for with the Bacon-Lowde equation for diffraction from ideally imperfect crystals [3]. This will overestimate the reflectivity of the deflector crystal resulting in the simulated gains being somewhat larger than what one would actually observe. (Note that the reflectivity is a function of the crystal speed. This has been included.) All of these simulations have been performed using the assumption that Si (111) crystals will be used as the monochromator ($\lambda \approx 6.27$ Å).

Two-dimensional projections of simulated Bragg reflections from a crystal having an isotropic 10° mosaic are shown in figure 1 for three different crystal speeds. Here the incident and final k_x and k_y values of the diffracted neutrons are represented by individual dots and the reference values are indicated by the solid lines. Two effects are evident. The first is that the phase space volume increases as the crystal velocity increases. This is because the Bragg reflection takes place at a lower angle in the Doppler frame. The second effect is that the diffracted beam tilts in phase space as the crystal velocity is changed. This tilt can be optimized so that the maximum number of neutrons have the correct energy to be backscattered from a Si (111) crystal. Note that this does not violate Liouville's theorem because the orientation, not the volume, of the final phase space element has been changed.

The most important information from the standpoint of increasing the flux of backscattering instruments is displayed in figure 2. Here the peak intensity (relative to that obtained for a crystal velocity of zero) is shown

as a function of speed for mosaics of 1°, 3°, 5°, 10°, and 20°. For mosaics of 3° or larger, the relative intensity increases from about 1 to a broad maximum, before decreasing again. For the parameters chosen here, the maximum gain is about 6 which occurs for a crystal with a 10° mosaic moving at about 300 m/s. The results for a 20° crystal show a smaller gain due to the decrease in the reflectivity. The results for a crystal having a mosaic of 1° appear somewhat unique. Here the intensity increases linearly with the crystal speed and has a relative value of only about 1/2 for a speed of 0. This is a result of the fact that a 1° mosaic is too small when compared to the divergence of the incident beam.

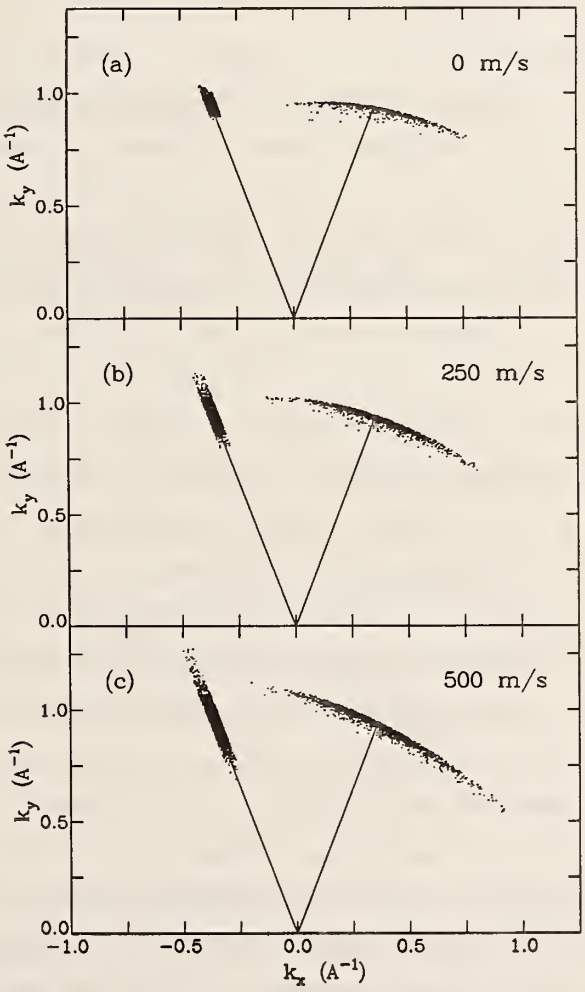

Figure 1. (a) Projection of a 3-dimensional simulation of Bragg diffraction from a stationary crystal with a mosaic of 10°. The dots represent the initial and final wave vectors of the diffracted neutrons. (b) Same view for a crystal speed of 250 m/s. Note that the initial phase space volume has expanded and the final volume has been "tilted" compared to the results obtained for the stationary crystal. (c) Crystal speed = 500 m/s.

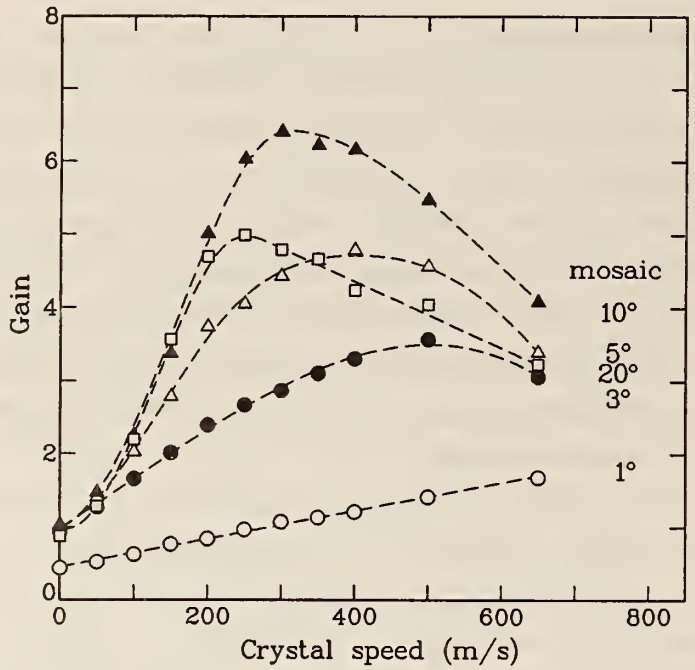

Figure 2. Peak intensity relative to that obtained for a stationary crystal. For a mosaic of 10°, the phase space transform leads to a gain of 6 for a crystal speed of 300 m/s. The dashed lines are guides to the eye.

The resulting gain factor of 6 would not be appreciably altered if supermirrors were developed to the point were it would be possible to fabricate guides with a critical angle twice that of Ni. However, if supermirrors suitable for focusing noses having even larger critical angles also became available the gain from the phase space transform would be reduced. For example, if the incident divergences were doubled (which would require a nose section having a critical angle of four times that of Ni) one would only attain a gain of 2-3 via the phase space transform instead of the value of 6 reported here. In addition, these simulations have shown that it is essential that the phase space crystal have an anisotropic mosaic to limit the vertical divergence and that the phase space transform technique may not be particularly useful as the sole monochromating device in an instrument because the final energy distribution is somewhat skewed to higher energies.

References

[1] J. Schelten and B. Alefeld, in Proc. Workshop on Neutron Scattering Instrumentation for SNQ, Maria Laach, 3-5 Sept. 1984, R. Scherm and H. H. Stiller, eds., report Jül-1954 (1984).

[2] The simulation of the converging guides was done using a program written by J. R. D. Copley.

[3] G. E. Bacon and R. D. Lowde, Acta Cryst. 1, 303 (1948).

SPIN POLARIZED INELASTIC NEUTRON SCATTERING SPECTROMETER (SPINS)

C. F. Majkrzak

Conceptual design work on an inelastic neutron scattering spectrometer to be situated on a neutron guide in the new NBS cold neutron facility is now in progress. The proposed machine is an innovative modification of a standard triple axis spectrometer with the capability of measuring spin-dependent cross sections. The use of state-of-the-art supermirror polarizers and a novel energy-dependent flipper will make it possible to obtain an energy resolution as good as about 10 μeV without prohibitive restriction of beam divergence. Although the four spin-dependent neutron cross sections can be measured, it will also be possible to use unpolarized beams when desired. The spectrometer will be capable of covering a range of incident neutron energies from 15 meV to 2 meV with resolutions from 1 meV down to about 10 μeV and with tunable instrumental resolution. In order to decouple the dependence of the energy resolution on the angular divergence of the beam, the proposed spectrometer will utilize a novel energy-dependent spin flipping device in conjunction with a pair of polarizing supermirrors as an energy analyser and/or monochromator preceding the sample as desired. The energy-dependent flipper is of the type first proposed by G. M. Drabkin [1]. Using this monochromating device, a very high energy resolution can be obtained even for a considerably divergent beam with a corresponding gain in intensity. The resolution function of the spectrometer can therefore be tuned for a particular experiment.

It should be emphasized that the proposed spectrometer is designed for both polarized and unpolarized beam experiments. The energy-dependent analyser device utilizes the neutron spin but does not require that the sample have a scattering cross section that is spin-dependent. Furthermore, the spectrometer will be designed to be completely flexible in choice of either PG

or energy-dependent flipper and pair of supermirrors at both the monochromator and analyser positions. This spectrometer should find wide application to problems in condensed matter physics and chemistry. For more details, see reference [2].

References

[1] G. M. Drabkin, Sov. Phys. JETP 43, 1107 (1962).

[2] C. F. Majkrzak, C. J. Glinka, and S. K. Satija, SPIE Conf. Proc. No. 983, to be published.

ON THE USE OF MULTIPLE-SLOT MULTIPLE DISK CHOPPER ASSEMBLIES TO PULSE THERMAL NEUTRON BEAMS

J. R. D. Copley
(University of Maryland and the National Bureau of Standards)

Single-slot disk choppers, illustrated in figure 1, are commonly used to pulse thermal neutron beams, but their use in high resolution applications is limited because the maximum transmitted beam intensity, given that the chopper is rotating at its maximum possible speed, is proportional to the square of the burst time of the chopper, which is proportional to the width of the incident beam. This means that in order to obtain high resolution using single-slot disk choppers it may be necessary to use an incident beam which is narrower than the available beam width, severely reducing the intensity at the sample position.

The transmitted intensity can be doubled, with no associated increase in the burst time, by doubling the beam width and using counter-rotating choppers [1] to double the effective chopping speed (fig. 2). In order to increase the intensity still further, without degrading the resolution, we propose [2] the use of multiply-slotted choppers in combination with a multiply-slotted beam mask. The first (and most practical) example of this concept requires two slots in each of two counter-rotating choppers and a mask (fig. 3), giving a transmitted beam intensity which is four times that of the single-slot single chopper arrangement, with no change in burst time. A further doubling may be achieved, with no change in the burst time, if three choppers (with relative angular frequencies ω, $-\omega$, and $\omega/2$) and a mask, each fitted with four slots, are employed. The purpose of the mask and the additional choppers in these systems is to suppress the early and late "satellite" bursts which would otherwise be permitted to occur.

(a)

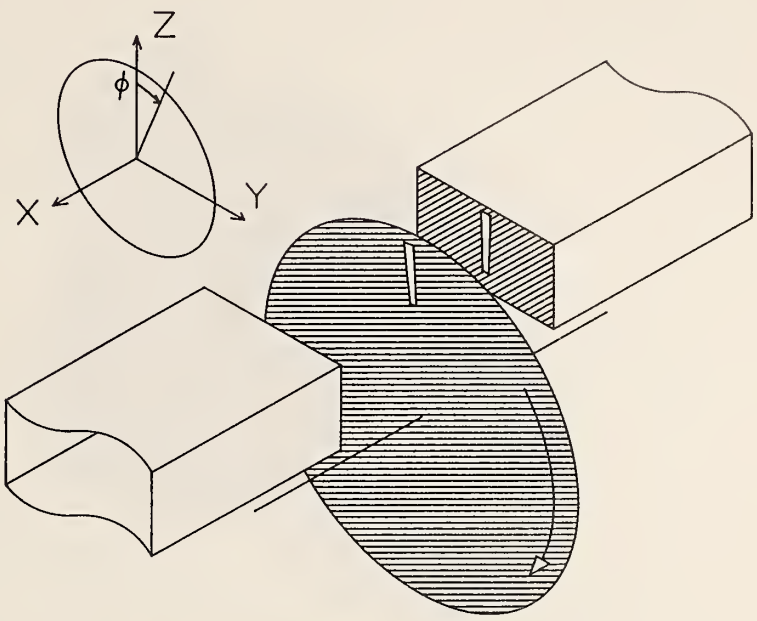

(b)

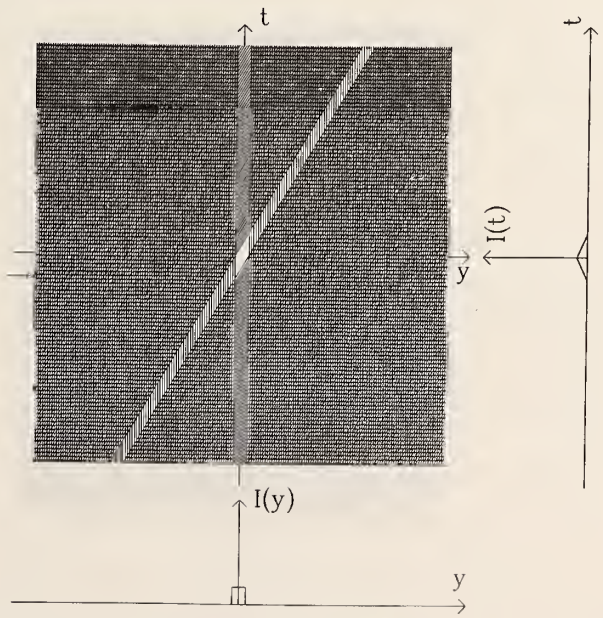

Figure 1. The single-slot single chopper assembly. (a) A schematic view of the setup. For clarity the width of the neutron guide is exaggerated. The width of the slots in the chopper and the mask is b and the chopper rotational frequency is ω. The burst time ΔT is b/v where $v = \omega R$. The system is shown at the start of a burst, $t = -\Delta T$. (b) The corresponding y-t diagram. The unhatched area represents the transmitted neutrons. The arrow to the left of the y-t diagram indicates the time associated with the schematic view of the assembly. Plots of intensity as functions of y and t are also shown.

(a)

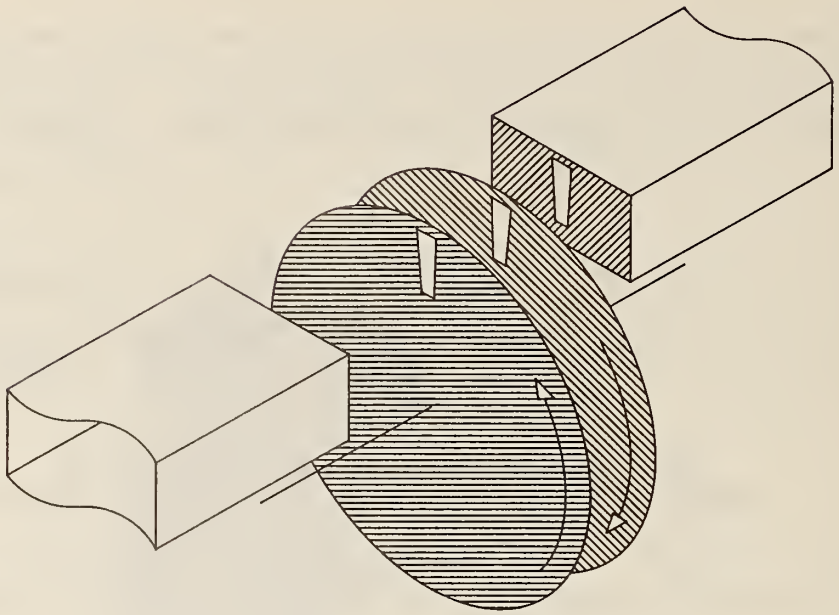

(b)

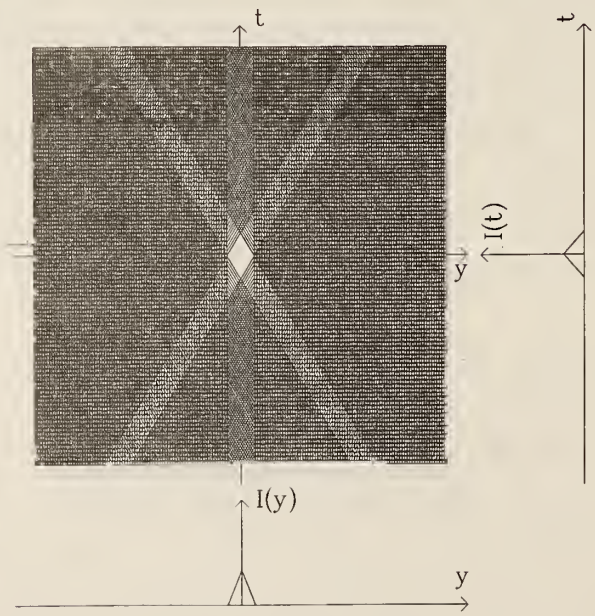

Figure 2. The single-slot double chopper assembly. (a) A schematic view of the setup. The width of the slots is 2b and the chopper rotational frequencies are ω and $-\omega$. The burst time is again b/v, and the system is shown at the time $t = \Delta T/2$: the choppers have passed the fully open position, and the transmitted intensity is one-half its maximum value. (b) The corresponding y-t diagram. See the caption to figure 1 (b).

(a)

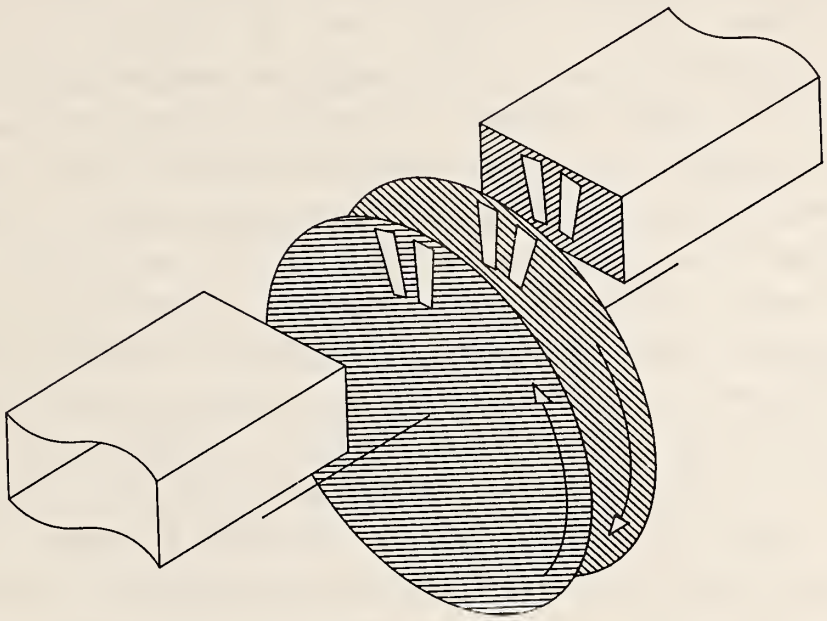

(b)

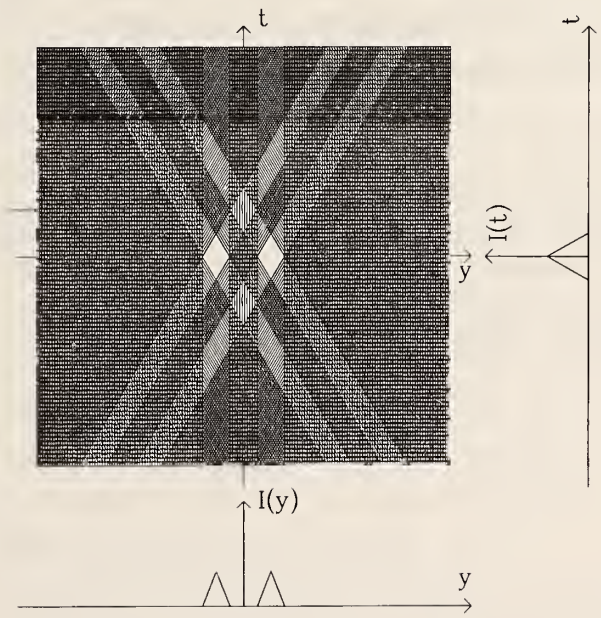

Figure 3. The double-slot double chopper assembly. (a) A schematic view of the setup. The width of the slots is 2b, the separation of their centres is 4b, and the chopper rotational frequencies are ω and $-\omega$. The burst time is again b/v, and the system is shown at the time $t = 2\ \Delta T$: the slots in the choppers are aligned, but the mask stops the unwanted satellite burst. (b) The corresponding y-t diagram. See the caption to figure 1 (b).

The effects of relative phasing errors in multiple chopper systems have been studied in considerable detail. The first effect is that the intensity of the principal burst is reduced, and to an extent this effect can be tolerated. The second and potentially much more damaging effect is that the satellite bursts are not necessarily completely suppressed. For example, if the width of a slot is 2b, the centre-to-centre adjacent slot separation is 2B, and the distance of the slots from the chopper axis is R, then relative phase angle deviations $|\delta\phi| > (B-2b)/R$ in a two-slot two chopper arrangement result in nonzero satellite burst intensity. To obviate this problem B/2b should be somewhat greater than unity, and the data acquisition system should be gated off whenever an unacceptable pulse (as defined above) occurs.

Our calculations, combined with information regarding achievable phase stability in actual disk chopper systems, have persuaded us to consider very seriously the idea of including the option of multiple chopper assemblies in the new high resolution time-of-flight instrument which is to be installed in the neutron guide hall. There are however certain other matters which must be considered, including the effects of nonzero radial extent of the slots in the choppers, nonzero separation between the choppers in a chopper assembly, and the spatial distribution of neutrons leaving a multiple-slot assembly.

References

[1] P. A. Egelstaff, Proc. of the First International Conference on the Peaceful Uses of Atomic Energy, Geneva, 1955 (United Nations, New York, Vol. 4, p. 70 (1956).

[2] J. R. D. Copley, Nucl. Instr. Meth.,(in press).

CALCULATIONS OF THE PERFORMANCE OF NEUTRON GUIDES

J. R. D. Copley
(University of Maryland and the National Bureau of Standards)

We have written a number of computer programs to investigate the behavior of parallel and converging neutron guides. The calculations are for the most part performed analytically in the case of straight-sided guides, whereas a Monte Carlo ray tracing technique is employed with curved guides and complex guide systems. The Monte Carlo calculations also serve as a check on the analytic calculations. Acceptance diagrams at the entrance, at the exit, and at points beyond the exit, are readily computed and plotted. These diagrams show the y-β distribution of the neutrons at the location of interest, where y is the spatial coordinate normal to the direction of the guide, and β measures the angle between the neutron direction and the guide direction. Guide gains and spatial and angular distributions may be computed using these acceptance diagrams. Most of the programs handle only one lateral guide dimension, but there is also a program which can be used to calculate the performance of a guide system with two lateral dimensions. Most of our effort has been devoted to calculations for straight-sided converging guides and for curved converging guides with the profile of a logarithmic spiral. We have also investigated the idea of placing additional blades within a straight-sided converging guide, blades which transmit the neutrons incident at angles higher than the critical angle for reflection by the guide.

The major conclusions from this work may be summarized as follows:

(i) Current density gains of order two or three are relatively easy to achieve using guides which converge in one lateral dimension, as long as the taper angle is correctly chosen and the converging section has a significantly higher critical angle (by a factor of order two) than the parallel section which precedes it: gains of order four or more appear to be extremely difficult to achieve.

(ii) The angular distribution of the neutrons exiting a converging guide is in general broad and highly non-uniform. The sample position should be close to the exit of a converging guide in order to reap as much benefit as possible from the increased current density at the exit.

(iii) Since the performance of a converging guide depends on the wavelength of the neutrons, the benefits of this type of device are most easily realized when it is designed to be used exclusively with a single choice of neutron wavelength.

Measurements of the performance of a converging guide system, described under "Supermirror Development" by C. F. Majkrzak et al. in this report, are in very good agreement with calculation. This gives us considerable confidence to use the results of calculations in the design of instruments.

THE SMITHSONIAN - NBS PROGRAM ON THE STUDYING OF ART OBJECTS BY NEUTRON METHODS.

Y. T. Cheng, M. J. Blackman, and J. S. Olin
(Smithsonian Institution and the National Bureau of Standards)

and

M. Ganoczy

1. The Application of Neutron Radiography and Activation Analysis to the Study of Ancient Bronzes

It is often desirable to have both the structural and compositional information available in addition to stylistic consideration in the study of ancient metal objects. X-ray radiography is utilized most commonly in structural analysis. The technique is useful except in cases where the object contains some high density materials such as lead and where organic substances and other low density contents inside the metal object are of interest. The compositional information generally is provided by detailed quantitative analysis of small samples taken from various inconspicuous places in the metal objects. The pitfalls for such a method are the common sampling difficulties: that the samples taken may not be true representations of the whole object and that the method is destructive. In this study, a neutron technique that combines neutron radiography and whole object neutron activation analysis was used to compliment the conventional approaches in providing structural and compositional information of a metal object.

The neutron radiography extends the ability to image the structure and the interior of a metal object beyond what can be accomplished with x-ray radiation, and the whole object neutron activation analysis (NAA) can give an

average composition of the major components in the object studied. The collection of 20 Tibet an Lo-Han figures from the National Museum of Natural History (fig. 1) was studied by the neutron technique. Five of the 20 religious figures still have their bottom seals in place, the rest have their seals and contents removed. High resolution neutron radiography was developed and applied to the five sealed figures to obtain clear images of the contents inside. The whole object NAA was carried out for the 15 opened figures. The whole object NAA differs from normal NAA in that: 1) it activates the entire object thus only a fraction of the neutron fluence needed for NAA study is required, 2) it uses a highly uniform neutron field to activate the test object so a proper averaging can be obtained. In addition, in whole NAA, the wall thickness of the test object, and to a lesser degree, the shape of the object and its alloying type all need to be considered and calibrated. The radiation released by the test object is very closely related to the thickness of the material being activated. This is because a truly uniform activation is difficult to achieve as neutrons are being attenuated more when they penetrate deeper into the material. The outer material can also shield the gamma radiation inside from being fully counted. A test calibration using copper cylinders with various wall thicknesses was conducted. The test shows that the detected radiation level per unit copper mass is an exponentially decreasing function of the cylinder wall thickness. A slight modification of the calibration was necessary to account for the fact that the shapes of these Tibetan figures were not cylindrical. Neutron radiographs of the 15 opened figures were digitized and evaluated by comparing with standards in deriving an average wall thickness for each figure. Each derived average wall thickness was then used to check against the calibration to obtain a corrected copper radiation level for that particular figure. Our initial result on the study of the Lo-Han figures indicates that they are in general alloys of copper and lead with small amounts of arsenic and indium. Gamma ray induced lead x-ray fluorescence was detected in the energy spectrum. Some figures also contain tin or low levels of antimony and zinc. The copper contents range from about 70% to 95% (see fig. 2).

Figure 1. The Tibetan bronze statues collection at the National Museum of Natural History.

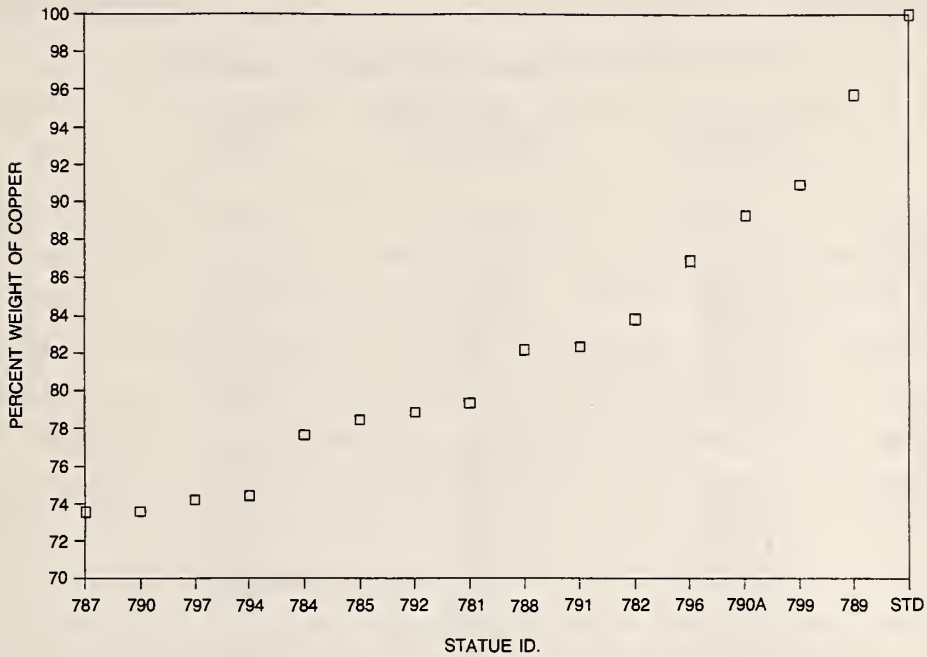

Figure 2. Percent weight content of copper in Tibetan bronze statues.

2. Neutron Activation Autoradiography

The study of works by Thomas W. Dewing using neutron activation autoradiography techniques continued with the paintings "Alma Thayer", "Lady Listening", "Lady in White #1", "Lady in White #2", and "Spinet". All were from the National Museum of American Art (NMAA). A Scholarly Studies proposal was submitted to the Office of Fellowships and Grants of the Smithsonian Institution and funding was granted to support art historian Dr. Susan Hobbs for collaboration in this continuing study. Meantime, the collaboration with NMAA has developed further. A new project, studying another prominent American artist Albert Pinkman Ryder has been initiated. His works are highly imaginative and "picture the inner reality of the mind and present to us the purest poetic imagery in the century." Four of the Ryder paintings from NMAA "Lord Ullin's Daughter", "Christ Appearing to Mary", "Pastoral Scene" and "Jonah" have been studied by autoradiography to date. Table 1 shows the neutron activation analysis result of the four paintings studied so far.

Table 1. Amount per unit area (mg/cm**2) in paintings by Albert P. Ryder

ELEMENT	LORD ULLIN'S DAUGHTER	CHRIST APPEARING TO MARY	PASTORAL STUDY	JONAH
NA SODIUM	0.486	1.101	1.470	1.018
MG MAGNESIUM	*	*	*	*
AL ALUMINIUM	0.930	2.055	1.667	1.788
CL CHLORINE	0.298	0.508	1.757	0.494
K POTASSIUM	0.106	0.150	0.111	0.505
CA CALCIUM	18.660	5.330	14.805	15.946
SC SCANDIUM	TRACE	TRACE	TRACE	TRACE
TI TITANIUM	*	*	*	*
V VANADIUM	*	0.002	0.003	*
CR CHROMINIUM	0.138	0.385	1.296	0.562
MN MANGANESE	0.179	0.108	0.139	0.100
FE IRON	1.257	6.487	6.316	4.722
CO COBALT	0.001	*	0.059	0.125
CU COPPER	*	0.089	*	*
ZN ZINC	2.147	0.824	18.716	12.751
AS ARSENIC	0.006	0.012	0.080	0.028
SE SELENIUM	*	*	2.159	0.003
BR BROMINE	0.011	0.009	0.025	0.005
SR STRONTIUM	0.030	1.206	1.293	1.214
AG SILVER	*	*	*	*
CD CADMIUM	*	*	0.322	0.012
IN INDIUM	*	TRACE	TRACE	TRACE
SN TIN	*	0.432	0.001	0.001
SB ANTIMONY	0.121	0.012	0.396	0.036
BA BARIUM	0.161	53.538	10.295	8.777
SM SAMARIUM	TRACE	TRACE	TRACE	TRACE
AU GOLD	0.001	0.002	0.001	TRACE
HG MERCURY	0.250	0.417	0.254	0.821
U URANIUM	*	*	*	*

Elements with "*" are not detected.

We wish to thank Dr. Paul Taylor, Department of Anthropology, National Museum of Natural History and Dr. Elizabeth Broun, Acting Director, National Museum of American Art. We also wish to acknowledge Fred Shorten's assistance in providing the photograph used for figure 1.

B. NON-RRD PROGRAMS

NEUTRON INTERACTIONS AND DOSIMETRY GROUP

J. A. Grundl

The Neutron Interactions and Dosimetry Group develops and applies well-characterized neutron fields and related capabilities for neutron dosimetry methods evaluation and standardization, for detector development and calibration, and for reaction cross-section measurements. Strong involvement with outside organizations, both in the federal and private sectors, includes many types of research and technology assistance programs as well as leadership roles on national and international standards and radiation policy making bodies.

A selection of accomplishments for FY 88, with emphasis on NBS reactor related activities, are outlined below in titled paragraphs. Projects that define the group's activities and major participants are included.

DOSIMETRY FOR MATERIAL PERFORMANCE ASSESSMENT

E. D. McGarry, D. Gilliam, C. Eisenhauer, and G. Lamaze

Dosimetry methods for monitoring the degradation of materials in high fluence neutron exposures are diverse. This project provides some form of measurement assurance, standardization, or methods development for nearly every approach to materials dosimetry employed in the United States. Interlaboratory measurement cooperation including substantial European participation are an important feature of this project.

1. Neutron Fluence Standards

These unique artifact standards are neutron sensors (activation foils generally) in which a radioactive species relevant for dosimetry is induced by irradiation in a standard neutron field. NBS maintains a variety of standard neutron fields to supply such neutron fluence standards to customers under NBS Spec. Publ. 250 Calibration Services and to the Nuclear Regulatory Commission (NRC) under a general consultation contract. These fluence standards provide benchmark referencing for dosimetry measurement methods used in the nuclear industry.

Of particular interest is the production of 30-year ^{137}Cs in fissionable foils of ^{238}U and ^{237}Np, and the production of 5.7-year ^{60}Co in copper by 30-day irradiations in the NBS ^{235}U Cavity Fission Source at the NBS reactor. Although long half-lives make these radioactive species difficult to produce in standard neutron fields, irradiations are carried out at some expense because long half-lives are especially appropriate for long-term neutron fluence monitoring in power reactors.

2. NBS-Westinghouse Cooperative Agreement

In a move to improve Quality Assurance (QA) methods associated with dosimetry procedures at commercial power reactors, NBS and Westinghouse have begun negotiating a cooperative agreement. Under this agreement, NBS will review the measurement techniques for reactor neutron dosimetry at Westinghouse to insure that direct measurement links exist with standard neutron fields at NBS. Westinghouse and NBS personnel have met and agreed upon important elements of a written agreement. Efforts are already underway to investigate some measurement discrepancies in power reactor data obtained with paired uranium detectors (PUD) neutron fluence detectors furnished by NBS.

3. Dosimetry Benchmarking for the HSST-Program

NBS is helping the NRC benchmark fast neutron dosimetry for an HSST steel testing program carried out by the Materials Engineering Associates (MEA) Corporation at the University of Buffalo's Pulstar Reactor. The focus of this activity is radioactive counting procedures at the Idaho Nuclear Engineering Laboratory (INEL) where analysis of all dosimetry involved in the MEA tests are performed. Comparisons of experimental dosimetry with neutron transport calculations were presented by NBS at the 14th ASTM- E10 Radiation Effects on Materials Symposium, in Andover, MA in June 1988.

4. Fission Spectrum Cross Section of $^{93}Nb(n,n')^{93m}Nb$

Because of its long half-life (16 years) and a low energy threshold (1 MeV), the Nb(n,n') reaction is a candidate for long term neutron fluence-monitoring. One drawback has been the lack of adequate cross-section information. Now, in cooperation with the universities of Illinois and Arkansas, the spectrum averaged cross sections of the niobium reaction have

been measured in the ^{235}U and ^{252}Cf standard fission neutron fields at NBS. Free-field neutron fluences at both irradiation facilities were established by neutron source emission-rate calibrations at the NBS $MnSO_4$ Bath Facility.

5. Benchmark Measurements in Commercial Power Reactors

Efforts continue to benchmark reference neutron dosimetry associated with fast neutron exposures of critical structures at nuclear power plants. The benchmark work focuses on both measurement of neutron exposures that cause embrittlement of steel and on the characterization of test reactor neutron environments used to study embrittlement models.

NBS is assisting the Babcock and Wilcox (B&W) Owner's Group conduct a full power cycle benchmark designed to check a variety of dosimetry methods, e.g., conventional foil activation versus solid-state track fission-event recorders. PUDs and lithium fluoride chips gamma sensors, both developed at NBS, are also included in this comprehensive dosimetry technique comparison.

PERSONNEL DOSIMETRY

R. Schwartz, C. Eisenhauer, J. Coyne, and E. Boswell

Standard neutron fields are developed and applied for calibration of radiation protection instrumentation and for the investigation and testing of new types of dose measuring techniques. Substantial responsibilities in national and international dosimetry methods research focuses on tissue dose modeling and tissue equivalent proportional counter measurements.

1. Calibration Service

Approximately 40 neutron radiation protection instruments were calibrated this year, the majority of them for nuclear power plants. The remotely operated detector positioner continues to operate well, minimizing exposure to personnel, speeding up data taking, and improving accuracy.

2. Performance Tests of Radiation Protection Instrumentation

In a joint project involving Harwell and the National Physical Laboratory in England, and the Naval Surface Warfare Center and Naval Research Laboratory in the United States, the properties of the new Chalk River "Bubble

Damage Detector" were investigated. The results of this work were sufficiently promising that this collaboration will continue under the auspices of the Naval Medical Command.

In an effort to understand the cause of the persistent slow drift in the 9" remmeters commonly used for neutron radiation protection measurements, a detailed study was made of the behavior of the 3BF proportional counters used as neutron detectors in these instruments. It was discovered that the drift is caused by an unfortunate combination of the somewhat unstable electronics in the remmeter instrument package, and the abysmal performance of the proportional counter. A good counter (readily available from other manufacturers) would eliminate the problem.

3. Tissue Equivalent Proportional Counter (TEPC) Studies

In a joint program with PTB and the University of Saarlands, a detailed study was made of the behavior of various configurations of TEPC's in the NBS filtered neutron beams. The purpose of this investigation was to learn how to improve the response of TEPC-based remmeters in the keV-to-100 keV neutron energy range. These types of remmeters are under active development at several laboratories in the United States and in Europe. It is recognized, however, that their performance needs to be improved in the energy region made accessible by our filtered beams. An immediate result of this study showed that the neutron dose due to contaminants in the beams as measured by the TEPC was in agreement with the predictions based on NBS ^{3}He and proton recoil spectroscopy. This work also demonstrated that the NBS filtered beams are, by a very significant margin, purer and of higher intensity than those available elsewhere.

4. International Standards Writing

The ISO Draft Standard Proposal, "Procedures for Calibrating and Determining the Energy Response of Neutron Measuring Devices Used for Radiation Protection," has been completely rewritten although further changes will have to be made. A draft of the chapter on calibrations, for the forthcoming ICRU publication "Determining of Dose Equivalents from External Radiation Sources - Part 3," has also been completed.

5. Data Acquisition Systems

The three Datacraft computers used for data acquisition at the linac and the 3-MV positive-ion accelerator for the past 13 years have been replaced. The new system consists of a Charles River Data System UV2403FT computer, MIZAR MZ9400 computer, and AST Research Inc. Premium/286 computer connected by a high speed local area network. The system is operational but will require some additional programming efforts.

RESEARCH AND TECHNOLOGY ASSISTANCE

all group members

Research activities and technology assistance are strongly coupled especially in neutron dosimetry. A multiplicity of institutional involvements, drawn to the group by unique irradiation facilities and measurement capabilities, encourages a variety of attractive projects and unavoidable responsibilities.

1. Neutron Lifetime Measurement

In collaboration with scientists of the Quantum Metrology Division, the University of Sussex, and the Central Bureau for Nuclear Measurements, an ambitious experimental program has been undertaken to improve previous measurements of the free neutron lifetime. The half-life for this most fundamental example of nuclidic disintegration is known to an accuracy of only ± 2.5%, while the half-lives of less stable particles such as the pion and the muon are known as much as 1400 times more accurately. The first lifetime data from this collaboration are expected between late August and early December 1988 from measurements at the Institut Laue-Langevin cold neutron guidehall in Grenoble, France. The experiment will next move to the new cold neutron guidehall at NBS for more exhaustive measurements. The group so far has carried out the absolute efficiency calibration of the ^{10}B neutron density monitor and will improve this calibration by means of a total absorption detector and an alpha-gamma coincidence calibration scheme. Group personnel also have participated in the Grenoble measurements.

2. Capture Cross-Section Measurement in ISNF

Spectrum-averaged cross sections for six reactions of interest in reactor physics have been measured in the Intermediate Energy Standard Neutron Field (ISNF). The ISNF neutron energy spectrum resembles a fast reactor spectrum, but with much less complexity. The ISNF neutron fluence is determined by fluence transfer from a calibrated ^{252}Cf fission source. The following spectrum-averaged cross sections were reported this year: $^{23}Na(n,\gamma)$ = 1.57 ± .10 mb, $^{45}Sc(n,\gamma)$ = 24.4 ± 0.8 mb, $^{59}Co(n,\gamma)$ = 36.3 ± 1.5 mb, $^{109}Ag(n,\gamma)$ = 23.8 ± 0.9 mb, $^{115}In(n,n')$ = 97.0 ± 2.5 mb, and $^{197}Au(n,\gamma)$ = 11 mb.

3. Fission Chamber Monitors at AFRRI

Neutron dosimetry at the Armed Forces Radiobiological Research Institute's reactor exposure room was put on a more stable basis by the installation and testing of two fission chamber monitors. The AFRRI staff has learned to operate these monitors confidently and have found them useful in resolving conflicting readings among other dosimetry systems. Linearity tests of reactor instrumentation, vs. NBS absolute fission chambers and tissue-equivalent ionization chambers were carried out over the full range of reactor power for the three most commonly used irradiation configurations.

4. Reactor Beam Calibrations

Absolute fission chambers and fissionable isotope mass standards were employed to determine absolute neutron fluence rates and improvement in the "capture flux" resulting from installation of the Cold Source at the NBS Research Reactor. These results influenced plans for further upgrading of the Cold Source.

5. Mass Assay of Ultra-Light Fissionable Deposits

Westinghouse Research Center, Pittsburgh is working cooperatively with NBS to establish mass scales for ultra-light fissionable deposits. These deposits, with masses in the picogram or sub-picogram range, are used with mica Solid Track Recorders (SSTR's) and represent a significant new dosimetry measurement technique. Currently achieved accuracy is better than 5%, the goal is 3% or better.

6. Paired Uranium Detectors (PUDs)

In 1984, PUDs were provided to Westinghouse Nuclear Technology Systems Division as backup dosimetry for ultra-lightweight SSTR neutron dosimeters. These dosimeters have been recovered and analyzed after an 18-month exposure in the Diablo Canyon power reactor. The results show a presently unexplained 15% discrepancy between the PUDs and SSTRs. NBS will now re-irradiate several of the PUD/SSTR pairs in a carefully controlled experiment in the NBS ^{235}U standard neutron field in an attempt to resolve the discrepancy.

7. LiF Chip Development and Application

A lithium fluoride crystal dosimeter package was returned to NBS after irradiation through a full fuel cycle in the cavity surrounding the reactor vessel at the Oconee 2 nuclear power plant. The sample retained virtually perfect optical quality, despite the heat and humidity of the environment. The gamma dose recorded was comfortably within the accurately readable range. This gamma dose data will be employed by the operating utility to confirm calculations of gamma and neutron dose as they affect the reactor vessel embrittlement and safe operating lifetime.

IRRADIATION AND CALIBRATION FACILITIES

E. D. McGarry, J. Grundl, C. Eisenhauer, and E. Boswell

Well-characterized neutron fields are built and maintained as permanent irradiation facilities providing certified fluences of pure fission neutrons, sub-MeV distributions, monoenergetic keV beams, and thermal neutrons. Passive and active detectors of all kinds are exposed in these neutron fields for response calibrations, for cross-section measurements, and for the investigation of new measurement techniques. A high intensity, neutron-driven gamma field operates for special purpose measurements.

A multi-purpose fission rate measurement capability is centered around the NBS "go anywhere" double fission chambers and the NBS set of fissionable isotope mass standards (FIMS). The Manganous Sulfate Bath is the primary neutron source strength calibration facility for the United States. Absolute neutron fluences for all fission-neutron-driven standard neutron fields at NBS are derived from source strength calibrations at this facility.

1. Cavity Fission Source Operations

Efforts to improve cavity fission source operations and calibration base documentation are continuing. A new general purpose shield cave for high and intermediate level radioactive components has been designed and shopwork on the shield walls has begun. When complete, this shield cave will greatly simplify irradiation operations at the reactor thermal column. New documentation describing the complicated path by which absolute fission neutron fluence rates are established are in final draft stage.

2. Scattering Corrections in the Cavity Fission Source

Corrections for neutron scattering in the hardware and irradiation samples of the cavity fission source are under review. Existing corrections are based on Monte Carlo calculations made by Los Alamos National Laboratory (LANL) for an earlier configuration of the cavity fission source with a different Cd box and Al enclosure. Furthermore, recent calibrations of solid state track recorders (SSTR's) involve a significantly different irradiation sample assembly. Recalculation of neutron scattering with the MCNP Monte Carlo code has yielded corrections for scattering in SSTR's that differ from the one calculated by LANL. We, therefore, recalculated scattering corrections with the MCNP Monte Carlo code. Corrections for scattering for SSTR's vary from - .006 for Ni reactors to + .018 for ^{235}U fissionable deposits.

NUCLEAR METHODS GROUP: OVERVIEW

R. F. Fleming
(Center for Analytical Chemistry)

The development and application of nuclear analytical techniques for greater accuracy, higher sensitivity and better selectivity are the goals of the Nuclear Methods Group. A high level of competence has been developed in reactor-based activation analysis, which includes instrumental and radiochemical neutron activation analysis (INAA and RNAA), as well as fast neutron activation analysis (FNAA). In addition, the group has a unique capability in neutron beam analysis with both prompt gamma activation analysis (PGAA) and neutron depth profiling (NDP). The NDP technique utilizes prompt charged particle emission to determine elemental distributions within the first few micrometers of a surface while the PGAA technique utilizes prompt gamma-ray

emission to measure the total amount of an element in a sample, regardless of its distribution. These techniques provide an arsenal of tools to address a wide variety of analytical problems in science and technology.

The activities of the past year have been highlighted by the initiation of the National Facility for Cold Neutron Research to be established at NBS during FY 89. The Group's involvement includes the design and construction of second generation instruments for PGAA and NDP. In addition, a facility is envisioned at which we will study the techniques for focusing neutron beams to increase the neutron intensity on a point. The combination of intense focussed beams applied to the existing analytical methods could result in greatly enhanced measurement capability. During FY 88 the cold source itself was installed and became operational, and construction of the guide hall will be completed during the the first quarter of FY 89. The Group's efforts have been aided substantially by its ability to use the existing cold neutron beams at the KFA Jülich facility. Plans are underway to include both the PGAA and NDP experimental systems in the first phase of implementation. A major grant from the Eastman Kodak Company is contributing to the timely development of NDP using cold neutrons.

The Group's contribution to the certification of Standard Reference Materials is illustrated by the multi-element measurements done on the SRM Bovine Serum, Buffalo River Sediment, and glass-film XRF standards. Work has been initiated on the new Orchard Leaves, Total Diet, Oyster Tissue, and a carbonaceous marine sediment, with Group members serving as the Technical Champion on each of these new SRM's. A new ability to quantify nitrogen in biological samples will result from this year's research to develop an NAA-liquid scintillation beta counting method exploiting the thermal neutron reaction 14N(n,p)14C and measuring the radioactive CO_2. This project is being done in collaboration with the University of Illinois.

The Group has taken an active role in the Bureau's program on high-temperature superconductivity, both in the measurement of impurities in starting materials and in final products, and in the determination of the actual stoichiometry of the metallic constituents. The effort this year has been in the development of accurate, rapid measurements of these materials by both NAA and PGAA.

The Biomonitoring Specimen Bank Research Project continued its support for other agencies' monitoring programs. These included the EPA human liver project, the NOAA National Status and Trends program, the NCI Micronutrient program, the IAEA/NBS/FDA/USDA Total Diet Study, and most recently, the NOAA Alaska Marine Mammal Project. Research has centered on banking protocols and improved analytical methodology. Our participation in intercalibration exercises with the project participants and the development of marine QA materials helped enhance the quality of the analytical results used in the assessment of the Nation's environmental health. Of major importance this year has been the completion of the reanalysis of 30 livers each from the 1982 and 1984 collections to quantify the stability of key elements under the carefully controlled storage conditions.

Bioanalytical research focused on the determination of metal species in various materials. Elements at trace and ultratrace levels have been determined in separated proteins and other macromolecules. The use of autoradiography to determine selenium has been added to the INAA and RNAA techniques. The occurrence of inorganic and organic compounds of tin in marine tissues is also being studied.

The strong interaction with industrial scientists using neutron depth profiling, prompt gamma activation analysis, and neutron activation analysis has continued with a growing number of guest workers, research associates, and joint publications. An important development this year has been the demonstration of two-parameter, coincidence spectroscopy for thin samples in collaboration with the group under Professor W.-K. Chu at the University of North Carolina and with Eastman Kodak. For appropriate samples this technique will increase the measurement sensitivity equivalent to a ten-fold increase in reactor neutron flux. The measurement of distributions of lithium and boron in metals, glasses, and polymers continues to produce important results.

The joint NBS/FDA/USDA study of trace elements in human diet, sponsored by the International Atomic Energy Agency, has completed its fourth year. A total of 40 minor and trace elements have been measured on the U.S. total diet material collected from several regions. In addition, measurements have been carried out on selected elements in diets received from countries participating in this global study. A candidate total diet material prepared in cooperation with OSRM is being evaluated as an elemental standard.

During the coming year the group will continue to improve the accuracy, productivity and sensitivity of nuclear methods as applied to elemental measurements. Problems to be addressed include those inherent in sample preparation, irradiation, radiochemical separation, counting and data reduction, with the goal of minimizing and quantifying the various sources of random and systematic errors in analysis by nuclear methods.

Particular attention will be paid to count rate dependent effects, gamma ray self-absorption, detector efficiency calibration, and monitor activation analysis. Maintaining full accuracy at high count rates using current generation data aquisition electronics is the goal of our count rate dependent studies. Accurate quantification of gamma ray self-absorption and measurement of the shape of the efficiency curve are required for accuracy in monitor activation analysis since matching of sample with primary standards is not done. The development of monitor activation analysis is part of the high temperature superconductivity effort to achieve rapid sample turnaround with minimum sacrifice of accuracy; however, the approach will also provide good quality control when used in parallel with traditional primary standard NAA.

MEASUREMENT OF SUPERCONDUCTOR STOICHIOMETRY BY NEUTRON ACTIVATION

R. M. Lindstrom and R. F. Fleming
(Inorganic Analytical Research Division)

Prompt and delayed neutron activation analysis have been applied to the nondestructive measurement of the major metals in small samples of $YBa_2Cu_3O_7$ superconductors, starting materials, and intermediate products. The small activation cross section and low gamma ray energies of Y-90m make the determination of yttrium imprecise in the presence of the large quantities of Cu-64 radioactivity. The physical parameters for neutron-capture prompt gamma-ray activation analysis (PGAA) are more attractive than delayed counting for stoichiometry measurements. The PGAA spectra of Y, Ba, and Cu show three, four, and six analytically useful gamma ray lines respectively, with nicely balanced intensities for the composition range of interest. A 100-mg sample gives a Poisson precision for yttrium (the weakest element) of 2% after only a 2-hour irradiation. Since the concentrations and atom ratios Y/Cu and Ba/Cu may be calculated immediately after the irradiation ends, the results can be returned within a day.

Atom Ratios in Superconductors and Unfired Precursors

Sample	Y/Cu	Ba/Cu	Sum
	Superconductors		
S3C	0.360 ± 0.007 (2.7%)	0.711 ± 0.007 (1.0%)	1.071 ± 0.031 (2.9%)
S4C	0.346 ± 0.007 (2.0%)	0.826 ± 0.014 (1.7%)	1.172 ± 0.031 (2.6%)
B7C	0.331 ± 0.006 (1.9%)	0.705 ± 0.014 (2.0%)	1.036 ± 0.015 (1.5%)
	Precursors		
P3C	0.367 ± 0.011 (3.1%)	0.737 ± 0.015 (2.1%)	1.104 ± 0.019 (1.7%)
P4D	0.334 ± 0.006 (1.7%)	0.777 ± 0.012 (1.6%)	1.111 ± 0.012 (1.3%)

Compositional measurements of substituted superconductors have been made in collaboration with the neutron scattering group. In these materials nominally 3-8% of the Cu had been substituted by Al, Fe, Ni, Zn, or Ga. Classical delayed activation analysis was used to measure the substituent and copper. An example is Fe-substituted 1:2:3 $YBa_2(Cu_{1-y}Fe_y)_3O_{7-x}$, where nominally y = 0.08. The sample was analyzed for three elements:

Element	g/g sample
Cu	0.238 ± 0.012
Ba	0.414 ± 0.024
Fe	0.0285 ± 0.0005

From the chemical formula,

atoms Fe / atoms Ba = 0.169 ± 0.010 = 3y / 2
atoms Fe / atoms Cu = 0.136 ± 0.007 = y / (1-y)

from which we have two measurements of the value of y:

y(Fe/Ba) = 0.115 ± 0.007
y(Fe/Cu) = 0.120 ± 0.007, which agree within errors.

In other samples the M/Cu ratios were not always found to be as expected:

"8% Al":	Al/Cu = 0.0872 ± 0.0025
"8% Ni":	Ni/Cu = 0.0880 ± 0.0018
"3% Ni":	Ni/Cu = 0.0308 ± 0.0012
"6% Zn":	Zn/Cu = 0.0654 ± 0.0015
"8% Ga":	Ga/Cu = 0.00024 ± 0.00002 Al/Cu = 0.0872 ± 0.0014

DETERMINATION OF AS, CD, CR AND MO IN THE NBS BOVINE SERUM STANDARD REFERENCE MATERIAL AT THE PPB LEVEL

R. R. Greenberg, R. Zeisler, and T. M. Sullivan
(Center for Analytical Chemistry)

As bioanalytical methods for trace element determinations have become more sensitive, biological and medical trace element research has included studies of many of the "difficult" elements such as Al, As, Cd, Cr, Mo, Mn, Sb and V. These elements are currently of interest, for example, in human blood-serum where they typically occur at the low ng/g level or below. The accurate determination of trace elements at these levels usually requires certified reference materials for method evaluation, and for quality assurance purposes. This need for low-level reference materials for accurate analyses of human-blood serum and related materials has been well documented. To help meet this need the National Bureau of Standards and the Department of Agriculture have cooperated in the production and certification of a frozen, Bovine Serum Standard Reference Material (SRM) with uncontaminated, or nearly uncontaminated levels of a wide variety of trace elements.

The certification of trace elements in this Bovine Serum (SRM 1598) was particularly difficult due to the very low levels on many of the elements of interest. A variety of analytical techniques has been used at NBS for the Bovine Serum certification. For several of these techniques, an extension of procedures beyond previously demonstrated measurement competence has been required. One of these analytical techniques, neutron activation analysis (NAA), was able to determine the concentrations of most of the elements desired for certification. In addition to the instrumental measurements made, a number of the difficult, low-level elements have been determined with appropriate pre- or post-irradiation chemical separations.

Two radiochemical separations have been used to reduce interferences from matrix activities such as from Na, Br and P, or in some cases to totally isolate the element of interest from essentially all other radionuclides. Post-irradiation separations are particularly useful for low-level determinations since no reagent blank has to be considered. Arsenic, along with Mo, has been determined using the inorganic ion exchanger HMD, and Cd along with Cu, have been determined in the eluent from the same samples using sequential extractions into solutions of bismuth and zinc diethyldithicarbamates in chloroform. This previously-developed procedure has been modified to include a predigestion step using a microwave oven. Dissolution was then completed with nitric and perchloric acids in a conventional manner (on a hot plate). The predigestion step allowed complete sample decomposition in two to three hours instead of the two days previously required to insure complete destruction of the organic sample matrix. This reduction in sample decay time improved the signal (number of counts) for As and Cd by factors of four and two respectively, and resulted in a comparable improvement in the detection limits. Arsenic and Cd were observed in the Bovine Serum at 0.15 and 0.093 ng/g respectively, while Mo was present at 11 ng/g.

Chromium has been also determined in an the Bovine Serum SRM following a post-irradiation extraction of Cr (VI) into a solution of tribenzylamine in chloroform. This newly developed procedure has also been applied to human blood and blood fractions, and is described elsewhere in this report. The Cr concentration in the Bovine Serum was 0.18 ng/g.

In addition to the elements determined after a radiochemical separation, three other biologically-important elements, Al, Mn and V, which are present at ng/g and sub-ng/g levels, have been determined previously in this material utilizing NAA combined with a pre-irradiation, chemical separation. These results, when combined with the results from other analytical techniques, will allow the certification of many of these difficult elements in a natural matrix material. The new Bovine Serum SRM should be of great value for method development, and for quality assurance purposes, when researchers analyze blood-serum or related materials.

MEASUREMENT OF CHROMIUM IN HUMAN BLOOD AND BLOOD FRACTIONS AT NATURAL (SUB-PPB) LEVELS

R. R. Greenberg and R. Zeisler
(Center for Analytical Chemistry)

Chromium was recognized as one of the elements essential for humans more than twenty-five years ago. However, at elevated concentrations, some forms of Cr are toxic and possibly even carcinogenic. In recent years, several analytical techniques have demonstrated the capability to accurately determine chromium at the naturally-occurring, ultratrace-levels normally found in uncontaminated samples of human serum. A variety of problems, however, have limited the determination of Cr to this single fraction of human blood. In view of the importance of this element, more detailed investigations of its occurrence and role at natural levels are needed, requiring even more sensitive analytical methods.

A reliable radiochemical procedure for Cr has been developed based upon neutron activation followed by a radiochemical separation. The separation procedure involves the liquid/liquid extraction of Cr(VI) into a 5% solution of tribenzylamine/chloroform, back-extraction into an aqueous solution (2 mol/L) of sodium hydroxide and precipitation as barium chromate. Radiochemical neutron activation analysis (RNAA) is one of the best analytical techniques currently available for trace and ultratrace level determination of Cr in biological materials. It possesses the sensitivity required to determine sub-manogram amounts of Cr, and the nearly blank-free nature of the technique allows chemical dissolution and separation of Cr from the sample matrix (after irradiation) without regard to reagent blank. In addition, NAA is free from chemical interferences, and most types of matrix effects which can interfere with other, non-nuclear, analytical techniques. However, the nuclear interference from the fast neutron reaction Fe-54(n, alpha)Cr-51, can be significant. This interference can be minimized, however, by using a highly thermalized facility such as the RT-4 facility of the NBS Research Reactor. In this facility, the measured Fe interference is 0.087 μg of Cr per gram of Fe, or approximately two orders of magnitude lower than at a typical light water reactor. The RT-4 interference is equivalent to a Cr blank of 0.039 ng of Cr per gram of whole blood for men, and 0.035 ng/g for women.

Chromium concentrations have been determined in whole-blood samples from nine individuals, and are listed in table 1. The Cr concentrations for eight

of these people were between 0.04 and 0.3 ng/g on a fresh weight basis. The ninth individual had a considerably higher level of Cr, and this is discussed below. Serum samples have been analyzed from seven of these individuals, and packed cells for two. Duplicate samples from a single collection have been run for the whole blood from one person and for the serum from a second. Both duplicate values are consistent with the observed counting statistics. In addition, blood from these two individuals has been sampled on two occasions more than one year apart. No differences in the Cr concentrations, above the analytical uncertainties, can be seen for subject B2 with time. A small, but real, increase in both the whole blood and serum Cr levels from B1 was observed. It should be noted that between the 1986 and 1987 sample collections, individual B1 was taking a daily dietary-supplement containing 200 μg of Cr in the form of an amino-acid chelate, while no supplement was taken prior to the 1986 collection. This factor of five increase in Cr intake, compared to the average American dietary intake of approximately 40% in the blood, and 90% in the serum. Since serum accounts for approximately 50% by weight, of whole blood in men, there appears to be no change in the Cr concentration in the packed cells of this individual. Thus the large increase in dietary Cr had only a relatively small effect, elevating the serum level for B1 from the second lowest concentration observed in this study, to the median value. Thus, at least for this individual, Cr levels in the blood may be under some type of bioregulatory mechanism.

An interesting observation can be made concerning individual T2. This person had concentrations of Cr in both whole blood and serum which were elevated by factors of 5-10 compared to the other individuals studied. Subsequent questioning revealed that this person has been diagnosed as a borderline diabetic, and has a family history of diabetes (mother). In view of the possible link between Cr and glucose metabolism, further studies of the Cr concentrations in whole blood and blood fractions from diabetics may be indicated. However, in view of the difficulty of accurate Cr determinations, at the naturally occurring levels in these materials, carefully validated analytical methods, and rigorous quality assurance procedures should be used for these studies.

Table 1. Chromium concentrations (ng/g) determined in human whole-blood, blood-serum, and packed cells (corrected for Fe interference)

Subject	Sample Date	Whole Blood	Blood Serum	Packed Cells
B1 Male	3/86	0.159 ± 0.023	0.102 ± 0.012	
B1 Male	3/86	0.160 ± 0.016		
B1 Male	9/87	0.226 ± 0.027	0.193 ± 0.021	
B2 Female	3/86	0.273 ± 0.019	0.378 ± 0.024	
B2 Female	3/86		0.445 ± 0.044	
B2 Female	9/87	0.292 ± 0.043	0.454 ± 0.044	
M1 Female	3/86	0.148 ± 0.019	0.117 ± 0.015	
T1 Male	3/86	0.340 ± 0.018		
D1 Male	3/86	0.150 ± 0.016	0.182 ± 0.027	
W1 Male	3/86	0.119 ± 0.025		
J1 Male	9/87	0.280 ± 0.036	0.258 ± 0.038	0.185 ± 0.027
R1 Male	9/87	0.038 ± 0.014	0.077 ± 0.010	
T2 Female	9/87	1.286 ± 0.048	1.743 ± 0.042	0.765 ± 0.058

Notes:
1. Concentrations are in ng/g, on a fresh weight basis.
2. Uncertainties are 1 sigma counting statistics.
3. Fe interferences applied for Cr:
   Whole blood (men) - 0.039 ng/g
   Whole blood (women) - 0.035 ng/g
   Packed cells (both) - 0.082 ng/g

NEUTRON ACTIVATION ANALYSIS OF MAJOR, MINOR, AND TRACE ELEMENTS IN MARINE SEDIMENTS

S. F. Stone, R. Zeisler, and B. J. Koster
(Center for Analytical Chemistry)

Neutron Activation Analysis (NAA) techniques are well established in the multi-element assay of geological materials. Similarly, applications of NAA to the analysis of marine sediments have been described. However, the different emphasis on elemental composition in studying and monitoring the health of the environment presents a new challenge to the analyst. To investigate as many elements as possible, previous multi-element procedures need to be re-evaluated and modified. In this work, we have utilized the NAA steps of a recently developed sequential analysis procedure [1] that obtained concentration for 45 biological and pollutant elements in marine bivalves. This procedure, with modification, was applied to samples of marine sediments collected for the National Oceanic and Atmospheric Administration (NOAA) National Status and Trends (NS&T) specimen banking program [2].

Duplicate samples of bottom sediments from more than 80 sites were collected and banked as part of the NS&T program during 1985-1987. Each sample consisted of a combination of aliquots from three stations per site. Each sample was obtained from a box core or grab sampler using a cylindrical Teflon corer. The top 3 cm of each core (approximately 50 g) were combined in a clean Teflon bag, or in later samples, in a clean Teflon jar. Two replicate station aliquots were taken to obtain two similar site samples of about 150 g each. The samples were sealed and stored in liquid nitrogen vapor freezers.

Samples selected for analysis were removed from cryogenic storage, thawed, and thoroughly mixed in their Teflon containers. After mixing, the samples were freeze-dried at -10 °C. The samples were ground/mixed using Teflon balls in Teflon jars and a Spex Mixer/Mill. Pellets were prepared for analysis with a Perkin-Elmer pellet press from the dry, homogenized material.

Neutron activation techniques were applied in sequence in order to obtain as much information as possible on the elemental composition of each sample. The samples were analyzed by either epithermal neutron activation analysis followed by thermal neutron activation analysis (NAA) or prompt gamma activation analysis (PGAA) followed by thermal NAA. The epithermal NAA irradiations were done at the University of Maryland reactor in College Park. Samples were irradiated inside boron nitride capsules at a fluence rate of

$2.1 \cdot 10^{16} n \cdot m^{-2} \cdot s^{-1}$ for 120 seconds. The National Bureau of Standards Research Reactor was used for the PGAA and thermal NAA irradiations, at fluence rates of $3.5 \cdot 10^{12} n \cdot m^{-2} \cdot s^{-1}$ for several hours and $2.8 \cdot 10^{17} n \cdot m^{-2} \cdot s^{-1}$ for 60 seconds and 8 hours, respectively.

Eighteen selected samples from 3 years of collection, 1985-1987, were analyzed. These samples represent both "clean" reference and presumed "contaminated" sites. A concentration profile from one site, MW2S138, Marina del Rey, CA, is shown in figure 1. Concentrations for 43 elements over nine orders of magnitude were obtained by PGAA and thermal NAA. A comparison of the concentrations of two pollutant elements for all investigated sites is given in figure 2. In addition, the Certified Reference Material (CRM) Sediment SD-N-1/2 from the International Atomic Energy Agency was analyzed using the combination of PGAA and thermal NAA. The results are shown in table 1. Good agreement with certified values can be seen for most elements, with the differences between the techniques dependent on counting statistics.

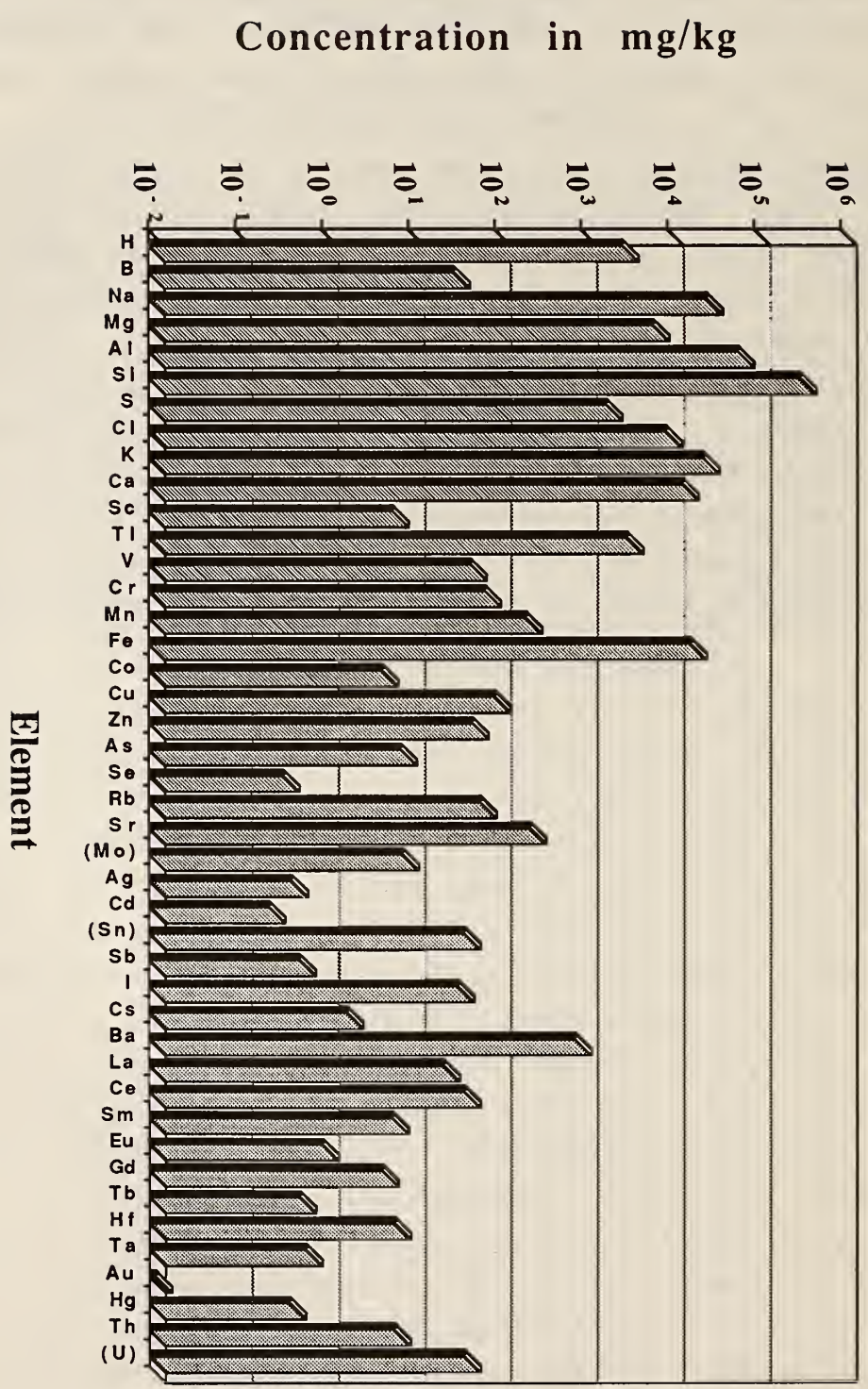

Figure 1. Concentration profile for MW2S138, Marina del Rey, California. Concentrations in mg/Kg, dry weight; (parentheses) indicates limit-of-detection.

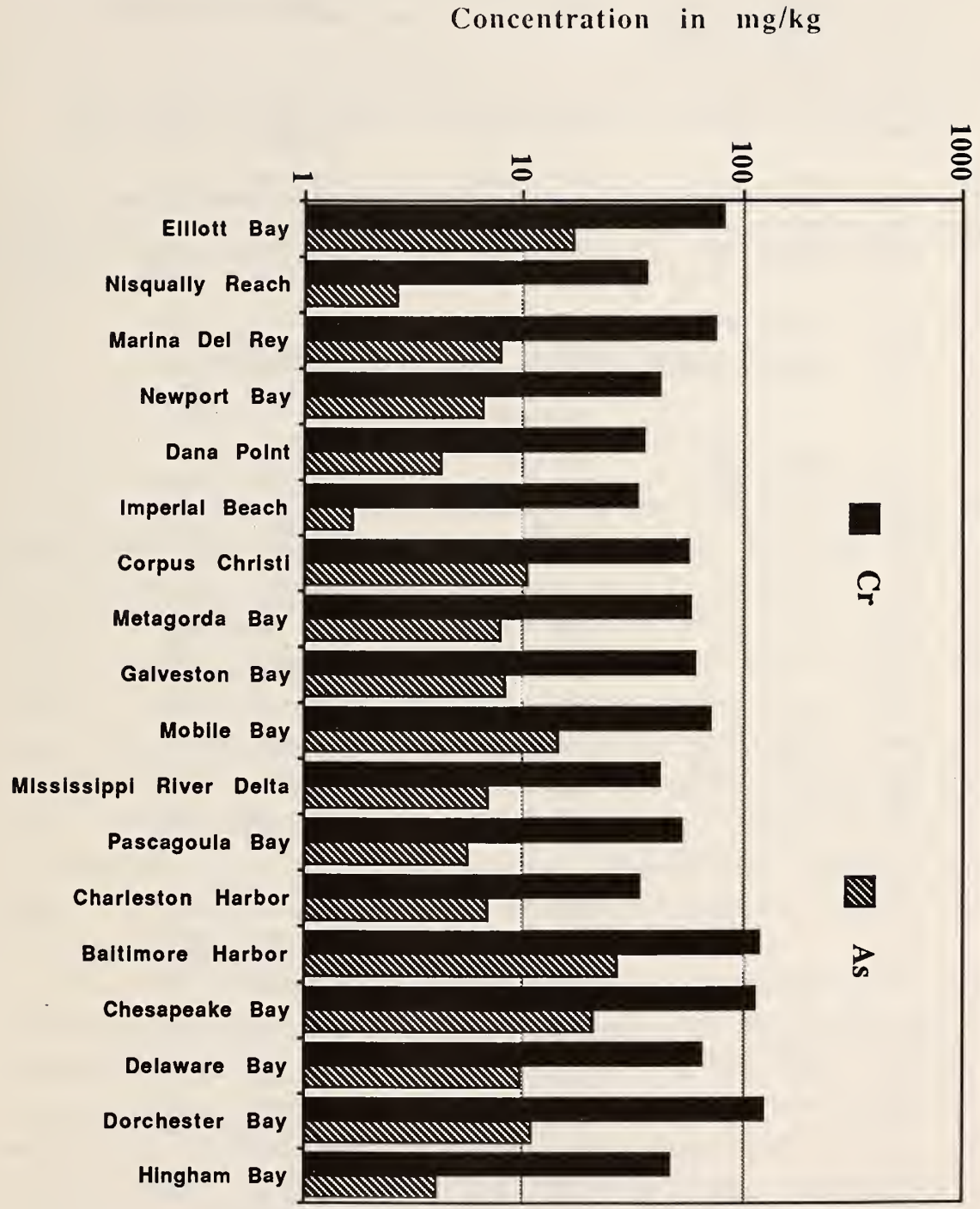

Figure 2. Comparison of Cr and As concentrations for 18 selected sediment samples. Concentrations in mg/Kg, dry weight.

Table 1. Results for IAEA/SEDIMENT SD-N-1/2

	PGAA	INAA	Certified (information*)
H %	1.257 ± 0.050		
B	87.7±1.5		
N %	2.3 ± 1.3		
Na %	0.62 ± 0.25	1.105 ± 0.010	1.04 (1.03 - 1.07)*
Mg %		0.86 ± 0.19	0.76 (0.74 - 0.79)*
Al %	2.52 ± 0.28	3.69 ± 0.03	3.75 (3.58 - 3.85)*
Si %	27.22 ± 0.93		28.05 (26.10 - 29.23)*
S	4100 ± 1200		
Cl	9290 ± 140	9840 ± 530	9040 (9040 - 9600)*
K %	1.522 ± 0.058	1.47 ± 0.16	1.54 (1.46 - 1.66)*
Ca %	5.03 ± 0.50	5.98 ± 0.19	5.32 (5.12 - 5.60)*
Sc		6.87 ± 0.06	7.10 (6.90 - 7.21)
Ti %	0.272 ± 0.002	0.293 ± 0.003	0.27 (0.24 - 0.31)*
V		77 ± 3	77.7 (65.0 - 80.7)
Cr		145 ± 16	149 (125 - 161)
Mn	850 ± 260	850 ± 13	777 (728 - 801)
Fe %	3.32 ± 0.20	3.69 ± 0.31	3.64 (3.53 - 3.78)*
Co		11.55±0.05	12.1 (11.2 - 12.7)
Cu		≤ 100	72.7 (68.1 - 75.2)
Zn		443 ± 6	439 (423 - 452)
As		56.3 ±0.4	50.0 (42.4 - 60.0)
Se		1.40 ± 0.25	2.90 (2.30 - 3.78)*
Rb		69.7 ±2.2	74.2 (68.6 - 77.0)
Sr		303 ±6	291 (277 - 303)
Mo		≤5.6	1.49 (1.30 - 2.60)*
Ag		1.80 ± 0.15	2.3 (2.0 - 3.2)
Cd	12.3 ± 0.49	8.11 ± 1.3	11.0 (10.0 - 12.0)
Sn		≤60	
Sb		3.79 ± 0.04	3.62 (3.20 - 3.95)
I		22 ± 5	20.5 (20.5 - 22.1)*
Cs		4.15 ± 0.06	4.9 (4.1 - 5.4)
Ba		292 ± 5	289 (276 - 310)
La		29.9 ±0.3	31.9 (30.0 - 35.5)
Ce		54.4 ± 0.6	60.3 (58.2 - 65.0)
Sm	5.52 ± 0.33	5.72 ± 0.12	5.58 (5.40 - 6.35)
Eu		1.132 ± 0.012	1.16 (1.12 - 1.30)
Gd	5.90 ± 0.45		
Tb		0.681 ± 0.021	0.86 (0.80 - 0.92)
Hf		8.61 ± 0.07	8.40 (7.45 - 8.77)*
Ta		1.03 ± 0.03	1.10 (0.83 - 1.20)*
Au		0.0307 ± 0.0012	0.04 (0.03 - 0.04)*
Hg		3.50 ± 0.18	1.46 (0.06 - 1.72)*
Th		6.47 ± 0.06	7.04 (6.85 - 7.20)
U		≤1.0	2.41 (2.29 - 2.53)

* Concentrations in mg/kg unless otherwise noted

References

[1] R. Zeisler, S. F. Stone, and R. W. Sanders, Anal. Chem. (submitted).

[2] G. G. Lauenstein, M. M. Schantz, S. A. Wise, and R. Zeisler, "Specimen Banking in the National Status and Trends Program: Development of Protocols and First Year Results," Oceans '86 Conference Record, IEEE, New York, N.Y., 586 (1986).

This work was supported in part by the Oceans Assessment Division, National Oceanic and Atmospheric Administration. The authors wish to acknowledge the assistance of Donald A. Becker and Manoranjani P. M. Tillekeratne in the epithermal NAA.

DETERMINATION OF TRACE ELEMENTS IN U.S. DIETS

V. Iyengar
(Center for Analytical Chemistry)

An international project sponsored by the International Atomic Energy Agency (IAEA), and supported by the National Bureau of Standards (NBS), the U.S. Food and Drug Administration (FDA) and the U.S. Department of Agriculture (USDA) is in progress. This study is designed to assess the daily dietary intake of certain dietary components by selected target populations in several countries. The countries involved are Australia, Brazil, China, Iran, Italy, Spain, Sudan, Sweden, Thailand, Turkey and the United States. Mixed total diets from these countries are being analyzed for caloric energy, phytate and fiber content, and minor and trace elements. Analysis for these constituents are being carried out in selected reference laboratories identified by the IAEA. The NBS is one such reference center to determine a select group of inorganic elements.

The U.S. efforts involve both as a collection center and as a reference laboratory. A part of the study was concerned with evaluating analytical approaches. Mainly neutron activation analysis was used in both the instrumental and radiochemical modes. Guidelines were developed for the preparation of mixed diet reference standards for quality control, and one material (Mixed Diet SRM 1548) is currently being characterized for certification. Simultaneously, collection of U.S. mixed diets based on the FDA Total Diet Study scheme was initiated. Until now six such collections have been completed from the following regions: Southeast (GA, TX, WV), North Central (IA, KS, OH), Northeast (NY, PA, RI), South (AL, LA, TX), West (AZ, CA, OR) and Central (IL, IN, WI). One portion of mixed diet from each of the

six collections has been stored in the Specimen Bank. Studies are also in progress to assess long-term stability of organic nutrients in mixed diets under different storage conditions [1-6].

Five of these diets have already been analyzed for vitamins, fiber, phytate and several minor and trace elements. Neutron activation analysis (instrumental and radiochemical) has been extensively used as a multielement analysis tool. The results obtained for several elements show remarkable agreement with the daily intake data calculated from the individual food analysis results of FDA-TDS study, confirming the validity of the mixed diet approach for monitoring the daily intake of minor and trace elements. The results did not indicate any significant inter-regional variations in the overall daily intake. This is attributable to the fact that these U.S. collections represent national diets due to standardized collection procedures of the TDS scheme. In the present study, analytical results obtained for over 30 elements for the mixed diet samples provide a basis for establishing baseline values for the daily dietary intake of a number of elements that are not covered by the FDA-TDS scheme.

References

[1] G. V. Iyengar, Trans Am. Nucl. Soc. 56, 233-34 (1988).

[2] G. V. Iyengar, J. T. Tanner, W. R. Wolf, and R. Zeisler, J. Res. Natl. Bur. Stand. (U.S.) 93, 360-362 (1988).

[3] G. V. Iyengar, Clin. Nutr. 6, 105-117 (1987).

[4] G. V. Iyengar, Clin. Nutr. 6, 143-153 (1987).

[5] G. V. Iyengar, Clin. Nutr. 6, 156-158 (1987).

[6] G. V. Iyengar, J. Jones, K. Cook, J. Tanner, and W. Wolf, Trans. Am. Nucl. Soc. 55, 177-178 (1987).

ATMOSPHERIC AND ENVIRONMENTAL STUDIES BY INSTRUMENTAL AND NEUTRON-CAPTURE PROMPT γ-RAY ACTIVATION ANALYSIS

G. E. Gordon and J. M. Ondov
(Department of Chemistry and Biochemistry, University of Maryland,)

We continue to make extensive use of instrumental neutron activation analysis (INAA) and neutron-capture prompt γ-ray activation analysis (PGAA) for continued development and testing of the methods themselves and to determine concentrations of about 40 elements in particles, gases, rain and fog from the atmosphere, in related source materials such as crustal dust and coal fly ash, and in standards appropriate for use in this field. By measuring concentrations of such a large number of species, we are able to identify contributions from certain types of air-pollution sources to the atmospheric burden at ambient sampling sites, a technique now known as "receptor Modeling." Examples of these studies are briefly discussed in the following sections.

1. Mauna Loa Observatory Studies

Since 1979, our group has collected airborne particle samples at Mauna Loa Observatory (MLO) on the island of Hawaii, as a part of the research program on remote area aerosols initiated by Prof. W. H. Zoller, now at the University of Washington. The MLO samples from February 1979 through January 1983 were collected and analyzed by J. R. Parrington [1]. Diane Hermann took over the project at that point and recently reported results through May 1985 in her thesis. There are several differences between her results and those of Parrington. First, she mainly analyzed only samples collected under conditions of downslope (DS) winds, which occur at night and bring down air from above Mauna Loa. These are good samples in which to observe very low concentrations of elements transported from long distances. Parrington also analyzed samples collected under unslope (US) wind conditions, which are less desirable because of their heavier loadings of marine aerosol, crustal material from the island and human activities on the island. The second major differences is that, starting in January 1983 Kilauea volcano has erupted every few weeks, and during May 1984, Mauna Loa volcano erupted for several weeks. The volcanoes presented an opportunity to observe their emissions in various phases of their eruptive cycles, but they created problems of interference with the observation of remote area aerosol compositions.

Table 1. Geometric means and standard deviations of elemental concentrations observed at Mauna Loa Observatory, February 1979 - May 1985

Element	Unit	Clean seasons Conc.	Geom. σ	No. Spls.	Dust seasons Conc.	Geom. σ	No. Spls.
Na	ng/m^3	8.5	2.4	168	24	2.3	124
Mg	ng/m^3	3.5	2	124	24	2.9	111
Al	ng/m^3	6.1	2.1	170	52	3.3	124
Cl	ng/m^3	6.3	3.3	136	6.8	2.7	101
K	ng/m^3	3.2	2	146	27	2.5	120
Ca	ng/m^3	4.6	2.3	156	55	3.6	122
Sc	pg/m^3	1.4	2.2	166	13	3.1	124
Ti	ng/m^3	0.87	1.9	117	4.5	2.7	108
V	pg/m^3	14	2	170	95	2.9	124
Cr	ng/m^3	1.6	3.7	135	1.6	3.7	95
Mn	pg/m^3	87	2.1	170	760	3.2	124
Fe	ng/m^3	5.8	2	162	41	2.9	124
Co	pg/m^3	3.7	2.5	162	20	2.6	123
Zn	ng/m^3	0.11	3.6	150	0.35	2.6	120
Ga	pg/m^3				23	3.6	65
As	pg/m^3	14	2.5	118	61	3.6	110
Se	ng/m^3	0.013	2.2	165	0.025	2.5	124
Br	ng/m^3	3	2.3	166	2.4	2.1	107
Rb	pg/m^3	24	2	52	140	2.8	112
Ag	pg/m^3	2.3	2.3	81	2.8	2	46
In	pg/m^3	0.36	2.5	21	0.67	2.6	27
Sb	pg/m^3	1.8	2.9	155	7	2.6	117
I	ng/m^3	1.7	1.7	169	1.3	1.7	119
Cs	pg/m^3	1.1	2.6	137	11	3.3	120
La	pg/m^3	3.2	2.9	155	42	3.7	121
Ce	pg/m^3	7.5	2.7	142	73	3.2	123
Sm	pg/m^3	0.57	3	131	6.4	3.1	112
Eu	pg/m^3	0.21	2.4	143	1.3	2.9	116
Tb	pg/m^3	0.19	2.4	56	0.97	2.5	87
Yb	pg/m^3	0.85	2.7	67	2.5	3.2	101
Lu	pg/m^3	0.41	2.8	34	0.57	2.7	81
Hf	pg/m^3	0.52	2.2	137	3.3	3	119
Ta	pg/m^3	0.3	1.9	80	1.1	2.5	92
W	pg/m^3	3.2	3.4	63	6.2	3	52
Au	pg/m^3	0.17	2.8	103	0.23	3.6	79
Th	pg/m^3	1.1	2.6	125	12	3.2	120
SO_4	ng/m^3	130	3	169	220	2.4	101

The major feature of the MLO data is the observation of large amounts of crustal dust from Asia every Spring, from February through June, the result of vast dust storms in loess regions of China. Table 1 shows the concentrations of elements observed during the dust and nondust seasons. Note the much greater concentrations of most elements, especially crustal elements, during the dust season.

The data were treated by various receptor-modeling methods to determine the sources of mass and of various elements. Evidence for the following

components was obtained: "normal" Asian dust, Asian anthropogenic materials, and Se-SO_4 component, marine aerosol, Hawaiian basalt and volatile volcanic emissions. Asian dust is not pure soil, but is soil contaminated by emissions from coal combustion in China. The Asian anthropogenic component is more highly enriched material from coal combustion. Note that during the clean seasons, wind trajectories suggest that both crustal and anthropogenic material come from North and Central America much of the time, but concentrations of most species are so low that we can't distinguish them chemically from the Asian sources. The Se-SO_4 component results from biological processes in the oceans, which release dimethyl sulfide, which is slowly converted to SO_2 gas and then to sulfate particles. The associated Se appears to arise from similar processes. Hawaiian basalt is a good representation of ash from the volcanoes. Table 2 shows the mass concentrations from the various sources during the dust and non-dust seasons.

Table 2. Source contributions (%) to total suspended particulate load at Mauna Loa Observatory during clean and dust seasons

Component	Clean season	Dust season
Se-SO_4	62.4	10.9
Continental dust	21.7	79.5
Marine aerosol	6.4	2.8
Anthropogenic	4.3	3.2
Basalt	2.7	1.9
Volcanic volcano	2.4	1.7
Mass conc. (ng/m^3)	600	2800

2. Deep Creek Lake Samples

In August/September 1983, various groups collected samples at a site near Deep Creek Lake, MD, an area strongly affected by emissions from distant coal-fired power plants in the Ohio River Valley and from nearby plants in WV, OH and PA. Ambient particulate samples were collected every 12 hrs with a dichotomous sampler, which sorted the particles every 12 hrs (diam < 2.5 μm) and a coarse fraction (2.5-10 μm). The particulate samples were analyzed by x-ray fluorescence (XRF) for about 17 elements. Our group then obtained fine fraction samples for all sampling periods and 22 coarse-fraction samples for further analysis by INAA for about 35 elements, including many that were also observed by XRF. A paper on the combined fine-fraction analyses has been

submitted to Atmos. Environ [2]. Results of the analyses are listed in table 3 along with INAA results for the 22 coarse-fraction samples. This paper mainly serves to introduce the data set to the atmospheric community, with rather little interpretation. We are now performing various receptor-model treatments of the data.

Table 3. Concentrations of elements observed at Deep Creek Lake (ng/m^3)

	Fine Fraction			Coarse Fraction		
	Average	Sig.	No. pts	Average	Sig.	No. pts
Na	32.3 ±	25.4	117	22.08 ±	20.72	22
Mg				119 ±	86	14
Al	55.6 ±	42.5	104	402 ±	527	22
Si	150.6 ±	83.3	120			
S	6754 ±	4252	120	1418 ±	1443	12
Cl	20.6 ±	30.3	104	14.61 ±	11.71	22
K	42.5 ±	21.2	120	150 ±	164	22
Ca	46.5 ±	31.9	120	705 ±	771	21
Sc	0.012 ±	0.011	116	0.09 ±	0.11	21
Ti				30 ±	43	22
V	0.862 ±	1.273	104	0.75 ±	0.74	22
Cr	0.86 ±	0.81	116	1.04 ±	1.80	20
Mn	3.07 ±	1.94	104	7.41 ±	8.40	22
Fe	58.84 ±	45.04	120	295 ±	332	22
Co	0.035 ±	0.033	116	0.11 ±	0.11	21
Zn	12.1 ±	9.1	116	3.06 ±	4.89	21
Ni	0.65 ±	1.16	106			
Ga	0.066 ±	0.131	111	0.11 ±	0.13	22
As	0.741 ±	0.627	111	0.20 ±	0.15	22
Se	2.40 ±	1.35	116	0.07 ±	0.12	21
Br	5.10 ±	2.46	120	2.01 ±	1.19	22
Rb				1.33 ±	1.48	15
Mo				0.31 ±	0.23	15
Cd	0.63 ±	0.87	111			
In				0.005 ±	0.008	18
Sb	0.64 ±	0.99	116	0.136 ±	0.354	22
I	0.56 ±	0.34	104			
Cs	0.030 ±	0.045	116	0.041 ±	0.047	22
Ba				4.85 ±	3.40	20
La	0.090 ±	0.129	111	0.257 ±	0.276	22
Ce	0.195 ±	0.182	116	0.647 ±	0.749	21
Sm	0.018 ±	0.048	111	0.048 ±	0.056	22
Eu	0.0027 ±	0.0062	116	0.009 ±	0.010	19
Tb				0.004 ±	0.005	14
Yb	0.0230 ±	0.0263	116	0.017 ±	0.020	22
Lu				0.004 ±	0.004	16
Hf	0.0024 ±	0.0092	116	0.026 ±	0.033	20
W	0.088 ±	0.142	111	0.040 ±	0.036	22
Pb	46.59 ±	19.3	120			

To determine compositions of particles emitted from coal-fired power plants near the DCL site, researchers from NEA, Inc. collected particulate samples from three large, nearby plants, the Ft. Martin, Harrison, and Pleasant plants. The samples were analyzed by XRF and, then, selected fine fraction samples were sent to our group for analysis by INAA. Both our results and those from XRF for elements that are marginal or impossible by INAA are listed in table 4. Because of the differing sizes of the plants, we have expressed the emissions in terms of the mass of each species (in pg) per unit energy produced (in J). Janet Joseph is attempting to interpret the results in her M.S. thesis. We had a priori hoped that emissions from the plants would be sufficiently distinctive as to allow us to identify them separately at the DCL site. Indeed, the data of table 4 reveal quite significant differences among the three plants. However, the area is so strongly influenced by emissions from more distant plants in the Ohio River Valley that it has so far not been possible to distinguish particles from the local plants from those of the more distant ones.

We also collected several sets of samples in the DCL area with a micro-orifice impactor, which separates particles of diam below about 2.5 μm into eight size fractions. These sample sets have also been analyzed by INAA for about 30 elements to provide detailed size distributions of very fine particles bearing the different elements. We see peaks in the size spectra at different diameters for different elements, suggesting that they were produced by different processes, or that some had been airborne for longer times than others, allowing for more coalescence or growth. Jeff Dodd is attempting to interpret the results in his M.S. thesis.

Table 4. Normalized emission factors of elements (pg/J) in fine particles

	Ft. Martin	Harrison	Pleasants
V_s (m/s)	15.4	27.1	23.0
A_s (m^2)	40.3	57.2	29.2
E (MWe)[a]	470	820	540
Na	3.9 ± 2.5	57 ± 16	4.4 ± 1.1
Al	46 ± 31	940 ± 440	160 ± 140
Si (XRF)	240 ± 115	320 ± 130	320 ± 140
S (XRF)	1570 ± 790	4260 ± 1450	2760 ± 1270
K	6.8 ± 4.1	82 ± 19	12 ± 6
Ca	8.6 ± 3.3	600 ± 160	120 ± 49
Sc	0.011 ± 0.009	0.26 ± 0.07	0.030 ± 0.012
Ti	2.0 ± 0.8	61 ± 19	8.6 ± 3.8
V	0.20 ± 0.08	6.5 ± 1.7	1.3 ± 0.6
Cr	0.31 ± 0.27	3.4 ± 1.0	1.3 ± 1.1
Mn	0.074 ± 0.035	3.9 ± 0.9	0.43 ± 0.19
Fe	23 ± 15	845 ± 201	122 ± 49
Co	0.042 ± 0.032	0.34 ± 0.09	0.037 ± 0.015
Ni (XRF)	1.4 ± 0.9	1.2 ± 0.3	0.33 ± 0.18
Cu	ND	ND	ND
Zn	0.57 ± 0.57	7.4 ± 3.0	2.4 ± 0.9
Ga	0.068 ± 0.038	1.4 ± 0.3	0.25 ± 0.11
As	0.42 ± 0.62	10 ± 2	5.4 ± 2.5
Se	65 ± 29	27 ± 7	23 ± 5
Br (XRF)	3.6 ± 0.9	2.4 ± 0.6	0.92 ± 0.39
Rb	ND	0.81 ± 0.20	0.12 ± 0.08
Sr	ND	28 ± 7	1.6 ± 1.3
Mo	ND	1.9 ± 0.7	0.45 ± 0.30
Ag	ND	0.15 ± 0.18	ND
Cd	ND	ND	ND
In	0.0010 ± 0.0011	0.011 ± 0.003	0.0020 ± 0.0009
Sb	0.10 ± 0.10	0.45 ± 0.19	0.27 ± 0.14
Cs	ND	0.11 ± 0.03	0.0095 ± 0.0052
Ba	0.79 ± 0.77	26 ± 6	7.8 ± 3.6
La	0.026 ± 0.020	0.45 ± 0.13	0.037 ± 0.014
Ce	ND	1.4 ± 0.4	0.17 ± 0.07
Nd	ND	0.63 ± 0.31	ND
Sm	0.017 ± 0.025	0.11 ± 0.03	0.025 ± 0.030
Eu	0.0014 ± 0.0009	0.024 ± 0.006	0.0035 ± 0.0023
Gd	ND	0.16 ± 0.16	ND
Tb	ND	0.018 ± 0.005	ND
Yb	ND	0.036 ± 0.009	ND
Lu	0.0016 ± 0.0015	0.011 ± 0.005	0.0013 ± 0.0008
Hf	0.0050 ± 0.0043	0.043 ± 0.018	0.0055 ± 0.0027
W	ND	0.22 ± 0.05	0.055 ± 0.032
Pb (XRF)	28 ± 10	9.2 ± 7.3	6.6 ± 1.7
Th	0.0092 ± 0.0057	0.17 ± 0.03	0.020 ± 0.006
U	0.016 ± 0.015	0.30 ± 0.07	0.075 ± 0.051

[a] All data were normalized to gross electrical generating load.

ND = not detected in greater than half of the samples.

V_s = stack gas velocity (Stevens, 1984).

A_s = stack cross sectional area (U.S. DOE, 1983).

E = gross electrical generating load (Stevens, 1984).

References

[1] J. R. Parrington, Ph.D. Dissertation, Dept. of Chemistry, University of Maryland, College Park, MD (1983).

[2] T. L. Vossler, C. W. Lewis, R. K. Stevens, T. G. Dzubay, G. E. Gordon, S. G. Tuncel, G. M. Russwurm, and G. J. Keeler, submitted to Atmos. Environ. (1988).

STABLE ISOTOPE TRACING OF ZINC IN INFANTS

G. E. Gordon and S. H. Harrison
(Department of Chemistry and Biochemistry, University of Maryland)

In cooperation with Dr. K. Sivasubramanian and coworkers of Georgetown University Medical Center, we are testing the use of enriched stable ^{70}Zn to trace the behavior of Zn in infants, especially preterm infants, who are often at considerable risk of Zn deficiency. The tracer consists of Zn enriched to 80% or more in ^{70}Zn (vs. its normal isotopic abundance of 0.6%) and is administered to the infant, usually in their infant formula. Samples of blood, urine and feces are collected as available for several days and the Zn is separated prior to irradiation in the NIST Reactor. The latter produces 245-day ^{65}Zn, 14-hr ^{69}Zn and 4-hr ^{71}Zn, whose activities are proportional to the masses of stable ^{64}Zn, ^{68}Zn and ^{70}Zn, respectively, in the samples. From the $^{70}Zn/^{68}Zn$ and $^{70}Zn/^{64}Zn$ ratios in the samples along with knowledge of the mass and ^{70}Zn abundance in the administered tracer, we can calculate the fraction of tracer that appears in the various body-pool samples. To date, six infants have been studied. Because of the smaller samples available from infants and less control of the sampling regime, they are much more difficult to study than the adult volunteers with whom the procedures were verified. However, preliminary results indicate that the procedure can be done, but with somewhat lower precision.

NEUTRON FILTERS FOR COLD NEUTRON BEAMS

C. A. Stone
(Center for Analytical Chemistry)

Single crystals have long been used to filter out the fast neutron component of a neutron beam while allowing thermal neutrons to pass through with little attenuation. Detailed comparisons of the performance of neutron filters have not been accomplished, primarily because of the limited data on the total neutron cross section for most materials. Freund [1] presented a semi-empirical method to determine the total neutron cross section of single crystals. This approach is simple and reproduces experimentally observed cross sections.

Extensive calculations have been carried out, following the method presented by Freund, to determine the optimum filters for cold neutron beams. Figure 1 shows the components to the total neutron cross section for sapphire. The component labeled SPH represents the single phonon scattering cross section and that labeled MPH represents the multiple phonon scattering cross section.

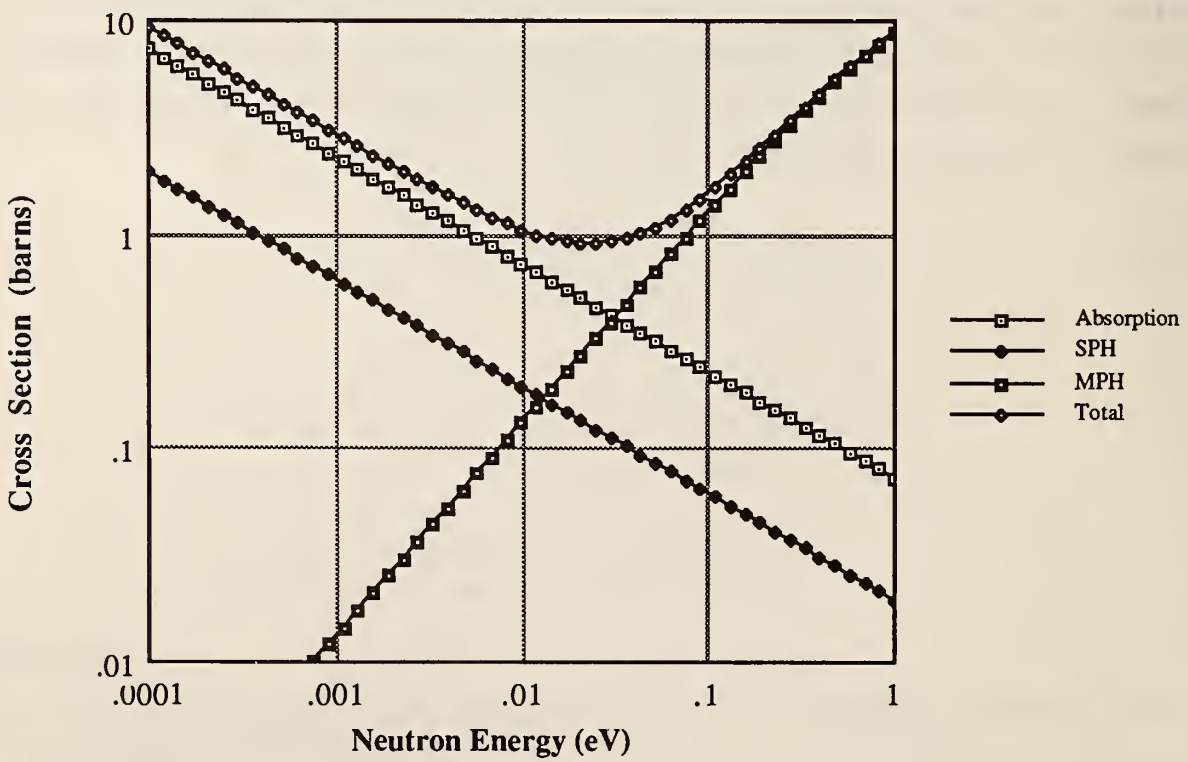

Figure 1. Neutron cross section for single crystal sapphire.

For several in-beam experiments, the relevant comparison between neutron filter choices is not necessarily the total transmission of neutrons through the crystal. Rather, it is the total neutron transmission versus a defined fast neutron transmission. In order to make this comparison, a set of "equivalent lengths" for filters was determined. The length of a given filter was defined as that which will attenuate the fast neutrons to a specified value. Table 1 shows the equivalent lengths for several filters. Each column is labeled with the fast neutron transmission in percent. Fast neutron cross sections, which were used to calculate the attenuation coefficients, were taken from reference [2]. The neutron transmission is shown in figure 2 for several filters with a fast neutron of transmission of 0.0001%.

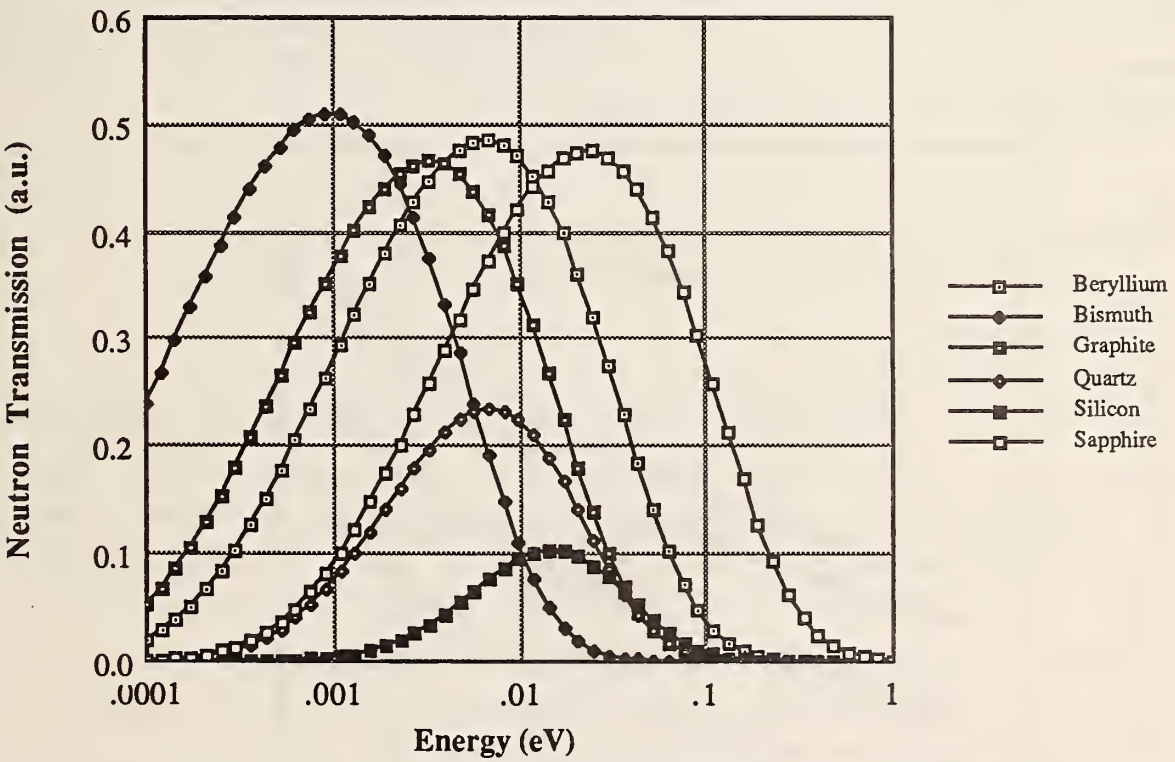

Figure 2. Neutron transmission for a 99.999% fast neutron attenuation.

Table 1. Lengths of various neutron filters which give equivalent fast neutron attenuation

Filter	Fast Neutron Scattering Cross Section (barns)	Density (g/cm^3)	Attenuation Coefficient (cm^{-1})	Filter Length for Fast Neutron Attenuation (cm) 99.9%	99.99%
Beryllium	6.151	1.85	0.760	9.1	12.1
Bismuth	9.300	9.8	0.26	26.3	35.1
Graphite	4.730	2.25	0.535	12.9	17.2
Quartz	9.5657	2.202	0.2111	32.7	43.6
Sapphire	13.1098	3.98	0.332	20.8	27.8
Silicon	2.0437	3.329	0.1021	67.7	90.2

Figure 3 shows the total neutron transmission for a series of filters as a function of the fast neutron transmission. A 77-K Maxwellian probability distribution was taken for the neutron spectrum shape and the crystal temperature was taken as 296 K. This figure clearly shows sapphire as the optimum choice for a cold neutron filter.

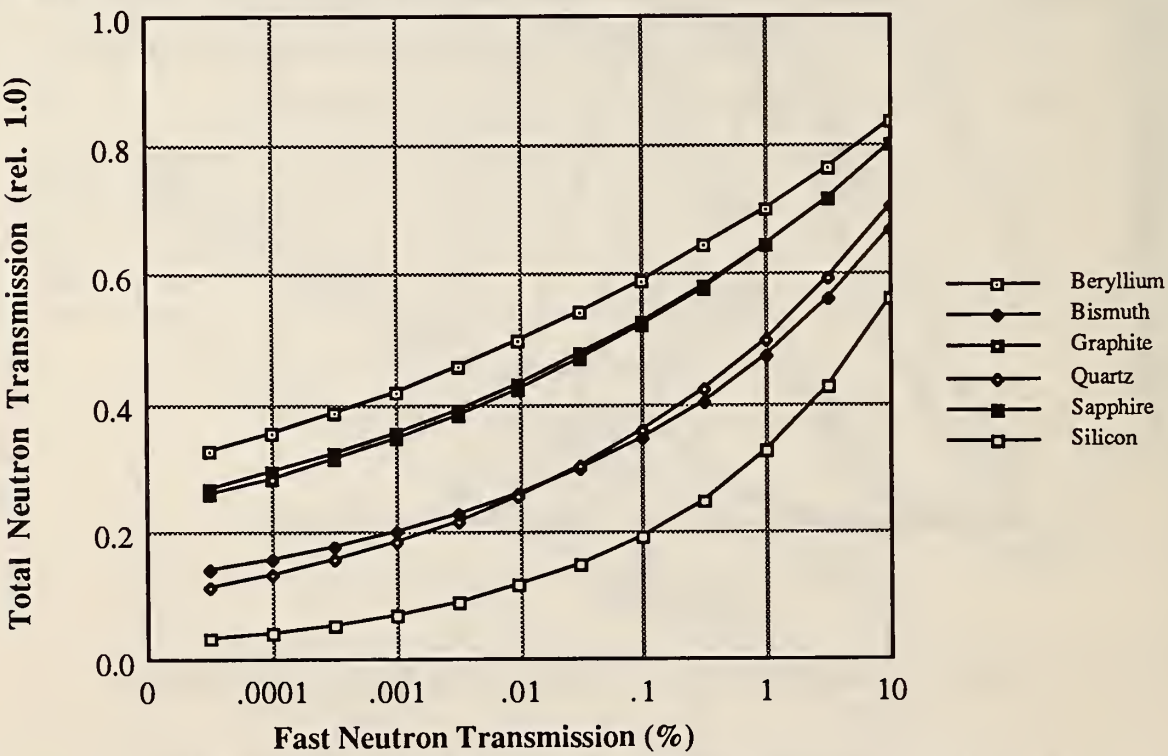

Figure 3. Total neutron transmission for 296 K neutron filters and 77 K (Maxwellian) neutrons.

References

[1] A. K. Freund, Nucl. Instr. Meth. 213, 495 (1983).

[2] S. F. Mughabghab, Neutron Cross Sections, Academic Press, Orlando, FL (1984).

REACTOR OPERATIONS AND SERVICES

T. Raby, J. Torrence, J. Ring, and N. Bickford

There were numerous activities this year that required extended reactor shutdown or operation at reduced power. Included among these are the installation of the cold neutron source, the beginning of construction of the new guide hall and confinement building annex, replacement of the shim arms, overhaul of the fuel transfer system and shipment of spent fuel. Two major problems were also encountered during this period, the failure of one of the main heat exchanger and the progressive leaks in the thermal shield cooling system. As a result, the reactor was on-line about 50% of the time at various power levels which is equivalent to about 35% had the reactor been operating at the full power level of 20 MW throughout.

Installation and testing of the cold source was a difficult and lengthy operation. The entire core was unloaded and the systems drained. The operation required almost 3 months. Construction of the new cold neutron facility complex was begun and is in progress. Shutdowns between operating cycles were extended to permit the contractor to do work near the confinement building. Application for license changes and associated safety analyses, to incorporate the new cold neutron guide tubes into the NBSR Technical Specifications was made to the Nuclear Regulatory Commission.

The shutdown period was used to perform major maintenance operations. The fuel transfer system was overhauled. The shim arms were replaced for the second time after 7 years of operation. The replacement took less than a month compared to nearly 6 months the previous time. Shipment of all spent fuel was completed. In all nine shipments were made involving 180 elements which is equal to all the previous shipments since the NBSR began operation.

For years, the thermal shield cooling system has been developing leaks. By 1988, approximately 70 out of 190 cooling tubes had to be isolated as leakers, or suspected leakers. The situation was close to becoming intolerable because of the significantly decreased cooling capacity. Recently a new method developed by National Nuclear Corporation of England was shown to be effective in sealing small leaks in inaccessible areas and in a hostile, highly radioactive environment. The treatment was applied to all proven leakers of the thermal shield over a 2-week period with very encouraging

initial results. The repaired system will be tested over the next several months under actual reactor operating conditions.

The main heat exchanger had developed several leaks in the past, one of which was so small that it could not be found from among 1200 U-tubes. The shutdown period was used to attempt to locate this small leak. Several suspect tubes were plugged following which the heat exchanger tested leak tight. Shortly thereafter, when the flow systems were refilled and returned to normal, major leaks developed suddenly, resulting in the loss of 400 gallons of heavy water. The leaks were traced to this same heat exchanger. Sixteen tubes were confirmed leakers and were plugged. The heat exchanger is being monitored until replacement heat exchangers can be obtained. This will take several years.

The operating staff now numbers 16, 15 of whom are licensed senior operators, and one in training for licensure. The staff is considerably smaller than that of comparable reactors. This requires each member of the staff to carry out duties and responsibilities significantly beyond that of routine shift operation of the reactor.

A summary of the operating statistics for the past year is presented in the following table. Fuel utilization continues to be the best in the country.

No. of equivalent days at 20 MW	126
Equivalent on-line time at 20 MW	35%
Average U-235 burnup	66%
No. of irradiations	675
Hours of irradiations	1850
Hours per irradiation	2.7

The same program of reactor irradiations continued. Irradiation services were provided to many organizations from within and outside NBS covering wide areas of research, applications, and standards.

ENGINEERING SERVICES

J. H. Nicklas and R. S. Conway

In addition to normal engineering and design services provided to reactor operations, experimenters and users, the engineering staff was involved in a continuing effort to upgrade the reactor systems, components and instrumentation. Among the major projects undertaken are:

New fuel elements have been qualified and are currently in production. These more heavily loaded elements will increase reactor core lifetime and will result in considerable cost savings throughout the fuel cycle, fewer shutdowns, and less handling for refueling.

For the first time, replacement shim arms were assembled with completely new mounting components. In the past, the old mounts which were highly radioactive had to be used. This required the entire assembly operation to be done remotely under water which required two months to complete. During this previous replacement, the old mounts were carefully inspected and the precise measurements needed to make new mounts were determined. The use of the new mounts eliminated the lengthy time required previously to disassemble the used shim arms from their mounts and reduced the shim-arm replacement time to less than two weeks. Because of the success of this procedure, another set of mounts was immediately fabricated for future use.

For years, the fuel transfer system has been causing problems because of the sticking transfer arms due to worn out bearings that we have not been able to replace because of their location. A unique tool has now been designed and fabricated to remove and replace some of the bearings. The first attempt to remove the bearings with the new tool will be made in the near future.

A long standing problem that has been getting progessively worse has been leaks in the thermal shield cooling tubes. These tubes are buried inside the biological shield and are not accessible. The system consists of many redundant individual tubes with separate valves enabling leaking tubes to be isolated. At the beginning of this year, more than 50 of the cooling tubes were isolated as known or suspected leakers. To address this problem we finally located a firm that has developed a method for sealing such leaks in highly radioactive environments. They were successful in sealing all but two or three of the leaks. A few have reopened during successive operating cycles, but, on the whole the results have been quite satisfactory. We

anticipate that periodic treatment will continue to be required, but it appears that sound and reliable operation of the thermal shield system can be maintained at reasonable cost.

The design drawings and specifications for the replacement of the main heat exchangers are in the final stages of completion. The existing heat exchangers have been the source of numerous problems resulting in significant loss of operating time and some loss of valuable heavy water. The new heat exchanger design will utilize advanced fabrication methods, testing procedures and new stainless steel alloys that are resistant to stress corrosion. This will assure their long life and reliable operation. A survey is being made to evaluate tube and heat exchanger manufacturers. Technical visits have already been made to several leading manufacturers across the country.

The cryogenic bismuth tip instrumentation project was completed. This instrumentation system monitors the temperature and rate of the D_2O and H_2O cooling water flow through the bismuth tip. This project involved installing stainless steel piping, tubing, venturi flow elements, transducers, alarm units, thermocouples, analog, and digital readout meters. The entire system including safety functions and alarms, was interfaced with the reactor console control room. This allows the operator to monitor performance and take corrective action as required. The final checkout and energizing of the bismuth tip instrumentation readout panels and alarms were completed on schedule.

NEUTRON ACTIVATION ANALYSIS AT THE FOOD AND DRUG ADMINISTRATION

W. C. Cunningham and D. L. Anderson
(Food and Drug Administration, Washington, DC)

The Food and Drug Administration (FDA) maintains a neutron activation analysis (NAA) facility in the reactor building of the National Bureau of Standards (NBS). Although this facility is directed by FDA's Center for Food Safety and Applied Nutrition, it provides agency-wide analytical support for special investigations and applications research. NAA complements other analytical techniques used at FDA and serves as a reference technique and confirmatory quality assurance (QA) tool.

During the past year, this facility provided support in all of the areas noted above. Radiochemical and instrumental NAA procedures (RNAA and INAA, respectively) continue as the prime analytical tools; however, during this year extensive efforts were directed to applying neutron-capture prompt gamma-ray activation analysis (PGAA) to FDA needs. PGAA provides a cross-check for some elements but is also sensitive for B, Cd, H and S and increases the capabilities of the FDA NAA facility. The combination of several nuclear techniques enables diverse multi-element information to be obtained for foods and related materials. This methods development and applications research was part of the ongoing FDA effort to improve overall analytical capabilities.

Research efforts continued this past year to accumulate general analytical information on food supplements. PGAA work was primarily to determine element concentrations and detection limits for these materials. INAA work focused on an examination of interferences and matrix effects. These materials are particularly interesting because many of them have both biological and mineral components in the same supplement. As a result, analytical approaches must be able to simultaneously handle problems associated with both. To date, more than 40 different product types have been analyzed by the nuclear techniques.

Preliminary work shows that PGAA was able to provide element concentrations for H, B, and Cl in virtually all supplements. Levels of C, N, Na, Si, S, K, and Ca were below detection limits in some materials but above in most. Levels of Al, Ti, Mn, Fe, Cu, Zn, Cd, Sm and Gd were above detection limits in only a few materials, predominantly the high-mineral supplements. Besides providing a general QA benefit for several elements, PGAA provides FDA's Element Research Section with specific added capabilities: It can be used to obtain element concentrations for H, C, N, Si and S and it serves as

an alternative technique to obtain element concentrations for B, Cd, Cl and K. Moreover, PGAA is an instrumental technique, it requires minimal test sample preparation, and it has a relatively short analysis time.

USE OF NAA IN CRIMINAL INVESTIGATIONS

Neutron Activation Analysis Unit
(Federal Bureau of Investigation, Washington, DC)

The Federal Bureau of Investigation (FBI) continues to utilize the NBSR for Neutron Activation Analysis (NAA) of various materials collected for their investigation of a wide range of criminal cases. Much of their investigation involves trace element comparisons of bullet leads and analysis of trace elements when the use of a handgun is suspected.

One case which utilized NAA involved a double homicide of a husband and wife. Fragments of bullets were removed from the husband's head. The trace elements in those fragments matched exactly with the trace elements in the unfired bullets found in the suspect's handgun and those still in the box at the suspect's residence. This match of trace elements provided a valuable clue in solving the crime.

Since NAA is sensitive and non-destructive, analysis of very small samples of evidence is possible with the added advantage of retaining the material for introduction during a trial.

REACTOR RADIATION DIVISION
460

R. S. Carter, Chief
T. M. Raby, Deputy Chief
E. C. Maxwell, Admin. Officer
M. Long, Admin. Assist.
*S. E. Tassey, Secretary
S. C. Shatzer, Clerk-Typist

Neutron Radiography
T. Cheng
**M. Ganoczy

Division Staff
R. Casella
B. Mozer
F. Shorten

REACTOR OPERATIONS

T. M. Raby, Chief
J. Torrence, Deputy Chief
C. Harrison, Secretary

Reactor Operations

R. Beasley
M. Bell
N. Bickford
M. Cassells
F. Clark
J. Clark
H. Dilks
L. Lindstrom
M. McDonald
W. Meuller
T. Meyers
J. Ring
R. Sprow
R. Stiber
A. Toth
D. Wilkinson

ENGINEERING SERVICES

J. H. Nicklas, Chief
*J. Spillman, Secretary

Mechanical Design

E. Guglielmo
J. Sturrock
M. Suthar

Electronics

J. Beatty
R. Conway
R. Hayes

NEUTRON CONDENSED MATTER SCIENCE

J. J. Rush, Group Leader
L. Roadarmel, Secretary
*L. Clutter, Clerk-Steno

Crystallography

#F. Beech
#C. Choi
#V. Himes
A. Mighell
#H. Prask
E. Prince (1/2)
W. Rymes
A. Santoro
*J. Stalick

Magnetic and Amorphous Materials

R. Erwin
#T. Giebultowicz
W. Knill
#W. Li
*J. Lynn
J. Rhyne
#M. Spano
#Y. Yu
#P. Klosowski

Materials Microstructure

N. Berk
D. Fravel (1/2)
C. Glinka (1/2)
J. Gotaas
J. LaRock (1/2)
S. Satija (1/2)

Chemical Materials

#J. Nicol
D. Neumann (1/2)
#S. Trevino
R. Williams (1/2)
T. Udovic (1/2)
E. Prince (1/2)
J. Grillo

COLD NEUTRON PROGRAM

J. M. Rowe, Manager
C. O'Connor, Admin. Assist.
P. Grimes, Clerk-Typist

Cold Neutron Program

#J. Copley
D. Fravel (1/2)
C. Glinka (1/2)
#G. Greene
+M. Kahn
P. Kopetka
J. LaRock (1/2)
Z. Majkrzak
D. Neumann (1/2)
S. Satija (1/2)
I. Schroder
T. Thai
T. Udovic (1/2)
R. Williams (1/2)
D. Pierce
M. Rinehart

*Part-time
+WAE, Coop, Intermittent
**Deceased
#Guest Scientist, Research Assoc. (Full Time)

NON-RRD NBS STAFF LOCATED AT REACTOR

Occupational Health and Safety Division (354)
- D. Brown
- C. Campbell
- I. Jensen
- F. Moore
- D. Nelson
- J. Shubiak
- L. Slaback

Ionizing Radiation Division (536)
- E. Boswell
- C. Eisenhauer
- D. Gilliam
- J. Grundl
- G. Lamaze
- E. McGarry
- R. Schwartz
- J. Coyne

Inorganic Analytical Research Division (551)
- D. Becker
- S. Carpenter
- G. Downing
- K. Fitzpatrick
- R. Fleming
- B. Grazman
- R. Greenberg
- G. Iyengar
- J. Langland
- R. Lindstrom
- J. Maki
- B. Norman
- S. Stone
- R. Zeisler

GUEST WORKERS AND COLLABORATORS

INSTITUTE FOR MATERIALS SCIENCE AND ENGINEERING (400)
- J. Cahn

Ceramics Division (420)
- J. Blendell
- E. Fuller
- G. Long
- C. Ostertag
- R. Roth
- W. Haller

Polymers Division (440)
- B. Bauer
- R. Briber
- F. Brinkman
- T. Chang
- C. Chiang
- J. Clark
- L. Coyne
- T. Davis
- C. Han
- S. Krueger
- G. Olsen
- R. Waterstrat
- W. Wu

Metallurgy Division (450)
- R. Fields
- R. Reno
- R. Shaefer
- R. Shull

Center of Basic Standards (520)
- M. Arif
- S. Dewey
- G. Greene

Surface Science Division (541)
- R. Cavanagh
- T. Madey

Organic Analytical Division (552)
- B. Koster
- L. Sander
- S. Wise

Gas and Particulate Science Division (553)
- C. Poston
- H. Rook
- J. Small
- C. Stone

Semiconductor Electronics Division (727)
- J. Ehrstein
- J. Marshall
- J. Suehle

Thermophysics Division (774)
- H. Hanley
- J. Straty

Armed Forces Institute of Pathology
- D. Nagarajan

Army Armament Research, Development and Engineering Center
- C. Choi
- H. Prask
- S. Trevino

Department of Agriculture
- G. Iyengar

Federal Bureau of Investigation
- R. Bilko
- R. Halberst
- R. Hargadon
- J. Haverkost
- K. Lundy
- C. Peters
- J. Riley
- D. Thompson

Food and Drug Administration
- D. Anderson
- W. Cunningham
- A. Kyah
- J. Tanner

National Institutes of Health
- J. Bennett
- M. Channing
- W. Eckelman
- M. Geller
- R. Finn
- R. Frank
- A. Katki
- R. Nossal

National Oceanic and Atmospheric Administration
- G. Lauenstein

Naval Research Laboratory
- D. Gubser
- P. S. Keath
- S. Lawrence
- M. Osofsky
- C. Roland
- P. Schoen
- L. Toth
- C. Trask
- R. Treanor
- S. Wolf

Naval Surface Weapons Center
- G. Riel
- M. Spano

Smithsonian Institution
- R. Bishop
- M. Blackman
- T. Chase
- Y. Cheng
- R. Cunningham
- J. Mishara
- E. Myers
- J. Olin

Argonne National Laboratory
- T. Brun
- P. Thiyagarajan

Battelle Pacific Northwest Laboratories
- L. Brackenbush
- F. Brauer
- G. Endres
- M. Failey
- R. Sanders

Brookhaven National Laboratory
- P. Boni
- D. Cox
- D. Gibbs
- A. Goldman

C.N.R.S. Grenoble, France
- B. Barbara
- M. Marezio
- S. Miraglia
- D. Tran Qui

ETH, Zurich, Switzerland
- I. Anderson

Energy Research Foundation
(The Netherlands)
J. Woittiez

Hahn-Meitner Institute
(Berlin)
D. Behne

Institut Laue-Langevin
Grenoble, France
A. Magerl
D. Richter
J. Soubeyroux

KFA Jülich, Germany
H. Grimm
R. Hempelmann
M. Stoepler

Los Alamos National Laboratory
T. Bowles
J. Eckert
R. Hjelm
R. Robinson
J. Wilkerson
M. Yethridge

Oak Ridge National Laboratory
J. Cable
J. Fernandez-Baca
J. Hayter
F. Kam
H. Mook
R. Nicklow
B. Sales
H. Smith

Risø National Laboratory
J. Bohr

Sandia National Laboratory
Z. Fisk

Alfred University
R. Snyder
R. Zhow

Auburn University
B. Taterchuck

Chalmers University of Technology
L. Sjölin
R. Alenljung

Colorado State University
A. Parker
J. Stille
J. Tsang

College of William and Mary
E. Schoe
R. Wright

Goethe University
W. Bauer
A. Bienok

Iowa State University
A. Goldman
R. Barnes

John Carroll University
J. Trivisonno

Johns Hopkins University
C. L. Chien
M. Creplak
A. Ganrin
D. Musser
F. Streitz
G. Xiao

Kyoto Institute of Technology
Q. Tran-Cong

Kyoto University (Japan)
H. Hasegawa
T. Hashimoto
Q. Trancong
S. Sakurai
Y. Shibayama

M.I.T.
J. Didiskein
M. Green
B. Wuensch

McMaster University
W. Clarke
R. Barr

Miami University (Ohio)
J. Cantrell

Michigan State University
T. D. Brewer
Y. Fan
A. Moini
T. Pinnavaia
S. Solin
M. S. Wang

Nagoya University
H. Choshi
Y. Matsushita
K. Mori
Y. Muroga
Y. Nahao
I. Nodo
R. Saguchi

Northwestern University
C. Sellers
J. Weertman

Ohio University
R. Cappelltetti

Oregon State Graduate School
P. Davis

Penn State University
L. Pilione
J. Yehoda

Purdue University
A. Overhauser

Rutgers University
R. Gerhardt

San Jose State University
P. Englert
A. Ling

Southwest Research Institute
R. Page

Temple University
J. Crow

Texas A&M University
E. Schweikert

Tokyo Institute of Technology
M. Okala

University of Annecy (France)
J. Bouillot

University of Antwerp (Belgium)
K. Michel

University of California (Davis)
P. Klavins
R. Shelton

University of California (Irvine)
V. Guinn

University of California
(Santa Barbara)
M. Eddy
J. Fint
D. Klingensmith
C. Levi
R. Odette
G. Stucky

University of California (San Diego)
J. Arnold
K. Nishiizumi

University of Cincinnati
H. Jackson
P. Boulchand

University of Exeter (U.K.)
R. Slade

University of Houston
P. Chu

University of Illinois
J. Anker
J. Borchers
B. Boyle
R. Du
C. Flynn
M. Salamon
H. Zabel

University of Illinois (Chicago)
M. Said
J. Kowel

University of London
C. Catlow
W. Jordon
B. Steele

University of Maryland
H. Ammon
A. Andrews
T. Clinton
J. Copley
J. Dodd
G. Gordon
M. Han
S. Harrison
D. Herman
J. Hoff
W. Li
J. Lynn
L. Mackie
J. Nicol
J. Ondov
A. Sheffield
S. Skanthakumar
J. Valette-Silver
W. Walters
H. Zhang

University of Massachusetts
S. Roy
R. Stein

University of Milan (Italy)
M. Zocchi

University of Michigan
D. Vincent

University of Missouri
R. Berliner
W. Ching
B. Hammouda
P. Schmidt
S. Werner
D. Worcester

University of Muenster
F. Kemper

University of Nancy (France)
P. Mangin

University of Nebraska
D. Sellmyer

University of North Carolina
W-K Chu
E. Frye
N. Parikh
M. Swanson

University of Notre Dame
J. Furdyna
T. Giebultowicz
P. Klosowski

University of Odense
E. Anderson

University of Pennsylvania
P. Davis

University of Peruglia
G. Alberti

University of Vermont
T. Flanagan

University of Virginia
T. Williamson

University of Washington
K. Mottet
W. Zoller

University of West Virginia
R. Kannan
M. Seehra

University of Wisconsin
D. Huber

Utah State University
T. Isenhour

Yale Univeristy
J. Flanagan

AT&T Bell Laboratories
F. Bates
R. Cava
H. Chen
D. Johnson
J. Mitchell
D. Murphy
J. Remeika
W. Rhodes
J. Riley
J. Rosedale
L. Scheemeyer
S. Sunshine
J. Waszazak
S. Yognasubiamian

PERSONNEL ROSTER

Aerospace Corporation
R. Bowman
J. Knudsen

Allied Corporation
G. Fish
A. Maeland
J. LaSalle

Atomic Energy of Canada, LTD
W. Lennard

Bell Communications Research Laboratories
P. Barboux
L. Greene
P. Miceli
J. Tarascon

Charles Evans & Assoc.
R. Fleming

CIDTECH
D. Carta

Directed Technologies, Inc.
N. Chesser

E. I. DuPont de Nemours Co.
D. Corbin
G. Jones
R. Shannon
F. Tebbe
C. Torardi

Eastman Kodak
T. Hossain
M. Landry
J. O'Reilly
C. Swanson
J. Tritten
H. Yang

Exxon
R. Busch
J. Huang
M. Kim
D. Lohse
R. Overfield
S. Sinha

G. E. Microelectronics Center
C. Tino

GTE Laboratories
G. Hamill

W. R. Grace
M. Wax
R. Wormsbecker

Hughes, Malibu
R. Wilson

IBM (San Jose)
G. Hadziioannou
T. Russel
S. Anastasiadis

Imperial Chemical Industries
J. Howard
H. Stanley

Intel Corporation
N. Cox

Lockheed EMSCO
D. Lindstrom

Research Triangle
N. Wadlen

Schumberger-Doll Research
N. Wada

Westinghouse-Hanford Corp.
W. McElroy

E. PUBLICATIONS

Abeles, B.; Yang, L.; and Majkrzak, C. F.; "Plasma Enhanced Exchange of H and D During Growth of Amorphous Semiconductor Superlattices," Proc. of the Materials Research Society Symposium on Surfaces, Superlattices and Thin Films, Boston, MA (1986).

Abeles, B.; Yang, L.; Leta, D. L.; and Majkrzak, C. F.; "Fast Diffusion of Interstital D in Amorphous Si,: J. of Non-Crystalline Solids 97 and 98, 353 (1987).

Ammon, H. L.; Choi, C. S.; and Reddy, S.; "Crystal Structure of 1, 4-Diidocubane," Acta Cryst. (in press).

Anderson, I. S.; Berk, N. F.; Rush, J. J.; and Udovic, T. J.; "Concentration and Temperature Dependence of Hydrogen Vibrations Along the C Axis for Hydrogen in Yttrium: Evidence of Dynamically Coupled Hydrogen Pairs," Phys Rev. B, 37, 4358 (1988).

Baur, W. H.; Bieniok, A.; Shannon, R. D.; Prince, E.; "Neutron Powder Diffraction Study and Thermogravimetry of Sodium Cesium Zeolite Rho," J. of Solid State Chem. (submitted for publication).

Berk, N. F.; Hardman-Rhyne, K. A.; "Analysis of SAS Data Dominated by Incoherent Multiple Scattering," J. Appl. Cryst. 21 (1988).

Bohr, J.; Gibbs, D.; Moncton, D. E.; D'Amico, K. L.; Majkrzak, C. F.; and Mohanty, K.; "Synchrotron X-ray Scattering Studies of Rare-Earth Metals," Proc. of the Workshop on X-ray and Neutron Scattering From Magnetic Materials, November 1987, Argonne, Il, Physica B, (to be published).

Borchers, J. A.; Salamon, M. B.; Du, R.; Flynn, C. P.; Erwin, R. W.; and Rhyne J. J.; "Magnetic Characterization of Er Y Superlattices," J. Appl. Phys. 63, 3458 (1988).

Bowman, R. C., Jr.; Cantrell, J. S.; Samwer, K.; Tebbe, J.; Rush, J. J.; "Properties of Amorphous Zr RhH Prepared From Glassy and Crystalline Alloys," Phys. Rev., B37, 8575 (1988).

Bowman, R. C., Jr.; Torgeson, D. R.; Barnes, R. G.; Maeland, A. J.; and Rush, J. J.; "Relationship of Hydrogen Site Occupancy to Diffusion Behavior in Crystalline and Amorphous Zr_2PdH_x, Z. Physik. Chem., (in press).

Bowman, R. C., Jr.; Maeland, A. J.; Venturini, E. L.; Rush, J. J.; and Cantrell, J. S.; "Studies of the Structure and Properties of Amorphous a-$Zr_{76}Fe_{24}H_x$," Z. Physik Chem., (in press).

Buchenau, U.; Monkenbusch, M.; Stamm, M.; Majkrzak, C. F.; and Nucker, N.; "Neutron Scattering Study of Relaxations and Vibrations in Molten Polyethylene," Proc. of the Workshop on Polymer Motion in Dense Systems, September 1987 (in press).

Cahn, J. W.; Gratias, D.; Mozer, B.; "Patterson-Fourier Analysis of the Icosahedral (Al_1Si)-Mu Alloy." Phys. Rev. B (in press).

Cahn, J. W.; Gratias, D.; Mozer, B.; "A 6-D Structural Model for the Icosahedral (Al_1Si)-Mu Quasicrystal," J. of Phy. Paris, France (in press).

Carr, M. J.; Chambers, W. F.; Melgaard, D. K.; Himes, V. L.; Stalick, J. K.; and Mighell, A. D.; "NBS/Sandia/ICDD Electron Diffraction Database," T.R. SAND87-1992, NTIS, 5285 Port Royal Road, Springfield, VA 22161.

Casella, R. C.; "Theoretical Models For High-Temperature Superconductivity," Nuovo Cimento D (in press).

Choi, C. S.; Prask, H. J.; "Orientation Distribution of Fiber-axes and Neutron Powder Diffraction Profiles." ICOTOM-8 Conference Proceedings by the Metallurgical Society of AIME (in press).

Copley, J.R.D.; "The Significance of Multiple Scattering in the Interpretation of Small Angle Neutron Scattering Experiments," J. of Applied Cryst. (in press).

Copley, J.R.D.; "On the Use of Multiple Slot Multiple Disk Chopper Assemblies to Pulse Thermal Neutron Beams," Nuclear Instruments and Methods in Physics Research A. (in press).

Copley, J.R.D. and Majkrzak, C. F.; "Converging Neutron Guides," Proc. of the 32nd Annual Int'l. Tech. Symposium on Optical and Optoelectronic Applied Science and Engineering, SPIE, August 1988, San Diego, CA (to be published).

DiNardo, R. P.; Majkrzak, C. F.; Neumann, D. A.; "Fabrication of Neutron Polarizing Multilayers by Sputtering," Proc. of the 32nd Annual Int'l. Tech. Symposium on Optical and Optoelectronic Applied Science and Engineering, SPIE, August 1988, San Diego (to be published).

Endoh, Y. and Majkrzak, C. F.; "Polarized Neutron Diffraction Studies of Magnetic Multilayer Structures," Chapter in a book on metallic superlattices, edited by T. Shinjo and T. Takada, Elsevier Science Publications (in press).

Erwin, R. W.; Rhyne, J. J.; Borchers, J.; Salamon, M. B.; Du, R.; and Flynn, C. P.; "Magneto-Elasticity and Structure of Er Y Superlattices," J. Appl. Phys. 63, 3461 (1988).

Fan, Y. B.; Solin, S. A.; Neumann, D. A.; Zabel, H.; and Rush, J. J.; "Elastic Neutron Scattering Studies of the Structure of Graphite Intercalated with Potassium and Ammonia," Phys. Rev., B36, 3386(1987).

Fernandez-Baca, J. A.; Lynn, J. W.; Rhyne, J. J.; and Fish, G. E.; "Low Temperature Spin Waves in Amorphous $Fe_{90-x}Ni_xZr_{10}$," J. Appl. Phys 63, 3749 (1988).

Fernandez-Baca, J. A.; Lynn, J. W.; Rhyne, J. J.; Fish, G. E.; "Study of the Long-wavelength Spin-wave Energies and Linewidths of the Amorphous Invar Alloy $Fe_{1-x}B_x$," Phys. Rev. B 36, 8497-8511 (in press).

Fowler, H. A.; Mozer, B.; and Sims, J.; "Triple Shell Symmetry in α-(Al,Si)-Mn," Phys. Rev. B37, 3906-3913 (1988).

Giebultowicz, T. M.; Rhyne, J. J.; Ching, W. Y.; Huber, D. L.; and Furdyna, J. K.; "Spin Dynamics in $Zn_{1-x}Mn_xTe$," J. Appl. Phys. 63, 3297 (1988).

Gotaas, J. A.; Lynn, J. W.; Shelton, R. N.; Klavins, P.; and Braun, H. F.; "Suppression of Superconductivity by Antiferromagnetism in $Tm_2Fe_3Si_5$," Phys. Rev. B 36, 7277-80 (1987).

Gotaas, J. A.; Rhyne, J. J.; Wenger, L. E.; and Mydosh, J. A.; "Magnetic Phase Transition in $Y_{0.97}Dy_{0.03}$," J. Appl. Phys. 63, 3577-9 (1988).

Gotaas, J. A.; Rhyne, J. J.; Wenger, L. E.; Mydosh, J. A.; "Magnetic Structure of $Y_{0.97}Er_{0.03}$," to be published in Proc. of the International Conference on Magnetism 1988.

Gotaas, J. A.; Said, M. R.; Kouvel, J. S.; Brun, T. O.; "Magnetic Structure of Cubic $Tb_{0.03}Y_{0.7}Ag$," to be published in Proc. of the International Conference on Magnetism 1988.

Gratias, D.; Cahn, J.W.; Mozer, B.; "Six-dimensional Fourier Analysis of Icosahedral $Al_{73}Mn_{21}So_6$ Alloy," Phys. Rev. B. (in press).

Gratias, D.; Cahn, J. W.; Bessiere, M.; Calvayrac, Y.; Lefebre, S.; Quivy, A.; Mozer, B.; "N-dimensional Crystallographic Description of the Icosahedral Phases; The Example of the $Al_{73}Mn_{21}Si_6$ Quasiperiodic Structure," Proc. of the NATO Conference, Acquafredda, Plenum (in press).

Grimm, H.; Stiller, H.; Majkrzak, C. F.; Rupprecht, A.; and Dahlborg, U.; "Observation of Acoustic Umklapp-Phonons in Water-Stabilized DNA by Neutron Scattering," Phys. Rev. Letts. 59, 1780 (1987).

Grimm, H.; Stiller, H.; Majkrzak, C. F.; and Rupprecht, A.; "Neutron Scattering Study of the Hydration Hull of DNA by H_2O/D_2O Exchange," Proc. of the Int'l. Conf. on Neutron Scattering, Grenoble, France, July 1988, Physica B (to be published).

Hanley, H.J.M.; Straty, G. C.; Glinka, C. J.; and Hayter, J. B.; "Low-Q Neutron Diffraction from Supercooled D-Glycerol," Molecular Physics, 62, 1165-1174 (1987).

Heise, W. H.; Lu, K.; Kuo, Y-J; Tatarchuk, B. J.; Udovic, T. J.; and Rush, J. J.; "Neutron Scattering Study of Hydrogen on Ruthenium Sulfide," J. Phys. Chem. (1988) (in press).

Himes, V. L.; and Mighell, A. D., "NBS*SEARCH: A Program to Search the Database," Data Commission of the Interntl Union of Crys., Chester, UK, Chap. 3.1, 144-155 (1987)

Himes, V. L.; Mighell, A. D.; Stalick, J. K.; Young, S. L.; Carr, M. J.; Anderson, R.; Holomany, M. A.; Jenkins, R.; Lyman, C. E.; "MAX-D Index for Phase Identification by Electron or X-ray Diffraction," U.S. Department of Commerce and the JCPDS-International Centre for Diffraction Data, Swarthmore, PA. 1988 (in press).

Himes, V. L. and Mighell, A.D.; "NBS Crystal Data: Compound Identification and Characterization Using Lattice-Formula Matching Techniques," Computerized Metallurgical Databases, published by The Metallurgical Society, 1988 (in press).

Hong, M.; Fleming, R. M.; Kwo, J.; Waszczak, J. V.; Mannaerts, J. P.; and Majkrzak, C. F.; "Magnetic Rare Earth Dy-Y Superlattices," J. Appl. Phys. 61, 4052 (1987).

Horton, J. C.; Squires, G. L.; Boothroyd, A. T.; Fetters, L. J.; Rennie, A. R.; Glinka, C. J.; and Robinson, R. A.; "Small-Angle Neutron Scattering from Star-Branched Polymers in the Molten State," Macromolecules (submitted for publication).

Krueger, S. and Nossal, R.; "SANS Studies of Interacting Hemoglobin in Intact Erythrocytes," Biophys. J. 53, 97 (1988).

Kwo, J.; Hong, M.; DiSalvo, F. J.; Waszczak, J. V.; and Majkrzak, C. F.; "Modulated Magnetic Properties of Synthetic Rare Earth Gd-Y Superlattices," Phys. Rev. B35, 7295 (1987).

Kwo, J.; Hong, M.; Hsieh, T. C.; Fleming, R. M.; McWhan, D. B.; Yafet, Y.; Majkrzak, C. F.; Gibbs, D.; Boni, P.; Goldman, A. I.; Cable, J. W.; Bohr, J.; and Grimm, H.; "Rare-Earth Magnetic Superlattices," Int'l Conf. on Magn., Paris, France, July, 1988, J. dePhysique (to be published).

Li, W-H.; Lynn, J. W.; Mook, H. A.; Sales, B. C.; and Fisk, Z.; "Long Range Antiferromagnetic Order of the Cu in Oxygen Deficient $RBa_2Cu_3O_{f6+x}$," Phys. Rev. B37, 9844 (1988) (Rapid Communications).

Li, W-H; Lynn, J. W.; Stanley, H. B.; Udovic, T. J.; Shelton, R. N.; and Klavins, P.; "Antiferromagnetic Structure and Crystal Field Splittings in the Cubic Heusler Alloys $HoPd_2Sn$ and ErP_2Sn," J. de Physique (1988) (submitted for publication).

Li, W-H; Lynn, J. W.; Stanley, H. B.; Udovic, T. J.; Shelton, R. N.; and Klavins, P.; "Crystal-Field Splittings in the Cubic Heusler Alloys $HoPd_2Sn$," (1988) (submitted for publication)

Loidl, A.; Knorr, K.; Rowe, J. M.; McIntyre, G. J.; "Glass and Phase Transitions in $(KBr)_{1-x}(KCN)_x$," Phys. Rev. B 37, 389-398 (1988).

Lynn, J. W.; Li, W-H.; and Li, q.; "Two-dimensional Character of the Magnetic Order in $ErBa_2Cu_3O_7$," Solid State Science, Vol. 1, 357-361 (1987).

Lynn, J. W.; Li, W-H.; Li, Q.; Ku, H. C.; Yang, H. D.; and Shelton, R. N.; "Magnetic Fluctuations and Two-Dimensional Ordering in $ErBa_2Cu_2O_7$," Phys. Rev. B 36, 2374-2377 (1987).

Lynn, J. W.; Li, W-H.; "Antiferromagnetic Order of the Cu in $RBa_2Cu_3O_{6+x}$," J. de Physique, (to be published).

Lynn, J. W.; and Li, W-H.; "Magnetic Order in $Ba_2Cu_3O_{6+x}$," Magnetism Conference, Vancouver, Canada, J. Appl. Phys. (to be published).

Lynn, J. W.; Li, W-H.; Mook, H. A.; Sales, B. C.; Fisk, Z.; "Nature of the Magnetic Order of Cu in Oxygen Deficient $NdBa_2Cu_3O_{6+x}$," Phys. Rev. Lett. 60, 2781 (1988).

Lynn, J. W. and Rhyne, J. J.; "Spin Dynamics of Amorphous Magnets," in Chap. 14 in Spin Waves and Magnetic Excitations, edited by A. S. Borovik-Romanov and S. K. Sinha, North Holland Physics Publishers, Amsterdam, 177 (1988).

Majkrzak, C. F.; Cable, J. W.; Kwo, J.; Hong, M.; McWhan, D. B.; Yafet, Y.; Waszczzak, J. V.; Grim, H.; and Vettier, C.; "Polarized Neutron Diffraction Studies of Gd-Y Synthetic Superlattices," J. Appl. Phys. 61, 4055 (1987).

Majkrzak, C. F.; Gibbs, D.; Boni, P.; Goldman, A. I.; Kow, J.; Hong, M.; Hsieh, T. C.; Fleming, R. M.; McWhan, D. B.; Yafet, Y.; Cable, J. W.; Bohr, J.; Grimm, H.; and Chien, C. L.; "Magnetic Superlattices," J. Appl. Phys., 63, 3447 (1988).

Majkrzak, C. F.; "Polarized Neutron Diffraction Studies of Synthetic Superlattices," Metallic Multilayers and Epitaxy, (The Metallurgical Society, Pittsburgh, PA (1988).

Majkrzak, C. F.; Neumann, D. F.; Copley, J.R.D.; and DiNardo, R. P.; "Fe-W Supermirrors for Polarizing Neutrons," Proc. of the 1987 Fall Meeting of the Materials Research Society (in press).

Majkrzak, C. F.; "Polarized Neutron Scattering: Some Current Methods and Applications," Proc. of the Int'l Conf. on Neutron Scattering, Grenoble, France, July 1988, Physica B (to be published).

Majkrzak, C. F.; "Applications of Supermirrors and Multilayers at the NBS Cold Neutron Research Facility," Proceedings of the 32nd Annual Int'l Tech. Symposium on Optical and Optoelectronic Applied Science and Engineering, SPIE, August 1988, San Diego, CA (to be published).

Majkrzak, C. F.; "Supermirrors," Proc. of the Workshop on X-ray and Neutron Scattering from Magnetic Matls, Nov. 1987, Argonne, IL, Physica B (to be published).

Majkrzak, C. F.; Cox, D. E.; and Lehmann, M. S.; "Neutron Diffraction," to appear as a chapter in Physical Methods of Chemistry, edited by Rossiter and Hamilton, John Wiley and Sons, Inc. (to be published).

Matsushita, Y.; Nakao, Y.; Saguchi, R.; Mori, K.; Choshi, H.; Muroga, Y.; Noda, I.; Nagasawa, K.; Chang, T.; Glinka, C. J.; and Han, C. C.; "Phase Contrast Matching in Lamellar Structures Composed of Mixtures of Labeled and Unlabeled Block Copolymers for Small-Angle Neutron Scattering," Macromol. (in press).

Mighell, A. D.; Stalick, J. K.; and Himes, V. L.; "NBS Crystal Data: Database Description and Applications," Crystallographic Databases: Information Content, Software Systems, Scientific Applications. Data Commission of the International Union of Crystallography, 134-143 (1987).

Neumann, D. A.; Zabel, H.; Rush, J. J.; Fan, Y. B.; Solin, S. A.; "Quasielastic Neutron Scattering Study of Rotations and Diffusion in Kc (NH)," J. of Phys. C. 20, L761 (1987).

Neumann, D. A.; Zabel, H.; Fan, Y. B.; Solin, S. A.; Rush, J. J.; "Neutron Scattering Study of Phonon-Libron Coupling in Potassium-Ammonia Intercalated Graphite," Phys. Rev. B37, 8424 (1988).

Neumann, D. A.; Zabel, H.; and Morkoc, H.; "Terracing in Strained-layer Superlattices," J. Appl. Phys. (in press).

Nicol, J. M.; Rush, J. J.; Kelley, R. D.; "Neutron Spectroscopic Evidence for Subsurface Hydrogen in Palladium," Phys. Rev. B36, 9315-17 (1987).

Nicol, J. M.; Udovic, T. J.; Rush, J. J.; and Kelley, R. D.; "Isotope Dilution Neutron Sectroscopy: A Vibrational Probe of Hydrogen/Deuterium Adsorbate Interactions on Palladium Black," Langmuir, 4, 294 (1988).

Nicol, J.M.; Rush, J. J.; and Kelley, R. D.; "Inelastic Neutron Scattering Studies of the Interaction of Hydrogen with Palladium Black," Surf. Sci. 197, 67-80 (1988).

Nicol, J. M.; Eckert, J.; Howard, J.; "The Dynamics of Molecular Hydrogen Adsorbed in CoNa-A Zeolite," J. Phys. Chem. (in press).

Osofsky, M.; Toth, L. E.; Lawrence, S.; Qadri, S. B.; Shih, A.; Mueller, D.; Hein, R. A.; Fuller, W. W.; Rachford, F. J.; Skelton, E. F.; Elam, T.; Gubser, D. U.; Wolf, S. A.; Gotaas, J. A.; Rhyne, J. J.; Kurtz, R.; Stockbauer, R.; "Experimental Program on High Temperature Oxide Superconductors at the Naval Research Laboratory," (to be published).

Parise, J. B.; McCarron, E. M.; Sleight, A. W.; Prince, E.; "Refinement of the Structure of β'-MoO_3," Maters. Sci. Forum (in press).

Prask, H. J.; Choi, C. S.; Chesser, N. J.; Rosasco, G. J.; "Ammonium Perchlorate Structure and Dynamics at Low Temperatures," J. Chem. Phys. 88, 5106-5122 (1988).

Prince, E.; "The Maximum Entropy Distribution Consistent with Observed Structure Amplitudes," Acta. Cryst. A. (submitted for publication).

Prince, E.; "An Alternative Approach to the Hauptman-Karle Determinantal Inequalities," Acta. Cryst. A. (in press).

Rhyne, J. J.; "Neutron Scattering in Intermetallics," Invited Paper, Intn'l Symposium on Magnetism of Intermetallic Compounds, Kyoto, Japan, J. Mag. and Mag. Matls. 70, 88 (1987).

Rhyne, J. J.; Erwin, R. W.; Borchers, J.; Salamon, M. B.; Du, R.; and Flynn, C. P.; "Magnetic Ordering in Rare-Earth Multilayers Studied by Neutron Diffraction," Invited Paper, 1987 Metallurgical Society Annual Meeting, Trans. Metallurgical Soc. (to be published in 1988).

Rhyne, J. J.; Erwin, R. W.; Fernandez-Baca, J. A.; and Fish, G. E.; "Magnetic Correlations in Amorphous Fe-Zr Alloys," J. Appl. Phys. 63, 4080 (1988).

Rush, J. J.; Berk, N. F.; Magerl, A.; Rowe, J. M.; and Provo, J. L.; "Anomalous Vibrations of Hydrogen Isotopes in β-phase Vanadium Hydride," Phys. Rev. B., Rapid Comm. 37, (1988).

Rush, J. J.; Udovic, T. J.; Hempelmann, R.; Richter, D.; and Driesen, G.; "Hydrogen Sites in Amorphous $Pd_{85}Si_{15}J_x$ Probed by Neutron Vibrational Spectroscopy," J. Phys. F (1988), in press.

Rush, J. J., "Research Opportunities and Planned Facilities at the Advanced Neutron Source," A.N.S. Trans., in press.

Schwarzenbach, D.; Abrahams, S. C.; Flack, H. D.; Gonschorek, W.; Hahn, T.; Marsh, R. E.; Prince, E.; Robertson, B. E.; Rollett, J. S.; Wilson, A.J.C.; "Report of the International Union of Crystallography Sub-committee on Statistical Descriptors," Acta. Crys. A. (submitted for publication).

Shelton, R. N.; McCallum, R. W.; Damento, M. A.; Gschneider, K. A.; Ku, H. C.; Yang, H. D.; Lynn, J. W.; "Effects of Crystal Anisotropy on Magnetization and Magnetic Order in Superconducting RBaCuO ?," Physica 148B, 285 (1987).

Slade, R. C.; Ramanan, A.; Nicol, J.; Rittar, C.; "Synthesis, "Characterization and Inelastic Neutron Scattering Spectra of Hydrogen Insertion Compounds of the Mixed V/Mo Oxide $V_9Mo_6O_{40}$, Mater. Res. Bull. 23, 647-651 (1988)

Spano, M. L. and Rhyne, J. J.; "Small Angle Neutron Scattering From Amorphous $ErFe_2$ and $HoFe_2$ Alloys, J. Appl. Phys. 63, 3752 (1988).

Spano, M. L.; Gotaas, J. A.; Rhyne, J. J.; "Neutron Scattering Study of Magnetic Order in a $Tb_{0.5}Dy_{0.5}$ Single Crystal," to be published in Proc. of the International Conference on Magnetism 1988.

Stamm, M. and Majkrzak, C. F.; "Investigation of Polymeric Thin Films by Total Reflection of Neutrons," American Chemical Society Preprints (1987).

Stanley, H. B. and Lynn, J. W.; "Antiferromagnetic Structure of the Cubic Superconductor $ErPd_2Sn$," J. Appl. Phys. 61, 3371-3373 (1987).

Torardi, C. C.; Reiff, W. M.; and Prince, E.; "Topochemical Li-ion Insertion into FeClMoO and Fe(MoO): Structure and Magnetism of LiFeClMoO and LiFe(MoO)," Mater. Sci. Forum (in press).

Tran Qui, D.; Handoune, S.; Soubeyeoux, J. L.; and Prince, E.; "Neutron Powder Diffraction Study of Solid Solution $Li_{1+x}Ti_{2-x}Ih_xP_3O_{12}$," J. of Solid State Chem. 72, 309-315 (1988).

Udovic, T. J.; Cavanagh, R. R.; Rush, J. J.; Wax, M. J.; Stucky, G. D.; Jones, G. A.; and Corbin D. R.; "Neutron Scattering Study of NH_4^+ Dynamics During the Deammoniation of NH_4-rho Zeolite," J. Phys. Chem. 91, 5968 (1987).

Udovic, T. J.; Cavanagh, R. R.; and Rush, J. J.; "Neutron Spectroscopic Evidence for Adsorbed Hydroxyl Species on Platinum Black," J. Am. Chem. Soc., 5590 (1988).

Wong-Ng, W.; Hubbard, C. R.; Stalick, J. K.; and Evans, E. H.; "Computerization of the ICDD Powder Diffraction Database. Critical Review of Sets 1 to 32," Powder Diffraction, 3, 12 (1988).

Xiao, G.; Cieplak, M. Z.; Musser, D.; Gavrin, A.; Streitz, F. H.; Chien, C. L.; Rhyne, J. J.; and Gotaas, J. A.; "Significance of Plane versus Chain Sites in High-Temperature Oxide Superconductors," Nature 332, 238-40 (1988).

Yu, H.; Kitano, T.; Kim, C.Y.; Amis, E. J.; Chang, T.; Landry, M. R.; Wesson, J. A.; Han, C. C.; Lodge, T. P.;and Glinka, C. J.; "Study of the Uniaxial Deformation of Rubber Network Chains by Small Angle Neutron Scattering," Advances in Elastomers and Rubber Elasticity, edited by J. Lal and J. E. Mark, Plenum Publishing Corp., 407-420 (1987).

Yu, S. C. and Lynn, J. W.; "X-ray Diffraction Studies of Amorphous $Ni_{92.24}Si_4.50B3.20C_{0.06}$," (submitted for publication).

Yu, S. C.; Lynn, J. W.; Rhyne, J. J.; Fish, G. E.; "Spin Wave Excitations in Amorphouse $Fe_{78}B_{13}Si_9$," J. Appl. Phys. 63, 4083 (1988).

Zabel, H.; and Neumann, D.; "Neutron Scattering Studies of Potassium-Ammonia Layers in Graphite," Can. J. Chem 66, 666 (1988).

INDEPENDENT PROGRAMS

Bauer, B. J.; Briber, R. M.; and Han, C. C.; "Small Angle Neutron Scattering Studies of Single Phase Interpenetrating Polymer Networks," Polymer Preprints (ACS), 28(2), 169 (1987).

Becker, D. A.; "Quality Assurance Techniques for Zinc Analysis by Neutron Activation," Trans. Am. Nucl. Soc. 55, 174 (1987).

Becker, D. A.; "Fast-Neutron INAA: Nickel Sensitivites and Fluence at Three Reactors," Trans. Am. Nucl. Soc. 56 , 193 (1988).

Bowman, R. C., Jr.; Downing, R. G.; and Knudsen, J. F.; "NDP Evaluations for Boron Implanted Compound Semiconductors," Trans. Am. Nucl. Soc. 55, 212 (1987).

Bowman, R. C., Jr.; Marks, J.; Downing, R. G.; Knudsen, J. F.; and To, G.A.; "Effects of Boron Implantation of Silicon Dioxide Passivated HgCdTe," Proc. Mater. Res. Soc. Sym. 90, 279, (1987).

Clark, W. B.; Koekebakker, M.; Barr, R.D.; Downing, R. G.; and Fleming, R. F.; "Analysis of Ultratrace Lithium and Boron by Neutron Activation and Mass-Spectrometric Measurement if ^{3}He and ^{4}He," Inter. J. of Appl. Radiation and Isotopes 38(9), 735-743 (1987).

Cox, J. N.; Hsu, R.; McGregor, P. J.; and Downing, R. G.; "NDP and FTIR Studies of Borophosphosilicate CVD Thin -Film Glasses," Trans. Am. Nucl. Soc. 55, 207 (1987).

Dzubay, T. G.; Stevens, R. K.; Gordon, G. E.; Olmez, I.; Sheffield, A. E.; and Courntey, W. J.; "A Composite Receptor Method Applied to Philadelphia Aerosol", Environ. Sci. Technol. 22, 46-52 (1988).

Dzubay, T. G.; Stevens, R. K.; Gordon, G. E.; Olmez, I.; Sheffield, A. E.; and Courtney, W. J.; "A Composite Receptor Method Applied to Philadelphia Aerosol", in Measurement of Toxic and Related Air Pollutants, S. Hochheiser and R. K. M. Jananty, eds. Air Pollution Control Assn., Pittsburgh, PA, 502-507 (1987).

Dzubay, T. G.; Morosoff, H.; Whitaker, G. L.; Yasuda, H.; Bazan, F.; Bennett, R. L.; Cooper, J.; Courtney, W. J.; Frazier, C. A.; Gatti, R. C.; Germani, M.; Gordon, G.; Hanamura, S.; Kellogg, R. B.; Rhodes, J. R.; and Schindler, J. S.; "Polymer Film Standards for X-ray Fluorescence Spectrometers", J. Trace and Microprobe Tech. 5, 327-341 (1988)

Eisenhauer, C. M.; Schwartz, R. B.; and McCall, R. C.; "Effect of Air Scatter on Calibration of Instruments for Detecting Neutrons, Radiation Protection Dosimetry 19, 2, 77-84 (1987).

Fleming, R. F. and Lindstrom, R. M.; "Precise Determination of Aluminum by Instrumental Neutron Activation," J. Radioanal. Nucl. Chem. 113, 35-42 (1987).

Gokmen, I.; Gordon, G. E.; and Aras, N. K.; "Application ofDifferent Activation Analysis Techniques for Determination of Trace Elements in Human Blood", J. Radioanal Nucl. Chem. 113, 453-459 (1987).

Greenberg, R. R. and Zeisler, R. L.; "A Radiochemical Procedure for the Determination of Chromium in Biological Materials," J. Radioanal. Nuc. Chem. (1987) (in press).

Greenberg, R. R.; Zeisler, R. L.; and Malozowski, S.; "Investigation of Natural Chromium Levels in Human Blood," J. Trace Elem. Electrolytes Health Dis., (1988) (in press).

Greenberg, R. R.; "Evaluation of Precision and Accuracy of Selenium Measurements in Biological Materials Using Neutron Activation Analysis," Trans. the Am. Nucl. Soc. 56, 148-9 (1988).

Greenberg, R. R.; Zeisler, R. L.; and Malozowski, S.; "Investigation of Natural Chromium Levels in Human Blood," to be submitted to Proc. Fifth Int'l Workshop on Trace Element Analytical Chemistry in Medicine and Biology.

Greenberg, R. R.; Zeisler, R. L.; Kingston, H. M.; and Sullivan, T. M.; "Neutron Activation Analysis of the NBS Bovine Serum Standard Reference Material Using Chemical Separations," to be submitted to Fresenius A. Anal. Chem.

Greenberg, R. R.; "Analysis of Atmospheric Particulate Samples Via Instrumental Neutron Activation Analysis," to be submitted Proc. of Conf. on Recent Developments in Monitoring Methods for Toxics in the Atmosphere.

Greenberg, R. R. and Zeisler, R. L.; "A Radiochemical Procedure for the Determination of Chromium in Biological Materials," J. Radioanal. Nucl. Chem. (1987) (in press).

Hadziioannou, G.; Cotts, P.; ten Brinke, G.; Han, C. C.; Lutz, P.; Strazielle, C.; Rempp, P.; and Kovacs, A.; "Thermodynamic and Hydrodynamic Properties of Dilute Solutions of Cyclic Polystyrenes," Macromol. 20, 493 (1987).

Han, C. C.; Sato, T.; Okada, M.; and Wu, C.; "Polymer Diffusion in an Interacting System," Polymer Preprints, ACS 28, 358(1987).

Han, C. C.; Okada, M.; Muroga, Y.; Tran-Cong, Q.; and McCrackin, F. L.; "Temperature, Composition and Molecule Weight Dependence of Binary Interaction Parameter for PS/PVME Blends," Polymer (in press).

Hasegawa, H.; Tanaka, T.; Hashimoto, T.; and Han, C. C.; "SANS and SAXS Studies on Molecular Conformation of a Block Polymer in Microphase Space. II. Contrast Matching Technique," Macromol. 20, 2120 (1987).

Han, C. C.; "Dynamics of Phase Separation in Binary Polymer Mixtures," Proceedings for the First Toyota Conference on "Molecular Conformation and Dynamics of Macromolecules in Condensed Systems," Inuyama, Japan, Sept. 29-Oct. 1, 1987.

Iyengar, G. V.; "Dietary Intake Studies of Nutrient and Selected Toxic Elements in Human Subjects: Analytical Approaches," Clin. Nutr. 6, 105-117 (1987).

Iyengar, G. V.; "Dietary Collection Procedures, " Clin. Nutr. 6, 143-153 (1987).

Iyengar, G. V.; "Practical Constraints in Monitoring Micronutrient Intake," Clin. Nutr. 6, 156-158 (1987).

Iyengar, G. V.; Jones, J.; Cook, K.; Tanner, J. T.; and Wolf, W. R.; "Comparison of Zinc Determination in Foods by Different Analytical Techniques," Trans. Am. Nucl. Soc. 55, 177-178 (1987).

Iyengar, G. V.; Stoeppler, M.; Thomassen, Y.; and Weiz, B.; "Quality Control," in Trace Elements in Health and Disease, Symposium Report, Environmental Health Series, World Health Organization, Regional Office, Copenhagen, Denmark, 26, 33-36 (1987).

Iyengar, G. V.; Tanner, J. T.; Wolf, W. R.; and Zeisler, R. L.; "Development of Multi-Purpose Reference Materials," J. Res. Natl. Bur. Stand. (U.S.) 93, 1-2 (1988).

Iyengar, G. V.; "The Role of Neutron Activation Analysis in Nutritional Biomonitoring Programs," Trans. Am. Nucl. Soc. 56, 233-234. (1988).

Iyengar, G. V.; "Biological Trace Element Research: A Multidisciplinary Science," Sci. Total Environ. 71, 1-5 (1988).

Iyengar, G. V. and Behne, D.; "Appropriate Reference Parameters for the Evaluation of Elemental Analysis Data From Biomedical Specimens," J. Res. Natl. Bur. Stands., (U.S.) 93, 326-328 (1988).

Iyengar, G. V. and Gopal-Ayengar, A. R.; Human Health and Trace E Elements Including Effects on High Altitude Populations, Ambio, XVII, 31-35 (1988).

Iyengar, G. V. and Woittiez, J. R. W.; "Trace Elements in Human Clinical Specimens: Evaluation of Literature Data to Identify Reference Values," Clin. Chem. 34, 474-481 (1988).

Iyengar, G. V.; Tanner, J. T.; Wolf, W. R.; Zeisler, R. L.; "Development of Multi-Purpose Biological Reference Materials," J. Res. Natl. Bur. Stands. (U.S.) 93, 360-362 (1988).

Iyengar, G. V.; Tanner, J. T.; Wolf, W. R.; and Zeisler, R. L.; "Development of Multi-Purpose Reference Materials," J. Res. Natl. Bur. Stand. (U.S.) 93, 1-2 (1988).

Jamieson, D.. N.; Bowman, R. C.; Adams, P. M.; Knudsen, J. F.; and Downing, R. G.; "Study of Boron Implantation in CdTe," in Fundamentals of Beam-Solid Interactions and Transient Thermal Processing, M. JU. Aziz, L. E. Rehn, and B. Stritzker, eds. 101, 299-304 (1988).

Knudsen, J. F.; Downing, R. G.; and Simons, D. S.; "NDP, SIMS, and Modeling of Boron Implantation Profiles in Silicon," Trans. Am. Nucl. Soc. 55, 210 (1987).

Lamaze, G. P.; Gilliam, D. M.; Willliams, A. P.; "Prompt Gamma as a Fluence Rate Monitor in Neutron Beam Experiments," J. of Radioanal. and Nucl. Chem. 123(2) (1988).

Lamaze, G. P. and Grundl, J. A.; "NBS Measurement Services: Activation Foil Irradiation With Californium Fission Sources, NBS Spec. Publ. 250-13 (1988).

Lamaze, G. P. and Grundl, J. A.; "NBS Measurement Services: Activation Foil Irradiation by Reactor Cavity Fission Sources, NBS Spec. Publ. 250-14 (1988).

Lauenstein, G. G.; Wise, S. A.; Zeisler, R. L.; Koster, B. J.; Schantz, M. M.; and Golembiewska, S. L.; National Status and Trends Program for Marine Environmental Quality Specimen Bank Project: Field Manual, NOAA Technical Memorandum NOS OMA 37, Rockville, MD, December 1987.

Lindstrom, R. M.; Zeisler, R. L.; and Rossbach, M.; "Activation Analysis Opportunities Using Cold Neutron Beams," J. Radioanal. Nucl. Chem. 112, 321-330 (1987).

Lindstrom, R. M.; Nuclear Analytical Methods in Standards Certification, in H. H. Ross, ed., "Comparison of Nuclear Analytical Methods With Competive Methods," (IAEA-TECDOC-435), International Atomic Energy Agency, Vienna, Austria 187-193 (1987).

Lindstrom, R. M.; "Measurement of Superconductor Stoichiometry by Prompt and Delayed Neutron Activation," Trans. Am. Nucl. Soc. 56, 231 (1988).

Lindstrom, R. M.; Analytical Standards in Silicon Analysis, Proc. IAEA Consultants' Meeting on the Need for Intercomparison and Reference Materials for Characterization of Silicon, (Gaithersburg, MD, 1987, IAEA-TECDOC), International Atomic Energy Agency, Vienna, Austria (1988) (in press).

Lindstrom, R. M.; Fleming, R. F.; and Rook, H. L.; "Neutron Microprobe: Prospects and Potential Applications, Microbeam Analysis 1988," Proc. 22nd Ann. Conf. Microbeam Analysis Soc. (1988).

Lindstrom, R. M.; Neutron Activation Analysis in Electronic Technology, (submitted for publication to the Electrochemical Society) (1988).

Matsushita, Y.; Nakao, Y.; Saguchi, R.; Mori, K.; Choshi, H.; Noda, I.; Nagasawa, N.; Chang, T.; Glinka, C. J.; and Han, C. C.; "Phase Contrast Matching in Lamellar Structures Composed of Mixtures of Labeled and Unlabeled Block Copolymer for Small Angle Neutron Scattering," Macromol. 21, 1802 (1988).

McGarry, E. D. and Boswell, E.; "Neutron Source Strength Calibrations," NBS Spec. Publ. 250-18 (1988).

Moody, J. R.; Greenberg, R. R.; Pratt, K.W.; and Rains, T. C.; "Recommended Inorganic Chemicals for Use as Calibrants," (submitted to Anal. Chem.).

Okada, M.; Sato, T.; and Han, C. C.; "Dynamics of Concentration Fluctuation on Both Sides of Phase Boundary," Proceedings for the International Meeting on Dynamics of Ordering Processes in Condensed Matter, Kyoto, Japan, August 27-30, 1987.

Olmez, I.; Gulovali, M. C.; Gordon, G. E.; and Henkin, R. I.; "Trace Elements in Human Parotid Saliva", Biol. Trace Elem, Res. (in press).

Riley, J. E., Jr. and Downing, R. G.; "Quantitative Determination of Boron in Semiconductors Using Neutron Depth Profiling," Trans. Am. Nucl. Soc. 55, 207 (1987).

Riley, J. E., Jr.; Downing, R. G.; and Fleming, R. F.; "Neutron Depth Profiling of Lithium in Lithium Niobate," Trans. Am. Nucl. Soc. 55, 214 (1987).

Riley, J. E., Jr. and Lindstrom R. M.; Determination of Boron in Borosilicate Glasses by Neutron Capture Prompt Gamma-Ray Activation Analysis," J. Radioanal. Nucl. Chem. 109, 109-115 (1987).

Rossbach, M.; Schärpf, O.; Kaiser, W.; Graf, W.; Schirmer, A.; Faber, W.; Duppich, J.; and Zeisler, R. L.; "The Use of Focusing Supermirror Neutron Guides to Enhance Cold Neutron Fluence Rates," Nucl. Instrum. Meth., (submitted for publication).

Rossbach, M.; Zeisler, R.; and Lindstrom, R. M.; PGNAA with Cold Neutrons - A Challenge for Chemical Analysis, Proc. International Symposium on the Utilization of Multi-Purpose Research Reactors, Grenoble, France, 19-23 October 1987: IAEA-SM-300-016, (1988) (in press).

Stone, S. F.; Zeisler, R. L.; and Gordon, G. E.; "Quantitative Determination of Proteins Using Polyacrylamide Gel Electrophoresis and Neutron Activation," J. Trace Elem. Electrolytes Health Dis. (1988) in press.

Stone, S. F.; Becker, D. A.; Koster, B. J.; Pella, P. A.; Sleater, G. A.; Tillekeratne, M. P. M.; Zeisler, R. L.; and Sanders, R. W.; "Inorganic Methods and Results for Marine Bivalves and Sediments," in Progress in Environmental Specimen Banking, NBS Spec. Publ. 740, 62-73 (1988).

Stone, S. F.; Zeisler, R.; and Koster,B. J.; "Neutron Activation Analysis of Major, Minor, and Trace Elements in Marine Sediments", Trans. Am. Nucl. Soc. 56, 228-229 (1988).

Stone, S. F.; Becker, D. A.; Koster, B. J.; Pella, P. A.; Sleater, G. A.; Tillekeratne, M.P.M.; and Zeisler, R. L.; Inorganic Analytical Methods and Results for Marine Bivalves and Sediments, in Progress in Environmental Specimen Banking, NBS Spec. Publ. 740, U.S. Government Printing Office, Washington, DC, 62-73 (1988).

Tuncel, S. G.; Gordon, G. E.; Olmez. I.; Parrington, J. R.; Shaw, R. W., Jr.; and Paur, R. J.; "Trace Element Concentrations on Fine Particles in the Ohio River Valley" in The Chemistry of Acid Rain I: Sources and Atmospheric Processes, R.W. Johnson and G. E. Gordon, eds., ACS Symp. Series No. 349, American Chemical Society, Washington, DC, 66-81 (1987).

Tuncel, G. and Zoller, W. H.; "Iridium in the South Pole Atmosphere: Estimation of a Meteoritic Component", Nature 329, 703-705 (1987).

Vossler, T. L.; Lewis, C. W.; Stevens, R. K.; Dzubay, T. G.; Gordon, G. E.; Tuncel, S. G.; Russwurm, G. M.; and Keeler, G. J.; "Composition and Origin of Summertime Air Pollutants at Deep Creek Lake, MD", (submitted to Atmos Environ.).

Williamson, T. G. and Lamaze, G. P.; "Niobium as a Neutron Dosimeter," Trans. Am. Nucl. Soc. 55, 553 (1987).

Williamson, T. G.; Lamaze, G. P.; Gilliam, D. M.; and Eisenhauer, C. M.; "Iron and Cadmium Capture Gamma Ray Photofission Measurements, Proceedings of Meeting on Theory and Practices in Radiation Protection and Shielding, Knoxville, TN.

Wise, S.A.; Zeisler, R. L.; and Goldstein, G. M.; eds., Progress in Environmental Specimen Banking, NBS Spec. Publ. 740, U.S. Government Printing Office, Washington, DC, 217 (1988).

Wise, S. A.; Koster, B. J.; and Zeisler, R. L.; Status of Specimen Banking Activities at the National Bureau of Standards, in Progress in Environmental Specimen Banking, NBS Spec. Publ. 740, U.S. Government Office, Washington, DC, 10-18 (1988).

Wu, W. and Gilmer, J. W.; "Molecular Weight Measured by Scattering Techniques in Random Block Copolymers," Poly. Comm. 28, 202 (1987).

Wu, W.; Hunston, D. L.; Yang, H.; and Stein, R. S.; "Epoxy Network Structure (IV) - A Neutron Scattering Study of Epoxies Swollen in A Deuterated Solvent," Macromol. 21(3), 756 (1988).

Wu, W. and Bauer, B. J.; "Network Structure in Epoxies (V) - Deformation Mechanism in Epoxies," Macromol. 21(2), 756 (1988).

Wu, W.; Bauer, B. J.; and Su, W.; "Network Structure in Epoxies (VI) - The Growth Process Investigated by Neutron Scattering," (submitted for publication).

Zeisler, R. L. and Becker, D. A.; "Determination of Zinc in a Monel Alloy by Compton Suppression Spectrometry," Trans. Am. Nucl. Soc. 55, 175 (1987).

Zeisler, R. L.; Stone, S. F.; and Sanders, R. W.; "Sequential Determination of Biological and Pollutant Elements in Marine Bivalves," Anal. Chem. (submitted for publication).

Zeisler, R. L.; Greenberg, R. R.; and Stone, S. F.; "Radiochemical and Instrumental Neutron Activation Analysis Procedures for the Determination of Low Level Trace Elements in Human Livers," J. Radioanal. Nucl. Chem. (1987) (in press).

Zeisler, R. L.; Greenberg, R. R.; Stone, S.F.; and Sullivan, T. M.; "Selenium Determinations for the Assessment of Sample Stability in Specimen Banking," Trans. Am. Nucl. Chem. (1987) (in press).

Zeisler, R. L. and Greenberg, R. R.; "Determination of Baseline Platinum Levels in Biological Materials," J. Trace Elem. Electrolytes Health Dis. (1988) (in press).

Zeisler, R. L.; Greenberg, R. R.; and Stone, S. F.; The Determination of Trace Elements in Human Livers, in Progress in Environmental Specimen Banking, NBS Spec. Publ. 740, U.S. Government Printing Office, Washington, DC, 82-90 (1988).

NBS-114A (REV. 2-8C)

U.S. DEPT. OF COMM. **BIBLIOGRAPHIC DATA SHEET** *(See instructions)*	1. PUBLICATION OR REPORT NO. NIST/TN-1257	2. Performing Organ. Report No.	3. Publication Date January 1989

4. TITLE AND SUBTITLE

NBS Reactor: Summary of Activities July 1987 Through June 1988.

5. AUTHOR(S)

Carol O'Connor, Editor

6. PERFORMING ORGANIZATION *(If joint or other than NBS, see instructions)*

NATIONAL INSTITUTE OF STANDARDS AND TECHNOLOGY
(formerly NATIONAL BUREAU OF STANDARDS)
U.S. DEPARTMENT OF COMMERCE
GAITHERSBURG, MD 20899

7. Contract/Grant No.

8. Type of Report & Period Covered
July 1987 through June 1988.

9. SPONSORING ORGANIZATION NAME AND COMPLETE ADDRESS *(Street, City, State, ZIP)*

Same as item #6 above.

10. SUPPLEMENTARY NOTES

☐ Document describes a computer program; SF-185, FIPS Software Summary, is attached.

11. ABSTRACT *(A 200-word or less factual summary of most significant information. If document includes a significant bibliography or literature survey, mention it here)*

This report summarizes all those programs which use the NBS Reactor. It covers the period for July 1987 through June 1988. The programs range from the use of neutron beams to study the structure and dynamics of materials through nuclear physics and neutron standards to sample irradiations for activation analysis, isotope production, neutron radiography, and nondestructive evaluation.

12. KEY WORDS *(Six to twelve entries; alphabetical order; capitalize only proper names; and separate key words by semicolons)*

activation analysis; cold neutrons; crystal structure; diffraction; isotopes; molecular dynamics; neutron; neutron radiography; nondestructive evaluation; nuclear reactor; radiation.

13. AVAILABILITY

☒ Unlimited

☐ For Official Distribution. Do Not Release to NTIS

☐ Order From Superintendent of Documents, U.S. Government Printing Office, Washington, D.C. 20402.

☒ Order From National Technical Information Service (NTIS), Springfield, VA. 22161

14. NO. OF PRINTED PAGES
227

15. Price

USCOMM-DC 6043-P80

*U.S. GOVERNMENT PRINTING OFFICE:1989-242-311:92628

NIST Technical Publications

Periodical

Journal of Research of the National Institute of Standards and Technology—Reports NIST research and development in those disciplines of the physical and engineering sciences in which the Institute is active. These include physics, chemistry, engineering, mathematics, and computer sciences. Papers cover a broad range of subjects, with major emphasis on measurement methodology and the basic technology underlying standardization. Also included from time to time are survey articles on topics closely related to the Institute's technical and scientific programs. Issued six times a year.

Nonperiodicals

Monographs—Major contributions to the technical literature on various subjects related to the Institute's scientific and technical activities.

Handbooks—Recommended codes of engineering and industrial practice (including safety codes) developed in cooperation with interested industries, professional organizations, and regulatory bodies.

Special Publications—Include proceedings of conferences sponsored by NIST, NIST annual reports, and other special publications appropriate to this grouping such as wall charts, pocket cards, and bibliographies.

Applied Mathematics Series—Mathematical tables, manuals, and studies of special interest to physicists, engineers, chemists, biologists, mathematicians, computer programmers, and others engaged in scientific and technical work.

National Standard Reference Data Series—Provides quantitative data on the physical and chemical properties of materials, compiled from the world's literature and critically evaluated. Developed under a worldwide program coordinated by NIST under the authority of the National Standard Data Act (Public Law 90-396). NOTE: The Journal of Physical and Chemical Reference Data (JPCRD) is published quarterly for NIST by the American Chemical Society (ACS) and the American Institute of Physics (AIP). Subscriptions, reprints, and supplements are available from ACS, 1155 Sixteenth St., NW., Washington, DC 20056.

Building Science Series—Disseminates technical information developed at the Institute on building materials, components, systems, and whole structures. The series presents research results, test methods, and performance criteria related to the structural and environmental functions and the durability and safety characteristics of building elements and systems.

Technical Notes—Studies or reports which are complete in themselves but restrictive in their treatment of a subject. Analogous to monographs but not so comprehensive in scope or definitive in treatment of the subject area. Often serve as a vehicle for final reports of work performed at NIST under the sponsorship of other government agencies.

Voluntary Product Standards—Developed under procedures published by the Department of Commerce in Part 10, Title 15, of the Code of Federal Regulations. The standards establish nationally recognized requirements for products, and provide all concerned interests with a basis for common understanding of the characteristics of the products. NIST administers this program as a supplement to the activities of the private sector standardizing organizations.

Consumer Information Series—Practical information, based on NIST research and experience, covering areas of interest to the consumer. Easily understandable language and illustrations provide useful background knowledge for shopping in today's technological marketplace.

Order the **above** *NIST publications from: Superintendent of Documents, Government Printing Office, Washington, DC 20402.*

Order the **following** *NIST publications—FIPS and NISTIRs—from the National Technical Information Service, Springfield, VA 22161.*

Federal Information Processing Standards Publications (FIPS PUB)—Publications in this series collectively constitute the Federal Information Processing Standards Register. The Register serves as the official source of information in the Federal Government regarding standards issued by NIST pursuant to the Federal Property and Administrative Services Act of 1949 as amended, Public Law 89-306 (79 Stat. 1127), and as implemented by Executive Order 11717 (38 FR 12315, dated May 11, 1973) and Part 6 of Title 15 CFR (Code of Federal Regulations).

NIST Interagency Reports (NISTIR)—A special series of interim or final reports on work performed by NIST for outside sponsors (both government and non-government). In general, initial distribution is handled by the sponsor; public distribution is by the National Technical Information Service, Springfield, VA 22161, in paper copy or microfiche form.

U.S. Department of Commerce
National Institute of Standards and Technology
(formerly National Bureau of Standards)
Gaithersburg, MD 20899